UNIVERSITÀ DEGLI STUDI DI PAVIA

DIPARTIMENTO DI INFORMATICA E SISTEMISTICA

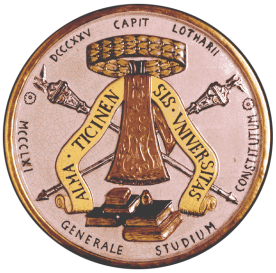

Sliding Mode Control:

theoretical developments and applications to uncertain mechanical systems

Claudio Vecchio

Advisor : Prof. Antonella Ferrara

Acknowledgments

This thesis is the result of a three years long research activity that I have carried out at the Department of Computer Engineering and Systems Science of the University of Pavia. I would like to thank some people who made a contribution to this thesis.

First of all, I would like to thank my advisor Antonella Ferrara for her constant support, suggestions and scientific guidance during all stages of my work.

I wish to thank all members of my department for providing a stimulating and collaborative working environment, in particular, Prof. Giuseppe De Nicolao, Prof. Giancarlo Ferrari-Trecate and Prof. Lalo Magni. I also thank my colleagues Luca Bossi, Luca Capisani, Riccardo Porreca, Matteo Rubagotti and Davide Raimondo for their help and their friendship. In particular, I want to express my gratitude to Davide Raimondo for his support and for all the fun we had together during these last eight years.

I would like to thank Massimo Canale, Lorenzo Fagiano, Alberto Massola, Prof. Sergio Savaresi and Mara Tanelli for their friendly collaboration.

I am particularly grateful to my parents Enzo and Gabriella, to my brother Luca, to my granparents Antonietta, Graziano, Luigi and Rosa and to my relatives Andrea, Giovanni and Simonetta for their everlasting love and support. Their suggestions have been an invaluable source of inspiration to grow up and to improve myself.

One special thank goes to Roby who gives me always a huge love and who makes every day of my life special.

Contents

Chapter 1

Introduction

1.1 Introduction and motivation

The control of dynamical systems in presence of uncertainties and disturbances is a common problem to deal with when considering real plants. The effect of these uncertainties on the system dynamics should be carefully taken into account in the controller design phase since they can worsen the performance or even cause system instability.

For this reason, during recent years, the problem of controlling dynamical systems in presence of heavy uncertainty conditions has become an important subject of research. As a result, considerable progresses have been attained in robust control techniques, such as nonlinear adaptive control, model predictive control, backstepping, sliding model control and others. These techniques are capable of guaranteeing the attainment of the control objectives in spite of modelling errors and/or parameter uncertainties affecting the controlled plant.

Among the existing methodologies, the Sliding Mode Control (SMC) technique turns out to be characterized by high simplicity and robustness. Essentially, SMC utilizes discontinuous control laws to drive the system state trajectory onto a specified surface in the state space, the so–called sliding or switching surface, and to keep the system state on this manifold for all the subsequent times.
In order to achieve the control objective, the control input must be designed with an authority sufficient to overcome the uncertainties and the disturbances acting on the system. The main advantages of this approach are two: first, while the system is on the sliding manifold it behaves as a reduced order system with respect to the original plant; and, second, the dynamic of the system while in sliding mode is insensitive to model uncertainties and disturbances.

However, in spite of the claimed robustness properties, the real–life implementation of SMC techniques presents a major drawback: the so–called chattering effect, i.e., dangerous high–frequency vibrations of the controlled system. This phenomenon is due to the fact that, in real–life applications, it is not reasonable to assume that the control signal can switch at infinite frequency. On the contrary, it is more realistic, due to the inertias of the actuators and sensors and to the presence of noise and/or exogenous disturbances, to assume that it switches at a very high (but finite) frequency. Chattering and the need for discontinuous control constitute two of the main criticisms to sliding modes control techniques, and these drawbacks are much more evident when dealing with mechanical systems, since rapidly changing control actions induce stress and wear in mechanical parts and the system could be damaged in a short time.

This work analyzes a quite recent development of sliding mode control, namely the second order sliding mode approach, which is encountering a growing attention in the control research community. Second order sliding mode techniques produce continuous control laws while keeping the same advantages of the original approach, and provide for even higher accuracy in realization.

The objective of this thesis is to survey the theoretical background of sliding mode control, in particular higher order sliding mode control, to show that the second order sliding mode approach is an effective solution to the above–cited drawbacks and to develop some original contribution to the theory and application of sliding mode control. Moreover, some important control problems involving uncertain mechanical systems are addressed and solved by means of the sliding mode control methodology in this thesis. In particular, the sliding mode control methodology will be applied to three different context:

- Automotive control;
- Control of nonholonomic systems;
- Multi–agent systems.

Apart from the robustness features against different kind of uncertainties and disturbances, the proposed control schemes have the advantage of producing low complexity control laws compared to other robust control ap-

proaches (H_∞, LMI, adaptive control, etc.) which appears particularly suitable in the considered contexts.

1.2 Thesis structure

The present thesis is organized as follows:

Chapter 2: Sliding mode control. In this chapter some of the basic notions of the sliding mode control theory are given.

Chapter 3: Higher order sliding mode control. The aims of this chapter are to provide a brief introduction to the higher order sliding mode control theory and to describe the main features and advantages of higher order sliding modes. In particular, the second order sliding mode control problem is described and several second order sliding mode controllers are presented.

Chapter 4: Automotive control. In this chapter some important application of the second order sliding mode control methodology to the automotive context are presented. In particular, second order sliding mode controllers for vehicle yaw stability, traction control for both vehicle and sport motorbike and a driver assistance system for a platoon of vehicles capable of keeping the desired inter–vehicular spacing, but also of generating a collision avoidance manoeuvre are designed.

Chapter 5: Stabilization of nonholonomic uncertain systems. The problem of controlling a class of nonholonomic systems in chained form affected by uncertainties is addressed and solved relying on second order sliding mode methodology. More specifically, the problem of stabilizing chained form systems affected by uncertain drift term and parametric uncertainties and by both matched and unmatched uncertainties is considered.

Chapter 6 Formation control of multi-agent systems. This chapter focuses on the control of a team of agents designated either as leaders or followers and exchanging information over a directed communication network. The generalized consensus state for a follower agent is defined as a target state that depends on the state of its neighbors. A decentralized control scheme based on sliding mode technique capable of steering the state of each follower agent to the generalized consensus state in finite time is presented.

Chapter 2

Sliding mode control

Contents

In this chapter some of the basic notions of the sliding mode control theory are given. The interested reader is referred to DeCarlo *et al.* (1988), Slotine and Li (1991), Utkin (1992), Edwards and Spurgeon (1998) and Perruquetti and Barbot (2002) for further details.

2.1 Introduction

Variable structure control (VSC) with sliding mode control was first proposed and elaborated by several researchers from the former Russia, starting from the sixties (Emel'yanov and Taran, 1962; Emel'yanov, 1970; Utkin,

1974). The ideas did not appear outside of Russia until the seventies when a book by Itkis (Itkis, 1976) and a survey paper by Utkin (Utkin, 1977) were published in English. Since then, sliding mode control has developed into a general design control method applicable to a wide range of system types including nonlinear systems, MIMO systems, discrete time models, large–scale and infinite–dimensional systems.

Essentially, sliding mode control utilizes discontinuous feedback control laws to force the system state to reach, and subsequently to remain on, a specified surface within the state space (the so–called sliding or switching surface). The system dynamic when confined to the sliding surface is described as an ideal sliding motion and represent the controlled system behaviour.

The advantages of obtaining such a motion are twofold: firstly the system behaves as a system of reduced order with respect to the original plant; and secondly the movement on the sliding surface of the system is insensitive to a particular kind of perturbation and model uncertainties.

This latter property of invariance towards so–called matched uncertainties is the most distinguish feature of sliding mode control and makes this methodology particular suitable to deal with uncertain nonlinear systems.

2.2 Problem statement

Consider the following nonlinear system affine in the control

$$\dot{x}(t) = f(t,x) + g(t,x)u(t) \tag{2.1}$$

where $x(t) \in \mathbb{R}^n$, $u(t) \in \mathbb{R}^m$, $f(t,x) \in \mathbb{R}^{n\times n}$, and $g(t,x) \in \mathbb{R}^{n\times m}$. The component of the discontinuous feedback are given by

$$u_i = \begin{cases} u_i^+(t,x), & \text{if} \quad \sigma_i(x) > 0 \\ u_i^-(t,x), & \text{if} \quad \sigma_i(x) < 0 \end{cases} \qquad i = 1,2,\ldots,m \tag{2.2}$$

where $\sigma_i(x) = 0$ is the i–th sliding surface, and

$$\sigma(x) = [\sigma_1(x),\, \sigma_2(x), \ldots,\, \sigma_m(x)]^T = 0 \tag{2.3}$$

is the $(n-m)$–dimensional sliding manifold.

The control problem consists in developing continuous function u_i^+, u_i^-, and the sliding surface $\sigma(x) = 0$ so that the closed–loop system (2.1)–(2.2) exhibit a sliding mode on the $(n-m)$–dimensional sliding manifold $\sigma(x) = 0$.

The design of the sliding mode control law can be divided in two phases:

1. Phase 1 consists in the construction of a suitable sliding surface so that the dynamic of the system confined to the sliding manifold produces a desired behaviour;

2. Phase 2 entails the design of a discontinuous control law which forces the system trajectory to the sliding surface and maintains it there.

The sliding surface $\sigma(x) = 0$ is a $(n-m)$–dimensional manifold in $\mathbb{R}^n$ determined by the intersection of the m $(n-1)$–sliding manifold $\sigma_i(x) = 0$. The switching surface is designed such that the system response restricted to $\sigma(x) = 0$ has a desired behaviour.

Although general nonlinear switching surfaces (2.3) are possible, linear ones are more prevalent in design (Utkin, 1977; DeCarlo *et al.*, 1988; Sira-Ramirez, 1992; Edwards and Spurgeon, 1998), Thus for the sake of simplicity, this chapter will focus on linear switching surfaces of the form

$$\sigma(x) = Sx(t) = 0 \tag{2.4}$$

where $S \in \mathbb{R}^{m \times n}$.

After switching surface design, the next important aspect of sliding mode control is guaranteeing the existence of a sliding mode. A sliding mode exists, if in the vicinity of the switching surface, $\sigma(x) = 0$, the velocity vectors of the state trajectory is always directed toward the switching surface. Consequently, if the state trajectory intersects the sliding surface, the value of the state trajectory remains within a neighborhood of $\{x|\sigma(x) = 0\}$. If a sliding mode exists on $\sigma(x) = 0$, then $\sigma(x)$ is termed a sliding surface. As seen in Fig. 2.1, a sliding mode on $\sigma(x) = 0$ can arise even in the case when sliding mode does not exist on each of the surface $\sigma_i(x) = 0$ taken separately.

An ideal sliding mode exists only when the state trajectory $x(t)$ of the controlled plant satisfies $\sigma[x(t)] = 0$ at every $t \geq t_0$ for some t_0. Starting from time instant t_0, the system state is constrained on the discontinuity surface, which is an invariant set after the sliding mode has been established.

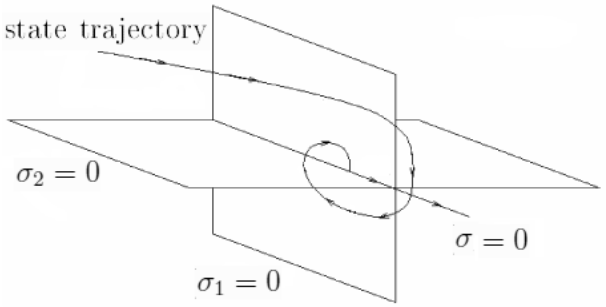

Figure 2.1: Sliding mode in the intersection of the discontinuity surfaces

This requires infinitely fast switching. In real systems are present imperfections such as delay, hysteresis, etc., which force switching to occur at a finite frequency. The system state then oscillates within a neighborhood of the switching surface. This oscillation is called chattering. If the frequency of the switching is very high compared with the dynamic response of the system, the imperfections and the finite switching frequencies are often but not always negligible.

2.3 Existence of a sliding mode

Existence of a sliding mode (Itkis, 1976; Utkin, 1977, 1992; Edwards and Spurgeon, 1998) requires stability of the state trajectory to the sliding surface $\sigma(x) = 0$ at least in a neighborhood of $\{x|\sigma(x) = 0\}$, i.e., the system state must approach the surface at least asymptotically. The largest such neighborhood is called the region of attraction. From a geometrical point of view, the tangent vector or time derivative of the state vector must point toward the sliding surface in the region of attraction (Itkis, 1976; Utkin, 1992) (see Fig. 2.2). For a rigorous mathematical discussion of the existence of sliding modes see Itkis (1976); White and Silson (1984); Filippov (1988); Utkin (1992).

The existence problem can be seen as a generalized stability problem, hence the second method of Lyapunov provides a natural setting for analysis. Specifically, stability to the switching surface requires to choose a generalized Lyapunov function $V(t, x)$ which is positive definite and has a

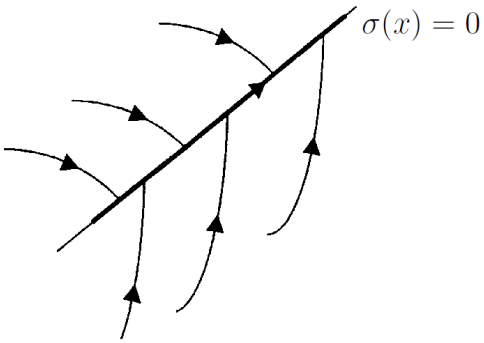

Figure 2.2: Attractiveness of the sliding manifold

negative time derivative in the region of attraction. Formally stated:

Definition 2.1 *A domain D in the manifold $\sigma = 0$ is a sliding mode domain if for each $\varepsilon > 0$, there is $\delta > 0$, such that any motion starting within a n–dimensional δ–vicinity of D may leave the n–dimensional δ–vicinity of D only through the n–dimensional δ–vicinity of the boundary of D (see Fig. 2.3).*

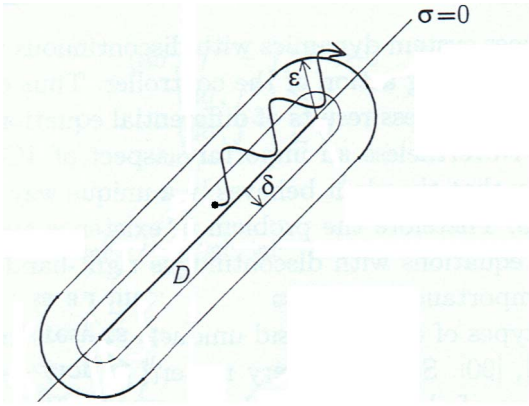

Figure 2.3: Two dimensional illustration of a sliding mode domain

Since the region D lies on the surface $\sigma(x) = 0$, dimension $[D] = n - m$. Hence:

Theorem 2.1 *For the $(n-m)$–dimensional domain D to be the domain of a sliding mode, it is sufficient that in some n–dimensional domain $\Omega \supset D$, there exists a function $V(t,x,\sigma)$ continuously differentiable with respect to all of its arguments, satisfying the following conditions:*

1. *$V(t,x,\sigma)$ is positive definite with respect to σ, i.e., $V(t,x,\sigma) > 0$, with $\sigma \neq 0$ and arbitrary t, x, and $V(t,x,0) = 0$; and on the sphere $\|\sigma\| = \rho$, for all $x \in \Omega$ and any t the relations*

$$\inf_{\|\sigma\|=\rho} V(t,x,\sigma) = h_\rho, \qquad h_\rho > 0 \tag{2.5}$$

$$\sup_{\|\sigma\|=\rho} V(t,x,\sigma) = H_\rho, \qquad H_\rho > 0 \tag{2.6}$$

   hold, where h_ρ, and H_ρ, depend on ρ ($h_\rho \neq 0$ if $\rho \neq 0$).

2. *The total time derivative of $V(t,x,\sigma)$ for the system (2.1) has a negative supremum for all $x \in \Omega$ except for x on the switching surface where the control inputs are undefined, and hence the derivative of $V(t,x,\sigma)$ does not exist.*

Proof: See Utkin (1977).

The domain D is the set of x for which the origin of the subspace $(\sigma_1 = 0, \sigma_2 = 0, \ldots, \sigma_m = 0)$ is an asymptotically stable equilibrium point for the dynamic system. A sliding mode is globally reachable if the domain of attraction is the entire state space. Otherwise, the domain of attraction is a subset of the state space.

The structure of the function $V(t,x,\sigma)$ determines the ease with which one computes the actual feedback gains implementing a sliding mode control design. Unfortunately, there are no standard methods to find Lyapunov functions for arbitrary nonlinear systems.

Note that, for all single input systems a suitable Lyapunov function is

$$V(t,x) = \frac{1}{2}\sigma^2(x)$$

which clearly is globally positive definite. In sliding mode control, $\dot{\sigma}$ will depend on the control and hence if switched feedback gains can be chosen so that

$$\dot{V}(t,x,\sigma) = \sigma\frac{\partial\sigma}{\partial t} < 0 \tag{2.7}$$

in the domain of attraction, then the state trajectory converges to the surface and is restricted to the surface for all subsequent time. This latter condition is called the reaching or reachability condition (Utkin, 1992; Edwards and Spurgeon, 1998) and ensures that the sliding manifold is reached asymptotically.

Condition (2.7) is often replaced by the so–called η–reachability condition (Utkin, 1977, 1992; Edwards and Spurgeon, 1998)

$$\dot{V}(t,x,\sigma) = \sigma\frac{\partial\sigma}{\partial t} \leq -\eta|\sigma| < 0 \tag{2.8}$$

which ensures finite time convergence to $\sigma(x) = 0$, since by integration of (2.8) one has

$$|\sigma[x(t)]| - |\sigma[x(0)]| \leq -\eta t$$

showing that the time required to reach the surface, starting from the initial condition $\sigma[x(0)]$ is bounded by

$$t_s = \frac{|\sigma[x(0)]|}{\eta}$$

The feedback gains which would implement an associated sliding mode control design are straightforward to compute in this case (Utkin, 1977; Slotine and Li, 1991; Sira-Ramirez, 1992; Zinober, 1994; Edwards and Spurgeon, 1998; Young *et al.*, 1999).

2.4 Existence and uniqueness of solution

The differential equations (2.1) and (2.2) do not formally satisfy the classical theorems on the existence and uniqueness of the solutions, since they have discontinuous right–hand sides. Moreover, the right–hand sides usually are not defined on the discontinuity surfaces. Thus, they fail to satisfy conventional existence and uniqueness results of differential equation theory. Nevertheless, an important aspect of sliding mode control design is the assumption that the system state behaves in a unique way when restricted to $\sigma(x) = 0$. Therefore, the problem of existence and uniqueness of differential equations with discontinuous right–hand sides is of fundamental importance. Various types of existence and uniqueness theorems can be found in Itkis (1976); Utkin (1977); Hajek (1979) and Filippov (1988).

One of the earliest and conceptually straightforward approaches is the method of Filippov (Filippov, 1988). This method is now briefly recalled as a background to the above referenced results and as an aid in understanding variable structure system behaviour on the switching surface.

Consider the following n–th order single input system

$$\dot{x}(t) = f(t, x, u) \tag{2.9}$$

with the following general control strategy

$$u = \begin{cases} u^+(t,x), & \text{if} \quad \sigma(x) > 0 \\ u^-(t,x), & \text{if} \quad \sigma(x) < 0 \end{cases} \tag{2.10}$$

The system dynamics are not directly defined on the manifold $\sigma(x) = 0$. In Filippov (1988), it has been shown that the state trajectories of (2.9) with control (2.10) on $\sigma(x) = 0$ are the solutions of the equation

$$\dot{x}(t) = \alpha f^+ + (1-\alpha) f^- = f^0, \qquad 0 \leq \alpha \leq 1 \tag{2.11}$$

where $f^+ = f(t, x, u^+)$, $f^- = f(t, x, u^-)$, and f^0 is the resulting velocity vector of the state trajectory while in sliding mode. The term α is a function of the system state and can be specified in such a way that the "average" dynamic of f^0 is tangent to the surface $\sigma(x) = 0$. The geometric concept is illustrated in Fig. 2.4.

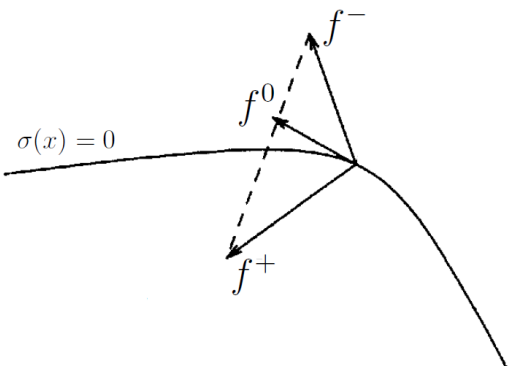

Figure 2.4: Illustration of the Filippov method

Therefore one may conclude that, on the average, the solution to (2.9) with control (2.10) exists and is uniquely defined on $\sigma(x) = 0$. This solution is called "solution in the Filippov sense". Note that this technique can be used to determine the behaviour of the plant in a sliding mode.

2.5 Sliding surface design

Filippov's method is one possible technique for determining the system motion in sliding mode as outlined in the previous section. In particular, computation of f^0 represents the "average" velocity $\dot{x}$ of the state trajectory restricted to the switching surface. A more straightforward technique easily applicable to multi–input systems is the equivalent control method, as proposed in Utkin (1977, 1992) and in Drazenovic (1969).
It has been proved that the equivalent control method produces the same solution of the Filippov method if the controlled system is affine in the control input while the two solutions may differ in more general cases.

The method of equivalent control can be used to determine the system motion restricted to the switching surface $\sigma(x) = 0$. The analytical nature of this method makes it a powerful tool for both analysis and design purposes.
Consider the following system affine in the control input

$$\dot{x}(t) = f(t,x) + g(t,x)u(t) \tag{2.12}$$

Suppose that, at time instant t_0, the state trajectory of the plant intercepts the switching surface and a sliding mode exists for $t \geq t_0$.
The first step of the equivalent control approach is to find the input u_{eq} such that the state trajectory stays on the switching surface $\sigma(x) = 0$. The existence of the sliding mode implies that $\sigma(x) = 0$, for all $t \geq t_0$, and $\dot{\sigma}(x) = 0$.

By differentiating $\sigma(x)$ with respect to time along the trajectory of (2.12) it yields

$$\left[\frac{\partial \sigma}{\partial x}\right] \dot{x} = \left[\frac{\partial \sigma}{\partial x}\right] [f(t,x) + g(t,x)u_{eq}] = 0 \tag{2.13}$$

where u_{eq} is the so–called equivalent control. Note that, under the action of the equivalent control u_{eq} any trajectory starting from the manifold $\sigma(x) = 0$ remains on it, since $\dot{\sigma}(x) = 0$. As a consequence, the sliding manifold $\sigma(x) = 0$ is an invariant set.
To compute u_{eq}, let us assume that the matrix product $[\partial\sigma/\partial x]g(t,x)$ is nonsingular for all t and x. Then

$$u_{eq} = -\left[\frac{\partial \sigma}{\partial x} g(t,x)\right]^{-1} \frac{\partial \sigma}{\partial x} f(t,x) \tag{2.14}$$

Therefore, given $\sigma[x(t_0)] = 0$, the dynamics of the system on the switching surface for $t \geq t_0$, is obtained by substituting (2.14) in (2.12), i.e.,

$$\dot{x}(t) = \left[I - g(t,x) \left[\frac{\partial \sigma}{\partial x} g(t,x) \right]^{-1} \frac{\partial \sigma}{\partial x} \right] f(t,x) \tag{2.15}$$

In the special case of a linear switching surface $\sigma(x) = Sx(t)$, (2.15) results in

$$\dot{x}(t) = \left[I - g(t,x) \left[Sg(t,x) \right]^{-1} S \right] f(t,x) \tag{2.16}$$

This structure can be advantageously exploited in switching surface design.

Note that (2.15) with the constraint $\sigma(x) = 0$ determines the system behaviour on the switching surface. As a result, the motion on the switching surface results governed by a reduced order dynamics because of the set of state variable constraints $\sigma(x) = 0$.

2.5.1 Order reduction

As mentioned above, in a sliding mode, the equivalent system must satisfy not only the n–dimensional state dynamics (2.15), but also the m algebraic equations given by $\sigma(x) = 0$. The use of both constraints reduces the system dynamics from an n–th order model to an $(n-m)$–th order model.

Specifically, suppose that the nonlinear system (2.1) is in sliding mode on the sliding surface (2.3), i.e., $\sigma(x) = Sx = 0$, with the system dynamics given by (2.16).

Then, it is possible to solve for m of the state variables in terms of the remaining $n-m$ state variables, if $rank[S] = m$. This latter condition holds under the assumption that $[\partial\sigma/\partial x]g(t,x)$ is nonsingular for all t and x.

To obtain the solution, solve for m of the state variables in terms of the $n-m$ remaining state variables. Substitute these relations into the remaining $n-m$ equations of (2.16) and the equations corresponding to the m state variables.

The resultant $(n-m)$–th order system fully describes the equivalent system given an initial condition satisfying $\sigma(x) = 0$.

2.5.2 The identificability property

The invariance property establishes that different systems may exhibit the same behaviour when constrained to evolve on the same manifold. Although any informations regarding the original plant seem to be lost during the sliding motion, it is possible to recover it through the analysis of the discontinuous plant input signal.

The response of a dynamic system is largely determined by the slow components of its input, while the fast components are often negligible. On the other hand, the equivalent control method requires the substitution of the actual discontinuous control with a continuous function which does not contain high-rate components.

On the basis of the above considerations, in Utkin (1992) it has been proved that the equivalent control coincides with the slow components of the input, and, under certain assumptions on the system dynamics, if the system remains within a δ–vicinity of the sliding manifold, the output of the first–order filter

$$\tau u_{av}(t) + u_{av}(t) = u(t) \tag{2.17}$$

where $u(t)$ is the actual control input, is close to the equivalent control according to the following relation

$$|u_{av}(t) - u_{eq}(t)| \leq k_0 |u_{av}(0) - u_{eq}(0)| e^{-\frac{t}{\tau}} + k_1 \tau + k_2 \delta + k_3 \frac{\delta}{\tau} \tag{2.18}$$

where k_0, k_1, k_2, k_3 are proper known constants. This result is not valid for systems nonlinear in the control law, as in such systems the dynamic plant response to the high-frequency terms cannot generally be neglected.

The expression (2.18) contains useful information on the criterion for properly choosing the filter time constant in order to achieve the best estimate. It is apparent that the right–hand side of (2.18) can be minimized if the time constant τ of the filter is taken to be proportional to $\sqrt{\delta}$, which leads to

$$|u_{av}(t) - u_{eq}(t)| \leq O(\sqrt{\delta}) \tag{2.19}$$

The filter time constant, that must be small enough as compared with the slow components of the control yet large enough to filter out the high–rate components, is to be chosen suitably matched with the size of the boundary layer.

This property of identificability constitutes one of the most important structural property of sliding mode control and it has been successfully applied for design purposes in various works (Hsu and Costa, 1989; Fu, 1991).

2.6 Controller design

The controller design is the second phase of the sliding mode control design procedure mentioned earlier. The problem is to choose switched feedback gains capable of forcing the plant state trajectory to the switching surface and of maintaining a sliding mode condition. The assumption is that the sliding surface has already been designed. In the considered case, the control is an m–vector $u(t)$ of the form (2.2).

2.6.1 Diagonalization method

The control design approach called diagonalization method (DeCarlo *et al.*, 1988) will be described in this subsection. The essential feature of these methods is the conversion of a multi–input design problem into m single input design problems.

This method is based on the construction of a new control vector u^* through a nonsingular transformation of the original control defined as

$$u^*(t) = Q^{-1}(t,x)\left[\frac{\partial \sigma}{\partial x}\right] g(t,x)u(t) \tag{2.20}$$

where $Q(t,x)$ is an arbitrary $m \times m$ diagonal matrix with elements $q_i(t,x)$, $i = 1, \ldots, m$, such that $\inf |q_i(t,x)| > 0$ for all $t \geq 0$ and all x.

The actual conversion of the m–input design problem to m single input design problems is accomplished by the $[\partial\sigma/\partial x]g(t,x)$–term with the diagonal entries of $Q^{-1}(t,x)$ which allows flexibility in the design, for example by weighting the various control channels of u^*. Often $Q(t,x)$ is chosen as the identity.

In terms of u^* the state dynamic becomes

$$\dot{x}(t) = f(t,x) + g(t,x)\left[\frac{\partial \sigma}{\partial x} g(t,x)\right]^{-1} Q(t,x)u^*(t) \tag{2.21}$$

Although this new control structure looks more complicated, the structure of $\dot{\sigma}(x) = 0$ permits to independently choose the m–entries of u^* to satisfy the sufficient conditions for the existence and reachability of a sliding mode.

Once u^* is known, it is possible to invert the transformation to yield the required u. To see this, recall that for existence and reachability of a sliding mode it is enough to satisfy the condition $\sigma(x)\dot{\sigma}(x) < 0$. In terms of u^*

$$\dot{\sigma}(x) = \frac{\partial \sigma}{\partial x} f(t,x) + Q(t,x)u^*(t) \tag{2.22}$$

Thus, if the entries u_i^{*+} and u_i^{*-} are chosen so as to satisfy

$$q_j(t,x)u_i^{*+} \quad < \quad -\sum_{j=1}^{n} \sigma_{ij} f_j(t,x) \quad \text{when } \sigma_j(x) > 0 \tag{2.23}$$

$$q_j(t,x)u_i^{*-} \quad > \quad -\sum_{j=1}^{n} \sigma_{ij} f_j(t,x) \quad \text{when } \sigma_j(x) < 0 \tag{2.24}$$

then sufficient conditions for the existence and reachability are satisfied where σ_{ij} equals the j–entry of $\nabla\sigma_j(x)$ which is the i–th row of $(\partial\sigma/\partial x)$. In particular, the conditions of (2.23) and (2.24) force each term in the summation of $\sigma^T\dot{\sigma}$ to be negative definite. As mentioned, the control actually implemented is

$$u(t) = \left[\frac{\partial \sigma}{\partial x} g(t,x)\right]^{-1} Q(t,x)u^*(t) \tag{2.25}$$

Note that other sufficient conditions for the existence of a sliding mode can also be used.

2.6.2 Other Approaches

In addition to the diagonalization method, different approaches have been proposed in the literature. A possible structure for the control of (2.2) is

$$u_i = u_{i_{eq}} + u_{iN} \tag{2.26}$$

where $u_{i_{eq}}$ is the i–th component of the equivalent control (which is continuous) and where u_{iN} is the discontinuous term of (2.2). For controllers

having the structure of (2.26), it results that

$$\begin{aligned}\dot{\sigma}(x) &= \frac{\partial\sigma}{\partial x}\dot{x} = \frac{\partial\sigma}{\partial x}[f(t,x)+g(t,x)(u_{eq}+u_N)] \\ &= \frac{\partial\sigma}{\partial x}[f(t,x)+g(t,x)u_{eq}] + \frac{\partial\sigma}{\partial x}g(t,x)u_N \\ &= \frac{\partial\sigma}{\partial x}g(t,x)u_N\end{aligned}$$

for the sake of simplicity, assume that $(\partial\sigma/\partial x)g(t,x) = I$. Then $\dot{\sigma}(x) = u_N$. This condition allows an easy verification of the sufficiency conditions for the existence and reachability of a sliding mode, i.e., the condition that $\sigma_i(x)\dot{\sigma}_i(x) < 0$ when $\sigma_i(x) \neq 0$. Below are different possible discontinuous control structures for u_N.

Relays with constant gains:

$$u_{iN} = -\alpha_i \ \text{sign}(\sigma_i(x))$$

where $\alpha_i > 0$, and the sign function is defined as

$$\text{sign}(x) = \frac{x}{|x|} = \begin{cases} 1, & \text{if } x > 0 \\ -1, & \text{if } x < 0 \\ 0, & \text{if } x = 0 \end{cases}$$

Observe that this controller satisfies the η–reaching condition (2.8) since

$$\sigma_i(x)\dot{\sigma}_i(x) = -\alpha_i|\sigma_i(x)| < 0, \qquad \text{if } \sigma_i(x) \neq 0$$

Hence a sliding mode on the surface $\sigma(x) = 0$ is enforced in finite time.

Relays with state dependent gains:

$$u_{iN} = -\alpha_i(x) \ \text{sign}(\sigma_i(x))$$

where $\alpha_i(x) > 0$, for all x. Again it is straightforward to check that the η–reaching condition (2.8) is satisfied

$$\sigma_i(x)\dot{\sigma}_i(x) = -\alpha_i(x)|\sigma_i(x)| < 0, \qquad \text{if } \sigma_i(x) \neq 0$$

Linear feedback with switched gains:

$$u_{iN} = \Psi x, \quad \Psi = [\Psi_{ij}] \qquad \Psi_{ij} = \begin{cases} \alpha_{ij}, & \sigma_i x_i > 0 \\ \beta_{ij}, & \sigma_j x_j < 0 \end{cases}$$

with $\alpha_{ij} > 0$ and $\beta_{ij} < 0$. Thus the reaching condition (2.7) is verified

$$\sigma_i(x)\dot{\sigma}_i(x) = \sigma_i(x)(\Psi_{i1}x_1 + \ldots + \Psi_{in}x_n) < 0$$

Linear continuous feedback:

$$u_N(x) = -L\sigma(x)$$

where $L \in \mathbb{R}^{m\times m}$ is a positive definite constant matrix. The reaching condition (2.7) is verified since

$$\sigma^T(x)\dot{\sigma}(x) = -\sigma^T(x)L\sigma(x) < 0, \qquad \text{if } \sigma_i(x) \neq 0$$

Univector nonlinearity with scale factor:

$$u_N(x) = -\frac{\sigma(x)}{\|\sigma(x)\|}\rho, \quad \rho > 0$$

which implies that

$$\sigma^T(x)\dot{\sigma}(x) = -\rho\|\sigma(x)\|, \qquad \text{if } \sigma_i(x) \neq 0$$

thus a sliding mode is enforced on $\sigma(x) = 0$ in finite time.

2.7 Sliding mode control of uncertain systems

The purpose of this section is to describe the performance of sliding mode control when applied to uncertain systems. The motivation for exploring uncertain systems is the fact that model identification of real-world systems introduces parameter errors. Hence, models contain uncertain parameters which are often known to lie within upper and lower bounds. A whole body of literature has arisen in recent years concerned with the stabilization of systems having uncertain parameters lying within known bounds (see for instance Krstić *et al.* (1995); Bartolini and Zolezzi (1996); Edwards and Spurgeon (1998); Isidori (1999); Young *et al.* (1999)). Such control

strategies are based on the second method of Lyapunov. On the other hand, sliding mode controls are based on the generalized Lyapunov second method. Hence, one expects some fundamental links in the two theories.

To represent uncertainties in the plant due to parameter uncertainties consider the following state dynamics

$$\dot{x}(t) = [f(t,x) + \Delta f(t,x,r)] + [g(t,x) + \Delta g(t,x,r)]u(t) \tag{2.27}$$

where r(t) is a vector function (Lebesgue measurable) of uncertain parameters whose values belong to some closed and bounded set. The plant uncertainties Δf and Δg are required to lie in the image of $g(t,x)$ for all values of t and x. This requirement is the so–called matching condition (Utkin, 1977; Slotine and Li, 1991; Edwards and Spurgeon, 1998; Perruquetti and Barbot, 2002).

Assuming that the matching conditions are satisfied, it is possible to lump the total plant uncertainty into a single vector $e(t,x(t),r(t),u(t))$ and represent the uncertain plant as

$$\dot{x}(t) = f(t,x) + g(t,x)u(t) + g(t,x)e(t,x,r,u) \tag{2.28}$$

with initial condition $x(t_0) = x_0$. With regard to a stabilization analysis of the above model (2.28), introduce the following definitions:

Definition 2.2 *Let $x(t)$: $[t_0,\infty) \to \mathbb{R}^n$ be a solution of (2.28). Then $x(t)$ is uniformly bounded if for each x_0 there is a positive finite constant, $d(x_0)$, $(0 < d(x_0) < \infty)$ such that $\|x(t)\|_2 < d(x_0)$ for all $t \in [t_0,\infty)$ where $\|\cdot\|_2$, is the usual Euclidean vector norm*

Definition 2.3 *The solutions to (2.28) are uniformly ultimately bounded with respect to some closed bounded set $S \subset \mathbb{R}^n$ if for each x_0 there is a non–negative constant $T(x_0,S) < \infty$ such that $x(t) \in S$ for all $t > t_0 + T(x_0,S)$.*

The problem is to find a state feedback $u(t,x)$ such that for any initial condition x_0 and for all uncertainties $r(t)$ a solution $x(t) : [t_0,\infty) \to \mathbb{R}^n$ of (2.28) exists and every such solution is uniformly bounded.

Different solutions can be found in the literature (see for instance Corless and Leitmann (1981) and the reference therein). In this section, the

so–called min–max approach proposed in Gutman and Palmor (1982) is discussed.

Consider a nominal system defined by

$$\dot{x}(t) = f(t,x), \qquad x(t_0) = x_0 \tag{2.29}$$

and assume that $x = 0$ is an equilibrium point, i.e., $f(t,0) = 0$ for all t. This approach requires that the nominal system is asymptotically stable, i.e.,

1. for any $\varepsilon > 0$, there is a $\delta(\varepsilon) > 0$ such that a trajectory starting within a $\delta(\varepsilon)$–neighborhood of $x = 0$ remains for all subsequent time within the ε–neighborhood of the origin
2. there is a δ_1 such that a trajectory originating within a δ_1–neighborhood of $x = 0$ tends to zero as $t \to \infty$.

If there exists a Lyapunov function $V(\cdot) : \mathbb{R} \times \mathbb{R}^n \to \mathbb{R}_+$ with a continuous derivative, and there exist functions $\gamma_i(\cdot)$, $i = 1,2,3$, of class $\mathcal{K}_\infty$ such that for all $(t,x) \in \mathbb{R} \times \mathbb{R}^n$

$$\gamma_1(\|x\|_2) \le V(t,x) \le \gamma_2(\|x\|_2) \tag{2.30}$$

and

$$\frac{\partial V}{\partial t}(t,x) + \nabla_x^T V(t,x)\, f(t,x) \le -\gamma_3(\|x\|_2) \tag{2.31}$$

then the nominal system (2.29) is uniformly asymptotically stable. The objective is to use this nominal Lyapunov function $V(\cdot)$ and bounds on the uncertainty $e(t,x,r,u)$ to develop sufficient conditions on the state feedback control $u = u(t,x)$ in order to guarantee the uniform boundedness of the closed loop state trajectory of (2.28).

According to the min-max approach, a Lyapunov function candidate for the closed loop plant (2.28), with $u = u(t,x)$, is again $V(t,x)$. The objective is to choose $u(t,x)$ so as to make the derivative of $V(t,x)$ negative on the trajectories of the closed loop system, i.e., choose $u = u(t,x)$ such that

$$\dot{V}(t,x) = \frac{\partial V}{\partial t} + (\nabla_x^T V)\dot{x} = \left[\frac{\partial V}{\partial t} + (\nabla_x^T V) f\right] + (\nabla_x^T V) g(u+e) < 0 \tag{2.32}$$

Since (2.31) holds, (2.32) is verified if $u = u(t,x)$ is chosen such that

$$\min_u \max_e (\nabla_x^T V) g(u+e) \le 0 \tag{2.33}$$

for all $(t,x) \in \mathbb{R} \times \mathbb{R}^n$ and all admissible controls and admissible uncertainties. Assuming that $g^T(t,x)\nabla_x V(t,x)$ is nonzero, the control

$$u = u(t,x) = -\frac{g^T(t,x)\nabla_x V(t,x)}{\|g^T(t,x)\nabla_x V(t,x)\|_2}\rho(t,x) \tag{2.34}$$

where $\rho(t,x)$ is a scalar function satisfying $\rho(t,x) \geq \|e(t,x,r,u)\|_2$, can be shown to satisfy (2.33) by direct substitution.
If $g^T(t,x)\nabla_x V(t,x)$ is zero then take

$$u \in \{u | u \in \mathbb{R}^m \quad \text{and} \quad \|u\| \leq \rho(t,x)\}$$

Note that the set

$$\{t, x \,|\, \sigma(t,x) = g^T(t,x)\nabla_x V(t,x) = 0\}$$

can be seen as a switching surface. In fact, control law (2.34) is discontinuous in the state since, for example, in the single input case it reduces to $u = -\ \text{sign}(g^T(t,x)\nabla_x V(t,x))$.

Since the above control is discontinuous it may excite unmodeled high-frequency dynamics of the plant.

2.7.1 Sliding mode controller design for uncertain systems

Consider again the uncertain system (2.28). In the sliding mode control approach it is not necessary for the nominal system (2.29) to be stable. However, the equivalent system, i.e., the restriction of (2.29) to the switching surface $\sigma(t,x) = 0$, must be asymptotically stable.
The sliding mode control control structure for system (2.29) will be

$$u = u_{eq} + u_N \tag{2.35}$$

where u_{eq} is the equivalent control for (2.29) assuming that all uncertainties $e(t,x,r,u)$ are zero and u_N is to be designed to account for nonzero uncertainties.

Considering the switching surface $\sigma(t,x) = 0$, one may compute

$$u_{eq} = -\left[\frac{\partial \sigma}{\partial x} g\right]^{-1} \left[\frac{\partial \sigma}{\partial t} + \frac{\partial \sigma}{\partial x} f\right] \tag{2.36}$$

assuming that $[\frac{\partial \sigma}{\partial x} g]$ is nonsingular and that $e(t, x, r, u) = 0$. It is now necessary to account for uncertainties and develop an expression for u_N.

As in the previous subsection, assume that

$$\|e(t, x, r, u)\|_2 \leq \rho(t, x)$$

where $\rho(t, x)$ is a non–negative scalar function. Also introduce the scalar function

$$\hat{\rho}(t, x) = \alpha + \rho(t, x)$$

where $\alpha > 0$. This particular structure simplifies some of the derivations. Before specifying the control structure, the most simple generalized Lyapunov function is chosen, i.e.,

$$V(t, x) = \frac{1}{2} \sigma^T(t, x) \sigma(t, x) \tag{2.37}$$

As usual, in order to insure the existence of a sliding mode and attractiveness to the surface, the reaching condition

$$\frac{dV}{dt}(t, x) = \dot{V} = \sigma^T \dot{\sigma} < 0$$

must be satisfied whenever $\sigma(t, x) \neq 0$, where

$$\dot{\sigma}(t, x) = \frac{\partial \sigma}{\partial t} + \frac{\partial \sigma}{\partial t} \dot{x}$$

The controller form given in (2.27) together with the controller of (2.34) suggests the sliding mode control form

$$u = u_{eq} + u_N = u_{eq} - \frac{g^T(t, x) \nabla_x V(t, x)}{\|g^T(t, x) \nabla_x V(t, x)\|_2} \rho(t, x) \tag{2.38}$$

when $\sigma(t, x) \neq 0$ and where

$$\nabla_x V(t, x) = \left[\frac{\partial \sigma}{\partial x}(t, x) \right]^T \sigma(t, x)$$

where $\nabla_x V(t, x)$ is the gradient of the generalized Lyapunov function (2.37). If $\sigma(t, x) = 0$, then set $u(t, x) = u_{eq}(t, x)$.

In order to verify the validity of this controller notice that

$$\dot{V} = \sigma^T \frac{\partial \sigma}{\partial t} + \sigma^T \frac{\partial \sigma}{\partial t} (f + gu + ge) \tag{2.39}$$

where t and x arguments have been omitted for notation simplicity. Substituting (2.38) into (2.39) it yields

$$\begin{aligned}\dot{V} &= \sigma^T\frac{\partial\sigma}{\partial t}+\sigma^T\frac{\partial\sigma}{\partial x}f-\sigma^T\frac{\partial\sigma}{\partial t}-\sigma^T\frac{\partial\sigma}{\partial x}f \\ &\quad -\left\|g^T\left(\frac{\partial\sigma}{\partial x}\right)^T\sigma\right\|_2\rho+\sigma^T\frac{\partial\sigma}{\partial x}ge\leq-\alpha\left\|g^T\left(\frac{\partial\sigma}{\partial x}\right)^T\sigma\right\|_2\end{aligned}$$

verifying the negative definiteness of $\dot{V}$. This establishes attractiveness to the switching surface.

2.8 Chattering

In real–life applications, it is not reasonable to assume that the control signal time evolution can switch at infinite frequency, while it is more realistic, due to the inertias of the actuators and sensors, and to the presence of noise and/or exogenous disturbances, to assume that it commute at a very high (but finite) frequency. The control oscillation frequency turns out to be not only finite but also almost unpredictable. The main consequence is that the sliding mode takes place in a small neighbour of the sliding manifold, whose dimension is inversely proportional to the control switching frequency (Utkin, 1992; Edwards and Spurgeon, 1998; Perruquetti and Barbot, 2002).

The notions of ideal sliding mode and real sliding mode is here adopted to distinguish the sliding motion that occurs exactly on the sliding manifold (analyzed in previous subsections assuming ideal control devices) from a sliding motion that, due to the non–idealities of the control law implementation, takes place in a vicinity of the sliding manifold, which is called boundary layer (see Fig. 2.5).

The effects of the finite switching frequency of the control are referred in the literature as chattering (Fridman, 2001*a*, 2003; Boiko *et al.*, 2004; Levant, 2007). Basically, the high frequency components of the control propagate through the system, therefore exciting the unmodeled fast dynamics, and undesired oscillations affect the system output. This can degrade the system performance or may even lead to instability. Moreover, the term chattering has been also designated to indicate the bad effect, potentially disruptive, that a switching control force/torque can produce on a controlled

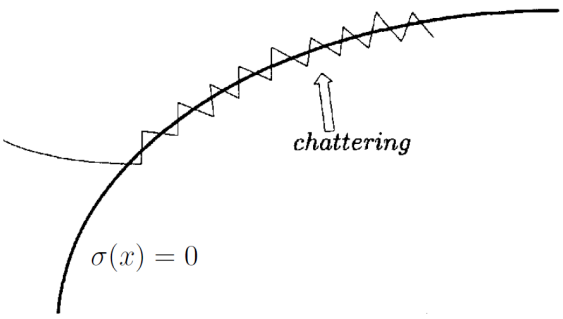

Figure 2.5: The chattering effect

mechanical plant (Bartolini, 1989; Slotine and Li, 1991; Young *et al.*, 1999; Levant, 2007).

Chattering and high control activity are the major drawbacks of the sliding mode approach in the practical realization of sliding mode control schemes (DeCarlo *et al.*, 1988; Utkin, 1992; Perruquetti and Barbot, 2002). In order to overcame these drawbacks, a research activity aimed at finding a continuous control action, robust against uncertainties and disturbances, guaranteeing the attainment of the same control objective of the standard sliding mode approach has been carried out in recent years (Sira-Ramirez, 1992; Levant, 1993; Bartolini *et al.*, 1998*b*).

The most used in practice approach is based on the use of continuous approximations of the sign$(\cdot)$ function (such as the $sat(\cdot)$ function, the $\tanh(\cdot)$ function and so on) in the implementation of the control law. A consequence of this method is that invariance property is lost. The system possesses robustness that is a function of the boundary layer width. It was pointed out in Slotine and Li (1991) that this methodology is highly sensitive to the unmodeled fast dynamics, and in some cases can lead to unacceptable performance. An interesting class of smoothing functions, characterized by a time-varying parameters, was proposed in Slotine and Li (1991), attempting to find a compromise between the chattering elimination aim and the possible excitation of the unmodeled dynamics. In conclusion, continuation approaches eliminate the high-frequency chattering at the price of losing invariance. The most recent and interesting approach for the elimination of chattering is represented by the second order sliding mode methodology (Levant, 1993; Bartolini *et al.*, 1998*b*; Levant, 2003), that will be extensively

detailed in Chapter 3.

2.9 Conclusions

In this chapter, the basic properties and interests of sliding modes have been discussed. The main advantages of the sliding mode control approach are the simplicity of both design and implementation, the high efficiency and the robustness with respect to matched uncertainties.
However, it has been shown that imperfections in switching devices and delays were inducing a high–frequency motion called chattering (the states are repeatedly crossing the surface rather than remaining on it), so that no ideal sliding mode can occur in practice. Chattering and high control activity were the reasons that fomented a generalized criticism towards sliding mode control.
To avoid chattering some approaches were proposed. The main idea was to change the dynamics in a small vicinity of the discontinuity surface in order to avoid real discontinuity and at the same time preserve the main property of the whole system. However, the trajectories of the controlled system remain in a small neighborhood of the surface and the robustness of the sliding mode were partially lost.
The most recent and interesting approach for the elimination of chattering is represented by the second order sliding mode methodology, that will be extensively detailed in Chapter 3 of the present thesis.

Chapter 3

Higher order sliding mode control

Contents

The aims of this chapter are to provide a brief introduction to the higher order sliding mode control theory and to describe the main features and advantages of higher order sliding modes.
In particular, the second order sliding mode control problem is described and several second order sliding mode controllers are presented since they are the most widely used in practice.

The interested reader is referred to Slotine and Li (1991), Levant (1993), Fridman and Levant (1996), Bartolini *et al.* (1999), Perruquetti and Barbot (2002) and Levant (2003) for further details.

3.1 Introduction

Sliding mode control (Utkin, 1992; Zinober, 1994; Edwards and Spurgeon, 1998) is considered to be one of the most effective control technique under

heavy uncertainty conditions. The control objectives are attained by constraining the system dynamics on a properly chosen surface by means of discontinuous control laws. This methodology provides for high accuracy and robustness with respect to a wide range of disturbances and uncertainties.

However, due to the presence of imperfections in actuators and sensors, such as hysteresis, delays, etc., and to the presence of noise and/or exogenous disturbances, this control approach may produce the dangerous chattering effect (Fridman, 2001*a*, 2003; Boiko *et al.*, 2004; Levant, 2007).

To avoid chattering different approaches have been proposed (see e.g. Slotine and Li (1991); Utkin (1992)). The main idea of such approaches was to change the dynamics in a small vicinity of the discontinuity surface in order to avoid real discontinuity and, at the same time, to preserve the main properties of the whole system. However, the ultimate accuracy and robustness of the sliding mode are partially lost.

On the contrary, higher order sliding modes generalize the basic sliding mode idea acting directly on the higher order time derivatives of the sliding variable instead of influencing its first time derivative like it happens in standard sliding modes. Keeping the main advantages of the original approach, at the same time they remove the chattering effect and provide for even higher accuracy in realization (Levant, 1993).

A number of higher order sliding mode controllers are described in the literature (Fridman and Levant, 1996; Bartolini *et al.*, 1998*b*, 1999; Perruquetti and Barbot, 2002; Levant, 2003)

The main problem in implementation of higher order sliding modes is the increasing information demand. Generally speaking, any r–th order sliding controller requires the knowledge of the time derivatives of the sliding variable up to the $(r-1)$–th order. The only exceptions are given by the twisting controller (Levant, 1993), the super–twisting controller (Levant, 1993) and the sub–optimal algorithm (Bartolini *et al.*, 1997*a*) which are second order sliding mode control algorithms.

For this reason these second order sliding mode controllers are the most widely used in practice among higher order sliding mode controllers because of their simplicity and of their low information demand and they will be presented in this chapter.

3.2 Sliding order and sliding set

Higher order sliding mode is a movement on a discontinuity set of a dynamic system understood in Filippov's sense (Filippov, 1988). The sliding order characterizes the dynamics smoothness degree associated to the motion constrained on the sliding manifold $\sigma(x) = 0$, and it can be defined as follows

Definition 3.1 *The sliding order r is the number of continuous total derivative, including the zero one, of the function $\sigma = \sigma(t, x)$ whose vanishing defines the equations of the sliding manifold.*

Note that the sliding order does not depend on the characteristic of the system zero dynamics (i.e. the state behaviour while constrained on the manifold) but it is associated only to the characteristic of the constrained motion.

Thus, higher order sliding mode is characterized by the fact that the derivatives of the sliding variable $\sigma(\cdot)$ converge to zero up to a certain order. This property can be formulated by introducing the definition of a new type of manifold, the so–called sliding set, on which an higher order sliding mode turns out to be established by definition.

Definition 3.2 *The sliding set of r–th order associated to the manifold $\sigma(t, x) = 0$ is defined by the equalities*

$$\sigma = \dot{\sigma} = \ddot{\sigma} = \ldots = \sigma^{(r-1)} = 0 \tag{3.1}$$

which form an r–dimensional condition on the state of the dynamic system.

A more precise definition of higher order sliding modes is that given in Fridman and Levant (1996), i.e.,

Definition 3.3 *Let the r–th order sliding set (3.1) be non–empty, and assume that it is locally an integral set in Filippov sense (Filippov, 1988) (i.e. it consists of Filippov trajectories of the discontinuous dynamic system). Then, the corresponding motion satisfying (3.1) is called an r–th order sliding mode with respect to the manifold $\sigma(t, x) = 0$ (see Fig. 3.1).*

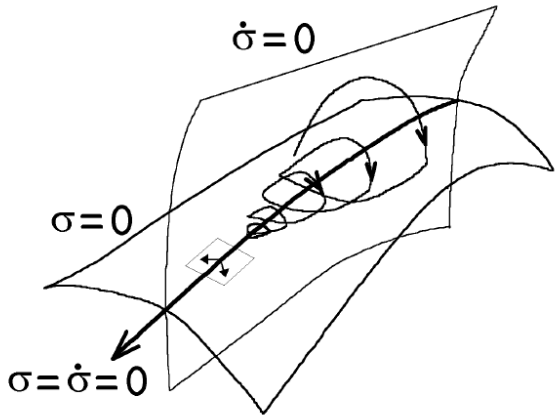

Figure 3.1: Second order sliding mode trajectory

Thus, if the task is to provide for keeping a constraint given by equality of a smooth function $\sigma = 0$, the sliding order is the number of continuous total derivatives of σ (including the zero one) in the vicinity of the sliding mode. The r–th derivative $\sigma^{(r)}$ is mostly supposed to be discontinuous or non–existent.

The standard sliding mode control described in Chapter 2 is of the first order since the sliding set is defined by $\sigma = 0$, and $\dot{\sigma}$ is discontinuous.

Higher order sliding mode behaviours may occur also when the relative degree r (Isidori, 1999) between the sliding variable and the control is higher than one, so that the control input appears explicitly in the higher derivatives of the constraint function (Levant, 2003).

Considering the real sliding behaviour, the sliding order establishes, in some sense, the velocity of the system motion around the sliding manifold. As a consequence, the switching imperfections cause the system trajectories to lie on a boundary layer of the sliding manifold whose size is smaller as the sliding order increases.

The main problem in implementation of higher order sliding modes is the increasing information demand. Generally speaking, any r–th order sliding controller keeping $\sigma = 0$, needs $\sigma, \dot{\sigma}, \ldots, \sigma^{(r-1)}$, to be available. The only exceptions are given by the twisting controller (Levant, 1993), the super–twisting controller (Levant, 1993) and the sub–optimal algorithm

(Bartolini *et al.*, 1997*a*, 1998*b*, 2001) which are second order sliding mode control algorithms.

3.3 Second order sliding mode

In this section a brief description of second order sliding mode control methodology is given. In second order sliding mode methodology, the control action affects directly the sign and the amplitude of $\ddot{\sigma}$, and a suitable switching logic, which can be based on both σ and $\dot{\sigma}$ or on σ and on the sign of $\dot{\sigma}$, guarantees the finite time convergence of the state to the sliding manifold $\sigma = \dot{\sigma} = 0$.

Second order sliding mode controllers are the most widely used in practice among higher order sliding mode controllers because of their simplicity and of their low information demand. In particular, the twisting controller, the super–twisting controller and the sub–optimal control algorithm are discussed because of their advantage of not requiring the knowledge of $\dot{\sigma}$.

3.3.1 The problem statement

Consider a dynamic single–input system of the form

$$\dot{x} = a(t,x) + b(t,x)u, \qquad \sigma = \sigma(t,x) \tag{3.2}$$

where $x \in \mathbb{R}^n$ is the system state, $u \in \mathbb{R}$ is the control input, and $a(t,x)$ and $b(t,x)$ are uncertain vector fields.

Let $\sigma(t,x) = 0$ be the chosen sliding manifold, then the control objective is to enforce a second order sliding mode on the sliding manifold $\sigma(t,x) = 0$, i.e.,

$$\sigma(t,x) = \dot{\sigma}(t,x) = 0 \tag{3.3}$$

in finite time.

Depending on the relative degree (Isidori, 1999) of the system, two different cases must be considered, i.e.,

A: relative degree $r = 1$, i.e., $\frac{\partial}{\partial u}\dot{\sigma} \neq 0$

B: relative degree $r = 2$, i.e., $\frac{\partial}{\partial u}\dot{\sigma} = 0$, $\frac{\partial}{\partial u}\ddot{\sigma} \neq 0$

Case A: In this case, the control problem can be solved relying on first order sliding mode control (see Chapter 2), nevertheless second order sliding mode control can also be used in order to avoid chattering. For this purpose $u(t)$ is considered as an output of some first order dynamic system and the time derivative of the plant control $\dot{u}(t)$ is regarded as an auxiliary control variable (Levant, 1993; Bartolini *et al.*, 1999).

A discontinuous control $\dot{u}$ steers the sliding variable σ to zero, keeping $\sigma = 0$ in second order sliding mode, so that the plant control u is continuous and the chattering is avoided (Levant, 1993; Bartolini *et al.*, 1998*b*).

The first and second time derivative of the sliding variable are given by

$$\dot{\sigma} = \frac{\partial}{\partial t}\sigma(t,x) + \frac{\partial}{\partial x}\sigma(t,x)[a(t,x) + b(t,x)u(t)] \tag{3.4}$$

$$\ddot{\sigma} = \varphi_A(t,x,u) + \gamma_A(t,x)\dot{u}(t) \tag{3.5}$$

where

$$\varphi_A(t,x,u) = \frac{\partial}{\partial t}\dot{\sigma}(t,x,u) + \frac{\partial}{\partial x}\dot{\sigma}(t,x,u)[a(t,x) + b(t,x)u(t)] \tag{3.6}$$

$$\gamma_A(t,x) = \frac{\partial}{\partial x}\sigma(t,x)b(t,x) \tag{3.7}$$

The control input u is understood as an unknown disturbance affecting the drift term $\varphi_A(t,x,u)$. The control derivative $\dot{u}$ is used as an auxiliary control variable to be designed in order to satisfy the control objective of steering σ and $\dot{\sigma}$ to zero. Note that the control time derivative $\dot{u}$ affects the $\ddot{\sigma}$ dynamics.

Case B: The control does not affect directly the dynamics of $\dot{\sigma}$, but it affects directly $\ddot{\sigma}$, i.e.,

$$\dot{\sigma} = \frac{\partial}{\partial t}\sigma(t,x) + \frac{\partial}{\partial x}\sigma(t,x)a(t,x) \tag{3.8}$$

$$\ddot{\sigma} = \varphi_B(t,x,u) + \gamma_B(t,x)u(t) \tag{3.9}$$

where

$$\varphi_B(t,x) = \frac{\partial}{\partial t}\dot{\sigma}(t,x,u) + \frac{\partial}{\partial x}\dot{\sigma}(t,x,u)a(t,x) \tag{3.10}$$

$$\gamma_B(t,x) = \frac{\partial}{\partial x}\dot{\sigma}(t,x,u)b(t,x) \tag{3.11}$$

It must be assumed that

$$\gamma_B(t,x) \neq 0 \tag{3.12}$$

which means that the sliding variable, understood as a system output, must have uniform relative degree two. In this case the actual control u is discontinuous.

Both cases A and B can be dealt with in an unified treatment, as the structure of the system to be stabilized is exactly the same, i.e., a second order uncertain system with affine dependence on the relevant control signal (the control derivative $\dot{u}$ in case A, the actual control u in case B).

For this reason, it will be addressed and solved the stabilization problem for the system

$$\left\{ \begin{array}{rcl} y_1(t) & = & \sigma(t,x) \\ \dot{y}_1(t) & = & y_2(t) \\ \dot{y}_2(t) & = & \varphi(\cdot) + \gamma(t,x)v(t) \end{array} \right. \tag{3.13}$$

As for the terms $\varphi(\cdot)$, and $v(t)$ they have different meaning and structure in cases A and B. More precisely:

Case A:

$$\varphi(\cdot) = \varphi_A(t,x,u) \tag{3.14}$$

$$v(t) = \dot{u}(t) \tag{3.15}$$

Case B:

$$\varphi(\cdot) = \varphi_B(t,x) \tag{3.16}$$

$$v(t) = u(t) \tag{3.17}$$

Remark 3.1 *As previously discussed, in case A, called the antichattering case, the second order sliding mode approach attains the control objective by means of a continuous control input. In fact, the actual discontinuous control signal $v(t)$ is the derivative of the plant input $u(t)$, which, obtained by integrating the discontinuous derivative, turns out to be continuous. The first order sliding mode control leads to the discontinuous control laws in this case.*

In case B, that is the relative degree two case, the actual control $u(t)$ is discontinuous. Note that the traditional first order sliding mode control methodology, if not properly coupled to state observers, fails to solve this problem.

The stabilization problem is solved under the assumption that $\dot{\sigma}$ is not available for measurements. This fact, together with the presence of model uncertainties, makes the problem not easily solvable. The existence of a solution is obviously critically related to the relevant assumptions on the uncertain dynamics.
The historical development of second order sliding mode control algorithms (Levant, 1993; Bartolini *et al.*, 1997*a*) starts considering the global boundedness assumption for the uncertainties, i.e., that in some neighbour of the sliding manifold (not necessarily small) the uncertain terms are bounded by known positive constants according to

$$|\varphi(\cdot)| \leq \Phi \tag{3.18}$$

$$0 < G_1 \leq \gamma(t,x) \leq G_2 \tag{3.19}$$

To summarize, the second order sliding mode control problem for n–th order systems of the type

$$\dot{x} = a(t,x) + b(t,x)u, \qquad \sigma = \sigma(t,x) \tag{3.20}$$

where $x \in \mathbb{R}^n$ is the system state, $u \in \mathbb{R}$ is the control input, and $a(t,x)$ and $b(t,x)$ are uncertain vector fields, can be reduced to the stabilization problem of a second order uncertain system, i.e.,

$$\begin{cases} y_1(t) &= y_2(t) \\ y_2(t) &= \varphi(\cdot) + \gamma(t,x)v(t) \end{cases} \tag{3.21}$$

where y_1 and y_2 represent the actual sliding variable and its derivative, respectively, y_2 is not available for measurement, and the uncertain terms φ, and γ are such that

$$|\varphi(\cdot)| \leq \Phi \tag{3.22}$$

$$0 < G_1 \leq \gamma(t,x) \leq G_2 \tag{3.23}$$

As previously discussed, depending on the relative degree r between the sliding variable and the actual control input, $v(t)$ may represent either the actual control or its derivative, and, correspondingly, also the uncertain drift term φ may depend on two different sets of variables.

3.3.2 The twisting controller

The so–called twisting controller is historically the first known second order sliding mode controller (Levantosky, 1985). This algorithm features twisting around the origin of the phase plane $\sigma O\dot{\sigma}$ (Fig. 3.2). This means that the trajectories perform rotations around the origin while converging in finite time to the origin of the phase plane. The absolute value of the intersections of the trajectory with the axes as well as the rotation times decrease in geometric progression. The control derivative value commutes at each axis crossing, which requires the availability of the sign of the sliding variable time derivative y_2.

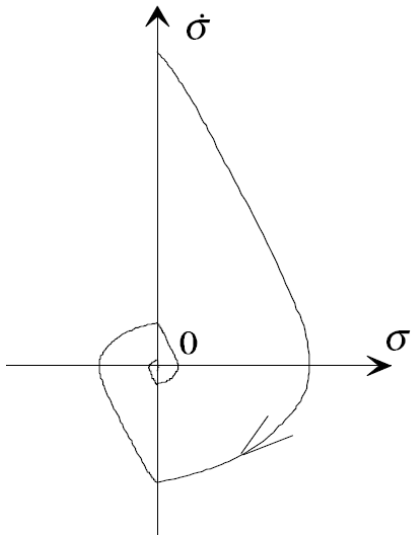

Figure 3.2: Twisting algorithm trajectory in the phase plane

According to Levantosky (1985) and Levant (1993) the following theorem can be proved:

Theorem 3.1 *Consider the auxiliary system (3.21) where the uncertain terms $\varphi(\cdot)$ and $\gamma(t,x)$ satisfy (3.22) and (3.23), respectively, and y_2 is not available for measurement but with known sign.*
Then, the control algorithm defined by the following control law

$$v(t) = \begin{cases} -V_m \text{ sign}(y_1) & \text{if} \quad y_1 y_2 \leq 0 \\ -V_M \text{ sign}(y_1) & \text{if} \quad y_1 y_2 > 0 \end{cases} \tag{3.24}$$

with V_M and V_m such that

$$V_M > V_m \tag{3.25}$$
$$V_m > 4\frac{G_2}{\sigma(0)} \tag{3.26}$$
$$V_m > \frac{\Phi}{G_1} \tag{3.27}$$
$$G_1 V_M - \Phi > G_2 V_m + \Phi \tag{3.28}$$

where $\sigma(0)$ is the initial value of the sliding variable, enforce a second order sliding mode on the sliding manifold $\sigma(t,x) = \dot{\sigma}(t,x) = 0$ in finite time.

Proof: See Levantosky (1985) and Levant (1993).

By taking into account the different limit trajectories arising from the uncertain dynamics of (3.21) and evaluating the time intervals between successive crossings of the abscissa axis, it is possible to define the following upper bound for the convergence time (Bartolini *et al.*, 1999)

$$\bar{t}_{tw} \leq t_{M1} + \frac{\Theta_{tw}}{1-\theta_{tw}}\sqrt{|y_{1_{M1}}|} \tag{3.29}$$

where $y_{1_{M1}}$ is the value of the y_1 variable at the first abscissa crossing in the $y_1 O y_2$ plane, t_{M1} is the corresponding time instant and

$$\Theta_{tw} = \sqrt{2}\frac{G_1 V_M + G_2 V_m}{(G_1 V_M - \Phi)\sqrt{G_2 V_m + \Phi}} \tag{3.30}$$
$$\theta_{tw} = \sqrt{\frac{G_2 V_m + \Phi}{G_1 V_M - \Phi}} \tag{3.31}$$

In practice, when y_2 is unmeasurable, its sign can be estimated by the sign of the first difference of the available sliding variable y_1 in a time interval τ, i.e.,

$$\text{sign}(y_2(t)) \approx \text{sign}(y_1(t) - y_1(t-\tau)) \tag{3.32}$$

In this latter case the system converge to a boundary layer of the sliding manifold which size is $O(\tau^2)$ and $O(\tau)$ as for y_1 and y_2, respectively (Levant, 1993).

3.3.3 The super–twisting controller

This control algorithm has been developed to control systems with relative degree one in order to avoid chattering. As for the twisting controller, the trajectories on the phase plane $\sigma O\dot{\sigma}$ are characterized by twisting around the origin as in Fig. 3.3. The continuous control law $u(t)$ is constituted by two terms. The first is defined by means of its discontinuous time derivative, while the other is a continuous function of the available sliding variable.

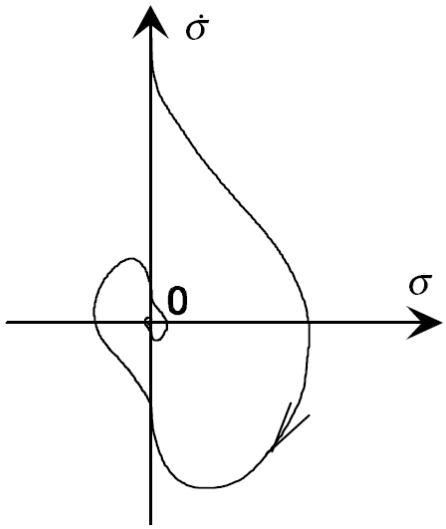

Figure 3.3: Super–twisting controller trajectory in the phase plane

Theorem 3.2 *Consider system (3.21) with its uncertain dynamics satisfying (3.22) and (3.23), y_2 is not available for measurement, and assume that the relative degree of the system is one.*

Then, the control algorithm defined by

$$u(t) = -\lambda|y_1|^{\rho}\ \mathrm{sign}(y_1) + u_1 \tag{3.33}$$

$$\dot{u}_1 = -\alpha\ sign(y_1) \tag{3.34}$$

with the constraints

$$\alpha > \frac{\Phi}{G_1} \tag{3.35}$$

$$\lambda^2 \leq \frac{4\Phi}{G_1^2}\frac{G_2(\alpha+\Phi)}{G_1(\alpha-\Phi)} \tag{3.36}$$

$$0 < \rho \leq 0.5 \tag{3.37}$$

is capable of enforcing a second order sliding mode on the sliding manifold $\sigma(t,x) = \dot{\sigma}(t,x) = 0$ *in finite time.*

Proof: See Levant (1993) and Levant (2003).

Note that the super–twisting algorithm does not need any information on the time derivative of the sliding variable.

3.3.4 The sub–optimal control algorithm

The so–called sub–optimal control algorithm was first proposed in Bartolini *et al.* (1997*a*). The name of this control algorithm put in evidence the fact that its switching logic is derived from the time–optimal control philosophy.

Relying on the assumption of being capable of detecting the extremal values of the sliding variable σ, i.e. the value of $\sigma(\bar{t})$ such that $\dot{\sigma}(\bar{t}) = 0$, the following theorem has been proved in Bartolini *et al.* (1997*a*).

Theorem 3.3 *Consider system (3.21) with its uncertain dynamics satisfying (3.22) and (3.23), and* y_2 *is not available for measurement. Assume that the sequence of the singular values of* $y_1(t)$, $y_{1_{Mk}} = y_1(t_{Mk})$, *with* t_{Mk} *such that* $y_2(t_{Mk}) = 0$, $k = 1, 2, \ldots$, *is available with ideal precision.*

Then, the control strategy

$$v(t) = -\alpha(t) V_M \text{ sign}\left[y_1(t) - \frac{1}{2}y_1(t_{Mk})\right] \tag{3.38}$$

where

$$\alpha(t) = \begin{cases} \alpha^* & \text{if } \; y_{1_{Mk}}\left[y_1(t) - \frac{1}{2}y_1(t_{Mk})\right] > 0 \\ 1 & \text{otherwise} \end{cases} \tag{3.39}$$

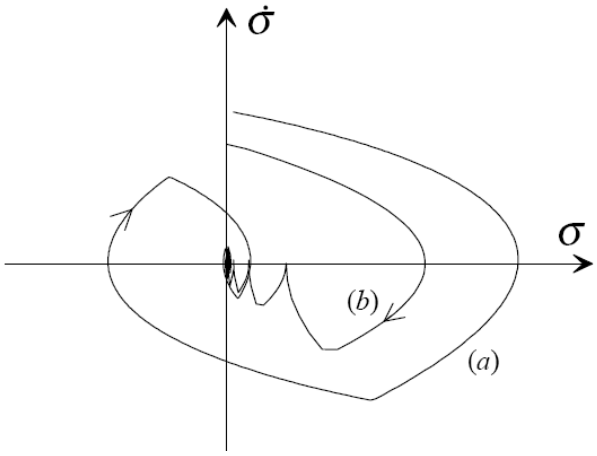

Figure 3.4: The two possible trajectories of the sub–optimal algorithm in the phase plane

and V_M *and* α^* *are such that*

$$V_M > \max\left\{\frac{\Phi}{\alpha^* G_1}; \frac{4\Phi}{3G_1 - \alpha^* G_2}\right\} \tag{3.40}$$

$$\alpha^* \in (0,1] \cap \left(0, \frac{3G_1}{G_2}\right) \tag{3.41}$$

is capable of enforcing a second order sliding mode on the sliding manifold $\sigma(t,x) = \dot{\sigma}(t,x) = 0$ *in finite time.*

Proof: See Bartolini *et al.* (1997*a*, 1998*b*) and Bartolini *et al.* (1999).

In Bartolini *et al.* (1998*b*), it was proved that in case of unit gain function the control law (3.38) can be simplified by setting $\alpha = 1$ and choosing $V_M > 2\Phi$.

As for the twisting controller, also in this case an upper bound for the convergence time can be found (Bartolini *et al.*, 1999)

$$\bar{t}_{so} \leq t_{M1} + \frac{\Theta_{so}}{1 - \theta_{so}} \sqrt{|y_{1_{M1}}|} \tag{3.42}$$

where $y_{1_{M1}}$ is the value of the y_1 variable at the first abscissa crossing in

the y_1Oy_2 plane, t_{M1} is the corresponding time instant and

$$\Theta_{so} = \frac{(G_1 + \alpha^* G_2)V_M}{(G_1 V_M - \Phi)\sqrt{\alpha^* G_2 V_M + \Phi}} \tag{3.43}$$

$$\theta_{so} = \sqrt{\frac{(\alpha^* G_2 - G_1)V_M + 2\Phi}{G_1 V_M - \Phi}} \tag{3.44}$$

Note that the commutation of the sign of $v(t)$ is anticipated with respect to the twisting controller case. The typical trajectories are different from those of the twisting and super–twisting algorithms, due to the anticipated commutation. Depending on the control parameters, both twisting around the origin (trajectory (a) in Fig. 3.4) and leaping, i.e., σ converge monotonically to zero with the consequent elimination of undesired transient oscillations, (trajectory (b) in Fig. 3.4) are allowed. Moreover, sub–optimal control algorithm features less convergence time and control effort as compared with both twisting and super–twisting controller.

The sub–optimal algorithm requires some device in order to detect the singular values $y_{1_{Mk}}$ of the available sliding variable $y_1 = \sigma$. This in not a particular drawback, as high-bandwidth peak detectors can be easily developed both in continuous and discrete time.
In the most practical case $y_{1_{Mk}}$ can be estimated by checking the sign of the quantity $\Delta(t) = [y_1(t-\tau) - y_1(t)]y_1(t)$ in which $\tau/2$ is the estimation delay. More specifically, the sequence $y_{1_{Mk}}$ can be estimated by means of the following approximate peak–detector proposed in Bartolini *et al.* (1998*a*).

Approximate peak–detector

Set $k = 0$, $y_{1_{M0}} = y_1(0)$; $y_1(t-\delta) = 0\ \forall t < \delta$.
Repeat, for any $t > \delta$, the following steps

- if $\Delta(t) = [y_1(t-\tau) - y_1(t)]y_1(t) < 0$ then

  $y_{1_{mem}} = y_1(t)$

  else

  $y_{1_{mem}} = y_{1_{mem}}$

- if $\Delta(t) < 0$ then

  $k = k + 1$

  if $\{y_{1_{mem}} y_{1_{Mk}} > 0\} \& \{|y_{1_{mem}}| < |y_{1_{Mk}}|\}$ then

$$y_{1_{Mk}} = y_{1_{mem}}$$

else

$$y_{1_{Mk}} = y_{1_M}$$

else

$$y_{1_{Mk}} = y_{1_{mem}}$$

The consequence is that y_1 and y_2 converge to a δ–vicinity of the origin, whose size is $O(\tau^2)$ and it defines the real accuracy featured by the algorithm.

Remark 3.2 *As for the real implementation, second order sliding mode control schemes have been proved to feature higher accuracy as compared with first order sliding mode control ones (Levant, 1993; Bartolini* et al.*, 1997*a*). The size of the boundary layer in which the real sliding motion occurs is $O(\delta^2)$ and $O(\delta)$ as for y_1 and y_2, respectively, where δ is the time delay between two successive switching of v. More specifically, the following steady state accuracy is guaranteed by the use of first order sliding mode control and second order sliding mode control respectively*

$$\begin{array}{cc} \textit{First order} & \textit{Second order} \\ \textit{sliding mode} & \textit{sliding mode} \\ |\sigma| \approx O(\delta) & \left\{ \begin{array}{lcl} |\sigma| & \approx & O(\delta^2) \\ |\dot{\sigma}| & \approx & O(\delta) \end{array} \right. \end{array} \tag{3.45}$$

The effectiveness of the sub–optimal algorithm was extended to larger classes of uncertain systems (Bartolini *et al.*, 1999). In particular, a generalization of the sub–optimal second order sliding mode control algorithm relevant to the form of the allowed uncertainties has been presented in Bartolini *et al.* (2001). More specifically, the approach proposed in Bartolini *et al.* (2001) is capable to deal with systems with state–dependent uncertainty of the form

$$|\varphi| \leq \Psi_0(y_1(t)) + \Psi_1(y_1(t))|y_2(t)| \tag{3.46}$$

where Ψ_0 and Ψ_1 are known non–decreasing functions.

3.4 Conclusion

In this chapter a brief introduction to the higher order sliding mode control theory is presented. Higher order sliding mode generalize the basic sliding

mode idea acting directly on the higher order time derivatives of the sliding variable instead of influencing its first time derivative like it happens in first order sliding mode.
Keeping the main advantages of first order sliding mode approach, i.e., high robustness feature and simple control laws, higher order sliding mode methodology provides for even higher accuracy in realization with respect to first order sliding mode and is capable of removing the dangerous chattering effect.

The second order sliding mode control problem has been discussed and several second order sliding mode controllers have been presented since they are the most widely used among higher order sliding mode control schemes. In particular, the twisting controller, the super–twisting controller and the sub–optimal control algorithm have been presented.
It has been shown that second order sliding mode approach is an effective solution to the drawbacks of first order sliding mode methodology, and can be successfully applied to solve a wide range of important practical problems.
Second order sliding mode techniques may become more popular in the industrial community since they are relatively simple to implement, they show a great robustness, and they are also applicable to complex problems.

Many important applications of second order sliding mode methodology to the automotive context and to the control of nonholonomic system will be presented in Chapters 4 and 5, respectively.

Chapter 4

Automotive control

Contents

Several traffic accidents happen every minute somewhere in the world as a result of a traffic accident. A number of manufacturers are pursuing the aim of reducing the frequency and severity of accidents by developing active and passive driving assistance systems (Bishop *et al.*, 2000). Active driver assistance systems aim to make the vehicle capable of perceiving its surroundings, interpret them, identify critical situations, and assist the driver in performing driving manoeuvres (Reichart *et al.*, 1995; Bishop *et al.*, 2000; Zheng *et al.*, 2004). The object is, at best, to prevent accidents completely and, at worst, to minimize the consequences of an accident for those concerned.

An example of these systems are intelligent speed adaptation, antilock braking system, vehicle stability control, brake assist, traction control, and seat belt pre–tensioning (Shladover *et al.*, 1991; Yoshida *et al.*, 2004).

The design of an active safety system for vehicle is a complicated problem. The main difficult arising in the design of such control schemes are due to the high nonlinearity of the system and to the presence of disturbances and parameter uncertainties (Gillespie, 1992; Genta, 1997). Indeed, since the vehicle operates under a wide range of conditions of speed, load, road friction, etc., an active control system has to guarantee stability robustly in face of disturbances and model uncertainties. Robustness of active vehicle systems is a widely studied topic and significant results have been proposed (see e.g. Ackermann and Sienel (1993); Ackermann *et al.* (1995); Güvenç *et al.* (2004); Canale *et al.* (2007); Canale and Fagiano (2008)).

The application of the sliding mode control theory to the automotive context appears to be quite appropriate because of its robustness properties, which make it particularly suitable to deal with uncertain nonlinear time–varying systems (see Chapters 2 and 3).
Apart from the robustness features against the uncertainty sources and disturbances typical of automotive applications, the sliding mode control methodology has the advantage of producing low complexity control laws compared to other robust control approaches (H_∞, LMI, adaptive control, etc.) which appears particularly suitable to be implemented in the Electronic Control Unit (ECU) of a controlled vehicle (Bartolini *et al.*, 1999; Fridman and Levant, 2002).

Indeed, different active safety control system based on the sliding mode control technique have been proposed in the literature (Haskara *et al.*, 2002; Vahidi and Eskandarian, 2003). For instance, sliding mode control has been adopted in the design of antilock braking system (Ünsal and Kachroo, 1999; Schinkel and Hunt, 2002), traction control system (Drakunov *et al.*, 1995; Haskara *et al.*, 2000; Lee and Tomizuka, 2003), automatic steering system (Ackermann *et al.*, 1995), vehicle yaw stability system (Kwak and Park, 2001; Stéphant *et al.*, 2007) and adaptive cruise control (Tomizuka *et al.*, 1995; Swaroop and Hedrick, 1996; Zhou and Peng, 2000). Many other driver assistance system designed relying on sliding mode methodology can also be found in the literature (see, e.g., the references therein cited).

Even if, in theory, sliding mode controllers are simpler and more efficient of most of the traditional as well as advanced devices (PID, adaptive, Lyapunov-based, high gain, etc.), they generate a discontinuous control action which has the drawback of producing high frequency chattering, with the consequent excessive mechanical wear and passengers' discomfort, due to the propagation of vibrations throughout the different subsystems of the controlled vehicle (Edwards and Spurgeon, 1998; Utkin *et al.*, 1999).

In order to reduce the vibrations induced by the controller, the solution adopted in most of the proposal appeared in the literature consists in the approximation of the discontinuous control signals with continuous ones. However, this kind of solution only generates pseudo–sliding modes (Edwards and Spurgeon, 1998; Utkin *et al.*, 1999). This means that the controlled system state evolves in a boundary layer of the ideal sliding subspace, featuring a dynamical behaviour different from that attainable if ideal sliding modes could be generated. So, even if from a practical viewpoint

this solution can produce acceptable results, the robustness features with respect to matched uncertainties are partially lost (Edwards and Spurgeon, 1998; Utkin *et al.*, 1999).

The solution to the problem in question, naturally leads to second order sliding mode. In contrast to higher order sliding modes, second order sliding modes have achieved a sufficient degree of formalization to be used in applications. Moreover, second order sliding mode control laws have a low information demand compared to higher order sliding mode control laws (Bartolini *et al.*, 1997*a*; Levant, 2003).

The second order sliding mode is given by the behaviour of the controlled system constrained on the sliding set $\sigma = \dot{\sigma} = 0$, $\sigma = 0$ being the sliding manifold, and it is attained in a finite time by means of a discontinuous control affecting directly only $\ddot{\sigma}$, and with unavailable $\dot{\sigma}$ (see Chapter 3).
As a result, a chattering–free control acting on the mechanical dynamics is obtained, since the discontinuity necessary to enforce a sliding mode is confined to the derivative of the control signal, while the control signal itself results in being continuous (Bartolini *et al.*, 1998*b*).
Furthermore, second order sliding mode controllers feature higher accuracy with respect to first order sliding mode controllers and the generated sliding modes are ideal, in contrast to what happens for solutions which relies on continuous approximations of the discontinuous control laws (Levant, 2003).

In this chapter some important application of the second order sliding mode control methodology to the automotive context will be presented.
In particular a second order sliding mode control for vehicle yaw stability is designed in Section 4.1. A traction control system based on second order sliding mode methodology is presented in Section 4.2 for vehicle and in Section 4.3 for sport motorbike. In Section 4.4 a driver assistance system for a platoon of vehicles capable of keeping the desired inter–vehicular spacing, but also capable, in case of detection of a possible collision with static or moving obstacles, of making a decision between the generation of an emergency braking or a collision avoidance manoeuvre is designed. The different modules of this latter safety system are design relying on sliding mode methodology.
The effectiveness of the control schemes presented in this chapter has been tested in simulations. All of them have shown good performances even in presence of disturbances and parametric uncertainties which are typical of the considered context, thus proving their validity.

4.1 Vehicle yaw control

In this section the problem of vehicle yaw control is addressed, using an active differential and yaw rate feedback. A reference generator, designed to improve vehicle handling, provides the desired yaw rate value to be achieved by the closed loop controller. The latter is designed using second order sliding mode (SOSM) methodology to guarantee robust stability in front of disturbances and model uncertainties, which are typical of the automotive context. A feedforward control contribution is also employed to enhance the transient system response.
The control derivative is constructed as a discontinuous signal, attaining a second order sliding mode on a suitably selected sliding manifold. Thus, the actual control input results in being continuous, as it is needed in the considered context.
Simulations performed using a realistic nonlinear model of the considered vehicle show the effectiveness of the presented approach.

The performance obtained with the designed SOSM controller are also compared by means of extensive simulation tests with that of another robust control scheme designed relying on the enhanced Internal Model Control (IMC) technique. The control structure is the same for both the control schemes.

The obtained results show the effectiveness of the control structure with both feedback controllers and highlight their respective benefits and drawbacks. This comparative study is a first step to devise a new mixed control strategy able to exploit the benefits of both the considered techniques.

Part of this section is taken from Canale *et al.* (2008*a*,*b*) and Canale *et al.* (2008*c*).

4.1.1 Introduction

Vehicle yaw dynamics may show unexpected dangerous behaviour in presence of unusual external conditions and during emergency manoeuvres, such as steering steps needed to avoid obstacles. Vehicle active stability systems aim to improve safety during emergency manoeuvres and in critical driving conditions (Rajamani, 2006). The employed actuators modify the vehicle dynamics by applying differential distribution of braking/driving forces or front and rear steering angles in a suitable way (see e.g. Ackermann and

Sienel (1993); Ackermann *et al.* (1995); Güvenç *et al.* (2004); Canale *et al.* (2007); Canale and Fagiano (2008)). Additionally, stability systems that do not rely on braking forces can be employed in normal driving situations, in order to improve the vehicle manoeuvrability. However, any stability system has a limited capability of generating the control action, due to actuator and tyre limits. This could deteriorate the control performances or cause vehicle instability. Moreover, since the vehicle operates under a wide range of conditions of speed, load, road friction, etc., the active control system has to guarantee safety (i.e. stability) performances robustly in face of disturbances and model uncertainties. Robustness of active vehicle systems is a widely studied topic and significant results have been proposed (see e.g.Ackermann and Sienel (1993); Ackermann *et al.* (1995); Güvenç *et al.* (2004); Canale *et al.* (2007); Canale and Fagiano (2008)).

In this section, the problem of yaw control is addressed considering a vehicle equipped with a Rear Active Differential (RAD) (Ippolito *et al.*, 1992; Avenati *et al.*, 1998), which exploits asymmetric distribution of left/right rear traction forces to apply suitable stabilizing yaw moments to the car. A yaw rate feedback is employed in the presented control structure, composed by a reference generator designed to improve vehicle handling, a closed loop controller, and a feedforward contribution. The feedback controller has to guarantee robust stability as well as good damping and readiness properties, while the feedforward contribution is used to further enhance the system performance in the transient phase. The robust control technique used to design the presented feedback controller is SOSM control (see Chapter 3).

To test in a realistic way the effectiveness of the presented control approach, simulations are performed using a detailed nonlinear 14 degrees of freedom vehicle model, which proves to give a good description of the vehicle dynamics as compared with real data.

4.1.2 Problem formulation and control requirements

The first control objective of any active stability system is to improve safety in critical manoeuvres and in presence of unusual external conditions, such as strong lateral wind or changing road friction coefficient. Moreover, the considered RAD device can be employed to change the steady state and dynamic behaviour of the car, improving its handling properties. In order to better introduce the control requirements, some basic concepts of lateral

vehicle dynamics are now recalled.
The vehicle inputs are the steering angle δ, commanded by the driver, and the external forces and moments applied to the vehicle center of gravity.
The most significant variables describing the behaviour of the vehicle are its speed $v(t)$, lateral acceleration $a_y(t)$, yaw rate $\dot{\psi}(t)$ and sideslip angle $\beta(t)$. Regarding the vehicle as a rigid body moving at constant speed v, the following relationship between $a_y(t)$, $\dot{\psi}(t)$ and $\dot{\beta}(t)$ holds

$$a_y(t) = v(\dot{\psi}(t) + \dot{\beta}(t)) \tag{4.1}$$

In steady state motion $\dot{\beta}(t) = 0$, thus lateral acceleration is proportional to yaw rate through the vehicle speed.

In this situation, let us consider the uncontrolled car behaviour: for each constant speed value, by means of standard steering pad manoeuvres it is possible to obtain the steady state lateral acceleration a_y corresponding to different values of the steering angle δ. These values can be graphically represented on the so–called *steering diagram* where the steering angle δ is reported with respect to the lateral acceleration a_y (see Fig. 4.1, dotted line). Such curves are mostly influenced by road friction and depend on the tyre lateral force–slip characteristics. At low acceleration the shape of the steering diagram is linear and its slope is a measure of the readiness of the car: the lower this value, the higher the lateral acceleration reached by the vehicle with the same steering angle, the better the manoeuvrability and handling quality perceived by the driver (Data and Frigerio, 2002). At high lateral acceleration the behaviour becomes nonlinear showing a saturation value, that is the highest lateral acceleration which the vehicle can reach.

The intervention of an active differential device can be considered as a yaw moment $M_z(t)$ acting on the car center of gravity: such a moment is capable of changing, under the same steering conditions, the behaviour of a_y, modifying the steering diagram according to some desired requirements. Thus, a target steering diagram (as shown in Fig. 4.1, solid line) can be introduced to take into account the performance improvements to be obtained by the control system.

In particular, such reference curves are chosen in order to decrease the steering diagram slope in the linear tract (which is related to the vehicle understeer gradient, see Rajamani (2006)), thus improving the vehicle manoeuvrability, and to increase the maximum lateral acceleration that can be reached. More details about the generation of such target steering diagrams

are reported in Subsection 4.1.4.1 and in a more extended form in Canale *et al.* (2007). Then, reference yaw rate values can be derived from the target steering diagrams, using equation (4.1) with $\dot{\beta} = 0$.

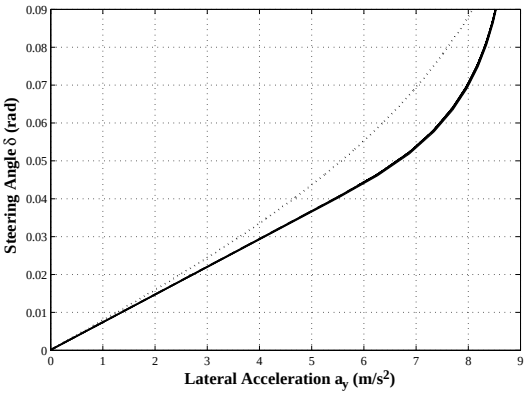

Figure 4.1: Uncontrolled vehicle (dotted), and target (solid) steering diagrams. Vehicle speed: 100 km/h

Therefore, the choice of yaw rate $\dot{\psi}$ as the controlled variable is fully justified, also considering its reliability and ease of measurement on the car. A reference generator will provide the desired values $\dot{\psi}_{ref}$ for the yaw rate $\dot{\psi}$ needed to achieve the desired performances by means of a suitably designed feedback control law.
As for the generation of the required yaw moment $M_z(t)$, in this section a full RAD is considered (see e.g. Ippolito *et al.* (1992); Avenati *et al.* (1998); Frediani *et al.* (2002) for further details).

A schematic of the considered RAD is reported in Fig. 4.2. This device is basically a traditional bevel gear differential that has been modified in order to transfer motion to two clutch housings, which rotate together with the input gear. Clutch friction discs are fixed on each differential output axle. The ratio between the input angular speed of the differential and the angular speeds of the clutch housings is such that the latter rotate faster than their respective discs in almost every vehicle motion condition (i.e. except for narrow cornering at very low vehicle speed), thus the sign of each clutch torque is always known and the torque magnitude only depends on the clutch actuation force, which is generated by an electro–hydraulic system whose input current is determined by the controller. The main

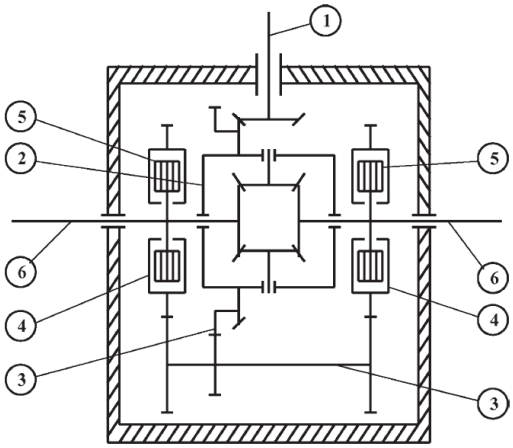

Figure 4.2: Rear Active Differential schematic. The input shaft 1 transfers driving power to the traditional bevel gear differential 2 and, through the additional gearing 3, to the clutch housings 4. Clutch discs 5 are fixed to the output axles 6.

advantage of this system is the capability of generating yaw moment of every value within the actuation system saturation limits, regardless of the input driving torque value and the speed values of the rear wheels. The considered device has a yaw moment saturation value of ±2500 Nm, due to the physical limits of its electro–hydraulic system.

The actuator dynamics can be described by the following first order model (Canale *et al.*, 2007)

$$G_A(s) = \frac{M_z(s)}{I_M(s)} = \frac{K_A}{1 + s/\omega_A} \tag{4.2}$$

where I_M is the input current originated by the controller and M_z is the actual yaw moment provided by RAD to the vehicle. The gain K_A depends on the geometry of the RAD, and ω_A is the bandwith of the electro–hydraulic valve.
The considered device has an input current limitation of ±1 A which corresponds to the range of allowed yaw moment values (i.e. ±2500 Nm) that can be mechanically generated.

As previously described, the improvements on the performances of the vehicle may be obtained using suitable modifications of the yaw dynamics in

steady state conditions. Moreover, in critical manoeuvring situations, such as fast path changing at high speed or braking and steering with low and non uniform road friction, the vehicle dynamics need to be improved in order to enhance stability and handling performances. Thus, the dynamic vehicle behaviour needs to satisfy good damping and readiness properties, which can be taken into account by a proper design of the feedback controller and the use of a feedforward action based on the driver input (i.e. δ) to increase system readiness. Indeed, the safety requirement (i.e. stability) needs to be guaranteed in face of the uncertainties arising from the wide range of the vehicle operating conditions of speed, load, tyre, friction, etc. Thus, a robust control design technique has to be used.

4.1.3 The Vehicle Model

The control design is carried out relying on a single track linear model of the vehicle (Rajamani, 2006; Genta, 1997), depicted in Fig. 4.3. This model is based on the assumption that the vehicle is travelling on a flat road with a low or zero longitudinal acceleration. Moreover, the wheel self–aligning moments are neglected and the longitudinal motion resistances are ignored compared to the tyre lateral forces. The relationship between the lateral force produced by a tyre and the sideslip angle is obtained by linearizing the so–called “Magic Formula" developed by Bakker and Pacejka (Pacejka, 2002) under the assumption of small sideslip angle. The dynamic generation mechanism of tyre forces is also modelled by introducing the tyre lateral relaxation lengths. The equations describing the motion of the vehicle are

$$\begin{aligned} &mv(t)\dot{\beta}(t) + mv(t)\dot{\psi}(t) = F_{yf,p}(t) + F_{yr,p}(t) \\ &J_z\ddot{\psi}(t) = aF_{yf,p}(t) - bF_{yr,p}(t) + M_z(t) \\ &F_{yf,p}(t) + \tfrac{l_f}{v(t)}\dot{F}_{yf,p}(t) = -c_f(\beta(t) + \tfrac{a}{v(t)}\dot{\psi}(t) - \delta(t)) \\ &F_{yr,p}(t) + \tfrac{l_r}{v(t)}\dot{F}_{yr,p}(t) = -c_r(\beta(t) - \tfrac{b}{v(t)}\dot{\psi}(t)) \end{aligned} \tag{4.3}$$

where m is the vehicle mass, J_z is the moment of inertia around the vertical axis, l is the wheel base, a and b are the distances between the center of gravity and the front and rear axles respectively, l_f and l_r are the front and rear tyre relaxation lengths, c_f and c_r are the front and rear tyre cornering stiffnesses. $F_{yf,p}$ and $F_{yr,p}$ are the front and rear tyre lateral forces, δ is the front steering angle, β is the vehicle sideslip angle, ψ is the vehicle yaw angle and v is the vehicle speed. The control variable is the yaw moment

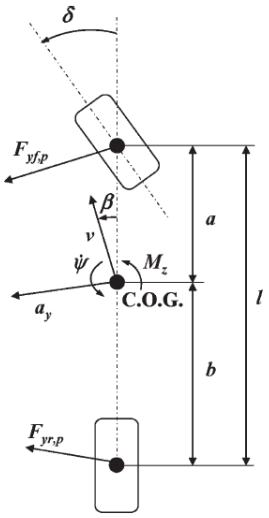

Figure 4.3: The single track model.

M_z applied by the RAD.
As previously mentioned, due to the high nonlinearity of the real vehicle system and to the presence of disturbances and modelling inaccuracies, typical of the considered context, the control system is designed relying on SOSM control, which is capable to deal in an effective way both disturbances and model uncertainties.

4.1.4 The Control Scheme

The adopted control structure is depicted in Fig. 4.4.

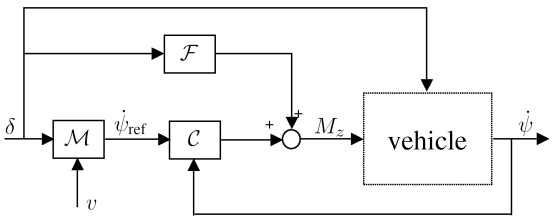

Figure 4.4: Considered control structure.

The desired yaw rate behaviour is produced by the yaw rate reference signal $\dot{\psi}_{\text{ref}}(t)$ which is generated relying on a nonlinear static map $\mathcal{M}$ which uses as inputs the front steering angle $\delta(t)$ and the vehicle speed $v(t)$. The feedback controller $\mathcal{C}$ is designed relying on the SOSM methodology (see Chapter 3) and has the aim to determine the yaw moment contribution needed to track the required yaw rate performances described by $\dot{\psi}_{\text{ref}}(t)$. In order to improve the yaw rate transient behaviour exploiting the knowledge of the driver action, a feedforward contribution $\mathcal{F}$ produced on the basis of the driver input $\delta(t)$ has been added.

Hence, in order to implement the presented control scheme on a real vehicle, the controlled vehicle must be equipped with sensors capable of measuring the yaw rate $\dot{\psi}$, the steering angle δ, and the wheels velocity, which are needed to estimate the vehicle speed v. All these sensors have low costs and are present in all the vehicles provided with a yaw control system.

4.1.4.1 Yaw Reference generator

As previously mentioned, the yaw rate reference is generated using a nonlinear static map, i.e.,

$$\dot{\psi}_{\text{ref}}(t) = f(\delta(t), v(t))$$

which uses as input the steering angle $\delta(t)$ and the vehicle speed $v(t)$. A nonlinear steady state single track vehicle model is adopted to compute the map values. The model equations are the following

$$\begin{aligned} m\, v\, \dot{\psi} &= F_{yf,p}(\beta, \dot{\psi}, \delta, F_{zf}) + F_{yr,p}(\beta, \dot{\psi}, F_{zr}) \\ a F_{yf,p}(\beta, \dot{\psi}, \delta, F_{zf}) &- b F_{yr,p}(\beta, \dot{\psi}, F_{zr}) + M_z = 0 \end{aligned} \tag{4.4}$$

where the front and rear tyre lateral forces $F_{yf,p}$ and $F_{yr,p}$ are computed considering the nonlinear tyre slip–lateral force relationship introduced in Pacejka (2002), i.e.,

$$\begin{aligned} F_{yf,p}(\alpha_f) &= D_f(C_f \arctan(B_f(\alpha_f) - E_f(B_f(\alpha_f) - \arctan(B_f(\alpha_f))))) \\ F_{yr,p}(\alpha_r) &= D_r(C_r \arctan(B_r(\alpha_r) - E_r(B_r(\alpha_r) - \arctan(B_r(\alpha_r))))) \end{aligned} \tag{4.5}$$

where α_f, α_r are the front and rear tyre sideslip angles respectively, which can be approximated as:

$$\alpha_f = \beta + a\frac{\dot{\psi}}{v} - \delta$$
$$\alpha_r = \beta - b\frac{\dot{\psi}}{v}$$

Coefficients B_f, C_f, D_f, E_f, B_r, C_r, D_r, E_r can be identified, for a given uncontrolled vehicle, using the experimental data collected during standard handling manoeuvres: the values employed in this section are reported in Subsection 4.1.5.

For each constant speed value v, the reference map $\mathcal{M}(\delta, v)$ is derived with a two–step procedure.

1. At first, equations (4.4) are numerically solved to obtain the uncontrolled vehicle steering diagram, i.e. the value of $a_y = \dot{\psi}\, v$ as function of the steering angle δ, with $M_z = 0$ (see Fig. 4.1, dotted line). Note that, since the tyre equations $F_{yf,p}(\cdot)$, $F_{yr,p}(\cdot)$ are not invertible in general (see e.g. Liaw *et al.* (2007)), two solutions of equations (4.4) can be found, given the same value of δ. However, only one of such solutions corresponds to a stable equilibrium point and it is therefore selected by the numerical procedure.

2. In the second step, the reference steering diagram is chosen according to some criteria, like improvement of the manoeuvrability with respect to the uncontrolled vehicle, as already pointed out in Subsection 4.1.2 (see e.g. Data and Frigerio (2002); Canale *et al.* (2007) for more details). In particular, the reference curves have been chosen to decrease the steering diagram slope in the linear tract, thus improving the vehicle manoeuvrability in the linear zone, and to increase the maximum lateral acceleration that can be reached (as can be seen in Fig. 4.1, solid line).

The nonlinear single track vehicle model (4.4) is also employed to verify that the designed reference steering diagrams correspond to feasible vehicle motion conditions, according to the actuator and tyre limits. The map of values of $\dot{\psi}_{\text{ref}}$ is obtained by designing a reference steering diagram for each value of velocity v within the working region of the vehicle. Fig. 4.5 shows an example of such a static reference map (see Canale *et al.* (2007) for a more detailed description on the map construction).

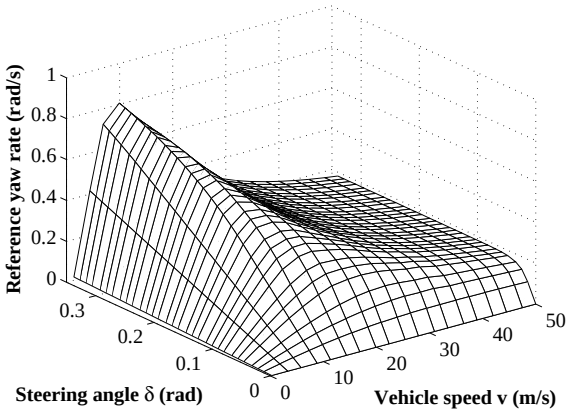

Figure 4.5: An example of yaw rate reference static map.

4.1.4.2 The feedforward component design

As previously discussed, in order to improve the yaw rate transient response a further control input generated by a feedforward controller $\mathcal{F}$ driven by the steering angle $\delta(t)$ is added (see Fig. 4.4). In order to design the feedforward controller, the following transfer functions in the Laplace domain are obtained from the vehicle model equations (4.3)

$$\dot{\psi}(s) = G_\delta(s)\delta(s) + G_M(s)M_z(s) \tag{4.6}$$

where

$$\begin{aligned} G_\delta(s) &= \frac{b_2 s^2 + b_1 s + b_0}{a_4 s^4 + a_3 s^3 + a_2 s^2 + a_1 s + a_0} \\ G_M(s) &= \frac{c_3 s^3 + c_2 s^2 + c_1 s + c_0}{a_4 s^4 + a_3 s^3 + a_2 s^2 + a_1 s + a_0} \end{aligned} \tag{4.7}$$

and

$$\begin{aligned} &a_4 = mJ_z l_f l_r,\ a_3 = mvJ_z(l_f + l_r) \\ &a_2 = J_z(mv^2 + c_f l_r + c_r l_f) + m(c_f a^2 l_r + c_r b^2 l_f) \\ &a_1 = v(J_z(c_f + c_r) + m(c_f a(a - l_r) + c_r b(b + l_f))) \\ &a_0 = c_f c_r l^2 - mv^2(c_f a + c_r b) \\ &b_2 = mvac_f l_r,\ b_1 = mv^2 ac_f,\ b_0 = vc_f c_r l \\ &c_3 = ml_f l_r,\ c_2 = mv(l_f + l_r) \\ &c_1 = mv^2 + c_f l_r + c_r l_f,\ c_0 = v(c_f + c_r) \end{aligned} \tag{4.8}$$

The feedforward contribution is computed by means of a linear filter $F(s)$ to match the open loop yaw rate behaviour given by (4.6) with the one described by an objective transfer function $T_\delta^{\text{des}}(s)$, i.e.,

$$\dot{\psi}(s) = T_\delta^{\text{des}}(s)\delta(s) \tag{4.9}$$

Thus, considering the transfer function (4.6) where $M_z(s)$ is computed as $M_z(s) = F(s)\delta(s)$ and $\dot{\psi}(s)$ is given by (4.9), the feedforward filter $F(s)$ is obtained as

$$F(s) = \frac{T_\delta^{\text{des}}(s) - G_\delta(s)}{G_M(s)} \tag{4.10}$$

Since the feedforward controller aims to improve the transient response only, its contribution should be zero in steady state conditions. To satisfy this condition, $T_\delta^{des}(s)$ and $G_\delta(s)$ must have the same static gain. Note that the presented procedure for feedforward design does not take explicitly into account the presence of the feedback controller.

4.1.4.3 Second order sliding mode control design

In the considered problem, the chosen sliding variable is the error between the actual yaw rate and the reference yaw rate, i.e.,

$$S(t) = \dot{\psi}(t) - \dot{\psi}_{ref}(t) \tag{4.11}$$

The control objective is to make this error vanish. By virtue of the use of sliding mode control it is possible to make the error converge to zero in finite time. To design the controller, it is useful to observe that the first and second time derivative of the sliding variable are, respectively,

$$\dot{S}(t) = (aF_{yf,p}(t) - bF_{yr,p}(t) + M_z(t))/J_z - \ddot{\psi}_{ref}(t) \tag{4.12}$$

$$\ddot{S}(t) = (a\dot{F}_{yf,p}(t) - b\dot{F}_{yr,p}(t) + \dot{M}_z(t))/J_z - \dddot{\psi}_{ref}(t) \tag{4.13}$$

Introducing the auxiliary variables $y_1(t) = S(t)$ and $y_2(t) = \dot{S}(t)$, (4.12) and (4.13) can be rewritten as

$$\begin{cases} \dot{y}_1(t) = \dot{S}(t) = y_2(t) \\ \dot{y}_2(t) = \ddot{S}(t) = \lambda(t) + \tau(t) \end{cases} \tag{4.14}$$

where $\tau(t) = M_z(t)/J_z$ is regarded as the auxiliary control variable and $\lambda(t) = (a\dot{F}_{yf,p}(t) - b\dot{F}_{yr,p}(t))/J_z - \dddot{\psi}_{ref}(t)$.

From the third and the fourth equation of (4.3), the quantity $\lambda(t)$ can be assumed to be bounded with known bound, i.e,

$$|\lambda(t)| \leq \Lambda \tag{4.15}$$

where $\Lambda > 0$ depends on the operating condition of the vehicle. From a physical point of view, (4.15) means that the lateral force produce by the tyres has a bounded first time derivative. Note that a conservative estimation for Λ can be determined on the basis of (4.3), (4.4), and the tyre characteristic.
Moreover, the quantity y_2 can be viewed as an unmeasurable quantity, being the first derivative of y_1 which depends on $\lambda(t)$ and $\tau(t)$.

The presented SOSM controller is of sub–optimal type (Bartolini *et al.*, 1997*b*). This implies that, under the assumption of being capable of detecting the extremal values $y_{1_{Max}}$ of the signal y_1, the following theorem can be proved:

Theorem 4.1 *Given system (4.14), where $\lambda(t)$ satisfies (4.15), and y_2 is not measurable, the auxiliary control law*

$$\tau(t) = \dot{M}_z(t)/J_z = -K_{SL}\ \text{sign}\left\{y_1(t) - \frac{1}{2}y_{1M}(t)\right\} \tag{4.16}$$

where the control gain K_{SL} is chosen such that

$$K_{SL} > 2\Lambda \tag{4.17}$$

and $y_{1M}(t)$ is a piece–wise constant function representing the value of the last singular point of $y_1(t)$ (i.e., the most recent value $y_{1M}(\bar{t})$ such that $\dot{y}_1(\bar{t}) = 0$), causes the convergence of the system trajectory to the origin of the plane, i.e., $y_1 = y_2 = 0$, in finite time.

Proof: The control law (4.16) is a sub–optimal SOSM control law. So, by following a theoretical development as that provided in Bartolini *et al.* (1997*b*) for the general case, it can be proved that the trajectories on the y_1Oy_2 plane are confined within limit parabolic arcs including the origin. The absolute values of the coordinates of the trajectory intersections with the y_1, and y_2 axis decrease in time. As shown in Bartolini *et al.* (1998*b*), under condition (4.15) the following relationships hold

$$|y_1(t)| \leq |y_{1M}(t)|, \qquad |y_2(t)| \leq \sqrt{|y_{1M}(t)|}$$

and the convergence of $y_{1M}(t)$ to zero takes place in finite time (Bartolini *et al.*, 1998*b*). As a consequence, also $y_1(t)$ and $y_2(t)$ tend to zero in finite time since they are both bounded by $\max\{|y_{1M}(t)|, |\sqrt{|y_{1M}(t)|}|\}$.

The saturation of the control input is taken into account relying on the approach proposed in Ferrara and Rubagotti (2008). Under the assumption that the saturation value of the RAD is such that

$$M_{z,sat} > aF_{yf,p}(t) - bF_{yr,p}(t) - J_z\ddot{\psi}_{ref}(t) \tag{4.18}$$

Then, the actual control law $M_z(t)$ is given by

$$\dot{M}_z(t) = \begin{cases} -M_z(t) & \text{if } |M_z(t)| \geq M_{z,sat} \\ J_z\tau(t) & \text{otherwise} \end{cases} \tag{4.19}$$

where $\tau(t)$ is given by (4.16) and $M_{z,sat}$ is the saturation value of the RAD, i.e., 2500 Nm. Note that assumption (4.18) implies that also a first order control law

$$M_z(t) = -M_{z,sat}\ \text{sign}\{S(t)\} \tag{4.20}$$

is capable of making $S(t) = 0$ in finite time. Yet, this is a discontinuous control law, which can produce the undesirable chattering effect.

As for the control design, the dynamic of the RAD actuator is neglected and the steady state gain of (4.2) is considered. Thus, the input current of the RAD is generated as

$$I_M(t) = M_z(t)/K_A \tag{4.21}$$

where $M_z(t)$ is obtained by integration of (4.19).

4.1.5 Simulation results

In order to show in a realistic way the effectiveness of the presented control approach, simulations of different manoeuvres are performed using a detailed nonlinear 14 degrees of freedom vehicle model. In particular, the model degrees of freedom correspond to the standard three chassis translations and yaw, pitch, and roll angles, the four wheel angular speeds and the four wheel vertical movements with respect to the chassis. Nonlinear characteristics obtained on the basis of measurements on the real vehicle have been employed to model the tyre, steer and suspension behaviour. The employed

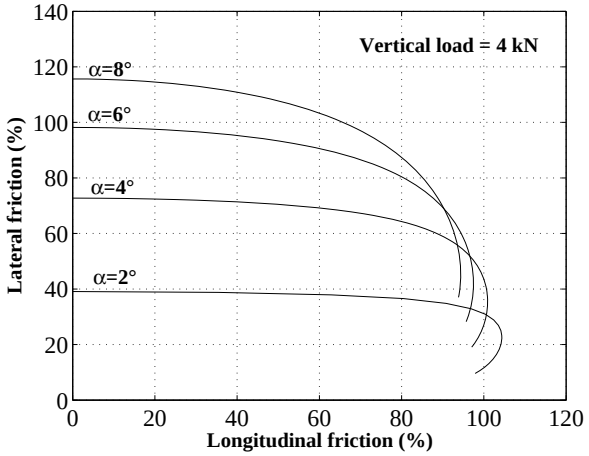

Figure 4.6: Front tyre friction ellipses considered in the 14 degrees of freedom model, with different values of lateral slip angle α, for a constant vertical load of 4 kN.

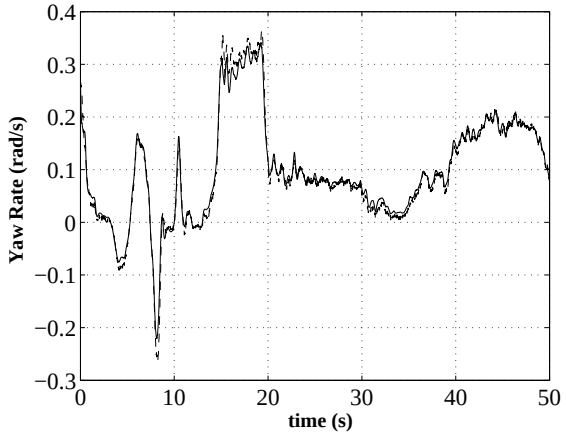

Figure 4.7: Comparison between the yaw rate real data (dashed) and that obtained with the considered model (solid).

tyre model is described e.g. in Genta (1997). It takes into account the interaction between longitudinal and lateral slip, as well as vertical tyre load and suspension motion, to compute the tyre longitudinal and lateral forces, as well as self–aligning moment. An example of the related tyre friction

ellipses is shown in Fig. 4.6, where the lateral friction coefficient is reported as a function of the exploited longitudinal friction (during traction) and of the tyre slip angle α. Asymmetrical friction ellipses for traction–braking longitudinal forces is also considered. Fig. 4.7 shows a comparison between the yaw rate measured on the real vehicle and the one obtained in simulation with the considered model. As can be seen, the model adopted in simulation gives a good description of the vehicle dynamics as compared with real data. To test the robustness feature of the designed control scheme, in the following manoeuvres, either the nominal vehicle configuration or a vehicle with increased mass (+ 300 kg, with consequent inertial and geometrical parameter variations) have been considered.

The parameters of the single track model (4.3) considered for the control design are as follow $v = 100\,\text{km/h} = 27.77\,\text{m/s}$, $m = 1715\,\text{kg}$, $J_z = 2700\,\text{kgm}^2$, $a = 1.07\,\text{m}$, $b = 1.47\,\text{m}$, $l_f = 1\,\text{m}$, $l_r = 1\,\text{m}$, $c_f = 95117\,\text{Nm/rad}$, $c_r = 97556\,\text{Nm/rad}$ while the parameters of the RAD model (4.2) considered in simulation are $K_A = 2500$ Nm/A and $\omega_A = 53.4$ rad/s.
The tyre slip–force characteristics (4.5) have been computed with the following parameters:
$B_f = 7.8$, $C_f = 1.3$, $D_f = 8824.5$, $E_f = -0.29$
$B_r = 13.0$, $C_r = 1.3$, $D_r = 6725.1$, $E_r = -0.16$

In principle, a value for the control gain K_{SL} in (4.16) can be found according to (4.17), relying on the knowledge of a suitable value of the bound Λ. However, in order to find a less conservative value of the control gain, one can also tune this parameter relying on simulation results, by choosing K_{SL} sufficiently high in order to guarantee the convergence to the sliding manifold and good performances. This latter approach is adopted and the chosen value of the control gain is $K_{SL} = 8000$.
The objective function for the feedforward controller has been chosen as

$$T_\delta^{\text{des}}(s) = \frac{56.7}{s + 10}$$

The bandwidth of the feedforward component has been chosen in simulation in order to achieve satisfactory performances.

4.1.5.1 Constant speed steering pad

The aim of this manoeuvre is to evaluate the steady–state vehicle performances: the steering angle is slowly increased (i.e. 1°/s handwheel velocity)

while the vehicle is moving at constant speed, until the vehicle lateral acceleration limit (about 8.6 m/s^2) is reached and the vehicle becomes unstable or the constant speed value cannot be kept. The results of this test, performed with a full load vehicle (+300 kg), are shown in Fig. The reference

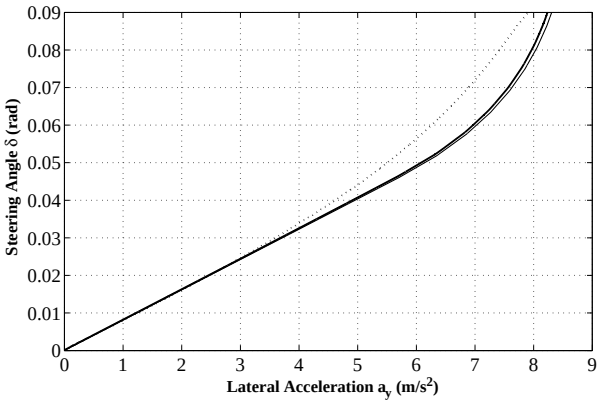

Figure 4.8: Steering pad test at 100 km/h. Comparison between the reference steering diagram (thin solid line) and the ones obtained with the full load (+300 kg) uncontrolled vehicle (dotted) and with the controlled vehicle (solid).

steering diagram and the one obtained with the controlled vehicle are practically superimposed: thus the target vehicle behaviour, characterized by a lower understeer gradient, is reached by the presented control system, which show good tracking performances also in the nonlinear tract of the diagram and with changed vehicle characteristics. A small tracking error can be noted in the nonlinear zone at quite high lateral acceleration values. This is due to the fact that the car does not reach the steady state conditions (i.e. $a_y(t) \neq \dot{\psi}(t)v(t)$) because of its increased inertial characteristics. Fig. 4.9 shows the course of the tracking error ($\dot{\psi}_{\text{ref}} - \dot{\psi}$) in the initial part of the manoeuvre: it can be noted that a chattering phenomenon occurs. The chattering effect is due to the fact that the presence of the unmodelled RAD actuator increases the relative degree of the system. As a consequence, the transient process converge to a periodic motion (Boiko *et al.*, 2007*a*,*b*). However, in the considered case the oscillations are too small to be perceived by the driver. A possible way to reduce the chattering is the use of lower values of the gain K_{SL} in the computation of the auxiliary control (4.16): however,

Table 4.1: Maximum and RMS reference tracking errors

Steering Pad	+300 kg	+200 kg	+100 kg	Nominal
$E_{\max}$	$6.0 \cdot 10^{-4}$	$6.6 \cdot 10^{-4}$	$6.8 \cdot 10^{-4}$	$2.3 \cdot 10^{-4}$
E_{rms}	$4.0 \cdot 10^{-8}$	$4.2 \cdot 10^{-8}$	$4.9 \cdot 10^{-8}$	$2.8 \cdot 10^{-7}$
Steer Reversal	+300 kg	+200 kg	+100 kg	Nominal
E_{rms}	$3.5 \cdot 10^{-3}$	$2.1 \cdot 10^{-3}$	$1.8 \cdot 10^{-3}$	$1.8 \cdot 10^{-3}$

the lower K_{SL} the worse the performance and robustness properties of the SOSM controller (Bartolini *et al.*, 1997*b*). Thus, a compromise has to be reached between limited chattering and good performances. The results of

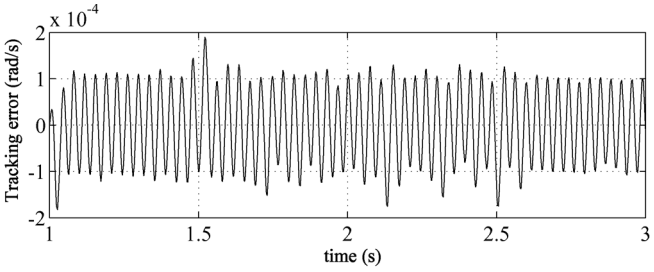

Figure 4.9: Steering pad test at 100 km/h, full load (+300kg) conditions. Tracking error during the initial part of the test.

a more complete analysis of the tracking performances obtained with the considered control strategies, for the steering pad manoeuvre, are reported in Table 4.1, in terms of maximum error $E_{\max}$ and root mean square error E_{rms}, i.e.,

$$E_{\max} = \max_{t \in [t_0, t_{\text{end}}]} |\dot{\psi}_{\text{ref}}(t) - \dot{\psi}(t)| \tag{4.22}$$

$$E_{\text{rms}} = \sqrt{\frac{1}{t_{\text{end}} - t_0} \int_{t_0}^{t_{\text{end}}} (\dot{\psi}_{\text{ref}}(t) - \dot{\psi}(t))^2 dt} \tag{4.23}$$

where t_0 and t_{end} are the starting and final test time instants respectively. It can be noted that the presented controller is able to achieve good tracking performance, with very low values of E_{rms} and $E_{\max}$. Similar results have been obtained for different speed values.

4.1.5.2 Steer reversal test

This test aims at evaluating the controlled car transient response performances: in Fig. 4.10 the employed steering angle behaviour is showed, corresponding to a maximum handwheel angle of 50°, with a handwheel speed of 400°/s. The manoeuvre has been performed at 100 km/h. The ob-

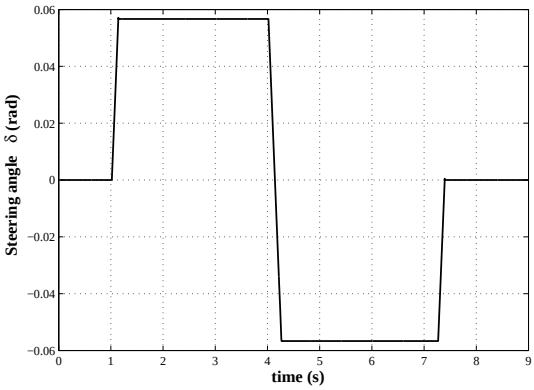

Figure 4.10: Steering angle reversal test input corresponding to 50° handwheel angle

tained yaw rate course shows that the controlled vehicle dynamic response in nominal conditions is well damped (see Fig. 4.11). The time evolution of yaw moment M_z is reported in Fig. 4.12. Table 4.1 shows the tracking performance obtained in the 50° steer reversal manoeuvre with varying mass values, with consequent changes of the other inertial and geometrical parameters, in terms of root mean square error E_{rms}. It can be noted that the presented SOSM controller achieves low values of E_{rms} also with increased mass, showing good robustness properties.

4.1.5.3 ISO double lane change

The aim of this manoeuvre is to test the effectiveness of the presented approach also in closed loop, i.e. in presence of the drivers' action. The ISO double lane change manoeuvre has been implemented as reported in Genta (1997), with constant test speed $v_{\text{ref}} = 100\,\text{km/h}$. The reference vehicle path in terms of yaw angle $\psi_{\text{ref}}(t)$ is reported in Fig. 4.13. The

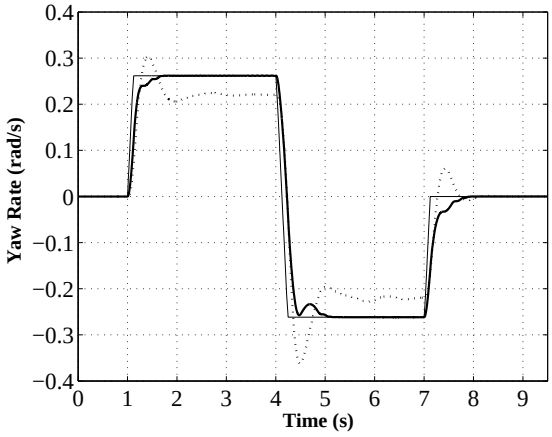

Figure 4.11: 50° steer reversal test at 100 km/h, nominal conditions. Comparison between the reference yaw rate course (thin solid line) and the ones obtained with the uncontrolled (dotted) vehicle and the controlled (solid) vehicle.

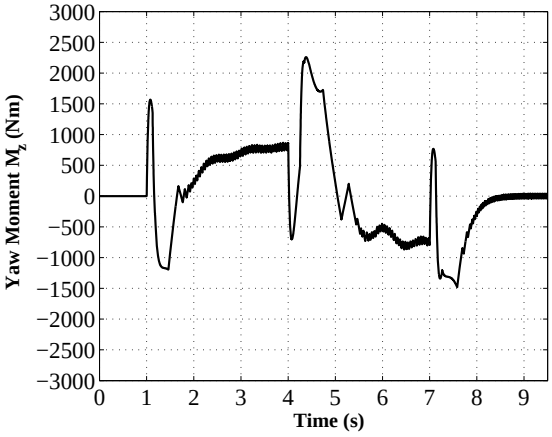

Figure 4.12: 50° steer reversal test at 100 km/h, nominal conditions. Time evolution of the yaw moment.

simple drivers' model described e.g. in Genta (1997) has been adopted

$$\delta(s) = \frac{K_d}{\tau_d\, s + 1} \left(\psi_{\text{ref}}(s) - \psi(s)\right)$$

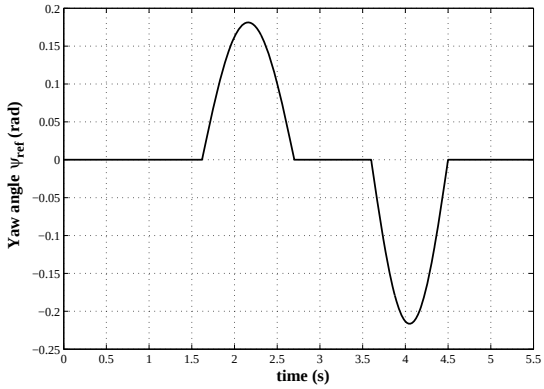

Figure 4.13: Reference yaw angle $\psi_{\text{ref}}(t)$ for the ISO double lane change test at 100 km/h

More complex drivers' model could be employed, however the purpose of the considered closed loop manoeuvre is to simply make a comparison between the handling properties of the uncontrolled vehicle and the controlled one, given the same driver model. The values of the driver gain K_d and of the driver time constant τ_d have been chosen as $K_d = 0.63$ and $\tau_d = 0.16\,\text{s}$. Note that the values of τ_d range approximately from $0.08\,\text{s}$ (experienced driver) to $0.25\,\text{s}$ (unexperienced driver), while the higher is the driver gain, the more aggressive is the driving action which could cause more likely vehicle instability. Fig. 4.14 shows the obtained results in terms of handwheel angle $\delta_H(t) = 15.4\,\delta(t)$: it can be noted that with the controlled vehicle the resulting driver input is less oscillating than the one obtained in the uncontrolled case, showing again that the considered control strategy achieves quite good improvements of the system damping properties.

4.1.6 A comparison between internal model control and second order sliding mode approaches to vehicle yaw control

The performance obtained with the SOSM control scheme previously described are compared with that of another robust control scheme designed relying on Internal Model Control (IMC) methodology.
Internal Model Control techniques are well established control methodolo-

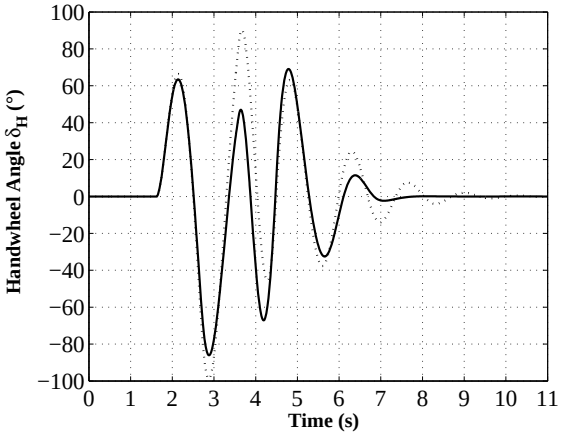

Figure 4.14: ISO double lane change at 100 km/h, handwheel input δ_H for the full load (+300 kg) uncontrolled vehicle (dotted) and the controlled vehicle (solid).

gies able to handle in an effective way both robustness (see Morari and Zafiriou (1989)) and saturation (see e.g. Zheng *et al.* (1994)) issues. More specifically, the enhanced Internal Model Control structure presented in Canale (2004), which guarantees robust stability as well as improved performances during saturation, will be employed.

The control structure of the IMC based control scheme is the same described in Subsection 4.1.4, i.e., it is composed of a reference map $\mathcal{M}$, a feedforward controller $\mathcal{F}$ and a robust feedback controller $\mathcal{C}$ which is designed relying on IMC control technique (see Fig. 4.4).

In order to compare the two approaches, the same reference map $\mathcal{M}$ is employed with both controllers. Note that, due to the different interaction of the feedforward controller with the considered IMC and SOSM feedback control laws, two different filters $\mathcal{F}$ are designed, in order to obtain the best performances in each case.

Part of the comparison study presented in this section is taken from Canale *et al.* (2008*b*) and Canale *et al.* (2008*c*).

4.1.7 IMC controller design

The design of the feedback controller in the case of Internal Model Control approach relies on H_∞ methodologies, to guarantee robust stability in presence of model uncertainty. In order to exploit this design technique, the linear model described by the transfer functions (4.6) is considered. Moreover, an unstructured description of the related uncertainty in the frequency domain is needed.

As the control input is the yaw moment M_z and the controlled output is the yaw rate $\dot{\psi}$, transfer function $G_M(s)$ given by (4.7) is used in the IMC feedback controller design.
In this framework, the considered model uncertainty is described by means of an additive linear model set of the form (see e.g. Skogestad and Postlethwaite (2005); Milanese and Taragna (2005)):

$$\mathcal{G}_M(G_M, \Gamma(\omega)) = \{G_M(s) + \Delta(s) : |\Delta(j\omega)| \leq \Gamma(\omega)\} \tag{4.24}$$

where $\Delta(s)$ is the considered model uncertainty, whose magnitude is bounded by function $\Gamma(\omega)$. In order to derive such model set, simulation data have been used. Such data have been generated using the 14 degrees of freedom nonlinear model adopted in simulation in Subsection 4.1.5 and considering the following uncertainty intervals for tyre parameters (0% to -20% front, 0% to +20% rear tyre cornering stiffness and ± 10% tyre relaxation lengths variations with respect to their nominal values), vehicle speed (± 30% of the nominal value) and vehicle mass (0% to +25% of the nominal value with consequent geometrical and inertial parameters changes).

The computed model set (4.24) is shown in Fig. 4.15, where the nominal transfer function magnitude behaviour is reported and compared with the obtained uncertainty bounds.

IMC techniques (see Morari and Zafiriou (1989)) based on H_∞ optimization are able to satisfy robust stability requirements in presence of input saturation (see e.g. Canale (2004)). A generic IMC structure is reported in Fig. 4.16. However, as discussed in Zheng *et al.* (1994), IMC control may deteriorate the system performances when saturation is active, even in absence of model uncertainty. In order to improve the performances under saturation, an enhanced robust IMC structure based on the anti-windup solutions presented in Zheng *et al.* (1994) has been proposed in Canale (2004). The control scheme considered in Canale (2004) gives rise to a nonlinear

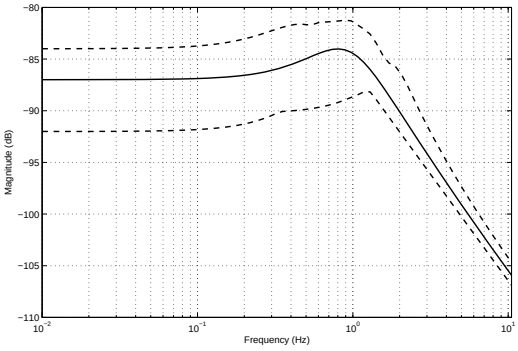

Figure 4.15: Model set $\mathcal{G}_M$: Nominal transfer function G_M (solid) and upper and lower uncertainty bounds (dashed).

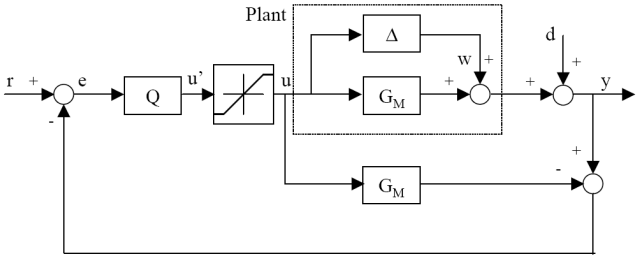

Figure 4.16: IMC scheme with model uncertainty and saturating input.

controller $\mathcal{Q}$, which replaces the linear controller $Q(s)$ in Fig. 4.16, made up by the cascade connection of a linear filter $Q_1(s)$ and a non linear loop $\mathcal{Q}_2$ as shown in Fig. 4.17. The design procedure can be summarized in the following steps:

1. A preliminary robust IMC controller $Q(s)$ is computed solving the following H_∞ optimization problem:

$$\begin{aligned} &Q(s) = \arg\min \left\| W_S^{-1}(s)\left(1 - G_M(s)\,Q(s)\right)\right\|_\infty \\ &\text{s.t. } \left\| Q(s)\,\bar{\Gamma}(s)\right\|_\infty < 1 \end{aligned} \tag{4.25}$$

where $\bar{\Gamma}(s)$ is suitable rational function with real coefficients, stable, whose magnitude strictly overbounds the frequency course $\Gamma(\omega)$ and $W_S(s)$ is a weighting function introduced to take into account a desired specification on the sensitivity function $(1 - G_M(s)Q(s))$

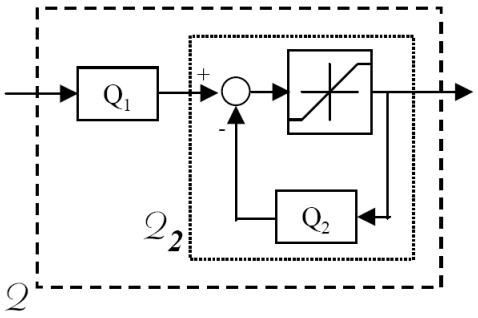

Figure 4.17: Nonlinear IMC enhanced controller.

2. Using controller $Q(s)$ computed in the previous step, a controller $Q_2(s)$, via the design of a preliminary filter $\bar{Q}_1(s)$, is obtained according to the criteria introduced in Zheng *et al.* (1994). It has to be noted that $Q_2(s)$ must ensure the stability of the non linear loop $\mathcal{Q}_2$ (see Fig. 4.17). To this end, an upper bound $\gamma_{\mathcal{Q}_2}$ on the H_∞ norm of $\mathcal{Q}_2$ has to be computed (see Canale (2004) for details). If $\gamma_{\mathcal{Q}_2}$ is finite then the stability of $\mathcal{Q}_2$ is guaranteed. In case that the stability of $\mathcal{Q}_2$ is not assured then a new IMC controller design has to be performed starting from point 1.

3. Then, the linear controller $Q_1(s)$ can be designed by means of the following H_∞ optimization problem:

$$\begin{aligned} &Q_1(s) = \arg\min \left\| W_S^{-1}(s) \left(1 - G_M(s)\tfrac{Q_1(s)}{1+Q_2(s)}\right)\right\|_\infty \\ &\text{s.t.} \|Q_1(s)\bar{\Gamma}(s)\gamma_{\mathcal{Q}_2}\|_\infty < 1 \end{aligned} \tag{4.26}$$

As described in Subsection 4.1.4.2, the feedforward controller is computed by means of a linear filter $F^{\text{IMC}}(s)$, designed to match the open loop yaw rate behaviour, given by (4.6), with the one described by an objective transfer function $T_\delta^{\text{des,IMC}}(s)$:

$$\dot{\psi}(s) = T_\delta^{\text{des,IMC}}(s)\delta(s) \tag{4.27}$$

Thus, the feedforward filter $F^{\text{IMC}}(s)$ is derived as:

$$F^{\text{IMC}}(s) = \frac{T_\delta^{\text{des,IMC}}(s) - G_\delta(s)}{G_M(s)} \tag{4.28}$$

As previously the dc-gains of $T_\delta^{\mathrm{des,IMC}}(s)$ and $G_\delta(s)$ must be the same. The weighting function $W_S(s)$ in (4.25)–(4.26), employed in the IMC design, and $T_\delta^{\mathrm{des,IMC}}(s)$ in (4.28), used for the feedforward design, are adjusted using simulation/experiments, in order to obtain the best overall performance.
Note that if the feedforward action had been implemented as shown in Fig. 4.4, the improvements introduced during saturation by the structure of Fig. 4.17 would influence only the feedback control contribution. This may cause a slight degradation on the control performance. In order to avoid such a degradation, in the case of IMC controller the feedforward contribution is injected at the reference level, obtaining the control scheme reported in Fig. 4.18. In such a structure, the feedforward action is realized by the

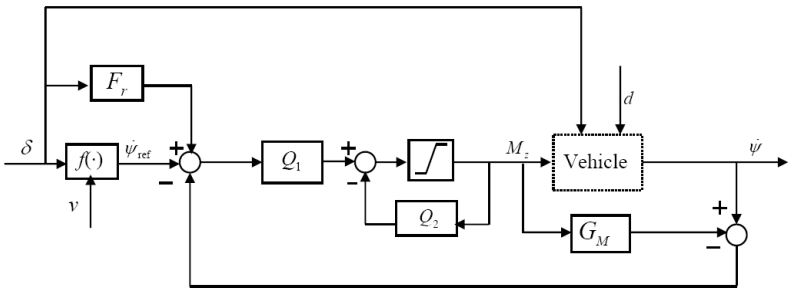

Figure 4.18: The control scheme for IMC control system.

linear filter $F_r(s)$, whose expression can be computed by straightforward manipulations as:

$$F_r(s) = \left(\frac{1 + Q_2(s)}{Q_1(s)} - G_M(s) \right) F^{\mathrm{IMC}}(s) \tag{4.29}$$

4.1.8 Simulation comparison tests

The IMC control design has been performed using transfer functions $G_\delta(s)$ and $G_M(s)$ defined in (4.6) computed at a nominal speed $v = 100\,\mathrm{km/h} = 27.77\,\mathrm{m/s}$ and with the same parameters adopted in Subsection 4.1.5. The following weighting function $W_S(s)$ has been used in the optimization problem (4.25):

$$W_S(s) = \frac{s}{s + 20} \tag{4.30}$$

Finally, in the feedforward design, the transfer function $T_\delta^{\mathrm{des,IMC}}(s)$ has been chosen as:

$$T_\delta^{\mathrm{des,IMC}}(s) = \frac{5.67}{1+\frac{s}{6}}$$

Transfer function $Q_2(s)$, employed in the anti-windup structure of the IMC controller, is the following:

$$Q_2(s) = \frac{72\,(s+39.13)\,(s+1.126)\,(s^2+21.85\,s+157)}{(s+54)(s^2+47.16\,s+562.3)(s^2+8.392\,s+61.89)}$$

Note that $Q_2(s)$ has to be strictly proper due to implementation issues.
Functions $W_S(s)$, $T_\delta^{\mathrm{des,IMC}}(s)$, have been chosen through simulations, to obtain the best performance for each control strategy.
As regards the SOSM sub–optimal controller designed in Subsection 4.1.4.3, the value of the control parameters are the same adopted in Subsection 4.1.5, i.e.,

$$K_{\mathrm{SL}} = 8000$$

and

$$T_\delta^{\mathrm{des,SL}}(s) = \frac{56.7}{s+10}$$

In order to show in a realistic way the performance obtained by the presented yaw control approaches, simulations have been performed using the detailed nonlinear 14 degrees of freedom Simulink model described in Subsection 4.1.5.

4.1.8.1 Constant speed steering pad

The aim of this manoeuvre is to evaluate the steady–state vehicle performance of the controlled vehicle. The constant speed steering pad test is the same described in Subsection 4.1.5.1. The results of this test, performed at 90 km/h with an increased mass (+300 kg) vehicle, are shown in Fig. 4.19, in terms of relative tracking error $(\dot{\psi}_{\mathrm{ref}} - \dot{\psi})/\dot{\psi}_{\mathrm{ref}}$: it can be noted that a smooth behaviour is obtained for the IMC control, while a chattering phenomenon occurs in the case of sliding mode controller as previously discussed. As previously discussed, the oscillations are too small ($\pm$ 0.04 %) to be perceived by the driver. The results of a more complete analysis of the tracking performances obtained with the considered control strategies, for the steering pad manoeuvre, are reported in Tables 4.2–4.3. It can be

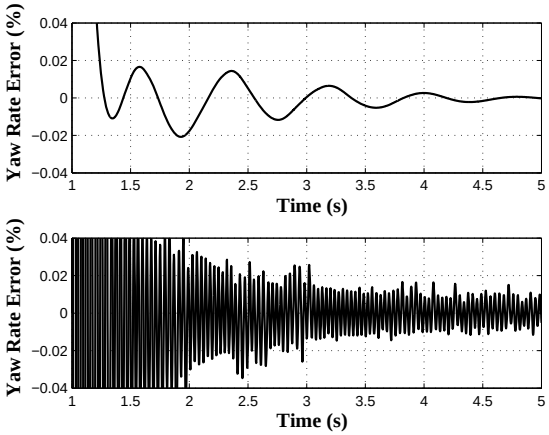

Figure 4.19: Steering pad test at 90 km/h. Relative tracking error behaviour during the initial part of the test for the IMC (upper) and SOSM (lower) control systems with increased mass (+300 kg) vehicle.

Table 4.2: Maximum reference tracking errors: steering pad manoeuvre at 90 km/h

$E_{\max}$	+300 kg	+200 kg	+100 kg	Nominal
IMC	$1.6 \cdot 10^{-4}$	$1.6 \cdot 10^{-4}$	$1.5 \cdot 10^{-4}$	$1.4 \cdot 10^{-4}$
SOSM	$6.0 \cdot 10^{-4}$	$6.6 \cdot 10^{-4}$	$6.8 \cdot 10^{-4}$	$2.3 \cdot 10^{-4}$

noted that both controllers are able to achieve good tracking performance, with very low values of E_{rms} and $E_{\max}$. The best results are obtained with the IMC controller, which appears to be more suited for the considered steady–state manoeuvre. Similar results have been obtained for different speed values.

4.1.8.2 Steer reversal test

The constant speed steering pad test is the same described in Subsection 4.1.5.2 and its aim is to evaluate the controlled car transient response performances.
Fig. 4.20 shows that the controlled vehicle dynamic response in nominal

Table 4.3: RMS reference tracking errors: steering pad manoeuvre at 90 km/h

E_{rms}	+300 kg	+200 kg	+100 kg	Nominal
IMC	$6.0 \cdot 10^{-10}$	$6.6 \cdot 10^{-10}$	$8.6 \cdot 10^{-10}$	$1.2 \cdot 10^{-9}$
SOSM	$4.0 \cdot 10^{-8}$	$4.2 \cdot 10^{-8}$	$4.9 \cdot 10^{-8}$	$2.8 \cdot 10^{-7}$

conditions is well damped with both the SOSM and the IMC controllers. The course of yaw moment M_z is reported in Fig. 4.21: it can be noted that the control input issued by the IMC controller saturates in all the transients during the test, while the SOSM controller is less aggressive. Both control systems are able to handle saturation effectively, without worsening of the performance. Table 4.4 shows the tracking performance obtained in the

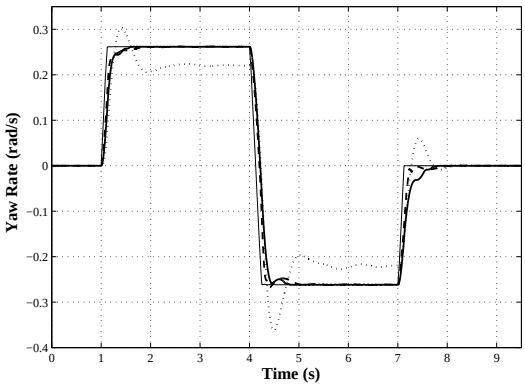

Figure 4.20: 50° steer reversal test at 100 km/h, nominal conditions. Comparison between the reference yaw rate course (thin solid line) and the ones obtained with the uncontrolled (dotted) vehicle and the Sliding Mode (solid) and IMC (dashed) controlled vehicles.

50° steer reversal manoeuvre with varying mass values, with consequent changes of the other inertial and geometrical parameters, in terms of root mean square error E_{rms} (4.23). Both controllers achieve low values of E_{rms} also with increased mass, showing good robustness properties. In this case, the difference between IMC and SOSM tracking performance is practically negligible.

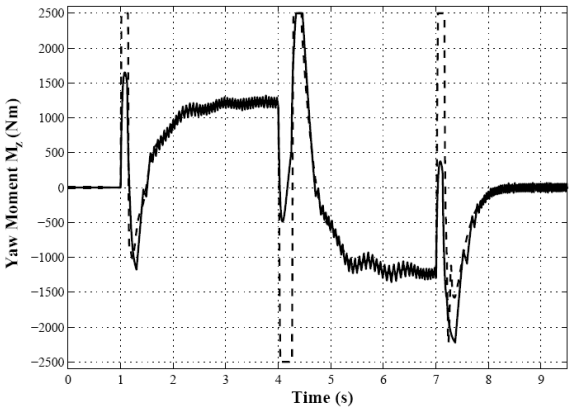

Figure 4.21: 50° steer reversal test at 100 km/h, nominal conditions. Comparison between the yaw moment courses obtained with the SOSM (solid) and IMC (dashed) controllers.

Table 4.4: RMS reference tracking errors: steer reversal test at 100 km/h

E_{rms}	+300 kg	+200 kg	+100 kg	Nominal
IMC	$3.1 \cdot 10^{-3}$	$1.8 \cdot 10^{-3}$	$1.4 \cdot 10^{-3}$	$1.1 \cdot 10^{-3}$
SOSM	$3.5 \cdot 10^{-3}$	$2.1 \cdot 10^{-3}$	$1.8 \cdot 10^{-3}$	$1.8 \cdot 10^{-3}$

4.1.8.3 Steering wheel frequency sweep

The steering wheel frequency sweep has been performed at 100 km/h in the frequency range 0-4 Hz, with a handwheel angle amplitude of 20°. The aim is to evaluate the bandwidth and resonance peak obtained with the considered control systems. In Table 4.5 the simulated behaviour of the transfer ratio $T_m(\omega) = |\dot{\psi}(\omega)|/|\dot{\psi}_{\text{ref}}(\omega)|$ is shown, putting into evidence the significant reduction of the resonance peak provided by the SOSM controller. A slightly higher resonance peak, but also a higher system bandwidth, are obtained with the IMC controller in the nominal case. With the increased mass (+300 kg) vehicle, the same resonance peak is obtained. The controlled vehicle performs better than the uncontrolled one with both the considered control techniques.

Table 4.5: Steering wheel frequency sweep at 100 km/h: bandwidth and resonance peak values

	Resonance Peak (dB)	Bandwidth (Hz)
Nominal uncontrolled	2.7	2.1
Nominal IMC	1.2	3
Nominal SOSM	0.9	2.8
+300 kg Uncontrolled	3.6	1.8
+300 kg IMC	2	2.5
+300 kg SOSM	2	2.3

Table 4.6: RMS reference tracking errors: Handwheel step at 100 km/h with lateral wind

E_{rms}	+300 kg	+200 kg	+100 kg	Nominal
IMC	$2.4 \cdot 10^{-4}$	$2.0 \cdot 10^{-4}$	$1.9 \cdot 10^{-4}$	$1.8 \cdot 10^{-4}$
SOSM	$4.0 \cdot 10^{-4}$	$3.7 \cdot 10^{-4}$	$4.2 \cdot 10^{-4}$	$3.2 \cdot 10^{-4}$

4.1.8.4 Steering step plus lateral wind disturbance

This test aims to evaluate the system performances in presence of external disturbances. A steering step with handwheel angle of 40° at 110 km/h, with a steering wheel speed of 400°/s is performed. Then, at time instant $t = 3\,\text{s}$ a quite strong lateral wind (100 km/h) acts on the vehicle. Such a disturbance is modelled by a lateral force $F_{y,\text{wind}} = 800$ N plus an external yaw moment $M_{z,\text{wind}} = 500$ Nm, both applied on the vehicle center of gravity. Fig. 4.22 shows the obtained results with the vehicle with increased mass (+300 kg): both control systems can reject the effects of the wind disturbance in an effective way, with practically the same behaviour. The obtained RMS errors with changing vehicle mass are reported in Table 4.6, showing that IMC control law performs slightly better than SOSM.

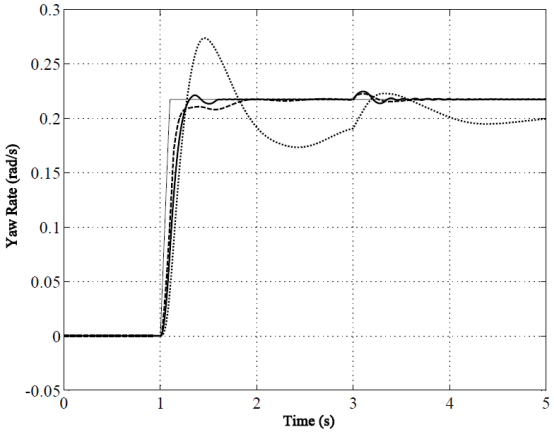

Figure 4.22: 40° Handwheel step at 110 km/h in presence of lateral wind, increased mass (+ 300 kg) vehicle. Reference yaw rate course (thin solid line) and those obtained with the uncontrolled vehicle (dotted) and the controlled vehicles with SOSM (solid) and IMC (dashed).

4.1.8.5 High speed braking in a turn

This test is employed by Mercedes to evaluate the performance of ESP® systems (see Nuessle *et al.* (2007)). The manoeuvre starts at 200 km/h on a curve with constant radius R=1000 m. A braking action with constant longitudinal deceleration $\overline{a}_x$ is then performed and the maximum yaw rate deviation $\Delta\dot{\psi}$, with respect to the initial steady–state value, within the first second after the braking is evaluated. The test is performed with increasing values of longitudinal deceleration and the resulting curves $\Delta\dot{\psi}(\overline{a}_x)$ are plotted. Fig. 4.23 shows the results obtained with the increased mass (+300 kg) vehicle. Similar results are obtained with the nominal configuration. It can be noted that the IMC and SOSM controlled vehicles show practically the same behaviour. Note that before a certain deceleration level (about 5.5 m/s^2 for the nominal vehicle and 4 m/s^2 for the increased mass one) the yaw rate deviation of the controlled vehicles is much lower than that of the uncontrolled one. Then, a sudden increase in $\Delta\dot{\psi}$ occurs for both the controlled vehicles, followed by a similar behaviour of the uncontrolled vehicle for even higher deceleration. This phenomenon is due to the fact that the particular stability system considered in this work, i.e. a rear active differential, is not well–suited to counterbalance the excessive oversteer given by

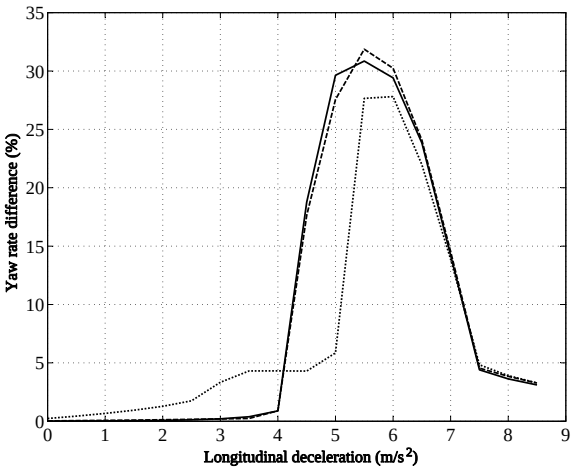

Figure 4.23: High speed braking in a turn, yaw rate difference $\Delta\dot{\psi}(\overline{a}_x)$ for the increased mass (+300 kg) uncontrolled vehicle (dotted) and controlled vehicles with SOSM (solid) and IMC (dashed) controllers.

this manoeuvre and leads to worse results than the uncontrolled vehicle. In fact, due to the interaction between tyre longitudinal and lateral forces, the intervention of the RAD may lead to saturate the lateral force at the rear wheels, thus exciting an oversteering behaviour instead of correcting it.

4.1.8.6 ISO double lane change

The aim of this manoeuvre is to test the effectiveness of the presented approaches also in closed loop, i.e. in presence of the driver's action. The ISO double lane change manoeuvre and the adopted driver model have been described in Subsection 4.1.5.3. Fig. 4.24 shows the obtained results, considering the increased mass (+300 kg) vehicle, in terms of handwheel angle $\delta_H(t) = 15.4\,\delta(t)$: it can be noted that with both IMC and SOSM the resulting driver input is less oscillating than the one obtained in the uncontrolled case, showing again that the considered control strategies achieve quite good improvements of the system damping properties. Fig. 4.25 shows the obtained courses of the control variable M_z: once more it can be noted that the SOSM controller is less aggressive than IMC but it leads to practically the same results.

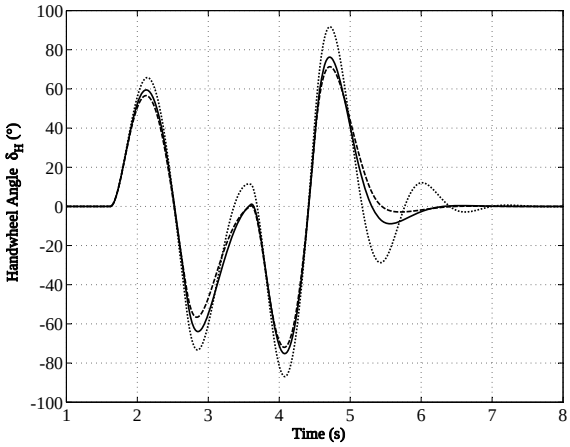

Figure 4.24: ISO double lane change at 100 km/h, handwheel input δ_H for the increased mass (+300 kg) uncontrolled vehicle (dotted) and controlled vehicles with SOSM (solid) and IMC (dashed)

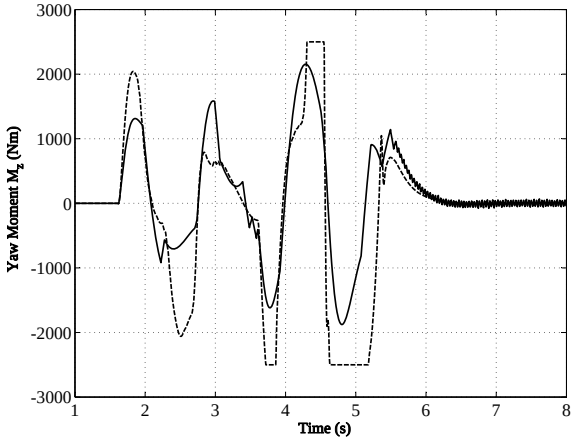

Figure 4.25: ISO double lane change at 100 km/h, control input M_z for the increased mass (+300 kg) controlled vehicle with SOSM (solid) and IMC (dashed)

4.1.9 Conclusions and future perspectives

In this section the problem of vehicle yaw control using yaw rate feedback and a Rear Active Differential has been investigated. The presented control

structure is composed by a reference generator, designed to improve vehicle handling, a feedforward contribution, which enhances the transient system response, and a feedback controller. The feedback controller is designed relying on the so–called second order sliding mode methodology which is capable of guaranteeing robust system stability in presence of disturbances and model uncertainties which are typical of the automotive context. The control scheme has been verified in simulation relying on an accurate 14 degrees of freedom vehicle model. The obtained results show the effectiveness of the presented control scheme. Quite good tracking performances have been obtained in steering pad manoeuvres and good transient performances have been achieved in steer reversal tests and in lane change manoeuvres. Simulation evidence has also assessed the robustness of the presented controller, since the considered manoeuvres have been performed with varying vehicle speed and mass.

Moreover, the performance of the presented SOSM control scheme are compared by means of extensive simulation tests, performed with an accurate 14 degrees of freedom vehicle model, with that obtained with the same control structure in which the robust feedback is designed relying on the enhanced Internal Model Control (IMC).
Small reference tracking errors have been obtained with both controllers during steering pad manoeuvres and good transient performances have been achieved in steer reversal tests. A slightly higher system bandwidth, but also a higher resonance peak, has been obtained by the IMC controller in the handwheel frequency sweep test. Quite good disturbance rejection properties and similar behaviours in oversteer contexts and closed loop lane change manoeuvres have been shown. The robustness of the employed controllers has been also tested, since the considered manoeuvres have been performed with varying vehicle speed and mass. The SOSM approach is able to handle the saturation of the control variable in an effective way, without extra conservativeness in control design. Moreover, SOSM control proved to be less aggressive with practically the same performances of the IMC controller. On the other hand, oscillations of the controlled variable are absent with the enhanced IMC controller, while it could be a serious issue in SOSM control. With both control techniques, stability in demanding oversteering conditions, like braking in a high speed turn, may be worse than the uncontrolled case, depending on the longitudinal deceleration level. This is due to the properties of the RAD, which is not well suited to stabilize the

vehicle in such situations.

Future works will aim to test stability and performance with low and non–uniform road friction coefficients and to compare the implementation issues of SOSM and IMC control laws, regarding required sampling period and computational complexity. Moreover, the possibility of combining these techniques will be also investigated, in order to exploit their respective benefits in vehicle stability control.

4.2 Traction control system for vehicle

During skid–braking and spin–acceleration, the driving force exerted by the tires reduces considerably and the vehicle cannot speed up or brake as desired. It may become very difficult to control the vehicle under these conditions. To solve this problem, a second order sliding mode traction controller is presented in this section. The controller design is coupled with the design of a suitable sliding mode observer to estimate the tire–road adhesion coefficient. The traction control is achieved by maintaining the wheels slip at a desired value. In particular, by controlling the wheels slip at the optimal value, the presented traction control enables anti–skid braking and anti–spin acceleration, thus improving the safety in difficult weather conditions, as well as the stability during high performance driving.

Part of this section is taken from Ferrara and Vecchio (2007*b*); Amodeo *et al.* (2007*a*,*b*) and Amodeo *et al.* (2008).

4.2.1 Introduction

In recent years, numerous different active control systems for vehicle have been investigated and implemented in production (Fodor *et al.*, 1998). Among them, the traction control of vehicles is becoming more and more important due to recent research efforts on intelligent transportation systems, and especially, on automated highway systems, and on automated driver assistance systems (see, for instance, Drakunov *et al.* (1995); Haskara *et al.* (2000); Kabganian and Kazemi (2001); Lee and Tomizuka (2003), and the references therein cited).

The objective of traction control systems is to prevent the degradation of the vehicle performances which occur during skid–braking and spin–acceleration. As a result, the vehicle performance and stability, especially under adverse external conditions such as wet, snowy or icy roads, are greatly improved. Moreover, the limitation of the slip between the road and the tire significantly reduces the wear of the tires.

The traction force produced by a wheel is a function of the wheel slip λ, of the normal force acting on a wheel F_z, and of the adhesion coefficient μ_p between road and tire, which, in turn, depends on road conditions (Gillespie, 1992; Genta, 1997). Since the adhesion coefficient μ_p is unknown and time–varying during driving, it is necessary to estimate such parameter on the

basis of the data acquired by the sensors. Because of its direct influence on the vehicle traction force, the wheel slip λ is regarded as the controlled variable in the traction force control system. The design of such a control system is based on the assumption that the vehicle velocity and the wheel angular velocities are both available on–line by direct measurements. As wheel angular velocity can be easily measured with sensors, only vehicle velocity is needed to calculate the wheel slip λ. The vehicle longitudinal velocity can be directly measured (Tomizuka *et al.*, 1995; Bevly *et al.*, 2003), indirectly measured (Borrelli *et al.*, 2006), and/or estimated through the use of observers (Ünsal and Kachroo, 1999; Kiencke and Nielsen, 2000). Since the problem of measuring the longitudinal velocity is out of the scope of this work, it is assumed that both the vehicle velocity and the wheel angular velocities are directly measured.

The main difficult arising in the design of a traction force control system is due to the high nonlinearity of the system and to the presence of disturbances and parameter uncertainties (Drakunov *et al.*, 1995; Buckholtz, 2002). Different sliding mode controllers have been proposed in the literature to solve the problem of controlling the wheel slip. For instance, sliding mode control is used to steer the wheel slip to the optimal value in order to produce the maximum braking force, and a sliding mode observer for the longitudinal traction force is proposed in Drakunov *et al.* (1995). A sliding mode based observer for the vehicle speed is proposed in Ünsal and Kachroo (1999). In Lee and Tomizuka (2003) a sliding mode control law that uses an online estimation of the tire/road adhesion coefficient is presented. Other different sliding mode approach to the traction control problem have been proposed in the literature (see, for instance, Gustafsson (1997); Xy *et al.* (2001); Haskara *et al.* (2002); Kang *et al.* (2005); Chikhi *et al.* (2005) and the references therein).

The traction control scheme presented in this section is designed relying on the second order sliding mode control methodology which features higher accuracy with respect to first order sliding mode control, and generates ideal sliding modes by means of continuous control actions while keeping the robustness feature typical of conventional sliding mode controllers (see Chapter 3).

The particular traction control problem addressed in this section is the so–called fastest acceleration/deceleration control (FADC) problem. It can be formulated as the problem of maximizing the magnitude of the traction

force in order to produce the maximum acceleration while driving and the smallest stopping distance during braking even on possible slippery road. This is attained by regulating the wheel slip ratio at the value corresponding to the maximum/minimum traction force. Since the reference slip ratios depend on the adhesion coefficient μ_p, which is unknown and time–varying during driving, the controller design is coupled with the design of a suitable sliding mode observer to estimate the tire–road adhesion coefficient. This makes the performance of the presented control system insensitive to possible variations of the road conditions, since such variations are compensated on–line by the controller.

This section is organized as follows. Subsection 4.2.2 is devoted to introduce the model of the vehicle dynamics, to specify the assumptions, and to state the control objectives. The second order sliding mode slip controller is presented in Subsection 4.2.3. A sliding mode observer for the tire/road adhesion coefficient is presented in Subsection 4.2.4 while the FADC problem is described in Subsection 4.2.5. Simulation results relevant to the designed controller are reported in Subsection 4.2.6, while some final comments are gathered in the last subsection.

4.2.2 Vehicle longitudinal dynamics

In this section, a nonlinear model of the vehicle is adopted (Genta, 1997). The vehicle is modeled as a rigid body and only longitudinal motion is considered. The difference between the left and right tires is ignored, making reference to the so–called bicycle model. The lateral, yawing, pitch and roll dynamics, as well as actuators dynamics are also neglected.

The resulting equations of motion for the vehicle are

$$
\begin{aligned}
m\dot{v}_x &= F_{xf}(\lambda_f, F_{zf}) + F_{xr}(\lambda_r, F_{zr}) - F_{loss}(v_x) && (4.31)\\
J_f\dot{\omega}_f &= T_f - R_f F_{xf}(\lambda_f, F_{zf}) && (4.32)\\
J_r\dot{\omega}_r &= T_r - R_r F_{xr}(\lambda_r, F_{zr}) && (4.33)\\
F_{loss}(v_x) &= F_{air}(v_x) + F_{roll} \\
&= c_x v_x^2 \cdot sign(v_x) + f_{roll} mg && (4.34)\\
F_{zf} &= \frac{l_r mg - l_h m\dot{v}_x}{l_f + l_r} && (4.35)\\
F_{zr} &= \frac{l_f mg + l_h m\dot{v}_x}{l_f + l_r} && (4.36)
\end{aligned}
$$

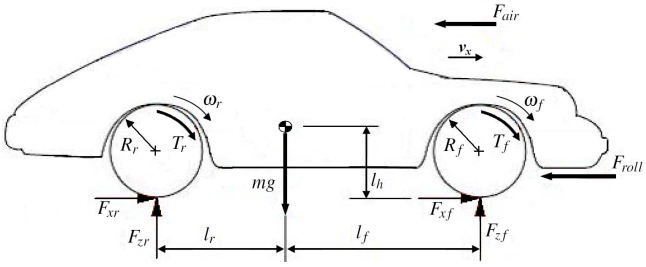

Figure 4.26: The vehicle model.

where v_x is the longitudinal velocity of the vehicle center of gravity, ω_f and ω_r are the angular velocity of the front and rear wheels, respectively, T_f and T_r are the front and rear input torque, λ_f and λ_r are the slip ratio at the front and rear wheel, respectively, F_{xf} and F_{xr} are the front and rear longitudinal tire–road contact forces, F_{zf} and F_{zr} are the normal force on the front and the rear wheel, F_{air} is the air drag resistance, and F_{roll} is the rolling resistance (see Fig. 4.26).
The vehicle parameters are the following: m is the vehicle mass, c_x is the longitudinal wind drag coefficient, f_{roll} is the rolling resistance coefficient, J_f and J_r are the front and rear wheel moment of inertia, respectively, R_f and R_r are the front and rear wheel radius, l_f is the distance from the front axle to the center of gravity, l_r is the distance from the rear axle to the center of gravity and l_h is the height of the center of gravity (see Fig. 4.26). The normal force calculation method (4.35)–(4.36) is based on a static force model, as described in Gillespie (1992), ignoring the influence of the suspension. This method gives a fairly accurate estimate of the normal force, especially when the road surface is fairly paved and not bumpy.
The longitudinal slip $\lambda_i,\ i \in \{f, r\}$, for a wheel is defined as the relative difference between a driven wheel angular velocity and the vehicle absolute velocity, i.e.,

$$\lambda_i = \begin{cases} \frac{\omega_i R_i - v_x}{\omega_i R_i}, & \omega_i R_i > v_x, \quad \omega_i \neq 0, \quad \text{acceleration} \\ \frac{\omega_i R_i - v_x}{v_x}, & \omega_i R_i < v_x, \quad v_x \neq 0, \quad \text{braking} \end{cases} \qquad i \in \{f, r\} \tag{4.37}$$

The wheel slip dynamics during acceleration can be obtained by differentiating (4.37) with respect to time, thus obtaining

$$\dot{\lambda}_i \quad = f_i^a + h_i^a T_i \qquad i \in \{f, r\} \tag{4.38}$$

where

$$f_i^a = -\frac{\dot{v}_x}{R_i\omega_i} - \frac{v_x F_{xi}}{J_i\omega_i^2} \quad i \in \{f, r\} \tag{4.39}$$

$$h_i^a = \frac{v_x}{J_i R_i \omega_i^2} \quad i \in \{f, r\} \tag{4.40}$$

The dynamics during braking can be analogously obtained by differentiating (4.37) for the brake situation and results in

$$\dot{\lambda}_i = f_i^b + h_i^b T_i \qquad i \in \{f, r\} \tag{4.41}$$

where

$$f_i^b = -\frac{R_i\omega_i\dot{v}_x}{v_x^2} - \frac{R_i^2 F_{xi}}{J_i v_x} \quad i \in \{f, r\} \tag{4.42}$$

$$h_i^b = \frac{R_i}{J_i v_x \omega_i^2} \quad i \in \{f, r\} \tag{4.43}$$

The traction force F_{xi} in the longitudinal direction generated at each tire is a nonlinear function of the longitudinal slip λ_i, of the normal force applied at the tire F_{zi}, and of the road adhesion coefficient μ_p (Genta, 1997). Different longitudinal tire/road friction model for vehicle motion control have been proposed in the literature, see e.g. Li *et al.* (2006). In this section, the so–called "Magic Formula" tire model developed by Bakker and Pacejka (Pacejka, 2002) is considered. This model is generally accepted as the most useful and viable model in describing the relationship between the slip ratio and the tire force. The model for the longitudinal force is as follow

$$F_{xi} = f_t(\mu_p, \lambda_i, F_{zi}) \qquad i \in \{f, r\} \tag{4.44}$$

where $\mu_p \in [0, 1]$ is the peak tire/road adhesion coefficient which depends on the road condition. Smaller values of μ_p correspond to more slippery road conditions. Fig. 4.27 shows typical λ–F_x curves for fixed F_z, for three different values of μ_p associated with the case of dry asphalt, wet asphalt and snowy road. Note that, from (4.44), one has that the longitudinal force produced by a wheel is bounded, i.e.,

$$|F_{xi}| \leq \Psi \qquad i \in \{f, r\} \tag{4.45}$$

The tire model (4.44) is a steady–state model of the interaction between the tire and the road. As for the transient tire behaviour it is assumed that,

being it due to tire relaxation dynamics (Kiencke and Nielsen, 2000), the traction force F_x has a bounded first time derivative, i.e.,

$$|\dot{F}_{xi}| \leq \Gamma \qquad i \in \{f, r\} \tag{4.46}$$

The controlled variable in the presented traction control system is the slip ratio at a wheel $\lambda_i,\ i \in \{f, r\}$, because of its strong influence on the traction force. Indeed, from (4.44), it is possible to adjust the traction force produced by a tire $F_{xi},\ i \in \{f, r\}$, to the desired value by controlling the wheel slip.

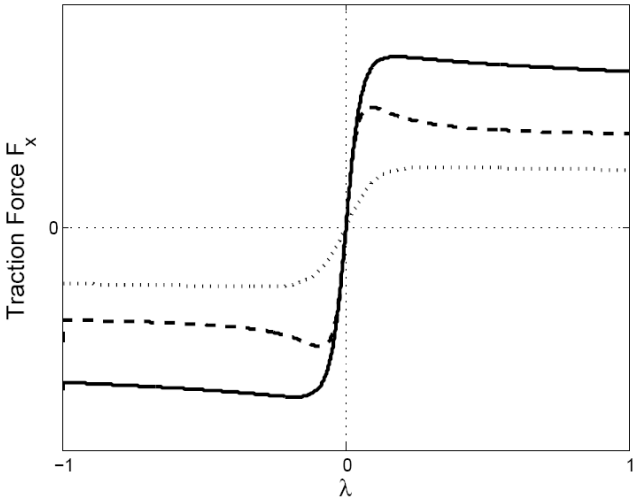

Figure 4.27: Typical λ–F_x curves for different road conditions (μ_p(dry asphalt) = 0.85 (solid), μ_p(wet asphalt) = 0.6, and μ_p(snow) = 0.3) and for fixed F_z.

4.2.3 The slip control design

As previously discussed, the controlled variable in the presented traction force control system is the slip ratio at a wheel $\lambda_i,\ i \in \{f, r\}$, because of its strong influence on the traction force. Indeed, it is possible to adjust the traction force produced by a tire $F_{xi},\ i \in \{f, r\}$, to the desired value by controlling the wheel slip. Thus the control objective of the control system is to make the actual slip ratio λ_i track the desired slip ratio $\lambda_{d,i}$.
The sliding variables are chosen as the error between the current slip and

the desired slip ratio, i.e.,

$$s_i = \lambda_{e_i} = \lambda_i - \lambda_{d,i} \qquad i \in \{f, r\} \tag{4.47}$$

As a consequence, the chosen sliding manifolds are given by

$$s_i = \lambda_{e_i} = \lambda_i - \lambda_{d,i} = 0 \qquad i \in \{f, r\} \tag{4.48}$$

and the objective of the control is to design continuous control laws $T_i,\ i \in \{f, r\}$, capable of enforcing sliding modes on the sliding manifolds (4.48) in finite time. Note that, once that the sliding mode is enforced, the actual slip ratio correctly tracks the desired slip ratio since on the sliding manifold $\lambda_{e_i} = 0$ and the control objective is attained in finite time.

The first and second derivatives of the sliding variable s_i in the acceleration case are given by

$$\begin{cases} \dot{s}_i &= f_i^a + h_i^a T_i - \dot{\lambda}_{d_i} \quad i \in \{f, r\} \\ \ddot{s}_i &= \varphi_i^a + h_i^a \dot{T}_i \qquad\qquad i \in \{f, r\} \end{cases} \tag{4.49}$$

where functions $\varphi_i^a,\ i \in \{f, r\}$, are defined as

$$\varphi_i^a = -\frac{\ddot{v}_x}{R_i\omega_i} + 2\frac{\dot{v}_x\dot{\omega}_i}{R_i\omega_i^2} - 2\frac{v_x\dot{\omega}_i^2}{R_i\omega_i^3} - \ddot{\lambda}_{d_i} - \frac{v_x\dot{F}_{xi}}{J_i\omega_i^2} \tag{4.50}$$

Note that the quantities $h_i^a,\ i \in \{f, r\}$, are known.
From (4.31), and (4.45), it yields

$$|\dot{v}_x| \leq \frac{2\Psi - F_{loss}(v_x)}{m} = f_1(v_x) \tag{4.51}$$

Taking into account the first time derivative of (4.31), (4.46), and (4.51), one has that

$$|\ddot{v}_x| \leq \frac{2\Gamma - 2c_x|\dot{v}_x||v_x|}{m} \leq \frac{2\Gamma - 2c_x f_1(v_x)|v_x|}{m} = f_2(v_x) \tag{4.52}$$

From (4.32), (4.33), and (4.45), it results

$$|\dot{\omega}_i| \leq \frac{R_i\Psi - T_i}{J_i} = f_{3i}(T_i) \qquad i \in \{f, r\} \tag{4.53}$$

Relying on (4.51), (4.52), and (4.53), and assuming, as it is the case in traction manoeuvres, $v > 0$, $\omega_r > 0$, $\omega_f > 0$, and $\lambda_i \in [0, 1)$ one has that

the quantities $\varphi_i^a,\ i \in \{f,r\}$, are bounded. From a physical viewpoint, this means that, when a constant torque $T_i,\ i \in \{f,r\}$, is applied, the second time derivative of the slip ratios is bounded.
To apply a second order sliding mode controller is not necessary that a precise evaluation of φ_i^a is available. It is only assumed that suitable bounds $\Phi_i^a(v_x,\omega_i,T_i)$ of φ_i^a, i.e.,

$$|\varphi_i^a| \ \leq \ \Phi_i^a(v_x,\omega_i,T_i) \qquad i \in \{f,r\} \tag{4.54}$$

are known.
As for the braking case, functions φ_i^b can be obtained following the same procedure described above for the acceleration case. As for φ_i^a, φ_i^b can be regarded as unknown bounded functions with known bounds $\Phi_i^b(v_x,\omega_i,T_i)$, i.e.,

$$|\varphi_i^b| \ \leq \ \Phi_i^b(v_x,\omega_i,T_i) \qquad i \in \{f,r\} \tag{4.55}$$

In order to design a second order sliding mode control law, introduce the auxiliary variables $y_{1,i} = s_i$ and $y_{2,i} = \dot{s}_i$. Then, system (4.49) can be rewritten as

$$\begin{cases} \dot{y}_{1,i} &= y_{2,i} \\ \dot{y}_{2,i} &= \varphi_i^j + h_i^j \dot{T}_i \end{cases} \qquad i \in \{f,r\},\ j \in \{a,b\} \tag{4.56}$$

where $\dot{T}_i$ can be regarded as the auxiliary control input (Bartolini *et al.*, 1997*b*).

Theorem 4.2 *Given system (4.56), where φ_i^j satisfies (4.54) and (4.55), and $y_{2,i}$ is not measurable, the auxiliary control law*

$$\dot{T}_i = -V_i \ \text{sign}\left\{ s_i - \frac{1}{2} s_{iM} \right\} \qquad i \in \{f,r\} \tag{4.57}$$

where the control gain V_i is chosen such that

$$V_i > \begin{cases} 2\Phi_i^a(v_x,\omega_i,T_i)/h_i^a & \textit{acceleration} \\ 2\Phi_i^b(v_x,\omega_i,T_i)/h_i^b & \textit{braking} \end{cases} \qquad i \in \{f,r\} \tag{4.58}$$

and s_{iM} is a piece–wise constant function representing the value of the last singular point of $s_i(t)$ (i.e., s_{iM} is the value of the most recent maximum or minimum of $s_i(t)$), causes the convergence of the system trajectory on the sliding manifold $s_i = \dot{s}_i = 0$ in finite time.

Proof: The control law (4.57) is a sub–optimal second order sliding mode control law. So, by following a theoretical development as that provided in Bartolini *et al.* (1998*b*) for the general case, it can be proved that the trajectories on the $s_i O\dot{s}_i$ plane are confined within limit parabolic arcs including the origin. The absolute values of the coordinates of the trajectory intersections with the s_i, and $\dot{s}_i$ axis decrease in time. As shown in Bartolini *et al.* (1998*b*), under condition (4.58) the following relationships hold

$$|s_i| \leq |s_{iM}|, \qquad |\dot{s}_i| \leq \sqrt{|s_{iM}|}$$

and the convergence of $s_{iM}(t)$ to zero takes place in finite time (Bartolini *et al.*, 1998*b*). As a consequence, the origin of the plane, i.e., $s_i = \dot{s}_i = 0$, is reached in finite since s_i and $\dot{s}_i$ are both bounded by $\max(|s_{iM}|, \sqrt{|s_{iM}|})$. This, in turn, implies that the slip errors $\lambda_{e_i},\ i \in \{f, r\}$, are steered to zero as required to attain the objective of the traction control problem.

4.2.4 The tire/road adhesion coefficient estimate

In order to identify the λ–F_x curve corresponding to the actual road condition, the control task has to estimate the tire/road adhesion coefficient μ_p. Different estimation technique for this parameter have been proposed in literature, most of them are based on the Bakker–Pacejka Magic Formula model. For instance, in Kiencke (1993), a procedure for real–time estimation of μ_p is presented, while in Gustafsson (1997) a scheme for identify different classes of roads with a Kalman filter and a least square algorithm is proposed. In Lee and Tomizuka (2003) a recursive least square algorithm (Ljung, 1999) is adopted to estimate the tire/road adhesion coefficient. A different approach is proposed in Ray (1997) where an extended Kalman filter is used to estimate the forces produced by the tires. A sliding mode observer for the longitudinal stiffnesses is proposed in Drakunov *et al.* (1995) and in M'sirdi *et al.* (2006), while a dynamical tire/road interaction model with a nonlinear observer to estimate the adhesion coefficient is presented in De Wit and Horowitz (1999).

In this subsection a first order sliding mode observer for the on–line estimation of the adhesion coefficient μ_p is designed. The presented observer has good robustness properties against disturbances, modeling inaccuracy and parameter uncertainties. Following the approach proposed in Lee and

Tomizuka (2003), a simplified tire model is considered instead of (4.44), i.e.,

$$F_{xi} = \mu_p f_t(\lambda_i, F_{zi}) \qquad i \in \{f, r\} \tag{4.59}$$

In order to design the sliding mode observer for μ_p, introduce the sliding variable

$$s_\mu = v_x - \hat{v}_x \tag{4.60}$$

where the longitudinal velocity v_x is assumed to be available for measurement and the dynamics of its estimate $\hat{v}_x$ is given by

$$\dot{\hat{v}}_x = \frac{1}{m}(\Omega - F_{loss}(v_x)) \tag{4.61}$$

where

$$\Omega = K\, sign(s_\mu) \tag{4.62}$$

is the control signal of the sliding mode observer.
In the sequel, for notation simplicity, the dependence of the tire force F_x on the slip ratio λ and on the normal force F_z will be omitted.
By differentiating (4.60) and substituting (4.31) one has that

$$\begin{aligned} \dot{s}_\mu &= \dot{v}_x - \dot{\hat{v}}_x = \frac{1}{m}(F_{xf} + F_{xr} - F_{loss}(v_x) - \Omega + F_{loss}(v_x)) \\ &= \frac{1}{m}(F_{xf} + F_{xr} - K\, sign(s_\mu)) \end{aligned} \tag{4.63}$$

In order to attain a sliding mode on the sliding manifold $s_\mu = 0$ in finite time, the gain K in (4.62) must be chosen so that the so–called reaching condition (Edwards and Spurgeon, 1998) is satisfied, i.e.,

$$s_\mu \dot{s}_\mu \leq -\eta |s_\mu| \tag{4.64}$$

where $\eta \in \mathbb{R}^+$. Substituting (4.63) in (4.64) one has that

$$s_\mu \dot{s}_\mu = \frac{1}{m}(F_{xf} + F_{xr} - K\, sign(s_\mu)) s_\mu \leq -\eta |s_\mu| \tag{4.65}$$

From (4.44), the following relationship holds

$$F_{xf} + F_{xr} \leq F_{zf} + F_{zr} = mg \tag{4.66}$$

If gain K in (4.62) is chosen such that

$$K > mg \geq F_{xf} + F_{xr} \tag{4.67}$$

then (4.64) is satisfied and the sliding motion on the sliding surface s_μ takes place in finite time.

The so–called equivalent control, denoted as Ω_{eq}, is defined in Utkin (1992) as the continuous control signal that maintains the system on the sliding surface $s_\mu = 0$ (see Chapter 2). Hence, the equivalent control can be calculated by setting the time derivative of the sliding variable $\dot{s}_\mu$ equal to zero, i.e.,

$$\dot{s}_\mu = \frac{1}{m}(F_{xf} + F_{xr} - \Omega_{eq}) = 0 \tag{4.68}$$

thus the equivalent control Ω_{eq} is given by

$$\Omega_{eq} = F_{xf} + F_{xr} \tag{4.69}$$

Assume that the front and rear wheel are on the same road surface, which is true for many driving situations, then (4.69) can be rewritten as

$$\Omega_{eq} = F_{xf} + F_{xr} = \mu_p[f_{t_f}(\lambda_f, F_{zf}) + f_{t_r}(\lambda_r, F_{zr})] \tag{4.70}$$

The equivalent control Ω_{eq} is close to the slow component of the real control which may be derived by filtering out the high frequency component of Ω using a low pass filter (Utkin, 1992), that is

$$\tau\dot{\hat{\Omega}} + \hat{\Omega} = \Omega \tag{4.71}$$

$$\Omega_{eq} \approx \hat{\Omega} \tag{4.72}$$

where τ is the filter time constant. The filter time constant should be chosen sufficiently small to preserve the slow components of the control Ω undistorted but large enough to eliminate the high frequency component. Thus, the condition $\tau \to 0$ where τ is the filter time constant, and $\delta/\tau \to 0$, where δ is the sample interval, should be fulfilled to extract the slow component equal to the equivalent control and to filter out the high frequency component (Marino and Tomel, 1992).

From (4.70) and (4.72), the estimated tire/road adhesion coefficient $\hat{\mu}_p$ is given by

$$\hat{\mu}_p = \frac{\hat{\Omega}}{f_{t_f}(\lambda_f, F_{zf}) + f_{t_r}(\lambda_r, F_{zr})} \tag{4.73}$$

Note that, from (4.70) and (4.72), one has that

$$\hat{\Omega} = F_{xf} + F_{xr} \tag{4.74}$$

Thus, $\hat{\Omega}$ can be regarded as a sliding mode observer to estimate the total longitudinal force exerted by the vehicle.

4.2.5 The fastest acceleration/deceleration control problem

The particular traction control problem taken into account is the so–called fastest acceleration/deceleration control (FADC) problem. It can be formulated as the problem of maximizing the magnitude of the traction force in order to produce the maximum acceleration while driving and the smallest stopping distance during braking even on possible slippery road.
Looking at the λ–F_x curve in Fig. 4.27, the maximum acceleration can be attained by the steering the slip λ to the value corresponding at the positive peak of the curve, namely λ_{Max}, i.e., considering the i–th axle,

$$\lambda_{d,i} = \lambda_{Max_i} \tag{4.75}$$

Beyond this value, the wheels begin to spin and the longitudinal force produced decrease and the vehicle cannot accelerate as desired. By maximizing the traction force between the tire and the road, the traction controller prevents the wheels from slipping and at the same time improves vehicles stability and steerability.
Similarly, the target slip to obtain the maximum braking force, i.e., the minimum braking distance, is determined as the slip value corresponding at the minimum of the λ–F_x curve, namely λ_{Min}. Thus, the maximum braking force can be attained by the steering the tire slip λ to λ_{Min}, i.e., considering the i–th axle,

$$\lambda_{d,i} = \lambda_{Min_i} \tag{4.76}$$

The position of λ_{Max_i} varies, depending on the actual λ_i–F_{xi} curve considered, and its value is generally unknown during driving. The same hold for λ_{Min_i}. As a consequence, the control task has to include the on–line searching of the peak slip. In the presented approach, this task is accomplished in two step:

1. the tire/road adhesion coefficient μ_p is estimated as described in Section 4.2.4, and the current λ_i–F_{xi} curve is identified.

2. for the acceleration case, the desired slip, i.e., the slip ratio corresponding to the maximum of the curve, is calculated by maximizing the function $\hat{F}_{xi} = f_{ti}(\hat{\mu}_p, \lambda_i, F_{zi})$

$$\lambda_{d,i} = \arg\min_{\lambda_i} \; -\hat{F}_{xi} = \arg\min_{\lambda_i} \; -f_{ti}(\hat{\mu}_p, \lambda_i, F_{zi}) \tag{4.77}$$

Table 4.7: Simulation parameters

Parameter	Value
m	1202 kg
$J_f = J_r$	1.07 kgm^2
l_f	1.15 m
l_r	1.45 m
l_h	0.53 m
c_x	0.4
f_{roll}	0.013
$R_f = R_r$	0.32 m

As for the braking case, the desired slip ratio corresponding to λ_{Min_i} is calculated by minimizing the function $\hat{F}_{xi}$, that is

$$\lambda_{d,i} = \arg\min_{\lambda_i} \quad f_{ti}(\hat{\mu}_p, \lambda_i, F_{zi}) \tag{4.78}$$

Note that, the minimum (maximum) of the function $\hat{F}_{xi}$ can be calculated, for instance, with a minimization algorithm without derivatives (Brent, 1973).

Note that different strategies have been proposed in the literature to find the slip ratio corresponding to the maximum of the λ–F_x curve (see, for instance, Drakunov *et al.* (1995); Haskara *et al.* (2000); Lee and Tomizuka (2003); Hong *et al.* (2006)).

4.2.6 Simulation results

The traction control presented in this section has been tested in simulation, considering a scenario with different road conditions. The vehicle is travelling at an initial velocity $v_x(0) = 20\,\mathrm{m/s}$, with initial slip ratios $\lambda_f(0) = \lambda_r(0) = 0.02$ and the control objective is to achieve the maximum acceleration. The nominal model parameters relevant to the case studied in simulation are indicated in Tab. 4.7 (Genta, 1997). The observer parameters are chosen as $K = 12000$ N, and $\tau = 0.005$ s.
In principle, a value for the control gains $V_i,\ i \in \{f, r\}$, in (4.57) can be

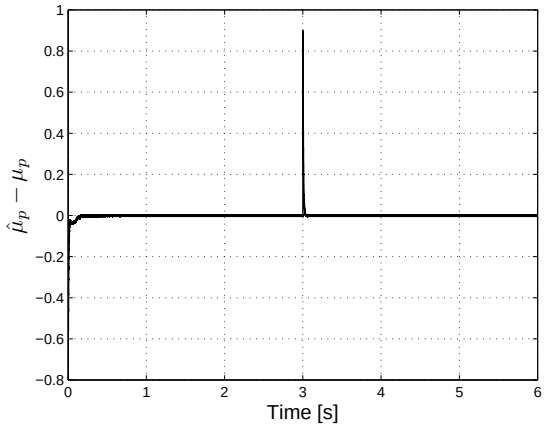

Figure 4.28: The actual road condition estimation error $\hat{\mu}_p - \mu_p$.

found according to (4.58), relying on the knowledge of a suitable value of the bounds Φ_i^a, and Φ_i^b. However, in order to find a less conservative value of the control gain, this parameter has been tuned relying on simulation results, by choosing $V_i,\ i \in \{f, r\}$, sufficiently high in order to guarantee the convergence to the sliding manifolds and good performances. Relying on this latter approach, the chosen value of the control gains are $V_f = V_r = 8000$ N/ms.
In the simulated scenario, the road condition is assumed to change at 3 s from dry asphalt ($\mu_p(dry) = 0.85$) to icy asphalt ($\mu_p(ice) = 0.1$). As shown in Fig. 4.28 the tire/road adhesion coefficient μ_p is correctly estimated with the presented sliding mode observer.
As described in Subsection 4.2.5, the desired slip ratios, $\lambda_{d,i},\ i \in \{f, r\}$, is calculated according to (4.77), i.e.,

$$\lambda_{d,i} = \arg\min_{\lambda_i} \quad -f_{ti}(\hat{\mu}_p, \lambda_i, F_{zi}) \qquad i \in \{f, r\}$$

Fig. 4.29 shows the time evolution of the desired slip ratio $\lambda_{d,f}$, and of the slip ratio λ_f for the front wheel obtained via the presented controller. The same quantities for the rear wheel are reported in Fig. 4.30. As one can note, after a finite time the slip of each wheels correctly tracks the desired value. This implies that the sliding quantities s_f and s_r are steered to zero in finite time as shown in Fig. 4.31. As can be seen in Fig. 4.32, the acceleration of the vehicle decreases at $t = 3$ s when the adhesion coefficient

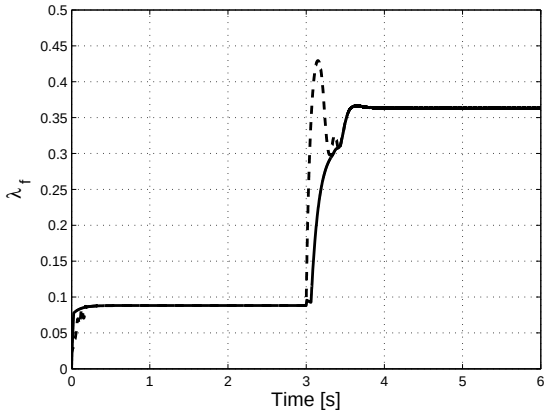

Figure 4.29: Time evolution of $\lambda_{d,f}$ (solid), and λ_f (dashed).

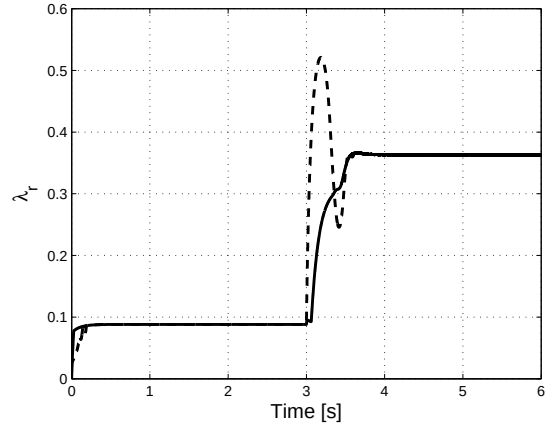

Figure 4.30: Time evolution of $\lambda_{d,r}$ (solid), and λ_r (dashed).

changes from 0.85 to 0.1 (from dry asphalt to icy road). This is due to the fact that the maximum acceleration that the vehicle can produce in the second part of the road (icy road) is lower than in the first part of the road (dry asphalt). Figs. 4.33 and 4.34 show the evolution of the control variables T_f and T_r, respectively, which, as expected, are continuous. Note that T_f is slowly decreasing while λ_f is constant due to the weight transfer (4.35)–(4.36). The opposite effect can be noted for T_r.

In order to exploit the robustness feature of the control scheme, the

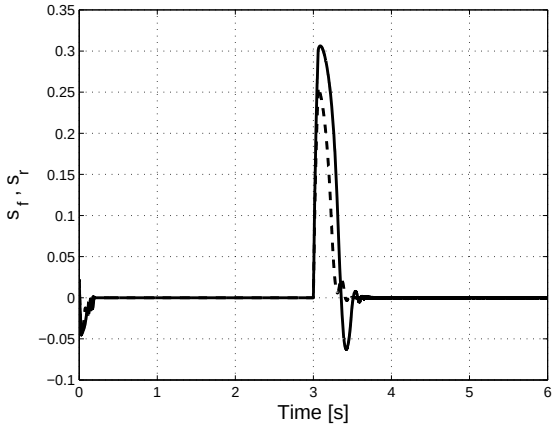

Figure 4.31: The sliding variables s_f (dashed), and s_r (solid).

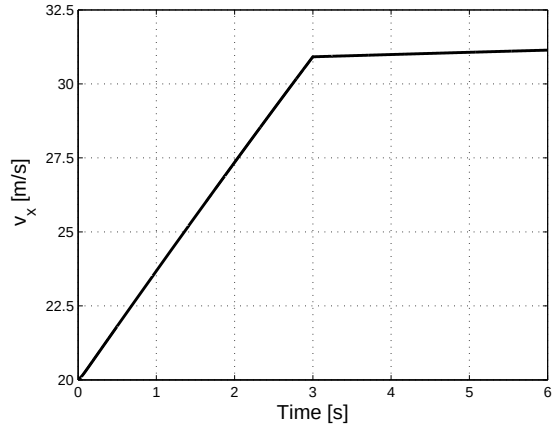

Figure 4.32: The time evolution of the longitudinal velocity v_x.

controlled system is tested in simulation in presence of model uncertainties and disturbances, and is compared with a first order sliding mode solution where the $sign(\cdot)$ function is approximated with the $sat(\cdot)$ function as in Lee and Tomizuka (2003).
The nominal model parameters are as in Tab. 4.7, while the real values for the mass, the wheels moment of inertia, and the wheels radius are $m = 1702$ kg, $J_f = J_r = 1.8$ kgm^2, and $R_f = R_r = 0.5$ m, respectively. Moreover, to

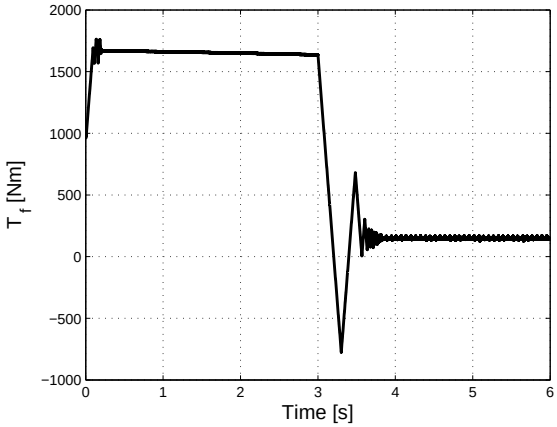

Figure 4.33: The control variable T_f.

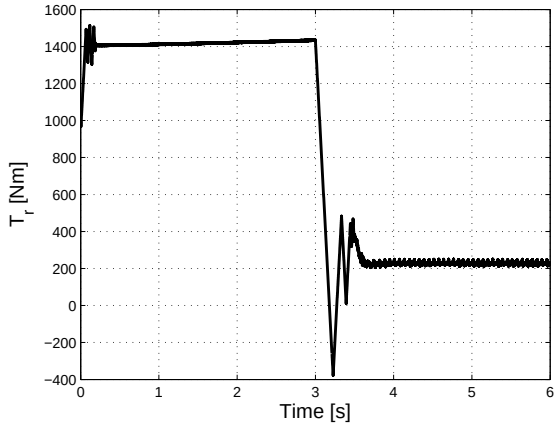

Figure 4.34: The control variable T_r.

model some matched disturbances, the real control input is calculated as

$$T_i(t) = \bar{T}_i(t) + A\sin(t) \quad i \in \{f, r\} \tag{4.79}$$

where $\bar{T}_i$ is the nominal control input given by (4.57), and A is the amplitude of the disturbances acting on the control input.
Figs. 4.36 and 4.35 show the simulation results obtained with the presented second order sliding mode control scheme, with $A = 300$ in (4.79). As expected, the presented control scheme results robust against parameter

uncertainties and matched disturbances. One can note that the tire/road adhesion coefficient is correctly estimated as shown in Fig. 4.36, and the sliding quantities s_f and s_r are steered to zero in finite time (see Fig. 4.35).

The simulation results for different values of the disturbances amplitude A

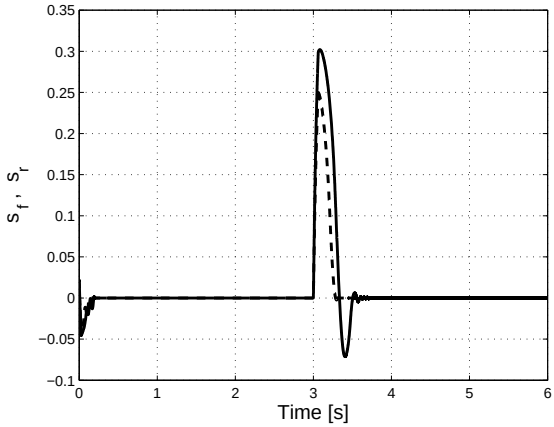

Figure 4.35: The time evolution of the sliding variables s_f (dashed), and s_r (solid) in presence of disturbances ($A = 300$ in (4.79)), and model uncertainties.

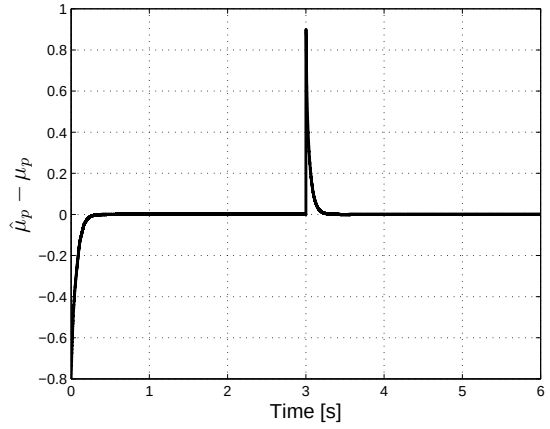

Figure 4.36: The road condition estimation error in presence of disturbances ($A = 300$ in (4.79)), and model uncertainties.

are reported in Table 4.8, where $SM1$ and $SM2$ stand for first order sliding mode controller and second order sliding mode controller, respectively, and MSE is the mean square error of the mean value of the slip errors, i.e., $s_i,\ i \in \{f, r\}$. As one can note, apart from the benefit due to the rise of continuous control actions, the presented controller also provides better performances with respect to the approximated first order sliding mode controller.

Table 4.8: Performance indexes

Controller	MSE	A
$SM1$	$1.4622 \cdot 10^{-3}$	100
$SM2$	$2.3022 \cdot 10^{-6}$	100
$SM1$	$1.8525 \cdot 10^{-3}$	200
$SM2$	$2.9251 \cdot 10^{-6}$	200
$SM1$	$2.7466 \cdot 10^{-3}$	300
$SM2$	$5.6467 \cdot 10^{-6}$	300
$SM1$	$3.0188 \cdot 10^{-3}$	400
$SM2$	$5.7753 \cdot 10^{-6}$	400

4.2.7 Conclusions and future works

A second order sliding mode traction force controller for vehicles has been presented in this section. The controller is capable of enforcing second order sliding modes, thus attaining the traction force control objective, by directly forcing to zero the slip errors in a finite time by means of a continuous control law.

The coupling of the presented controller with a suitably designed sliding mode observer, which enables to estimate on–line the tire–road adhesion coefficient, makes the described approach insensitive to possible variations of the road conditions. Simulations results have demonstrated the possible effectiveness of the described control system even in presence of disturbances and parameter uncertainties. Moreover, the second order sliding mode control scheme provides for a higher accuracy with respect to first order sliding mode.

Future work needs to be devoted to discuss and verify the coupling of the presented traction force controller with throttle angle and brake controllers, taking into account the actuators dynamics, as well as vehicle pitch dynamics.

4.3 Traction Control for Sport Motorcycles

In this section the analysis and design of a safety-oriented traction control system for ride-by-wire sport motorcycles based on the Second Order Sliding Mode (SOSM) methodology is addressed. The controller design is based on a nonlinear dynamical model of the rear wheel slip, and the modeling phase is validated against experimental data measured on an instrumented vehicle. To comply with practical applicability constraints, the position of the electronic throttle body is used as control variable and the effect of the actuator dynamics is thoroughly analyzed. After a discussion on the interplay between the controller parameters and the tracking performance, the final design effectiveness is assessed via MSC BikeSim®, a full-fledged commercial multibody motorcycle model.

Part of this section is taken from Vecchio *et al.* (2008) and Vecchio *et al.* (2009).

4.3.1 Introduction and Motivation

Nowadays, four-wheeled vehicles are equipped with many different active control systems which enhance driver's and passengers' comfort and safety. In the field of two-wheeled vehicles, instead, the development of electronic control systems is still in its infancy. However, the importance of active control for traction and braking has been recently recognized also for motorcycles (Corno *et al.*, 2008*b*). The motivation for this is twofold: on one hand, in the racing context, these systems are designed to enhance vehicle performance; on the other hand, in the production context, the same control systems are intended to enhance the safety of non-professional bikers, whose number is steadily increasing mainly due to traffic congestion and high oil price.

Little or no previous work has been done on the problem of rear wheel slip dynamics analysis and Traction Control (TC) for two-wheeled vehicles, whereas the same problem has been addressed on four-wheeled vehicles (see Section 4.2). TC increases safety and performance by controlling the slip of the rear (driving) wheel. As is well known, the wheel slip is related to the force exerted by the tire via the friction curves (Kiencke and Nielsen, 2000; Cossalter, 2002). By keeping the slip of the tire at the peak of the longitudinal curve, one achieves the best performance and, at the same

Figure 4.37: The acceleration phase during the final part of a curve: a critical condition where a TC system can help the rider obtaining the best performance (Philip Island 2008 - SBK World Championship).

time, improves safety (see Fig. 4.37). If the peak is surpassed there is only a marginal loss of longitudinal force but a dramatic loss of lateral force, which could cause a fall during cornering.
Consider Fig. 4.38, which shows a schematic view of the overall TC problem for motorbikes. As can be seen, the control problem in its most general view is comprised of three different control sub-problems.

The first one (see the dashed oval box with label ① in Fig. 4.38) concerns the servo-control of the Electronic Throttle Body (ETB), which is the considered actuator. Note that electronic control of throttle in motorbikes has been only recently introduced (Beghi *et al.*, 2006; Corno *et al.*, 2008*a*); before the introduction of such a technology, engine torque was (and still is) mainly modulated via spark advance control. By anticipating or delaying the spark in the cylinders, it is possible to control the generated torque. Thus, the control sub-problem ① in Fig. 4.38 could in principle need to address spark advance control, or, in a more sophisticated system, a combination of spark advance and ETB control, as it is commonly done in F1 cars.

Once the actuator controller has been designed, an outer loop for controlling the rear wheel slip needs to be designed (dashed oval box with label ② in Fig. 4.38). This step, which has been addressed for four-wheeled vehicles in Section 4.2, has not yet been treated in the literature for motorbikes and constitutes the main topic of this section. However, even though it constitutes the most important task to be solved for TC control, rear wheel slip control is not the last design step. In fact, as shown in Fig. 4.38, the

slip controller needs a target wheel slip to track. In two-wheeled vehicles, when moving in a curve, there is a trade–off between longitudinal and lateral forces (see e.g., Sharp *et al.* (2004)). When on a curve, in fact, a TC system should provide the largest possible amount of longitudinal force for transferring the traction torque to the ground, while guaranteeing sufficient lateral force for negotiating the curve.

Thus, the last building block of a TC system (dashed oval box with label ③ in Fig. 4.38) is a supervisory unit which, based on a measure or an estimation of the roll angle, selects the optimal target slip. The roll angle estimation with low-cost sensors is still an open problem (first results on this topic can be found in Boniolo *et al.* (2008)), so that the supervisory block ③ for TC systems has not yet been addressed in the literature for motorbikes and is topic of ongoing research.

Note that, as far as control systems design is concerned, dealing with motorcycle dynamics is far more subtle than dealing with for four-wheeled vehicles. In fact, it is common practice to design most active control systems for cars based on simplified dynamical models (e.g., the quarter-car model and the half-car model for braking control systems and the single-track model for active stability control (Kiencke and Nielsen, 2000)), while complete vehicle models are employed mostly for testing and validation phases. In two-wheeled vehicles, instead, the presence of a single axle, together with the peculiar suspensions, steer and fork geometry, makes it difficult to devise appropriate simplified models.

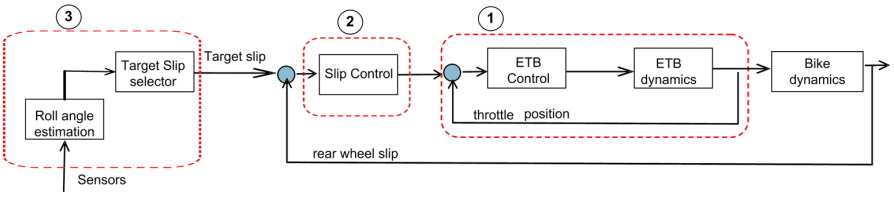

Figure 4.38: A schematic view of the overall TC problem.

Hence, the effort of analyzing well-defined driving conditions seems to be the key for a comprehensive understanding of motorcycles dynamics. Such an approach is well confirmed in the scientific literature of this field (see Sharp (1971); Cossalter *et al.* (1999); Limebeer *et al.* (2001); Sharp (2001); Sharp and Limebeer (2001); Cossalter *et al.* (2004)). Note that, although this approach is well suited for dynamic analysis, it may not be easily used

for control systems design, as its results are strongly dependent on many (uncertain) system parameters, and this makes it difficult to validate them on a real vehicle.

In this section the analysis and design of a safety-oriented rear wheel slip control system for ride-by-wire sport motorcycles is carried out relying on the so-called Second Order Sliding Mode (SOSM) approach.

The contents of this section are as follows. For controller design, a simple yet adequate analytical model of the rear wheel slip is derived in Subsection 4.3.2. Then, the SOSM controller is designed in Subsection 4.3.3 based on the wheel slip dynamical model only, disregarding, in this phase, the actuator dynamics, so as to work on a model with relative degree equal to one. This allows to obtain, thanks to the presented control approach, a continuous control variable. Further, Subsection 4.3.4 investigates the real traction dynamics by means of experimental data measured on an instrumented vehicle, and discusses the analytical model validation. Finally, in Subsection 4.3.5 a simulation study is presented to investigate the closed-loop properties in presence of the actuator dynamics and to assess the validity of the presented approach on MSC BikeSim®, an accurate commercial multibody motorcycle model.

4.3.2 Dynamical Model

For the preliminary design of traction control algorithms in motorcycles, the rear wheel slip dynamics need to be modeled. To this aim, focusing on straight-line traction manoeuvres, the following dynamical model can be employed

$$J_r\dot{\omega}_r = -r_r F_{x_r} + T \tag{4.80}$$

$$J_f\dot{\omega}_f = -r_f F_{x_f} \tag{4.81}$$

$$m\dot{v} = F_{x_r} + F_{x_f} \tag{4.82}$$

where ω_f and ω_r are the angular speeds of the front and rear wheel, respectively, v is the longitudinal speed of the vehicle body, T is the driving torque, F_{x_f} and F_{x_r} are the front and rear longitudinal tire-road contact forces, $J_f = J_r = J$, m and $r_f = r_r = r$ are the wheel inertias, the vehicle mass, and the wheel radii, respectively. Note that, for simplicity, the front and rear wheel inertias and the wheel radii are assumed to be equal and

indicated with J and r, respectively. The system is nonlinear due to the dependence of F_{x_i}, $i = \{f, r\}$, on the state variables v and ω_i, $i = \{f, r\}$. The expression of F_{x_i} as a function of these variables is involved and influenced by a large number of features of the road, tire, and suspension; however, it can be well-approximated as follows (see Kiencke and Nielsen (2000))

$$F_{x_i} = F_{z_i}\, \mu(\lambda_i, \beta_{i_t}; \vartheta), \quad i = \{f, r\} \tag{4.83}$$

where F_{z_i} is the vertical force at the tire-road contact point and $\mu(\cdot, \cdot; \vartheta)$ is a function of

- the longitudinal slip $\lambda_i \in [0, 1]$, which, during traction, is defined as

$$\lambda_i = \frac{\omega_i r - v}{\omega_i r} \tag{4.84}$$

- the wheel side-slip angle β_{i_t}.

Vector ϑ in $\mu(\cdot, \cdot; \vartheta)$ represents the set of parameters that identify the tire-road friction condition. Since for traction manoeuvres performed along a straight line one can set the wheel side-slip angle equal to zero ($\beta_{i_t} = 0$), the dependence of F_{x_i} on β_{i_t} can be omitted and the μ function can be denoted as $\mu(\cdot; \vartheta)$.

Remark 4.1 *It is worth mentioning that the results presented in this section remain valid even in the case when $\beta_{i_t} = 0$. In fact, changes in β_{i_t} cause a shift in the peak position of the $\mu(\cdot; \vartheta)$ curve and act as a scaling factor (in this resembling the effect of changes in the vertical load). Accordingly, as the controller is designed assuming no knowledge both of the current road conditions and of the value of the vertical load, it can handle non-zero values of β_{i_t}.*

Many empirical analytical expressions for function $\mu(\cdot; \vartheta)$ have been proposed in the literature. A widely-used expression (see Kiencke and Nielsen (2000)) is

$$\mu(\lambda; \vartheta) = \vartheta_1(1 - e^{-\lambda\vartheta_2}) - \lambda\vartheta_3 \tag{4.85}$$

where ϑ_i, $i = 1, 2, 3$, are the three components of vector ϑ. By changing the values of these three parameters, many different tire-road friction conditions can be modeled. In Fig. 4.39 the shape of $\mu(\lambda; \vartheta)$ in four different conditions is displayed.

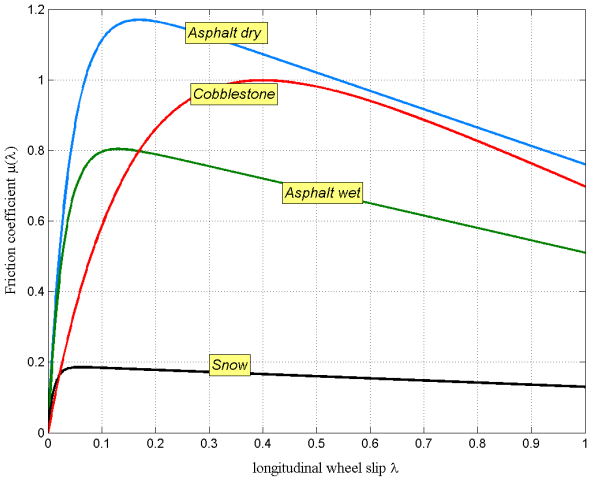

Figure 4.39: Behaviour of the function $\mu(\lambda;\vartheta)$ in different road conditions.

From now on, for ease of notation, the dependency of μ on ϑ will be omitted, and the function in equation (4.85) will be referred to as $\mu(\lambda)$. Note that from (4.85) one has that the longitudinal force produced by a wheel is bounded, i.e.,

$$|F_{xi}| \leq \Psi, \qquad i \in \{f, r\} \tag{4.86}$$

The tire model (4.85) is a steady–state model of the interaction between the tire and the road. As for the transient tire behaviour it is assumed that, being it due to tire relaxation dynamics (Kiencke and Nielsen, 2000) the traction forces F_{xi} have a bounded first time derivative, i.e.,

$$|\dot{F}_{xi}| \leq \Gamma, \qquad i \in \{f, r\} \tag{4.87}$$

By employing system (4.80)–(4.82), it is important to highlight the rear wheel slip dynamics. To this aim, in order to use the wheel slip definition in (4.84), a measure or a reliable estimate of the vehicle speed is needed. As is discussed in Tanelli *et al.* (2008*b*) for the case of braking control, vehicle speed estimation for two-wheeled vehicle is an open problem.

For traction control purposes, however, the problem of vehicle speed estimation is eased by the fact that the only driven wheel is the rear one, so that, in principle, the front wheel linear speed should provide a reasonable

estimate of the vehicle speed. Again, the suspension and pitch dynamics, which in two-wheeled vehicles are much more coupled with longitudinal dynamics than they are in cars, should warn that the use of the front wheel speed might provide non precise speed estimates in very strong acceleration phases. However, as in practice no alternative (or more accurate) vehicle speed estimate has been made available yet, the definition of the *relative* rear wheel slip is introduced, namely

$$\lambda_{r,r} = \frac{\omega_r r - \omega_f r}{\omega_r r} \tag{4.88}$$

which is nothing but equation (4.84) with $\omega_f r$ replacing v. This quantity is what can be actually measured on commercial motorbikes. Along this line, the *absolute* rear wheel slip $\lambda_{r,a}$ is defined as the quantity computed as in (4.84) using the true vehicle speed v.

In what follows it is assumed that the longitudinal dynamics of the vehicle (expressed by the state variable v) are significantly slower than the rotational dynamics of the wheels (expressed by the state variables λ_i or ω_i) due to the differences in inertia. Henceforth, v is considered as a slowly time-varying parameter when analyzing the evolution in time of λ_i (see e.g., Johansen *et al.* (2003); Tanelli *et al.* (2008*a*)). Under this assumption, equation (4.82) (center of mass dynamics) is neglected, and the model reduces to that of the wheels dynamics only. Further, in system (4.80)–(4.82) the state variables are v and ω_i. As λ_i, v and ω_i are linked by the algebraic equation (4.84), it is possible to replace ω_i with λ_i as state variable. Specifically, let us analyze the *absolute* rear wheel slip $\lambda_{r,a}$. Considering equations (4.80) and (4.82) (the front wheel dynamics (4.81) only affect the vehicle speed equation in the driving torque to rear slip dynamic relation), and considering the absolute slip definition in (4.84) together with the longitudinal force description in (4.83), the absolute rear wheel slip dynamics can be written as

$$\begin{aligned} \dot{\lambda}_{r,a} = \frac{v}{\omega_r^2 r}\dot{\omega}_r - \frac{1}{\omega_r r}\dot{v} \;\; = \;\; & -\frac{(1-\lambda_{r,a})^2 r}{Jv}\Big\{ [rF_{z_r}\mu(\lambda_{r,a}) - T] \\ & + \frac{J}{r\,m\,(1-\lambda_{r,a})}\left(F_{z_r}\mu(\lambda_{r,a}) + F_{z_f}\mu(\lambda_f)\right)\Big\} \end{aligned} \tag{4.89}$$

In Subsection 4.3.3, the SOSM controller will be designed taking into account the absolute wheel slip dynamics. However, its intrinsic robustness properties allow to employ the same controller also when the relative wheel

slip is used as controlled variable, as will be shown in Subsection 4.3.5.
Even though the SOSM controller is designed based on the nonlinear wheel slip dynamics, in order to be able to validate the analytical model against the frequency response estimates obtained on the basis of experimental data collected on an instrumented vehicle (see Section 4.3.4), the slip dynamics is linearized so as to obtain a transfer function description.
To this aim, the absolute slip dynamics in (4.89) is considered and the system equilibria are computed. Thus, $\dot{\lambda}_{r,a} = 0$ is considered and the equilibrium points characterized by a constant longitudinal slip value $\lambda_{r,a} = \bar{\lambda}_{r,a}$ are computed (note that the equilibrium characterized by $\mu(\lambda) = 0$ and $T = 0$ is meaningless for traction control purposes as it corresponds to the coasting-down condition with no torque applied). From equation (4.89) it is easy to find that the equilibrium values for the driving torque T are given by

$$\bar{T} = rF_{z_r}\mu(\bar{\lambda}_{r,a}) + \frac{J}{rm(1-\lambda_{r,a})}\left(F_{z_r}\mu(\lambda_{r,a}) + F_{z_f}\mu(\lambda_f)\right) \tag{4.90}$$

According to the assumption of regarding v as a slowly varying parameter, the model is linearized around an equilibrium point defined by $\delta T = T - \bar{T}$ and $\delta\lambda_{r,a} = \lambda_{r,a} - \bar{\lambda}_{r,a}$. Defining the slope of the $\mu(\lambda)$ curve around an equilibrium point as

$$\mu_1(\bar{\lambda}) := \left.\frac{\partial\mu(\lambda)}{\partial\lambda}\right|_{\lambda=\bar{\lambda}}$$

the linearized absolute wheel slip dynamics have the form

$$\begin{aligned}\dot{\delta\lambda}_{r,a} \;=\; & \left\{\frac{F_{z_r}}{\bar{v}}\left[\frac{2(1-\bar{\lambda}_{r,a})}{J}r^2 + \frac{1}{m}\right]\mu(\bar{\lambda}_{r,a})\right. \\ & + \left[\frac{(1-\bar{\lambda}_{r,a})^2 F_{z_r}}{\bar{v}}\left(\frac{r^2}{J}+\frac{1}{m}\right)\right]\mu_1(\bar{\lambda}_{r,a}) \\ & \left. + \frac{\bar{\lambda}_{r,a}}{m\bar{v}}F_{z_f}\mu(\bar{\lambda}_f) - \frac{2(1-\bar{\lambda}_{r,a})r}{J\bar{v}}\bar{T}\right\}\delta\lambda_{r,a} + \frac{(1-\bar{\lambda}_{r,a})^2 r^2}{\bar{v}}\delta T\end{aligned} \tag{4.91}$$

From the linearized dynamics (4.91) it is immediate to derive the expression of the first-order transfer function $G_{\lambda_{r,a}}(s)$, which will be employed in Subsection 4.3.4 for model validation against experimental data.

4.3.3 The traction controller design

The SOSM controller will be designed based on the nonlinear absolute rear slip dynamics only, disregarding the actuator dynamics (see Subsec-

tion 4.3.4). This allows us to work on a plant model with relative degree one, thus exploiting the possibility of designing a continuous control law. The effect of the actuator dynamics will be taken into account in the simulations, and its impact on the closed-loop system analyzed in Subsection 4.3.5. The traction controller is designed to make the rear wheel slip $\lambda_{r,a}$ tracks the desired value λ_r^*. The error between the current slip and the desired slip is chosen as the sliding variable, i.e.,

$$s_{r,a} = \lambda_{r,a} - \lambda_r^* \tag{4.92}$$

and the control objective is to design a continuous control law $\mathcal{T}$ capable of steering this error to zero in finite time. Then, the chosen sliding manifold is given by

$$s_{r,a} = 0 \tag{4.93}$$

The first and second derivatives of the sliding variable $s_{r,a}$ are

$$\left\{ \begin{array}{lcl} \dot{s}_{r,a} & = & \dot{\lambda}_{r,a} - \dot{\lambda}_{r,a}^* \\ \ddot{s}_{r,a} & = & \varphi_{r,a} + h_{r,a}\dot{\mathcal{T}}_r \end{array} \right. \tag{4.94}$$

where $\dot{\lambda}_{r,a}$ is given by (4.89), and h_r and φ_r are defined as

$$h_{r,a} := \frac{v}{J\omega_r^2 r} = \frac{(1-\lambda_{r,a})^2 r}{Jv} \tag{4.95}$$

$$\begin{aligned} \varphi_{r,a} &:= -\frac{\ddot{v}}{r\omega_r} + 2\frac{\dot{v}\dot{\omega}_r}{r\omega_r^2} - 2\frac{v\dot{\omega}_r^2}{r\omega_r^3} - \ddot{\lambda}_{r,a}^* - \frac{v\dot{F}_{x_r}}{J\omega_r^2} \\ &= \frac{r(1-\lambda_{r,a})^2}{Jv}\left\{ \frac{2(-rF_{x_r}+T)}{v}[m(F_{x_f}+F_{x_r}) \right. \\ &\quad -r(1-\lambda_{r,a})(-rF_{x_r}+T)] - r\dot{F}_{x_r} \\ &\quad \left. -\frac{J(\dot{F}_{x_r}+\dot{F}_{x_f})}{rm(1-\lambda_{r,a})} \right\} - \ddot{\lambda}_{r,a}^* \end{aligned} \tag{4.96}$$

Combining (4.82) with (4.86), it yields

$$|\dot{v}| \leq \frac{2\Psi}{m} = f_1 \tag{4.97}$$

Further, taking into account the first time derivative of (4.82), (4.87), and (4.97), one has that

$$|\ddot{v}| \leq \frac{2\Gamma}{m} = f_2 \tag{4.98}$$

Finally, from equations (4.80) and (4.86), it results

$$|\dot{\omega}_r| \leq \frac{-r\Psi + T}{J} = f_3(T) \tag{4.99}$$

Relying on (4.97), (4.98), and (4.99), and assuming, as it is the case in traction manoeuvres, $v > 0$, $\omega_r > 0$ and $\lambda_{r,a} \in [0, 1)$ one has that $\varphi_{r,a}$ is bounded. From a physical viewpoint, this means that, when a constant driving torque T is applied, the second time derivative of the rear wheel slip is bounded.
Note that in order to design a SOSM controller it is not necessary that a precise evaluation of $\varphi_{r,a}$ is available. It is only assumed that a suitable bound of $\varphi_{r,a}$, i.e., $\Phi_r(v, \omega_r, T)$ such that

$$|\varphi_{r,a}| \quad \leq \quad \Phi_r(v, \omega_r, T) \tag{4.100}$$

is known. Similar considerations can be made for $h_{r,a}$ which can be regarded as an unknown bounded function with the following known bounds

$$0 < \Gamma_{r1}(v, \omega_r) \leq h_{r,a} \leq \Gamma_{r2}(v, \omega_r) \tag{4.101}$$

In order to design a second order sliding mode control law, introduce the auxiliary variables $y_1 = s_{r,a}$ and $y_2 = \dot{s}_{r,a}$. Then, system (4.94) can be rewritten as

$$\begin{cases} \dot{y}_1 &= y_2 \\ \dot{y}_2 &= \varphi_{r,a} + h_{r,a}\dot{\mathcal{T}} \end{cases} \tag{4.102}$$

where $\dot{\mathcal{T}}$ can be regarded as an auxiliary control input (Bartolini *et al.*, 1999). As a consequence, the control problem can be reformulated as follows: given system (4.102), where $\varphi_{r,a}$ and $h_{r,a}$ satisfy (4.100) and (4.101), respectively, and y_2 is unavailable for measurement, design the auxiliary control signal $\dot{\mathcal{T}}$ so as to steer y_1, y_2 to zero in finite time.
Under the assumption of being capable of detecting the extremal values s_{rM} of the signal $y_1 = s_{r,a}$, the following result can be proved.

Theorem 4.3 *Given system (4.102), where $\varphi_{r,a}$ and $h_{r,a}$ satisfy (4.100) and (4.101), respectively, and y_2 is not measurable, the auxiliary control law*

$$\dot{\mathcal{T}} = -\eta V_r \ \text{sign}\left(s_{r,a} - \frac{1}{2}s_{rM}\right) \tag{4.103}$$

$$\eta = \begin{cases} \eta^* & \textit{if} \quad [s_{r,a} - s_{rM}/2]s_{rM} > 0 \\ 1 & \textit{if} \quad [s_{r,a} - s_{rM}/2]s_{rM} \leq 0 \end{cases}$$

where V_r is the control gain, η is the so–called modulation factor, and s_{rM} is a piece–wise constant function representing the value of the last singular point of $s_r(t)$ (i.e., the most recent value s_{rM} such that $\dot{s}_{r,a}(t_M) = 0$), causes the convergence of the system trajectory to the sliding manifold $s_{r,a} = \dot{s}_{r,a} = 0$ in finite time, provided that the control parameters η^* and V_r are chosen so as to satisfy the following constraints

$$\eta^* \in (0,1] \cap \left(0, \frac{3\Gamma_{r1}}{\Gamma_{r2}}\right) \tag{4.104}$$

$$V_r > \max\left\{\frac{\Phi_r}{\eta_r^*\Gamma_{r1}}, \frac{4\Phi_r}{3\Gamma_{r1} - \eta^*\Gamma_{r2}}\right\} \tag{4.105}$$

Proof: The control law (4.103) is a sub–optimal second order sliding mode control law. So, by following a theoretical development as that provided in Bartolini *et al.* (1998*b*) for the general case, it can be proved that the trajectories on the $s_{r,a}O\dot{s}_{r,a}$ plane are confined within limit parabolic arcs including the origin. The absolute values of the coordinates of the trajectory intersections with the $s_{r,a}$, and $\dot{s}_{r,a}$ axis decrease in time. As shown in Bartolini *et al.* (1998*b*), under condition (4.104) the following relationships hold

$$|s_{r,a}| \leq |s_{rM}|, \qquad |\dot{s}_{r,a}| \leq \sqrt{|s_{rM}|}$$

and the convergence of $s_{rM}(t)$ to zero takes place in finite time (Bartolini *et al.*, 1998*b*). As a consequence, the origin of the plane, i.e., $s_{r,a} = \dot{s}_{r,a} = 0$, is reached in finite since $s_{r,a}$ and $\dot{s}_{r,a}$ are both bounded by $\max(|s_{rM}|, \sqrt{|s_{rM}|})$. This, in turn, implies that the traction control objective is attained.

Finally, note that in the automotive context one needs the designed controller to provide acceptable performance also in presence of disturbances and measurement errors. As is well known, SM control is very attractive to deal with uncertain systems, but its formulation allows to formally take into account only the so-called matched disturbances (see Chapter 3). However, in the considered application, one has to handle also measurements errors, i.e., unmatched disturbances. Thus, in order to obtain better performance in the presence of unmatched disturbances an error prefiltering block have been added to the controller. Specifically, the sliding variable (4.92) is low pass filtered via a first order filter with a cut-off frequency of

30 Hz. Note that the filter bandwidth is much higher than that of the wheel dynamics (which ranges from approximately 5 to 10 Hz, depending on the vehicle speed), so that there is no significant performance degradation due to filtering-induced delay. A comparison of the SOSM controller performance with and without error prefiltering in presence of both matched and unmatched disturbances will be shown in Subsection 4.3.5.

4.3.4 The complete motorcycle traction dynamics

To better evaluate the suitability for TC design of the dynamical model presented in Subsection 4.3.2, it is compared with the data collected on a hypersport motorbike which has been used to perform experiments tailored to the identification of actual rear wheel slip dynamics. The considered motorbike is propelled by a 1000cc 4-stroke engine; it weights about 160 kg (without rider) and can deliver more than 200 HP. For confidentiality reasons other details of the motorbike are kept undisclosed. The vehicle is equipped with

- an Electronic Throttle Body (ETB) which allows to electronically control the position of the throttle valve independently of the rider's request;
- an Electronic Control Unit (ECU) that allows to control the throttle. The clock frequency of the ECU is 1 kHz;
- two wheel encoders to measure the wheels angular velocity;
- a 1-dimensional optical velocity sensor. This sensor measures the true longitudinal velocity and it will be used to compute the instantaneous absolute rear wheel slip.

4.3.4.1 Signal processing

The main issues related with the signal processing phase needed to employ the measured signals for the identification of the rear wheel slip dynamics is now presented.

Rolling Radius Calibration
To estimate the linear wheel velocity the rolling radius of the wheel is

needed; the rolling radius can be estimated, using the optical velocity sensor, with a coasting down test. The test consists of a slow deceleration with the transmission disengaged. In this way, the wheel slip can be assumed to be null; all the braking force can be attributed either to aerodynamic drag or rolling friction. The true velocity reading, as measured by the optical head, can be used to calibrate the rolling radius by solving the following minimization problems

$$r_f = \underset{r_f}{\operatorname{argmin}} \int_{t_0}^{t_1} |\omega_f r_f - v_{true}| \, dt$$
$$r_r = \underset{r_r}{\operatorname{argmin}} \int_{t_0}^{t_1} |\omega_r r_r - v_{true}| \, dt$$

This calibration provides all the elements needed to have an accurate estimate of the linear velocity of the wheels.

Optical Velocity Sensor
The optical sensor is equipped with a built-in moving average filter with a window of 128 ms; the filter has the effect of a low pass filter with a bandwidth of around 3.5 Hz. The filter introduces a phase shift in the velocity signal; all the other signals, not being filtered, have no phase shift. In order to rigorously solve this issue, all the signals should be filtered by the same moving average filter; this is not feasible because it would filter all the frequencies above 4 Hz, removing most of the interesting dynamics. Filtering the longitudinal velocity at 4 Hz does not remove any interesting dynamics because the longitudinal velocity of the vehicle is slower than the slip dynamics. This problem is approximately solved by delaying all the signals of 64 ms; it is trivial to show that the phase shift introduced by the moving average filter is equivalent to a pure delay of 64 ms up to 8 Hz.

4.3.4.2 Experimental Identification

In order to identify the slip dynamics, a frequency sweep response has been employed. The test was carried out on a 3.5 km straight dry asphalt patch; the rider is asked to bring the motorcycle to a given constant engine speed in a given gear. After steady state conditions are reached, the rider presses a button which starts the test. The throttle control is taken over by the ECU and the excitation signal (a frequency sweep) is applied around the neighborhood of the initial condition. In the following, reference is made

to the absolute rear wheel slip $\lambda_{r,a}$, which is defined as in (4.84). Fig. 4.40 shows the set-point and output throttle position, the engine speed variation and the rear wheel slip measured during a frequency sweep test. For confidentiality reasons, the time scale is omitted.

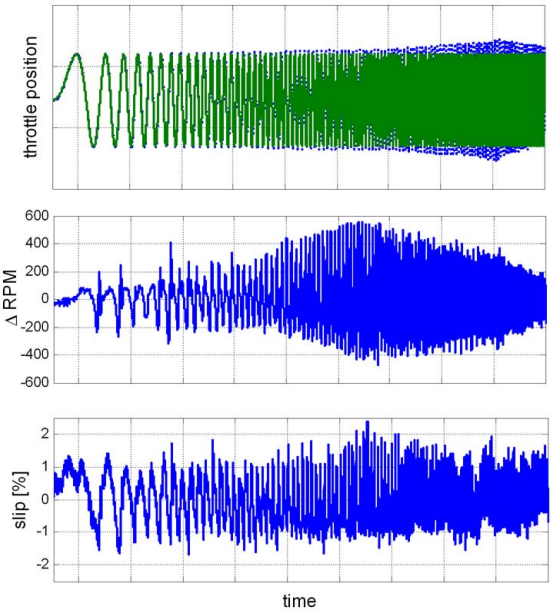

Figure 4.40: Plot of (top): throttle position set point (solid line) and throttle output position (dotted line); (middle) engine speed variation; (bottom) absolute rear wheel slip.

From the experiments, the throttle set point position θ^o and the absolute rear wheel slip $\lambda_{r,a}$ are recorded to estimate the frequency response $\hat{G}_{\lambda_{r,a}}(j\omega)$. Such a non parametric estimate of the frequency response is obtained by windowed spectral analysis of the input/output cross-spectral densities (Pintelon and Schoukens, 2001) and is shown with the dashed line in Fig. 4.41. For confidentiality reasons, the frequencies in Fig. 4.41 are shown normalized with respect to the closed loop frequency of the servo-loop throttle control (ω_c).

From Fig. 4.41 it can be observed that the measured slip dynamics has a resonance around 0.7-0.8 ω_c. The fact that this resonance is visible also on the engine speed (see middle plot in Fig. 4.40) suggests that it is due to

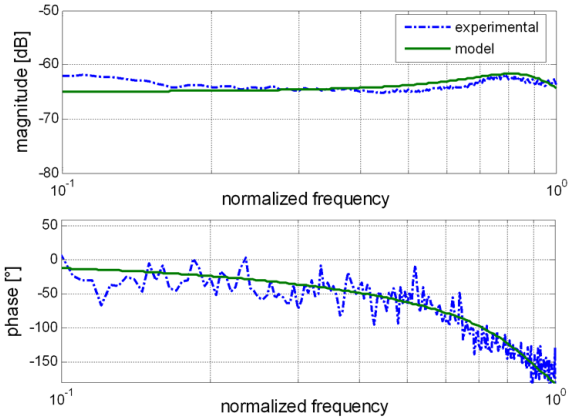

Figure 4.41: Experimental frequency response (dashed line) and analytical transfer function (solid line) from throttle set-point to rear wheel slip.

the transmission elasticity.
Therefore, to complement the analytical wheel slip model (4.91) so that it accounts for the additional dynamic elements which emerge in the measured data, the actuator dynamics and the transmission elasticity need to be considered.

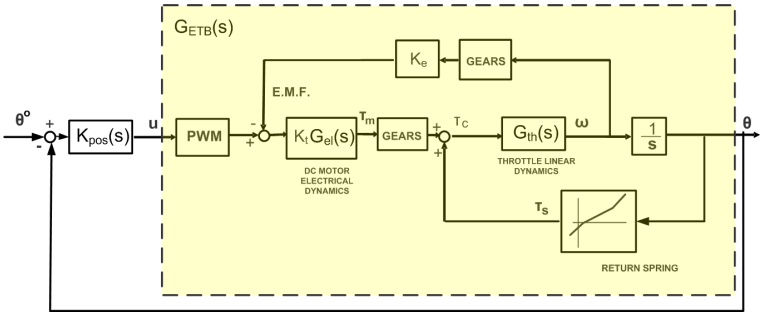

Figure 4.42: Schematic representation of the electronic throttle architecture.

Actuator model
The considered actuator is an Electronic Throttle Body (ETB), which is comprised of butterfly valves actuated by an electrical motor through a reduction system. Fig. 4.42 shows the system-theoretic representation of

the throttle control system. As can be seen, it comprises the electrical part of the DC motor dynamics $G_{el}(s)$, the mechanical DC motor component due to the electromotive force F_e and the outer ETB system made by the planetary gear, the return spring and the LTI throttle dynamics $G_{th}(s)$. The system is completed by the position control loop which regulates the throttle position θ to a desired set-point θ^o.

This mechanical system is rendered complex by packaging, cost and reliability constraints. These constraints give rise to dominant friction and backlash behaviour in the transmission, making the control of the valve difficult (Deur *et al.*, 2004). The packaging constraints are even more strict when the system is being designed for racing motorcycles. For traction control purposes, it is interesting to model the dynamics of the controlled ETB, which, as discussed in Corno *et al.* (2008*a*), can be described in terms of the transfer function (see also Fig. 4.42)

$$G_{ETB}(s) = \nu(\omega_e)\frac{1}{\tau s + 1}e^{-ds}, \tag{4.106}$$

that is a first-order low-pass filter with time-varying gain $\nu(\omega_e)$, where ω_e is the engine speed, and a pure delay d.

Transmission model

For modeling the transmission elasticity, a mass-spring-damper description has been chosen, which can be therefore represented by means of the following second-order transfer function

$$G_{transm}(s) = \frac{\omega_n^2}{s^2 + 2\xi\omega_n s + \omega_n^2}, \tag{4.107}$$

where the natural frequency $\omega_n = \sqrt{k/m}$ and $\xi = c/2\sqrt{k\,m}$ and m, c and k are the mass, damping coefficient and spring stiffness of the transmission, respectively.

Thus, the overall analytical model of the motorbike dynamics $G_{m-bike,TC}(s)$ (see also Fig. 4.38) is

$$G_{m-bike,TC}(s) = G_{th}(s)\, G_{\lambda_{r,a}}(s)\, G_{transm}(s),$$

and it is given by the cascade of the controlled ETB dynamics (4.106), the transmission (4.107) and the analytical transfer function $G_{\lambda_{r,a}}(s)$ derived from the linearized model (4.91). The overall transfer function is shown

with the solid line in Fig. 4.41. As can be appreciated, the fitting between measured data and the analytical model can be regarded as quite satisfactory. Note that the fitting is better for frequencies above 0.3 ω_c, whereas it worsens at lower frequencies. This is due to the fact that only a few periods of the periodic excitation can be completed at low frequency because of track length constraints, and this results in a poor quality of the frequency response estimate because of the very limited number of data points available.
Note that, as both the ETB and the transmission dynamics are characterized by 0dB DC gain and roll-off frequencies higher than that of the vehicle dynamics, the approach of designing the SOSM controller based on the wheel slip dynamics only is sensible. In fact, the boundedness constraints on which it relies are still valid also in presence of these additional dynamics. In the next subsection, the effects of such dynamic elements on the closed-loop performance will be analyzed and discussed.

4.3.5 Simulation Results

This subsection is devoted to assess the performance of the presented SOSM controller via a simulation study. A relatively simple Simulink-based in-plane motorcycle model (Tanelli *et al.*, 2008*b*), which takes into account tire elasticity and tire relaxation dynamics and models the ETB dynamics is considered first. As a first step, the controller performance in presence of the actuator dynamics, which have been neglected in the controller design are analyzed. Then, the controller robustness is investigated when the relative wheel slip is used as controlled variable. Further, a sensitivity analysis of the controller performance with respect to the SOSM controller gain V_r is provided, which allows to highlight interesting trade-offs between tracking performance and settling time.
Further, to validate the presented SOSM controller in a setting as close as possible to real on-bike experiments, some simulation results obtained on a full-fledged commercial motorcycle simulator (the Mechanical Simulation Corp. MSC BikeSim® simulation environment, based on the AutoSim symbolic multibody software (Sharp *et al.*, 2005)), which also models transmission and engine dynamics and provides a very accurate description of the road-tire interaction forces (Sharp *et al.*, 2004) are presented.

All the simulations have been carried out with fixed step integration and

a sampling frequency of 1 kHz, which is that available on vehicle ECUs.

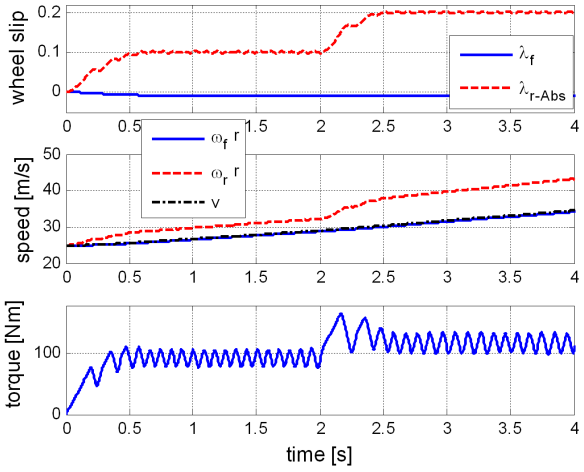

Figure 4.43: Plot of (top): front (solid line) and absolute rear (dashed line) wheel slip (top); (middle): front (solid line) rear (dashed line) and vehicle (dash-dotted line) speed; (bottom): driving torque in traction manoeuvre where the slip set-point is changed from $\lambda_r^* = 0.1$ to $\lambda_r^* = 0.2$ at $t = 2$s with absolute rear slip $\lambda_{r,a}$ as controlled variable.

4.3.5.1 Simulation Results on the in-plane motorcycle model

Figure 4.43 shows the time histories of the closed-loop absolute rear wheel slip, vehicle and wheel speeds and driving torque in a traction manoeuvre where the slip set-point is changed from $\lambda_r^* = 0.1$ to $\lambda_r^* = 0.2$ at $t = 2$s with absolute rear slip $\lambda_{r,a}$ as controlled variable. It is interesting to note that the front wheel slip in the top-plot of Fig. 4.43 is negative and not equal to zero. Namely, the front wheel provides a braking torque. This fact can be explained by observing that the front wheel has a kinetic energy given by $\frac{1}{2}J\bar{\omega}_f^2$, where $\bar{\omega}_f$ is the front wheel rotational speed at the beginning of the traction manoeuvre, and J is the inertia of the front wheel (Corno *et al.*, 2008*b*). Unfortunately, unlike the case of braking control (where the same phenomenon appears as an induced traction torque at the rear wheel when only the front brake is used), where in principle the rear brake can be used to compensate for this *flywheel* effect, in traction control it cannot be counteracted, as no driving torque can be applied to the front wheel.

The results in Fig. 4.43 show that the SOSM controller provides good tracking performance, which are maintained even if (with no controller modifications) the same manoeuvre is carried out with relative rear slip $\lambda_{r,r}$ as controlled variable, as shown in Fig. 4.44. One can appreciate also the effect of the SOSM controller in making the control variable continuous (with sawtooth-like behaviour).

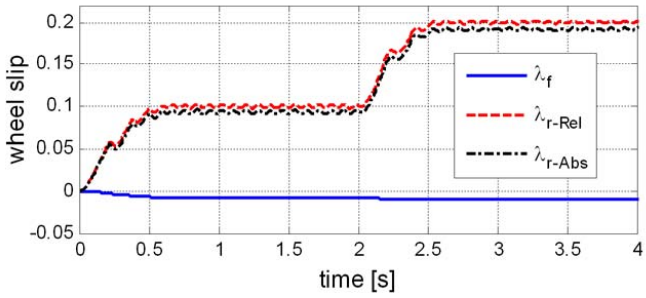

Figure 4.44: Plot of relative (dashed line), absolute (dash-dotted line) rear wheel slip and front (solid line) wheel slip in traction maneuver where the slip set-point is changed from $\lambda_r^* = 0.1$ to $\lambda_r^* = 0.2$ at $t = 2$s with relative rear slip $\lambda_{r,r}$ as controlled variable.

Inspecting Fig. 4.44, note that the wheel slip exhibits small oscillations: analyzing the period of such oscillations one finds that it corresponds to the actuator bandwidth. Such oscillations are due to the fact that the presence of the unmodelled ETB dynamic increases the relative degree of the system (note that the pure delay in (4.106) has been modeled via a second order Padé approximation, hence with no additional increase in the relative degree). As a consequence, the transient process converge to a periodic motion (Boiko *et al.*, 2007*b*). However, the amplitude of such oscillations is very small and can be well tolerated in the specific application. Instead, the use of a higher order sliding mode controller, which would be needed in principle to formally deal with a plant with relative degree higher than one by means of a continuous control law, is not advisable in automotive control, as higher order derivatives of the controlled variable need to be computed and this cannot be done reliably due to measurements noise.

It is interesting to investigate the closed-loop system sensitivity with respect to the SOSM controller gain. To this end, refer to Fig. 4.45, where the relative rear wheel slip and the driving torque is shown with nominal

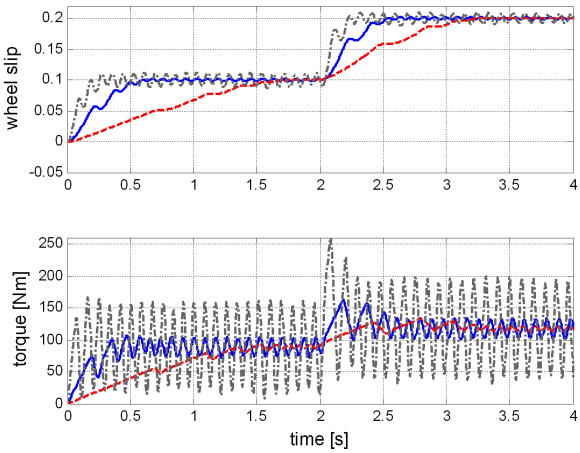

Figure 4.45: Plot of (top): relative rear wheel slip; (bottom): driving torque in a traction manoeuvre where the slip set-point is changed from $\lambda_r^* = 0.1$ to $\lambda_r^* = 0.2$ at $t = 2$s with relative rear slip $\lambda_{r,r}$ as controlled variable and with controller gains V_r (solid line), $5\,V_r$ (dash-dotted line) and $0.2\,V_r$ (dashed line).

controller gain values V_r, increased gain $5\,V_r$ and reduced gain $0.2\,V_r$. What emerges from these results is a clear trade-off between the actuator-induced oscillations amplitude and settling time. Increasing the controller gain by a factor of 5 (see the dash-dotted line in Fig. 4.45), the settling time can be nearly halve, but the price to pay are larger oscillations. The converse holds for the case of decreased gain values (dashed-line in the same figure). This feature is quite interesting for the considered application. As a matter of fact, acceleration manoeuvres on slippery roads are much more difficult to handle at low speeds. In fact, the rear wheel slip dynamics are inversely proportional to the vehicle speed, as can be seen in equation (4.89). As such, the slip dynamics get faster, hence more difficult to control for human drivers, as speed decreases. Thus, at low speeds one would willingly lose tracking performance in exchange for increased (and guaranteed) safety. It is topic of ongoing work the design of an adaptive SOSM controller, where the gains are tuned according to the vehicle speed.

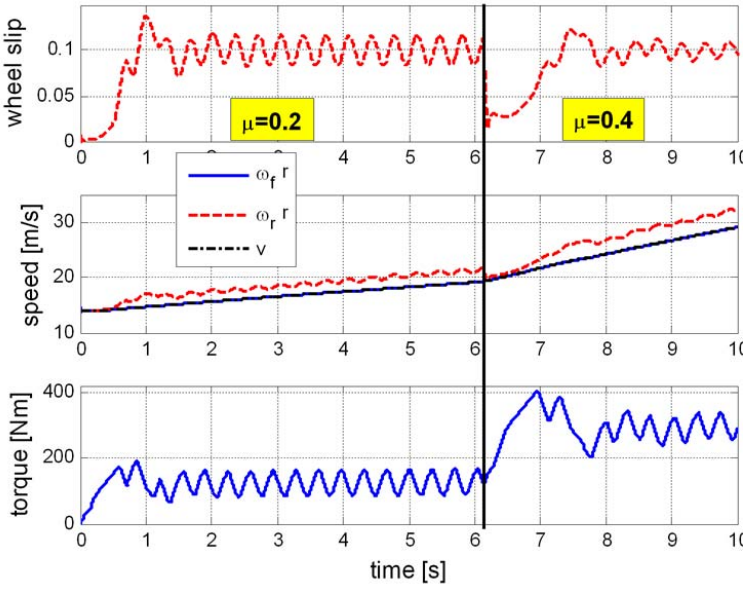

Figure 4.46: Plot of (top): relative rear wheel slip; (middle): front wheel (solid line) rear wheel (dashed line) and vehicle (dash-dotted line) speed; (bottom): driving torque in a traction maneuver on the full multibody simulator where a μ-jump from $\mu = 0.2$ to $\mu = 0.4$ with relative rear slip $\lambda_{r,r}$ as controlled variable.

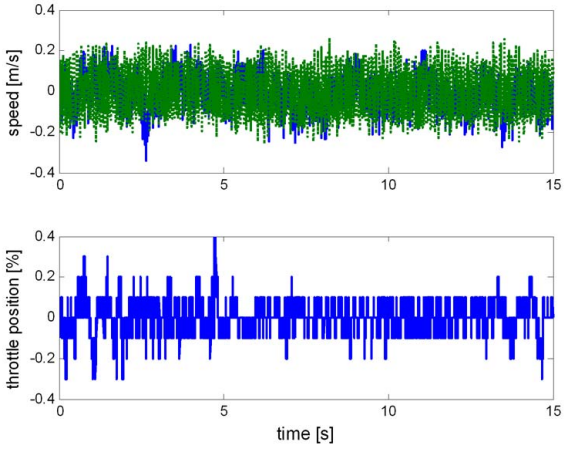

Figure 4.47: Plot of (top): measured noises on front (solid line) and rear (dotted line) wheel speed; (bottom) measured noise on the throttle position.

4.3.5.2 Simulation Results on a full multibody simulator

The controller performance are now tested on the full multibody simulator MSC BikeSim®.
To consider challenging yet realistic situations, note that in traction control applications it is crucial that the control algorithm can correctly manage sudden changes in the road conditions, which possibly occur during strong accelerations. Such a situation is often referred to as a μ-jump. Figure 4.46 shows the time histories of the relative rear wheel slip, vehicle and wheel speeds and driving torque in a traction manoeuvre on the full multibody simulator where a μ-jump from $\mu = 0.2$ to $\mu = 0.4$ with relative rear slip $\lambda_{r,r}$ as controlled variable.

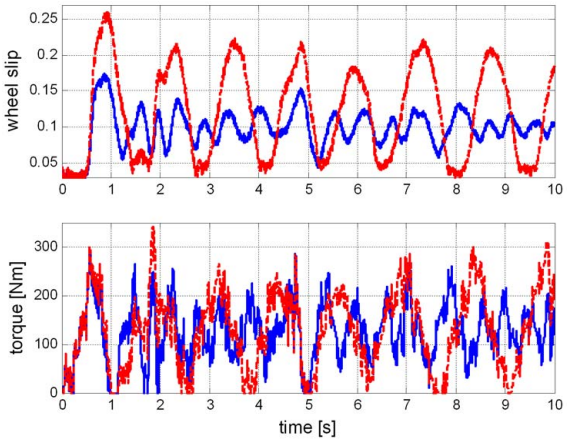

Figure 4.48: Plot of (top): relative rear wheel slip with (solid line) and without (dashed line) error pre-filtering; (bottom): driving torque with (solid line) and without (dashed line) error pre-filtering in a traction maneuver on the full multibody simulator fed with measured noises.

Further, Fig. 4.46 shows that the designed controller can guarantee safety also in very critical manoeuvres. As can be seen, however, tracking the wheel slip in face of the more realistic vehicle model offered by the full multibody simulator (where also engine and transmission are modeled) is more critical, and this results in slightly increased oscillations amplitude than encountered with the simpler model. However, the results are still more than acceptable for a real vehicle implementation.

Finally, disturbances need to be taken into account. As discussed in Subsection 4.3.3, to handle both matched and unmatched disturbances a SOSM controller scheme complemented with error prefiltering is considered. Further, in order to validate the controller in a realistic setting, the employed noises used in these simulations are front and rear wheel speeds and throttle position noise measurement errors which have been recorded on the instrumented vehicle and are shown in Fig. 4.47. Note that the wheel speed errors magnitude is such that the induced oscillations on the relative wheel slip are approximately of ± 0.02.

The results of these simulations are shown in Fig. 4.48, where the behaviour of the relative wheel slip and the driving torque is shown both with and without error prefiltering. As can be seen, with error prefiltering the closed-loop behaviour of the rear wheel slip exhibits oscillations of much smaller magnitude than without error prefiltering, so that the traction control systems can guarantee safety even in the presence of real-life disturbances, thereby confirming the suitability of the presented SOSM controller for motorcycle traction control applications.

4.3.6 Concluding remarks and outlook

The analysis and design of a safety-oriented traction control system for ride-by-wire sport motorcycles based on a Second Order Sliding Mode (SOSM) control approach has been addressed in this section. An analytical model of the rear wheel slip dynamics has been provided, taking into account the difficulties of having a reliable vehicle speed estimate. The model has been validated against experimental data collected on an instrumented vehicle. The presented controller effectiveness has been assessed on a full-fledged multibody motorcycle model and taking into account both matched and unmatched disturbances, so as to confirm its practical applicability. Ongoing work is being devoted to devise an adaptation of the controller gains in order to achieve high safety levels also at low speed, which is a very critical situation for traction control.

4.4 Collision avoidance strategies and coordinated control of a platoon of vehicles

Recent research has shown that the longitudinal control of platoons of vehicles is appropriate to improve the traffic capacity of road networks while maintaining the safety distance between vehicles. The possibility of reducing the number of accidents involving pedestrians or other vulnerable road users (VRUs), like cyclists and motorcyclists, by providing the control systems of the vehicles of the platoon with some collision detection and avoidance capabilities is investigated in this section.

The presented control system allows to maintain a desired distance from the preceeding vehicle, and, as a novelty with respect to other proposals, to avoid the collision with VRUs present on the road. The control scheme is realized by means of a supervisor, which make the decision on which is the appropriate current control mode for each controlled vehicle, and manage the switches among low–level controllers.

Part of this section is taken from Ferrara and Vecchio (2006*a*,*b*,*c*,*d*, 2007*a*); Ferrara *et al.* (2008*f*); Ferrara and Vecchio (2008*b*) and Ferrara and Vecchio (2008*c*)

4.4.1 Introduction

During recent years, a number of initiatives and research developments have been devoted to investigate how safety in urban and highway transportation networks can be increased by means of on–board intelligent driver assistance systems. For instance, it has been observed that the exploitation of the capacity of transportation networks can be enforced if the vehicles flow is harmonized by making the vehicles move at uniform speeds, while respecting the safety distance constraints.

Different cruise control algorithms have been proposed and analyzed in the literature (see, for instance, Chien *et al.* (1994); Swaroop and Hedrick (1996); Xy *et al.* (2001); Zambou *et al.* (2004)). More specifically, in Zambou *et al.* (2004) a vehicle–follower control system for vehicles within a platoon, using a model–based predictive approach for the control law, is presented; in Zhang *et al.* (1999), a cruise control is described, which uses information about the relative speed and spacing from the preceding and the following

vehicles; in Swaroop and Hedrick (1996), the automatic vehicle following system proposed adopts a constant spacing policy; in Yip (1997) a first order sliding mode adaptive cruise control strategies has been proposed; in Bom *et al.* (2005) a cruise control strategy based on nonlinear decoupling laws is presented; in Khatir and Davison (2004) decentralized non–identical linear controllers for a large platoon of vehicles are described.

The key elements of a coordinated control systems for passenger vehicles are various. Surely, an important issue in this context is inter–vehicular communication. This can influence an important control objective to be attained by the vehicle controllers which is string stability (Swaroop and Hedrick, 1996). String stability ensures that spacing errors decrease as they propagate downstream through the platoon. The stability of the string of automated vehicles depends on the information available for feedback and on how such information are processed to generate the vehicle control (Brogliato and De Wit, 1999). Sheikholeslam and Desoer (Sheikholeslam and Desoer, 1990) showed that string stability cannot be achieved for platoons with constant inter–vehicle spacing under autonomous operation, and proposed a scheme which guarantees string stability, assuming that the lead vehicle is transmitting its velocity and acceleration information to all the other vehicles of the platoon. This approach is also used in Hallouzi *et al.* (2004); Swaroop and Hedrick (1996); Zambou *et al.* (2004), and it yields stable platoons with small inter–vehicle spacings at the cost of introducing and maintaining continuous inter–vehicle communication. Yet, the presented control scheme is designed relying on the result of Chien and Ioannou (Chien *et al.*, 1994), which proves that the string stability of the platoon can be guaranteed in autonomous operation if a speed–dependent spacing policy is adopted. In this way, the communication overhead can be avoided.

While the problem of cruise control, regarded as the longitudinal control of the vehicles of the platoon to maintain the correct spacing and uniform velocity of the vehicles, has been deeply explored by researchers, only few works address the possibility of enriching the vehicle controllers with the capability of autonomously reacting to the presence of moving or static obstacles on the road. This aspect is described in this section and a cruise control system with collision avoidance features is presented.

The idea is to provide the control system of each vehicle of the platoon with a supervisor (Fig. 4.49) which receives the data from the car sensors (for instance radar, laser, stereo–vision systems, etc.).

In normal situations, the control system mode is a “cruise mode" in which, apart from the leader vehicle, which is autonomously driven by its driver, all the other vehicles of the platoon are controlled so as to keep the desired safety distance, which is calculated according to the constant time headway policy, and to guarantee, in steady–state, uniform velocities. The cruise control component of the control scheme is designed by following a second order sliding mode approach.

At any time instant when new data are collected by the sensors, a collision detection test is performed by the supervisor of each vehicle, relying on the concept of collision cone presented in Chakravarthy and Ghose (1998). When a possible collision is detected, the control system of the involved vehicle switches to the “collision avoidance mode". The vehicle stops to follow the preceding vehicle, since the higher priority control objective is to avoid the collision with the obstacle. The supervisor makes the decision on which action, between an emergency braking and the generation of a collision avoidance manoeuvre, is the appropriate choice in the current situation. When a collision avoidance manoeuvre is necessary and feasible, the supervisor activates a high level controller which, on the basis of the data received from the sensors, and of some computed quantities, establishes if the car has to perform the movement to avoid the obstacle, or if it has to return to the original driving direction, since the obstacle has been avoided. This implies that there are two low level dedicated controllers capable of attaining the two different aims. Both of them are designed through a first order sliding mode control approach, acting on two control variables: traction/braking force and wheels steering angle.

The emergency braking module indicated in Fig. 4.49 can be realized via a simple open–loop automatic action designed so as to completely exploit the braking capability of the vehicle.

The effectiveness of the control scheme has been tested in simulation in presence of model uncertainties and disturbances, and with a realistic pedestrian model obtained from real data in order to evaluate its performance in a realistic scenario.

4.4.2 The vehicle model

The considered platoon consists of $n+1$ vehicles. It is assumed that all the vehicles of the platoon are identical, and that the so–called bicycle model

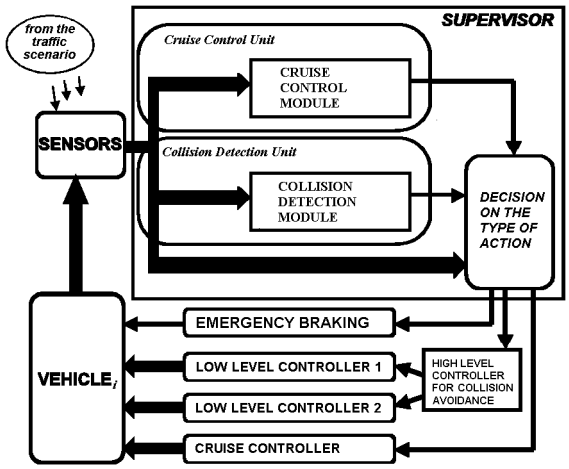

Figure 4.49: Scheme of the automatic control system

(Genta, 1997) can be adopted to give a sufficiently accurate representation of their longitudinal and lateral dynamics. The model of the i–th vehicle is

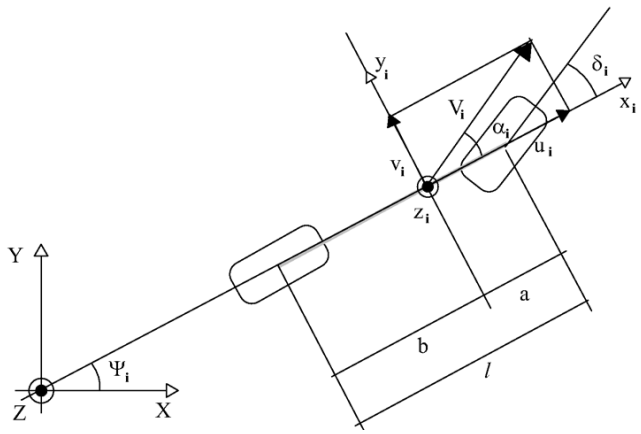

Figure 4.50: The bicycle model

the following

$$\begin{cases} \dot{u}_i &= \frac{1}{M}\Big(Mv_ir_i - Mfg + u_i^2(fK_1 - K_2) \\ &+ c_f\frac{v_i+ar_i}{u_i}\delta_i + T_i\Big) \\ \dot{v}_i &= \frac{1}{M}\Big(- Mu_ir_i - (c_f + c_r)\frac{v_i}{u_i} \\ &+ (bc_r - ac_f)\frac{r_i}{u_i} + c_f\delta_i + T_i\delta_i\Big) \\ \dot{r}_i &= \frac{1}{J_z}\Big((bc_r - ac_f)\frac{v_i}{u_i} - (b^2c_r + a^2c_f)\frac{r_i}{u_i} \\ &+ ac_f\delta_i + aT_i\delta_i\Big) \\ \dot{X}_i &= u_i\cos(\psi_i) - v_i\sin(\psi_i) \\ \dot{Y}_i &= u_i\sin(\psi_i) + v_i\cos(\psi_i) \\ \dot{\psi}_i &= r_i \end{cases} \tag{4.108}$$

where, u_i, v_i and r_i are the longitudinal velocity, the lateral velocity and the yaw rate, respectively; X_i and Y_i are the position coordinates of the vehicle with respect to the road coordinate system; ψ_i is the yaw angle of the vehicle (see Fig. 4.50), and all the other parameters are shown in Table 4.9. The two control signals are δ_i, the wheels steering angle, and T_i, the traction force at the contact point between tire and ground.

Table 4.9: Vehicle model parameters

	Parameter	Value
M	Mass of the vehicle	1480 kg
f	Rotating friction coefficient	0.02
J_z	Inertial moment around z–axis	2350 kgm^2
a	Distance from front tyres to center of mass	1.05 m
b	Distance from rear tyres to center of mass	1.63 m
c_f	Front tyres cornering stiffness	135000 N/rad
c_r	Rear tyres cornering stiffness	95000 N/rad
K_1	Aerodynamic lift coefficient	0.005 Ns^2/m^2
K_2	Aerodynamic drag coefficient	0.41 Ns^2/m^2

4.4.3 Cruise Control Mode

In this section the Second Order Sliding Mode (SOSM) technique (see Chapter 3) is adopted for the design of the cruise control component of the control system.

In the considered platoon of vehicles, the 0–th vehicle is the so–called leader, and it is assumed that its speed and acceleration are arbitrary. The objective of the longitudinal control of the i–th vehicle, with $i = 1, 2, \ldots, n$, is to maintain the safety distance from the preceding vehicle. The safety distance is calculated in accordance with the Constant Time–Headway (CTH) policy, which is commonly suggested as a safe practice for human drivers, and is frequently used in ACC designs (Chien *et al.*, 1994). The safety distance given by the CTH policy is

$$S_{d_i}(u_i(t)) = S_{d_0} + hu_i(t) \tag{4.109}$$

where S_{d_0} is the distance between stopped vehicles, and h is the so–called headway time. Thus, considering the i–th vehicle, with $i = 1, 2, \ldots, n$, the spacing error is given by

$$e_i(t) = S_{d_i}(u_i(t)) - d_i(t) = S_{d_0} + hu_i(t) - X_{i-1}(t) + X_i(t) \tag{4.110}$$

where $d_i(t) = X_{i-1}(t) - X_i(t)$, is the longitudinal distance between the i–th vehicle and the $(i-1)$–th vehicle. This quantity can be measured, for instance, by a laser or radar sensor mounted on the front of the vehicles.

The chosen sliding variable is the spacing error, i.e.,

$$S_i(t) = e_i(t) = X_i(t) - X_{i-1}(t) + S_{d_0} + hu_i(t) \tag{4.111}$$

and the control problem is to design a control law capable of making the sliding variable vanishes in finite time.
To design a SOSM control law for the longitudinal dynamic of the i–th vehicle, introduce the following auxiliary system

$$\begin{cases} \dot{\sigma}_{i1}(t) = \dot{S}_i(t) = \sigma_{i2}(t) \\ \dot{\sigma}_{i2}(t) = \ddot{S}_i(t) = \chi_i(t) + w_i(t) \end{cases} \tag{4.112}$$

where $\chi_i(t) = \dot{u}_i(t) - \dot{u}_{i-1}(t)$, and signal $w_i(t) = h\ddot{u}_i(t)$ can be regarded as an auxiliary control input. The term $\chi_i(t)$ in (4.112) represents the difference between the longitudinal acceleration of two adjacent vehicles. Such value is

bounded by mechanical and physical limits (Genta, 1997), i.e., $|\dot{u}_i(t)| \leq \Gamma$, $\forall i$, where Γ is the maximum longitudinal acceleration/deceleration that a vehicle can produce. Moreover, the following relationships holds

$$|\chi_i(t)| \leq 2\Gamma \qquad i = 1, 2, ..., n \tag{4.113}$$

Following the sub–optimal control approach (Bartolini *et al.*, 1998*b*), the auxiliary control input in (4.112) can be designed as

$$w_i(t) = -W_M \ \text{sign}\left\{S_i(t) - \frac{1}{2}S_{i_{Max}}(t)\right\} \tag{4.114}$$

where $W_M > 4\Gamma$, and $S_{i_{Max}}(t)$ is a piece–wise constant function producing the value of the last singular point of $S_i(t)$ (i.e., the most recent value $S_i(t)$ such that $\dot{S}_i(t) = 0$).

To determine the traction force T_i to be applied to generate the desired longitudinal acceleration, it is necessary to consider the model of the longitudinal dynamics of the vehicle. From (4.108), with $v_i = 0$ (null lateral speed), and $\delta_i = 0$ (null steering angle), it follows that the force to be applied is

$$T_i(t) = Ma_{des_i}(t) - Mfg - u_i^2(t)(fK_1 - K_2) \tag{4.115}$$

where $a_{des_i}(t)$ is calculated from (4.114) as

$$a_{des_i}(t) = \frac{1}{h}\int_0^t w_i(\tau)d\tau \tag{4.116}$$

The control law (4.115) can be analyzed in analogy with that presented in Bartolini *et al.* (1999). It can be proved that the control law (4.115) enforces a second order sliding mode on the sliding manifold $S_i(t) = \dot{S}_i(t) = 0$ in finite time. From (4.111), this implies that the spacing error between the i–th and the $(i-1)$–th vehicle, and its first time derivative are steered to zero in a finite time t_i^*, i.e., $e_i(t) = \dot{e}_i(t) = 0$, $\forall\, t \geq t_i^*$.

4.4.3.1 The string stability of the platoon

String stability is usually defined as the requirement that disturbances on the spacing errors e_i are attenuated as they propagate along the platoon (Swaroop and Hedrick, 1996). To analyse the string stability of the platoon of vehicles controlled via the second order sliding mode control approach

previously described, it is possible to consider the system in sliding mode $S_i(t) = \dot{S}_i(t) = 0$ and determine the so-called equivalent control (Bartolini *et al.*, 1998*b*) by setting $\ddot{S}_i(t) = 0$ in (4.112), that is,

$$\ddot{S}_i(t) = a_i(t) - a_{i-1}(t) + h\dot{a}_i(t) = 0 \tag{4.117}$$

From (4.117), the auxiliary equivalent control is

$$w_{i_{eq}}(t) = h\dot{a}_{i_{eq}} = a_{i-1}(t) - a_i(t) \tag{4.118}$$

Then, the acceleration of the i–th vehicle produced by the auxiliary equivalent control is

$$a_{i_{eq}} = \frac{1}{h}\int (a_{i-1}(t) - a_i(t)) = \frac{1}{h}v_{i-1}(t) - v_i(t) \tag{4.119}$$

Under the assumption that all the vehicles are identical, the following equivalence between transfer functions

$$G(s) = \frac{V_i(s)}{V_{i-1}(s)} = \frac{E_i(s)}{E_{i-1}(s)} \tag{4.120}$$

where V_i and E_i are the Laplace transform of the speed and of the separation error of the i–th vehicle, has been proved in Zhou and Peng (2000). In the considered case, by Laplace transforming (4.119), one has

$$G_i(s) = \frac{V_i(s)}{V_{i-1}(s)} = \frac{1}{1 + hs} \tag{4.121}$$

where one can note that the headway time h, which characterises the separating strategy between two subsequent vehicles, determines the position of the pole of the transfer function $G(s)$. To conclude about the string stability of the platoon of controlled vehicles, one has to verify if the necessary and sufficient conditions (Brogliato and De Wit, 1999)

$$\|G\|_\infty = \max_\omega |G(j\omega)| \leq 1, \qquad g(t) \geq 0 \tag{4.122}$$

where $g(t)$ is the impulse response, are satisfied. The first condition is satisfied since

$$\max_\omega |G(j\omega)| = \max_\omega \sqrt{\frac{1}{1 + \omega^2 h^2}} \leq 1, \qquad \forall h > 0 \tag{4.123}$$

As for the second condition, by determining the inverse Laplace transform of $G(s)$, one has

$$g(t) = \frac{1}{h}e^{-t/h} \tag{4.124}$$

for $t > 0$. Since $h > 0$, it follows that $g(t) > 0$, so that the string stability of the platoon is proved.

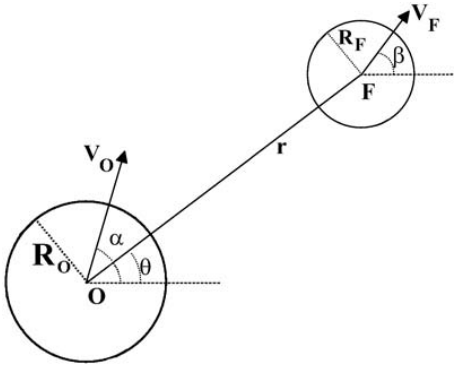

Figure 4.51: The collision cone

4.4.4 Collision Avoidance Mode

Now the point is to enrich the control system capabilities in order to make the platoon of vehicles able to avoid the collision with static or moving obstacles. In this subsection, for the sake of simplicity, a single vehicle will be considered, even if, in the sequel, it will be assumed that all the controlled vehicles of the platoon will possess the collision avoidance capability. For this reason the subscript i is omitted. Moreover, the following two assumptions are made: both the vehicle and the obstacles move on a two-dimensional space; their velocities (modulus and direction), during the sampling interval, are constant.

The collision detection task is performed relying on the so–called collision cone (Chakravarthy and Ghose, 1998), in alternative to the different procedure presented in Petti and Fraichard (2005).
In Fig. 4.51, let O and F represent the car and the obstacle to be avoided, respectively, and r is the distance between their centers. The velocities of O and F are denoted by V_F and V_O, respectively. In a polar–coordinates reference frame centred on the vehicle O, the motion of the object F with respect to the car O is described by the two speed components V_r and V_θ

$$\begin{cases} V_r = V_F \cos(\beta - \theta) - V_O \cos(\alpha - \theta) \\ V_\theta = V_F \sin(\beta - \theta) - V_O \sin(\alpha - \theta) \end{cases} \tag{4.125}$$

In Chakravarthy and Ghose (1998) it has been proved that two circular moving objects, with radius R_O and R_F respectively, moving at constant

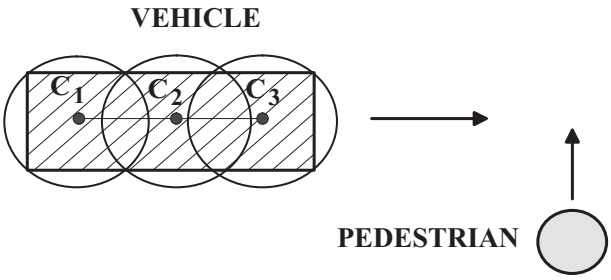

Figure 4.52: The area occupied by the car and the pedestrian represented by circles

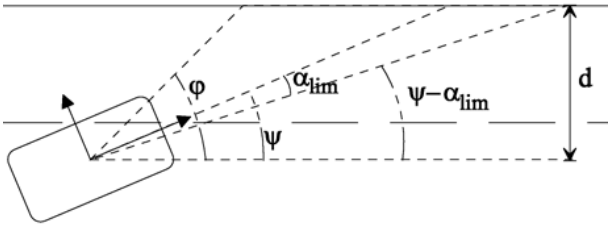

Figure 4.53: The left road border case

velocities will collide if and only if their initial conditions satisfy

$$V_\theta(t_0)^2 \leq p^2 V_r(t_0)^2 \quad \text{and} \quad V_r(t_0) < 0 \tag{4.126}$$

with $p = (R_O + R_F)/\sqrt{r(t_0)^2 - (R_O + R_F)^2}$ and t_0 being the initial time instant. The "collision cone" is defined by all those values of $\eta_c = \alpha(t_0) - \theta(t_0)$ that satisfy (4.126).

The collision cone concept can be applied to the detection of possible collisions between a car and the pedestrians crossing the road or other VRUs. The area occupied by the car plus some margins is represented by means of circles suitably positioned on the vehicle as indicated in Fig. 4.52. The collision cone idea can be extended to the road borders by relying on trigonometric considerations. Making reference to Fig. 4.53 and considering the circle of radius R_{car} placed on the front side of the vehicle as in Fig. 4.52, the resulting collision cone with respect to the left road border will be given by the set of angles

$$\mathcal{N}_{Lrb} = \{-\alpha_{lim}, \varphi - \psi\} \tag{4.127}$$

where $\alpha_{lim} = \psi - \arcsin\{(d - R_{car})/(|V_{car}|t_{react})\}$, in which d is the distance between the car and the left road border, $|V_{car}|$ is the module of the car velocity vector, t_{react} is the minimum reaction time of the driver assumed equal to 1.5 s, φ is the maximum allowed angle between the car direction and the road border, and ψ is the angle between the current car direction and the road border.
The algorithm used for collision detection, apart from the collision cone extremes, also produces as an output a discrete value variable, named *collision*, the value of which is a code associated with the various situations and used by the supervisor to generate the suitable corresponding action. The values used in our case are listed below:
4: Collision cannot be avoided acting only on α;
3: Future collision with the road border detected;
2: Future collision with the obstacle detected;
1: A collision is going to occur in a time greater than t_{react};
0: No collision detected;
Taking into account the value of the *collision* variable, an appropriate set of angles for which a collision is predicted is obtained by the union of the collision cones that have the collision variable value greater than or equal to 2. This latter set will be called, on the whole *collision cone*. The extreme of this set nearest to the current vehicle velocity vector will be the set point for the direction of the velocity vector. If the supervisor realizes that the manoeuvre is not feasible, i.e, the value of the *collision* variable is 4, an emergency braking is produced so as to reduce, at least, the energy at the impact. Otherwise, a high level controller in charge of the generation of the manoeuvre is activated.

The movement of the vehicle during the collision avoidance manoeuvre is divided into two phases: *Phase 1*, collision avoidance movement; *Phase 2*, re–entry movement. The two low level controllers for collision avoidance indicated in Fig. 4.49 have been designed relying on a sliding–mode control approach (Utkin, 1992).
The controller which is activated in Phase 1 (*low level controller 1*) has the aim to steer the velocity vector of the controlled car outside the *collision cone*. To this end, the control system acts simultaneously on the steering wheels and on the vehicle speed. The controller which is activated in Phase 2 (*low level controller 2*) makes the car track the reference trajectory given

by a line parallel to the road border and distant from it of an offset (equal to 1.5 m in our case).

Actually, the presented control laws are applied, when necessary, in a decentralized way to each controlled vehicle of the platoon. Future work will be devoted to investigate the possibility of introducing communication between vehicles in order to perform more complex collision avoidance manoeuvre.

To generate the steering command in Phase 1, introduce the sliding quantity

$$S_1 = \dot{\xi} + \lambda_{11}\xi + \lambda_{12}\int_0^t \xi \mathrm{d}\tau \tag{4.128}$$

where λ_{11}, and λ_{12} are design parameters, and ξ represents the error between the actual vehicle direction and the border of the collision cone closer to the actual vehicle direction, i.e., $\xi = \alpha_{car} - \alpha_c$. Then, the control law can be chosen as

$$\delta = -\frac{K_{S_1}}{\Delta} sign\,(\Delta)\; sign\,(S_1) \tag{4.129}$$

where K_{S_1} is a positive design parameter which takes into account the physical and passenger comfort limits, and $\Delta = a(c_f + T)/J_z$.

To generate the steering command in Phase 2, introduce the sliding quantity

$$S_1' = \dot{y}_s + \lambda_{11}' y_s + \lambda_{12}' \int_0^t y_s \mathrm{d}\tau \tag{4.130}$$

where λ_{11}', and λ_{12}' are design parameters on which the dynamics of the vehicle depend once the sliding manifold is reached, and y_s represents the reference lateral distance from the road border. The control law can be chosen as

$$\delta = -K_{S_1'} sign\left(S_1'\right) \tag{4.131}$$

where $K_{S_1'}$ is a positive design parameter that takes into account the physical and passenger comfort limits.

As for the velocity control in Phase 1 and 2, suppose to set a reference velocity V_d, and define the error variable $\varepsilon = V - V_d$ and the sliding surface

$$S_2 = \varepsilon \tag{4.132}$$

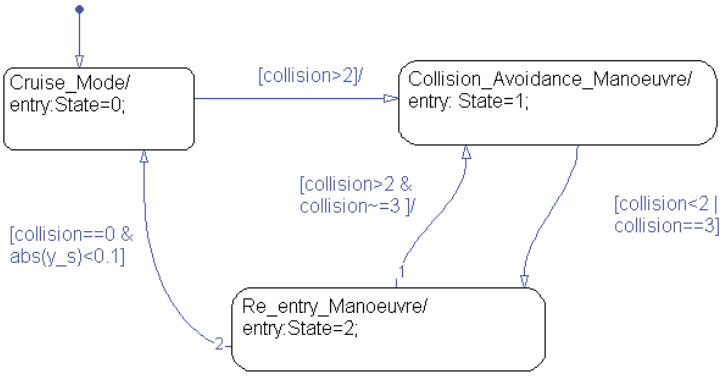

Figure 4.54: Control stateflow chart

Then, a discontinuous control law can be designed as

$$T = -K_{S_2} sign\,(S_2) \tag{4.133}$$

with K_{S_2} positive and sufficiently high so as to attain $S_2 = 0$ in finite time. In Phase 1, the reference velocity V_d is determined, at any sampling instant, as the velocity magnitude which could force the velocity vector outside the collision cone, even without acting on the steering angle. Instead, in Phase 2, V_d is chosen as the velocity magnitude of the vehicle before entering Phase 1.

4.4.5 Coordinated control of the platoon with collision avoidance

Fig. 4.54 depicts the state flow scheme which implements the supervisor of the control system of each controlled vehicle. The automatic control system, during operations, can be in one of three possible states, which differs for the different control objectives and references.

State 0: In this state no collision is detected and the vehicle i is in its lane. The goal of the controlled vehicle is to follow the preceding vehicle at the correct safety distance. The traction force T_i is given by (4.115). The leader of the platoon is totally controlled by its driver that cruises at an arbitrary speed. In this state, the steering control is performed manually by

Table 4.10: Vehicles initial conditions

Vehicle	X_i	Y_i	V_i	ψ_i
0	100 m	0 m	20 m/s	0 rad
1	50 m	0 m	10 m/s	0 rad
2	0 m	0 m	10 m/s	0 rad

the driver. If the supervisor of a vehicle detects a possible future collision the control system state switches from State 0 to State 1.

State 1: Only the vehicles interested by the event "future collision with an obstacle" undergo a switch of their control from State 0 to State 1. The steering command, in this state, is generated automatically as indicated in (4.129), while the traction force to be applied by the low level controller is that given in (4.133). When all the obstacles have been correctly avoided, the control system state switches to State 2 and the vehicle starts the re–entry manoeuvre to return to the original driving path.

State 2: To perform the re–entry manoeuvre, the traction force to be applied is that indicated in (4.133), while the steering command is given in (4.131). When the vehicle has reached the original driving path and no other obstacle is detected, the control system state will return to State 0.

4.4.6 Simulation Results

The presented automatic system has been tested in simulation, considering a situation in which the platoon is composed by a leader vehicle and two follower vehicles. The parameters of the model used for simulations are shown in Table 4.9. The initial positions (see Fig 4.55) and velocities of the vehicles are reported in Table 4.10. The leader of the platoon starts travelling in its lane keeping its velocity constant. The parameters which characterize the spacing policy are chosen as $h = 2\,\mathrm{s}$, and $S_{d_0} = 1\,\mathrm{m}$.
The control parameters used in simulation are: $W_M = 4\,\mathrm{g}$, $\lambda_{11} = 1000$, $\lambda_{12} = 1$, $K_{S_1} = 18$, $\lambda'_{11} = 1.8$, $\lambda'_{12} = 0.001$, $K_{S'_1} = 0.2$, $K_{S_2} = 100$. In this simulation case, it is assumed that three pedestrians are present on the road. The initial position (see Fig 4.55), and velocities of the pedestrians are reported in Table 4.11. In order to model the complex pedestrian

Table 4.11: Pedestrians initial conditions

Pedestrian	X_{Pi}	Y_{Pi}	$v_{x_{Pi}}$	$v_{y_{Pi}}$
1	110 m	−1.5 m	−3 m/s	0.275 m/s
2	150 m	0 m	−1 m/s	0 m/s
3	230 m	2.5 m	0 m/s	−0.27 m/s

behaviour in a simple, yet representative way, the integrated random walk model proposed in De Nicolao *et al.* (2007) has been adopted. Indicating with X_{Pi} the position of the i–th pedestrian, with $v_{x_{Pi}}$ her/his velocity along the abscissa axis, one has

$$\begin{cases} \dot{X}_{Pi}(t) &= v_{x_{Pi}}(t) \\ \dot{v}_{x_{Pi}}(t) &= \omega_{xi}(t) \\ \omega_{xi} &\sim WGN(0, \sigma_x^2) \end{cases} \tag{4.134}$$

where $WGN(0, \sigma_x^2)$ stands for White Gaussian Noise with zero expectation and variance equal to σ_x^2. An analogous model can be set up for the other direction of motion, i.e.,

$$\begin{cases} \dot{Y}_{Pi}(t) &= v_{y_{Pi}}(t) \\ \dot{v}_{y_{Pi}}(t) &= \omega_{yi}(t) \\ \omega_{yi} &\sim WGN(0, \sigma_y^2) \end{cases} \tag{4.135}$$

On average, the pedestrian follows the nominal trajectory determined by the initial velocity. Nevertheless, in a particular simulation, the actual trajectory will randomly differ from the nominal one. The variance of such a difference grows with time and reflects the increasing uncertainty on the predicted final position of the pedestrian. The existence of a nominal trajectory is what motivates the choice of an integrated random walk in place of a simple random walk model. The value for σ_x^2, and σ_y^2 used in simulation are $\sigma_x^2 = 0.82$, and $\sigma_y^2 = 0.5$. These parameters have been identified on the basis of real data on pedestrians' crossing, as illustrated in De Nicolao *et al.* (2007).

In order to test the robustness feature of the presented control schemes, the actual parameters of the vehicles are assumed to be different from their nominal values, i.e., $M = 1850\,\text{kg}$, $f = 0.05$, $C_f = 120000$ N/rad, $C_r = 80000\,\text{N/rad}$, $k_1 = 0.002\,\text{Ns}^2/\text{m}^2$, and $k_2 = 0.21\,\text{Ns}^2/\text{m}^2$. The vehicles are approximated with a circle of radius $R_{car} = 1.25\,\text{m}$ centerd in the

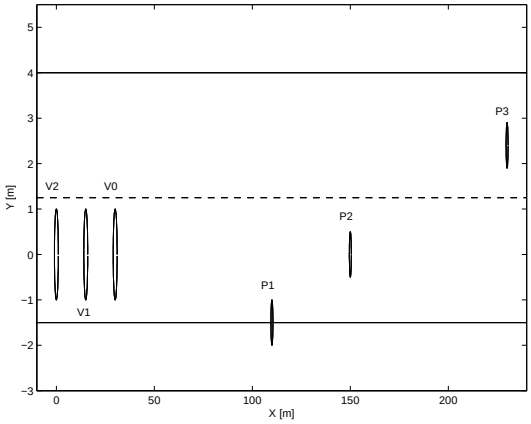

Figure 4.55: Initial positions of the vehicles of the platoon, and of the pedestrians (t=0s)

center of gravity of the vehicle, while pedestrians are approximated with a circle of radius $R_p = 0.5\,\mathrm{m}$. Moreover, to take into account some external disturbances affecting the vehicle model in matched forms (Edwards and Spurgeon, 1998), the control input are calculated as

$$\begin{aligned} T_i &= \bar{T}_i + d_i + e_i \sin(t + f_i) \\ \delta_i &= \bar{\delta}_i + g_i \sin(t + h_i) \end{aligned} \tag{4.136}$$

where $\bar{T}_i$, and $\bar{\delta}_i$ are the nominal control signals, computed, on the basis of the current "control mode", according to the equations illustrated in this section, and all the other parameters are reported in Table 4.12.

Table 4.12: Disturbance parameters

Vehicle	d_i	e_i	f_i	g_i	h_i
0	300	20	$pi/4$	0.15	$\pi/2$
1	100	40	0	0.1	0
2	200	10	$\pi/2$	0.2	$\pi/2$

Figs. 4.56 and 4.57, represent the positions of the vehicles of the platoon, and of the pedestrians at time $t = 5\,\mathrm{s}$, and $t = 10\,\mathrm{s}$, respectively, and their trajectories, starting respectively from $t = 0\,\mathrm{s}$, and $t = 5\,\mathrm{s}$, are represented

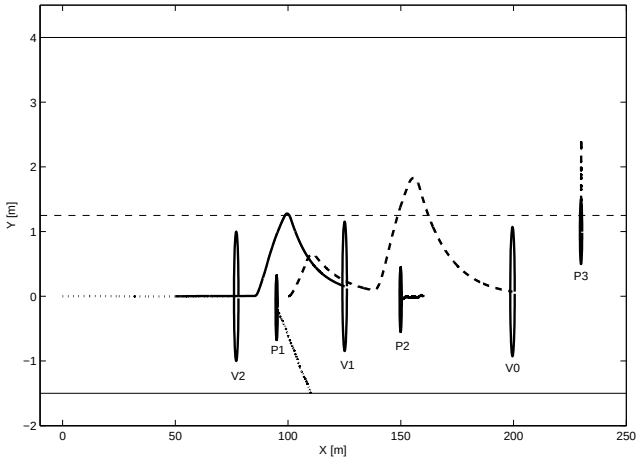

Figure 4.56: Positions of the vehicles of the platoon, and of the pedestrians (t=5s)

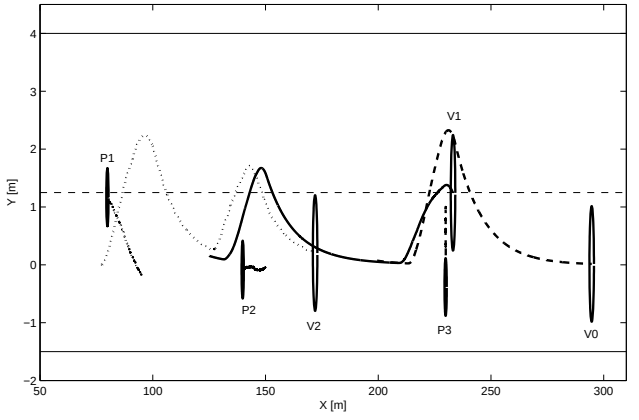

Figure 4.57: Positions of the vehicles of the platoon, and of the pedestrians (t=10s)

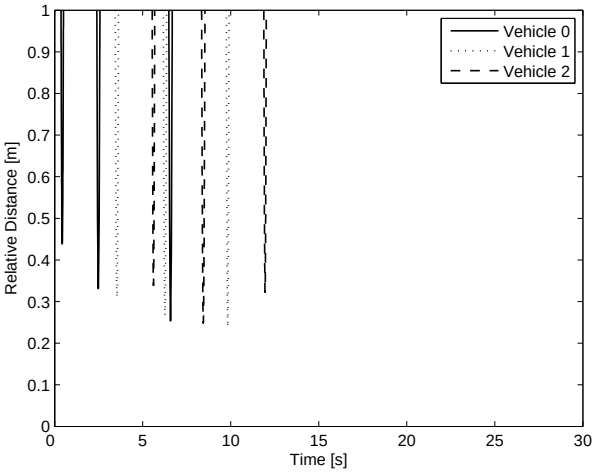

Figure 4.58: Minimum value of the relative distances vehicles-pedestrians

by a line. The minimum values of the relative distances between the vehicles and the pedestrians are illustrated in Fig. 4.58. The minimum relative distance is zoomed so as to show that it is always different from zero (no collision has occurred). The inter–vehicular spacing between vehicle 0 and 1, and between vehicle 1 and 2 are shown in Figs. 4.59 and 4.60, respectively. One can note that Vehicle 1 reaches the safety distance from Vehicle 0 only when the three pedestrians have been avoided. Vehicle 2, instead, reaches the safety distance from Vehicle 1 before the event “possible collision detected" occurs. When the collision is detected, Vehicle 2 stops to follow the preceding vehicle to perform an emergency manoeuvre to avoid the pedestrian. This manoeuvre causes the loss of the safety distance from Vehicle 1. The fact that, during the manoeuvre to avoid the pedestrian, Vehicle 2 can collide with Vehicle 1 is prevented, in the sense specified in the theoretical development, by the collision detection capability of the control system: indeed, during the manoeuvre also the other vehicles of the platoon are regarded as possible obstacles, and, if necessary, a collision cone is generated also with respect to them. The collision avoidance manoeuvre is generated, if feasible, in order to avoid the collision with all the detected obstacles. The safety distance from preceeding vehicle is reached again after the end of the emergency manoeuvre. This situation takes place again when Vehicle

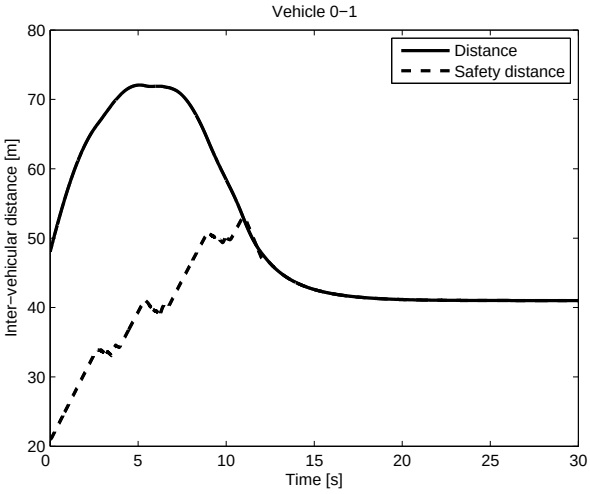

Figure 4.59: Spacing between vehicle 0 and 1

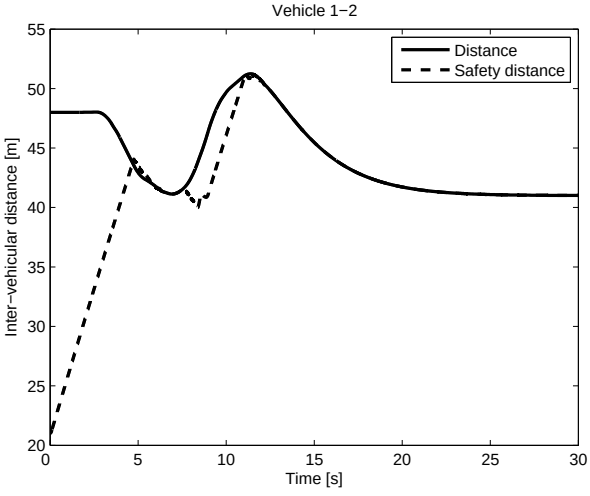

Figure 4.60: Spacing between vehicle 1 and 2

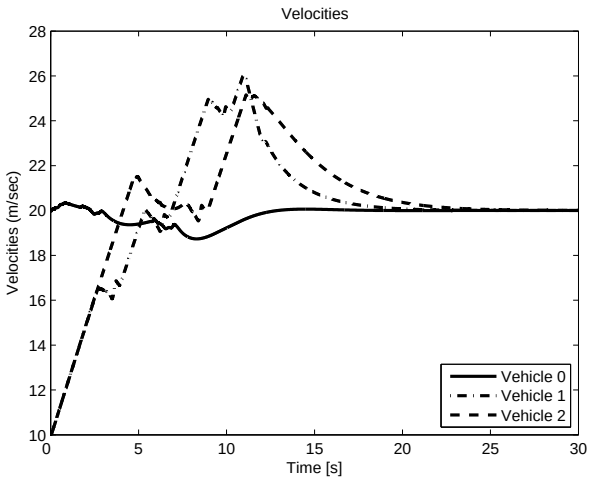

Figure 4.61: The evolution of the velocities of the vehicles

2 detects the second and the third pedestrian. After the last pedestrian has been avoided, Vehicle 2 attains again the desired inter–vehicular spacing with respect to Vehicle 1, and it correctly keeps this spacing until the end of simulation. Moreover, after that the three pedestrians have been correctly avoided, all the vehicles reach the same velocity as the leader vehicle, as shown in Fig. 4.61.

4.4.7 Conclusions and future works

This section explores the possibility of designing a driver assistance system for vehicles capable of keeping the desired inter–vehicular spacing, so as to have a coordinated motion of a platoon of vehicles, but also capable, in case of detection of a possible collision with static or moving obstacles, to make a decision between the generation of an emergency braking or a collision avoidance manoeuvre. The automatic driver assistance system presented in this section makes the controlled vehicle operates in two possible automatic modes: a “cruise mode" and a “collision avoidance mode". While in “cruise mode", the control objective is to maintain the safety distance from the preceding vehicle, so as to increase traffic capacity, while improving safety. If the supervisor detects a future collision with an obstacle, the

control system switches to the “collision avoidance mode", and generates a suitable automatic action choosing between an emergency braking, and a collision avoidance manoeuvre. Simulation evidence has been provided demonstrating the feasibility of the presented approach even in presence of disturbances and parametric uncertainties. The addressed control problem could be also regarded as an hybrid control problem. Future works will be devoted to investigate the problem from this point of view in particular as for as the stability issues are concerned and to the design of second order sliding mode low level controllers for the “collision avoidance" module. The possibility of introducing communication between vehicles in order to perform more complex collision manoeuvre will be the topic of future research. Clearly, apart from the necessity of experiments to evaluate the concept, a number of crucial aspects still need to be analyzed: the psycho–physical issues regarding the driver and the passengers of the cars controlled via the automatic system here presented, as well as the type of driving skills required to the driver so that she/he does not act as an antagonist of the control system during emergencies.

Chapter 5

Stabilization of nonholonomic uncertain systems

Contents

In this chapter the problem of controlling a class of nonholonomic systems in chained form affected by two different kind of uncertainties is addressed.
The control of nonholonomic systems is quite complex, since this class of systems, very common in practical applications, like wheeled mobile robots, does not satisfy the well–known Brockett's necessary smooth feedback stabilization condition (Kolmanovsky and McClamroch, 1995). The control problem is further complicated whenever uncertainties of various nature affect the nonholonomic system model.
In particular, a class of nonholonomic systems in chained form affected by two different kind of uncertainties is considered in this chapter. More specifically, the problem of stabilizing chained form systems affected by uncertain drift term and parametric uncertainties is addressed in Section 5.2, while in Section 5.3 the same problem is solved for a class of chained form systems affected by both matched and unmatched uncertainties.
The design methodologies described in this chapter are both based on suitable transformations of the system model so that, on the basis of the transformed system state, it is possible to design a particular sliding manifold, as well as to re–formulate the control problem in question as a second order sliding mode control problem. As a consequence, the control input results in being continuous, thus more acceptable in the considered context.
Simulation results show the effectiveness of the control schemes presented in this chapter.

Part of this chapter is taken from Ferrara *et al.* (2006); Ferrara and Vecchio (2008*a*); Ferrara *et al.* (2008*b*,*c*,*d*) and Ferrara *et al.* (2008*e*).

5.1 Introduction

Nonholonomic systems have been the object of research for control theorists for many years (Kolmanovsky and McClamroch, 1995; De Wit *et al.*, 1996). This particular class of nonlinear systems commonly arises in finite dimensional mechanical systems where nonintegrable constraints are imposed on the motion, like wheeled mobile robots and wheeled vehicles (Kolmanovsky and McClamroch, 1995; De Wit *et al.*, 1996).

In Murray and Sastry (1993), the class of systems in chained form was introduced as a possible way to represent a wide class of nonholonomic systems. Indeed, many nonlinear mechanical systems with nonholonomic constraints on velocities can be locally, or globally, converted to the chained form under coordinate change and state feedback. Nonholonomic chained systems have the following form

$$\begin{cases} \dot{x}_0 &= u_0 \\ & \vdots \\ \dot{x}_i &= x_{i+1}u_0, \qquad 1 \leq i \leq n-1 \\ & \vdots \\ \dot{x}_n &= u_1 \end{cases} \tag{5.1}$$

where $x_0 \in \mathbb{R}$, $x = [x_1, \ldots, x_n]^T \in \mathbb{R}^n$, and u_0, u_1, are the scalar control variables. As stated in Murray and Sastry (1993), a chained system (5.1) is maximally nonholonomic, which is equivalent to claim that system (5.1) is completely controllable.
The main problem in controlling this class of systems is due to the fact that nonholonomic systems do not satisfy Brockett's necessary smooth feedback stabilization condition (Brockett, 1983) as shown in Ryan (1994). To overcome this problem, several nonlinear approaches have been proposed. In particular, most of them are based on a discontinuous transformation of the system states and on a backstepping–based design procedure (see, for instance Krstić *et al.* (1995); Astolfi (1996); Jiang (2000); Ge *et al.* (2003) and the references therein cited).
The control problem of this class of systems is further complicated whenever uncertainties of various nature affect the nonholonomic system model. A possible approach to control nonholonomic uncertain systems is sliding mode control (Guldner and Utkin, 1995; Floquet *et al.*, 2003).
Yet, the application of the sliding mode methodology to the control problem of a nonholonomic system affected by some kind of uncertainties does not appear to be straightforward. Some preliminary steps to transform the system into a suitable form need to be taken.

In Section 5.2, the problem of stabilizing a chained form system in presence of parametric uncertainties and uncertain drift term is addressed, while in Section 5.3 the same problem is solved for a class of chained form systems affected by both matched and unmatched uncertainties.

5.2 Chained form systems affected by uncertain drift term and parametric uncertainties

In this section a class of systems in chained form affected by uncertain drift nonlinearity and parametric uncertainties is considered.
Following the idea already developed in Bartolini *et al.* (2000) with reference to nonlinear uncertain systems in some triangular feedback forms, the possibility of coupling a partial transformation of the nonholonomic uncertain system via a backstepping–based procedure with a second order sliding mode control approach (Bartolini *et al.*, 1997*a*; Levant, 2003) is investigated.
More specifically, a discontinuous state transformation (Astolfi, 1996) and a partial backstepping procedure (Krstić *et al.*, 1995) are applied to the perturbed nonholonomic system. In this section, it has been proved that the tuning law for the unknown parameters and the virtual control laws obtained via the backstepping procedure make the error state of the transformed system input–to–state–stable (Isidori, 1999). Then, the control problem is solved designing a particular sliding manifold on which the input of the error system is steered to zero thus making the error state globally asympotically stable.
Moreover, to circumvent the problem of the chattering effect (Fridman, 2001*b*; Levant, 2007), the design procedure is carried out relying on the second order sliding mode methodology (see Chapter 3).
It should be noted that the coupling of backstepping with sliding mode control has been first investigated in Bartolini *et al.* (2000). On the other hand, higher–order sliding modes have already been applied to the stabilization of a three wheeled vehicle in Floquet *et al.* (2003). As a novelty with respect to other proposals, the second order sliding mode control presented in this section is able to deal with parametric uncertainties thanks to the introduction of a suitably designed adaptive mechanism.

5.2.1 The problem statement

The considered uncertain chained form system is of the following form

$$\begin{cases} \dot{x}_0 &= u_0 + \phi_0^T(x_0)\theta \\ &\vdots \\ \dot{x}_i &= x_{i+1}u_0 + \phi_i^T(u_0, x_0, \overline{x}_i)\theta \qquad 1 \leq i \leq n \\ &\vdots \\ \dot{x}_n &= \gamma(u_0, x_0, x) + \beta(u_0, x_0, x)u_1 + \phi_n^T(u_0, x_0, x)\theta \end{cases} \tag{5.2}$$

where $x = [x_1, x_2, \ldots, x_n]^T$, $[x_0, x^T]^T \in \mathbb{R}^{n+1}$ are the system states, $\overline{x}_i = [x_1, \ldots, x_i]^T$, u_0 and u_1 are scalar control inputs, $\phi_0(x_0) \in \mathbb{R}^l$ and $\phi_i(u_0, x_0, \overline{x}_i) \in \mathbb{R}^l$, $1 \leq i \leq n$, are vectors of smooth nonlinear functions, $\theta \in \mathbb{R}^l$ is a vector of unknown bounded constant parameters, $\beta(u_0, x_0, x)$ is a known scalar function such that $\beta(u_0, x_0, x) \neq 0$, and $\gamma(u_0, x_0, x)$ is an uncertain bounded scalar function with bounded first time derivative. In particular, it is assumed that the bounds are known, i.e.,

$$|\gamma(u_0, x_0, x)| \leq G_1 \tag{5.3}$$

$$|\dot{\gamma}(u_0, x_0, x)| \leq G_2 \tag{5.4}$$

where G_1 and G_2 are positive constants. Note that in Ge *et al.* (2003) adaptive state feedback control strategy based on the backstepping procedure were proposed for the class of system (5.2) with $\gamma(u_0, x_0, x) = 0$ and $\beta(u_0, x_0, x) = 1$. As in Jiang (2000) and Ge *et al.* (2003), in this section it is assumed that for ϕ_0 there is a known smooth function vector φ_0 such that

$$\phi_0(x_0) = x_0\varphi_0(x_0) \tag{5.5}$$

and for $\phi_i, 1 \leq i \leq n$, there are some known smooth function vectors φ_i such that

$$\phi_i(x_i) = \sum_{j=1}^{i} x_j\varphi_j(u_0, x_0, \overline{x}_i) \tag{5.6}$$

Assumptions (5.5) and (5.6) imply that the nonlinearities $\phi_i, 0 \leq i \leq n$, satisfy a triangularity structure requirement. Note that this assumption is a quite common assumption in the framework of robust and adaptive nonlinear control (Krstić *et al.*, 1995). As a consequence, the origin is a possible

equilibrium point of system (5.2). Moreover, the first time derivatives of ϕ_i, $0 \leq i \leq n$, are assumed to be bounded, i.e.,

$$|\dot{\phi}_i| < \Delta_i, \qquad 0 \leq i \leq n \tag{5.7}$$

Then, taking into account the foregoing problem formulation, the control objective is to design adaptive control laws u_0 and u_1 such that $[x_0, x^T]^T \to 0$ as $t \to \infty$, and all the other signals in the closed–loop system are bounded. Note that the triangular structure of system (5.2) allows us to design the control inputs u_0 and u_1 in two separate steps. The control input u_0 is designed so as to globally asymptotically stabilize the x_0–subsystem, which is described by the first equation of (5.2), while the control input u_1 takes into account the x–subsystem given by the remaining equations in (5.2).

5.2.2 The control signal u_0

In this subsection, the case $x_0(t_0) \neq 0$ is considered. The case when $x_0(t_0) = 0$ will be dealt with in Subsection 5.2.6. when $x_0(t_0) \neq 0$, the following theorem can be proved.

Theorem 5.1 *Consider the chained form uncertain system (5.2). Then, for any initial condition $x_0(t_0) \neq 0$, the control law u_0 given by*

$$u_0(x_0, \hat{\theta}_0) = x_0 g_0(x_0, \hat{\theta}_0) \tag{5.8}$$

$$g_0(x_0, \hat{\theta}_0) = -\varphi_0^T(x_0)\hat{\theta}_0 - \sqrt{k_0^2 + (\varphi_0^T(x_0)\hat{\theta}_0)^2} \tag{5.9}$$

where $k_0 > 0$ and $\hat{\theta}_0$ is an estimate of θ, and the following update law for parameter $\hat{\theta}_0$

$$\dot{\hat{\theta}}_0 = \tau_0 = \Gamma x_0 \phi_0(x_0), \quad \Gamma = \Gamma^T > 0 \tag{5.10}$$

can globally asymptotically regulate the state x_0 to zero, i.e. $\lim_{t\to\infty} x_0(t) = 0$. Moreover, since $x_0(t_0) \neq 0$ is assumed, u_0 ensures that x_0 does not cross zero $\forall t \in [t_0, \infty)$.

Note that, $1/g_0(x_0, \hat{\theta}_0)$ is well defined since, from (5.9), one has that $g_0(x_0, \hat{\theta}_0) \neq 0$, $\forall\, x_0, \hat{\theta}_0$.

Proof: Consider the Lyapunov function candidate

$$V_0 = \frac{1}{2}x_0^2 + \frac{1}{2}\tilde{\theta}_0^T \Gamma^{-1} \tilde{\theta}_0 \tag{5.11}$$

where $\tilde{\theta}_0 = \theta - \hat{\theta}_0$. The first time derivative of (5.11) is

$$\begin{aligned}\dot{V}_0 &= x_0\left[x_0\left(-\varphi_0^T(x_0)\hat{\theta}_0 - \sqrt{k_0^2 + (\varphi_0^T(x_0)\hat{\theta}_0)^2} + \varphi_0^T(x_0)\theta\right)\right] \\ &\quad -\tilde{\theta}_0^T\Gamma^{-1}\dot{\hat{\theta}}_0 \\ &= -x_0^2\sqrt{k_0^2 + (\varphi_0^T(x_0)\hat{\theta}_0)^2} - \tilde{\theta}_0^T\Gamma^{-1}(\dot{\hat{\theta}}_0 - \tau_0) \\ &\leq -k_0 x_0^2 \end{aligned} \tag{5.12}$$

by using LaSalle's Invariant Theorem (LaSalle, 1960), one can conclude that $\hat{\theta}_0$ is bounded and $x_0 \to 0$ as $t \to \infty$.
Moreover, by applying the control law (5.8) to system (5.2), the solution $x_0(t)$ of the closed–loop system is given by

$$x_0(t) = x_0(t_0)e^{-\int_{t_0}^{t}\lambda(s)ds} \tag{5.13}$$

where $\lambda(s) = -\varphi_0^T\tilde{\theta}_0(s) + \sqrt{k_0^2 + (\varphi_0^T\hat{\theta}_0(s))^2}$. Note that, since $x_0(t_0) \neq 0$ is assumed, u_0 can guarantee that x_0 does not cross zero $\forall t \in [t_0, \infty)$.

5.2.3 Discontinuous state scaling

As proved in Subsection 5.2.2, the control law (5.8) can globally asymptotically regulate the state x_0 to zero. However, in doing so, the control u_0 will converge to zero as $t \to \infty$. This causes a serious problem since, in the limiting case, when $u_0 = 0$, the x–subsystem is uncontrollable via the control input u_1. As in Jiang (2000) and in Ge *et al.* (2003), to overcome the loss of controllability of the x–subsystem in the limiting case, the following discontinuous state scaling transformation is performed (Astolfi, 1996)

$$z_i = \frac{x_i}{x_0^{n-i}}, \quad 1 \leq i \leq n \tag{5.14}$$

The discontinuous state coordinate transformation (5.14) possesses the property of increasing the resolution around a given point (Arnold, 1996) so that x_0 cannot converge to zero before x_i, $i = 1, \ldots, n$. By applying the

state transformation (5.14) to system (5.2), it yields

$$\begin{aligned}
\dot{z}_i &= \frac{\dot{x}_i}{x_0^{n-i}} - (n-i)\frac{x_0^{n-i-1}\dot{x}_0 x_i}{x_0^{2(n-i)}} \\
&= \frac{u_0 x_{i+1}}{x_0^{n-i}} + \frac{\phi_i^T\theta}{x_0^{n-i}} - (n-i)\frac{x_i}{x_0^{n-i+1}}(u_0 + \phi_0^T\theta) \\
&= g_0 z_{i+1} - (n-i)g_0 z_i + \left[\frac{\phi_i}{x_0^{n-i}} - \frac{(n-i)\phi_0 z_i}{x_0}\right]^T\theta \\
&= g_0(x_0,\hat{\theta}_0)z_{i+1} + f_i(x_0,z_i,\hat{\theta}_0) + \psi_i^T(x_0,\overline{z}_i,\hat{\theta}_0)\theta \qquad (5.15)
\end{aligned}$$

where

$$f_i(x_0,z_i,\hat{\theta}_0) = -(n-i)g_0(x_0,\hat{\theta}_0)z_i \qquad (5.16)$$

$$\psi_i(x_0,\overline{z}_i,\hat{\theta}_0) = \frac{\phi_i(u_0,x_0,\overline{x}_i)}{x_0^{n-i}} - \frac{(n-i)\phi_0(x_0)z_i}{x_0} \qquad (5.17)$$

Then, the resulting z–subsystem is given by

$$\begin{cases} \dot{z}_i = g_0(x_0,\hat{\theta}_0)z_{i+1} + f_i(x_0,z_i,\hat{\theta}_0) + \psi_i^T(x_0,\overline{z}_i,\hat{\theta}_0)\theta \\ \dot{z}_n = \gamma(u_0,x_0,x) + \beta(u_0,x_0,x)u_1 + \phi_n^T(u_0,x_0,x)\theta \end{cases} \qquad (5.18)$$

where $\overline{z}_i = [z_1,\ldots,z_i]^T, 1 \le i \le n-1$.

5.2.4 The backstepping procedure

Most of the control schemes appeared in the literature capable of stabilizing an uncertain nonholonomic system are based on the backstepping procedure (Krstić *et al.*, 1995) (see for instance Bartolini *et al.* (2000); Jiang (2000); Ge *et al.* (2003) and the reference therein). Following the ideas already developed in Bartolini *et al.* (2000) and in Scarratt *et al.* (2000) with reference to nonlinear uncertain systems in some triangular feedback forms, the possibility of coupling a partial transformation of the nonholonomic system via a backstepping–based procedure with a second order sliding mode control approach (Bartolini *et al.*, 1997*a*) is investigated.
The problem is complicated by the presence of parametric uncertainties affecting the system which are not the kind of uncertainties naturally dealt with by sliding mode control.

The backstepping design procedure (Krstić *et al.*, 1995) in case of single input systems and with reference to a regulation objective consists in the step–by–step construction of a transformed system with state

$$e_i = z_i - \alpha_{i-1} \tag{5.19}$$

$i = 1, \ldots, n$, where α_i, with $\alpha_0 = 0$, is the so–called virtual control signal at the design step i. The virtual controls for the system with state $e = [e_1, \ldots, e_n]^T$ are computed to drive e to the equilibrium point $[0, \ldots, 0]^T$. The equilibrium point is proved to be stable through a standard Lyapunov analysis. Moreover, the Lyapunov functions themselves, computed at each step, are used to determine the most suitable α_i.

In this section, a modified backstepping procedure is presented to transform the state system in order to design a particular sliding manifold upon which a second order sliding mode is enforced.

5.2.4.1 Step 1

With reference to system (5.18), the following quantities are defined

$$e_1 = z_1 \tag{5.20}$$

$$e_2 = z_2 - \alpha_1 \tag{5.21}$$

By differentiating (5.20),

$$\dot{e}_1 = \dot{z}_1 = g_0 z_2 + f_1 + \psi_1^T \theta = g_0 e_2 + g_0 \alpha_1 + f_1 + \psi_1^T \theta \tag{5.22}$$

Consider the Lyapunov function candidate

$$V_1 = \frac{1}{2} e_1^2 + \frac{1}{2} \tilde{\theta}^T \Gamma^{-1} \tilde{\theta} \tag{5.23}$$

where $\tilde{\theta} = \theta - \hat{\theta}$, and $\hat{\theta}$ is an estimate of θ, and its first time derivative

$$\dot{V}_1 = e_1 (g_0 e_2 + g_0 \alpha_1 + f_1 + \psi_1^T \theta) - \tilde{\theta}^T \Gamma^{-1} \dot{\hat{\theta}} \tag{5.24}$$

Choosing the virtual control α_1 and the tuning function τ_1 as

$$\alpha_1 = \frac{1}{g_0} (-k_1 e_1 - f_1 - \psi_1^T \hat{\theta}) \tag{5.25}$$

$$\tau_1 = \Gamma \psi_1 e_1 \tag{5.26}$$

where $k_1 > 0$, from (5.24) one has

$$\dot{V}_1 = -k_1 e_1^2 + e_1 e_2 g_0 - \tilde{\theta}^T \Gamma^{-1} (\dot{\hat{\theta}} - \tau_1) \tag{5.27}$$

5.2.4.2 Step i

Define

$$e_{i+1} = z_{i+1} - \alpha_i \tag{5.28}$$

and then

$$\begin{aligned}\dot{e}_i &= g_0 e_{i+1} + g_0\alpha_i + f_i + W_i^T\theta - \frac{\partial\alpha_{i-1}}{\partial x_0}u_0 \\ &\quad - \sum_{k=1}^{i-1}\frac{\partial\alpha_{i-1}}{\partial z_k}(g_0 z_{k+1} + f_k) - \frac{\partial\alpha_{i-1}}{\partial\hat{\theta}_0}\tau_0 - \eta_i\dot{\hat{\theta}} \end{aligned} \tag{5.29}$$

where

$$\eta_i(x_0, \overline{z}_i, \hat{\theta}_0, \hat{\theta}) = \frac{\partial\alpha_{i-1}(x_0, \overline{z}_i, \hat{\theta}_0, \hat{\theta})}{\partial\hat{\theta}} \tag{5.30}$$

$$\begin{aligned}W_i(x_0, \overline{z}_i, \hat{\theta}_0, \hat{\theta}) &= \psi_i(x_0, \overline{z}_i, \hat{\theta}_0) - \frac{\partial\alpha_{i-1}(x_0, \overline{z}_i, \hat{\theta}_0, \hat{\theta})}{\partial x_0}\phi_0 \\ &\quad - \sum_{k=1}^{i-1}\frac{\partial\alpha_{i-1}(x_0, \overline{z}_i, \hat{\theta}_0, \hat{\theta})}{\partial z_k}\psi_k(x_0, \overline{z}_i, \hat{\theta}_0)\end{aligned} \tag{5.31}$$

Consider the Lyapunov function candidate

$$V_i = V_{i-1} + \frac{1}{2}e_i^2 \tag{5.32}$$

yielding

$$\begin{aligned}\dot{V}_i &= -\sum_{j=1}^{i-1}k_j e_j^2 - \tilde{\theta}^T\Gamma^{-1}[\dot{\hat{\theta}} - (\tau_{i-1} + \Gamma W_i e_i)] - h_{i-1}(\dot{\hat{\theta}} - \tau_{i-1}) \\ &\quad + e_i[e_{i-1}g_0 + g_0 e_{i+1} + g_0\alpha_i + f_i + W_i^T\hat{\theta} - \frac{\partial\alpha_{i-1}}{\partial x_0}u_0 \\ &\quad - \sum_{k=1}^{i-1}\frac{\partial\alpha_{i-1}}{\partial z_k}(g_0 z_{k+1} + f_k) - \frac{\partial\alpha_{i-1}}{\partial\hat{\theta}_0}\tau_0 - \eta_i\dot{\hat{\theta}}]\end{aligned} \tag{5.33}$$

Choosing the virtual control α_i and tuning function τ_i as

$$\begin{aligned}\alpha_i &= \frac{1}{g_0}[-k_i e_i - e_{i-1}g_0 - f_i - W_i^T\hat{\theta} + \frac{\partial\alpha_{i-1}}{\partial x_0}u_0 \\ &\quad + \sum_{k=1}^{i-1}\frac{\partial\alpha_{i-1}}{\partial z_k}(g_0 z_{k+1} + f_k) + \frac{\partial\alpha_{i-1}}{\partial\hat{\theta}_0}\tau_0 + \eta_i\tau_i \\ &\quad - h_{i-1}\Gamma W_i]\end{aligned} \tag{5.34}$$

$$\tau_i = \tau_{i-1} + \Gamma W_i e_i \tag{5.35}$$

(5.33) yields

$$\dot{V}_i = -\sum_{j=1}^{i-1} k_j e_j^2 - \tilde{\theta}^T \Gamma^{-1}(\dot{\hat{\theta}} - \tau_i) - h_i(\dot{\hat{\theta}} - \tau_i) + e_i e_{i+1} g_0 \quad (5.36)$$

where

$$h_i(x_0, \overline{z}_i, \hat{\theta}_0, \hat{\theta}) = h_{i-1}(x_0, \overline{z}_i, \hat{\theta}_0, \hat{\theta}) + e_i \eta_i(x_0, \overline{z}_i, \hat{\theta}_0, \hat{\theta}) \quad (5.37)$$

with $h_1(x_0, z_1, \hat{\theta}_0, \hat{\theta}) = 0$.

5.2.4.3 Step $n-1$

Introduce

$$e_n = z_n - \alpha_{n-1} \quad (5.38)$$

then

$$\begin{aligned} \dot{e}_{n-1} = {} & g_0 e_n + g_0 \alpha_{n-1} + f_{n-1} + W_{n-1}^T \theta - \frac{\partial \alpha_{n-2}}{\partial x_0} u_0 \\ & - \sum_{k=1}^{n-2} \frac{\partial \alpha_{n-2}}{\partial z_k}(g_0 z_{k+1} + f_k) - \frac{\partial \alpha_{n-2}}{\partial \hat{\theta}_0} \tau_0 - \eta_{n-1} \dot{\hat{\theta}} \end{aligned} \quad (5.39)$$

Consider the Lyapunov function candidate

$$V_{n-1} = V_{n-2} + \frac{1}{2} e_{n-1}^2 \quad (5.40)$$

From (5.34) and (5.35), at step $n-1$, the virtual control and the tuning function, respectively, result in

$$\begin{aligned} \alpha_{n-1} = {} & \frac{1}{g_0}[-k_{n-1} e_{n-1} - e_{n-2} g_0 - f_{n-1} - W_{n-1}^T \hat{\theta} + \frac{\partial \alpha_{n-2}}{\partial x_0} u_0 \\ & + \sum_{k=1}^{n-2} \frac{\partial \alpha_{n-2}}{\partial z_k}(g_0 z_{k+1} + f_k) + \frac{\partial \alpha_{n-2}}{\partial \hat{\theta}_0} \tau_0 + \eta_{n-1} \tau_{n-1} \\ & - h_{n-2} \Gamma W_{n-1}] \end{aligned} \quad (5.41)$$

$$\tau_{n-1} = \tau_{n-2} + \Gamma W_{n-1} e_{n-1} \quad (5.42)$$

Then (5.40) yields

$$\begin{aligned} \dot{V}_{n-1} = {} & -\sum_{j=1}^{n-1} k_j e_j^2 - \tilde{\theta}^T \Gamma^{-1}(\dot{\hat{\theta}} - \tau_{n-1}) - h_{n-1}(\dot{\hat{\theta}} - \tau_{n-1}) \\ & + e_n e_{n-1} g_0 \end{aligned} \quad (5.43)$$

where, h_{n-1} is given by (5.37).
In contrast to the standard procedure adopted in Jiang (1996) and in Ge *et al.* (2003), the backstepping procedure is stopped at step $n-1$ instead of step n. The update law for parameter $\hat{\theta}$ is chosen as

$$\dot{\hat{\theta}} = \tau_{n-1} \tag{5.44}$$

and (5.43) gives

$$\dot{V}_{n-1} = -\sum_{j=1}^{n-1} k_j e_j^2 + e_n e_{n-1} g_0 \tag{5.45}$$

By relying on the concept of input-to-state stability (Isidori, 1999), the following result can be proved.

Theorem 5.2 *The dynamic system*

$$\begin{cases} \dot{e}_1 &= \dot{z}_1 \\ \dot{e}_2 &= \dot{z}_2 - \dot{\alpha}_1 \\ & \vdots \\ \dot{e}_{n-1} &= \dot{z}_{n-1} - \dot{\alpha}_{n-2} \end{cases} \tag{5.46}$$

where z_i, $i = 1, \ldots, n-1$, are defined in (5.14), α_i, $i = 1, \ldots, n-1$, as in (5.34), is input–to–state–stable (ISS) (Isidori, 1999) with respect to $e_n g_0$ and, if $e_n g_0 \to 0$ then

$$\lim_{t \to \infty} \|\eta\| = 0$$

where $\eta = [e_1, \ldots, e_{n-1}]^T$.

Proof: The Lyapunov funcion (5.40) is an ISS Lyapunov function (Isidori, 1999). Indeed, from (5.45) one has that

$$\forall\, |e_{n-1}| \geq \frac{|e_n g_0|}{\sigma k_{n-1}} \Rightarrow \dot{V}_{n-1} \leq -\sum_{j=1}^{n-2} k_j e_j^2 - k_{n-1}(1-\sigma) e_{n-1}^2 \tag{5.47}$$

where $\sigma \in (0,1)$.
This implies that there exist a function $\chi(\cdot,\cdot)$ of class $\mathcal{KL}$ and a function $\omega(\cdot)$ of class $\mathcal{K}$ (called ISS gain function) such that, for any initial state $\eta(0)$ one has that

$$\|\eta(t)\| \quad \leq \quad \chi(\|\eta(0)\|, t) + \omega(\|e_n g_0\|_\infty) \tag{5.48}$$

Hence, if $e_n g_0$ is bounded, then $\|\eta\|$ is bounded. Moreover, if $e_n g_0 \to 0$ then $\eta \to 0$ (Isidori, 1999).

5.2.5 The control signal u_1

From (5.48) one can observe that it is possible to steer η to zero with a control law u_1 capable of steering e_n to zero. In the approach presented in this section, a second order sliding mode control law is designed to steer to zero not only e_n but also its first time derivative $\dot{e}_n$ in finite time. This implies that a second order sliding mode is generated. As a result, while $\dot{u}_1$ is constructed as a discontinuous signal, guaranteeing the attainment of a second order sliding mode on the sliding manifold, the actual control u_1 is continuous and thus more acceptable, in terms of chattering, in systems of mechanical nature (Levant, 2007).

5.2.5.1 The second order sliding mode control

To design the second order sliding mode controller the chosen sliding variable s is

$$s = e_n = z_n - \alpha_{n-1} \tag{5.49}$$

The first and second time derivatives of (5.49) are given by

$$\begin{aligned} \dot{s} &= \gamma + \beta u_1 + W_n^T\theta - \frac{\partial \alpha_{n-1}}{\partial x_0}u_0 - \sum_{k=1}^{n-1}\frac{\partial \alpha_{n-1}}{\partial z_k}(g_0 z_{k+1} + f_k) \\ &\quad - \frac{\partial \alpha_{n-1}}{\partial \hat{\theta}_0}\tau_0 - \eta_{n-1}\tau_{n-1} \qquad (5.50) \\ \ddot{s} &= \dot{\gamma} + \dot{\bar{u}}_1 + \dot{W}_n^T\theta \qquad (5.51) \end{aligned}$$

where control signal u_1 is designed as

$$\begin{aligned} u_1 &= \frac{1}{\beta}\Big[\frac{\partial \alpha_{n-1}}{\partial x_0}u_0 + \sum_{k=1}^{n-1}\frac{\partial \alpha_{n-1}}{\partial z_k}(g_0 z_{k+1} + f_k) \\ &\quad + \frac{\partial \alpha_{n-1}}{\partial \hat{\theta}_0}\tau_0 + \eta_{n-1}\tau_{n-1} + \bar{u}_1\Big] \end{aligned} \tag{5.52}$$

and $\bar{u}_1$ is an auxiliary control signal to be specified. Now, by using the sliding variable and its first time derivative as states of a new dynamical system, i.e., by introducing the auxiliary variables $y_1 = s$ and $y_2 = \dot{s}$, equations (5.49)–(5.51) can be rewritten as

$$\begin{cases} \dot{y}_1 = y_2 \\ \dot{y}_2 = \xi(x_0, x, \hat{\theta}_0, \hat{\theta}, \theta, u_0, u_1) + \dot{\bar{u}}_1 \end{cases} \tag{5.53}$$

The auxiliary system (5.53) is a double integrator affected by the matched uncertainty term

$$\xi(x_0, x, \hat{\theta}_0, \hat{\theta}, \theta, u_0, u_1) = \dot{\gamma} + \dot{W}_{n-1}^T \theta$$

Relying on assumptions (5.3)–(5.7) and on the previous results, the term ξ is uncertain but its components are bounded, i.e.,

$$|\xi(x_0, x, \hat{\theta}_0, \hat{\theta}, \theta, u_0, u_1)| \leq F \tag{5.54}$$

where $F > 0$ is assumed to be a known constant. Note that the quantity y_2 can be viewed as an unmeasurable quantity. Then, the following theorem can be proved:

Theorem 5.3 *Given system (5.53), where $\xi(x_0, x, \hat{\theta}_0, \hat{\theta}, \theta, u_0, u_1)$ satisfies (5.54), and y_2 is not measurable, the control signal (5.52) with $\bar{u}_1$ given by*

$$\dot{\bar{u}}_1(t) \;=\; -U_{Max}\ \text{sign}\{y_1(t) - \frac{1}{2} y_{1_{Max}}\} \tag{5.55}$$

where

$$U_{Max} > 2F \tag{5.56}$$

and $y_{1_{Max}}$ is a piece–wise constant function representing the value of the last singular point of $y_1(t)$ (i.e., the most recent value $y_{1_{Max}}$ such that $\dot{y}_1(t) = 0$) causes the convergence of the system trajectory to the origin of the $y_1 O y_2$ plane in finite time.

Proof: The control law (5.55) can be classified as a sub–optimal second order sliding mode control law, and by following a theoretical development as that provided in Bartolini *et al.* (1999) for the general case, it can be proved that the trajectories on the $y_1 O y_2$ plane are confined within limit parabolic arcs which include the origin. The absolute values of the coordinates of the trajectory intersections with the y_1, and $\dot{y}_1$ axis decrease in time. This condition ensures a contraction of the elements of the sequence $\{y_{1_{Max}}\}$. Moreover, it can be proved that under condition (5.56),

$$|y_1(t)| < |y_1(0)| + \frac{1}{2} \frac{|y_2(0)|^2}{U_{Max}} \tag{5.57}$$

$$|y_2(t)| \leq \sqrt{|y_{1_{Max}}(t)|} < \sqrt{|y_1(0)| + \frac{1}{2}\frac{|y_2(0)|^2}{U_{Max}}} \tag{5.58}$$

hold, as shown in Bartolini *et al.* (1999), and that the convergence of $y_{1_{Max}}$ to zero takes place in finite time. Clearly, if $y_{1_{Max}} \to 0$, then $y_1 \to 0$ and $y_2 \to 0$ in finite time, because they are both bounded by $\max(|y_{1_M}|, \sqrt{|y_{1_M}|})$.

5.2.6 The case $x_0(t_0) = 0$

For $x_0(t_0) = 0$, different schemes can be used for different classes of systems. In this chapter, the adaptive switching proposed in Ge *et al.* (2003) is adopted because this approach is rather general and also capable of solving the finite time escape problem for systems with non–Lipschitz nonlinearities.
When $x_0(t_0) = 0$, the control signal u_0 is chosen as

$$u_0 = x_0 g_0 + u_0^* \tag{5.59}$$

where g_0 is given by (5.9), $\hat{\theta}_0$ is updated by (5.10), and $u_0^* \in I\!R^+$ is a constant. Choosing the Lyapunov function (5.11), its first time derivative is given by

$$\dot{V}_0 \leq -k_0 x_0^2 + u_0^* x_0 \tag{5.60}$$

which leads to the boundedness of x_0 and $\hat{\theta}_0$. Applying control law (5.59), the time evolution of x_0 for the closed–loop system is given by

$$x_0(t) = e^{-\int_{t_0}^{t} \lambda(s)ds} \int_{t_0}^{t} u_0^* e^{\int_{t_0}^{s} \lambda(\tau)d\tau} ds + x_0(t_0) e^{-\int_{t_0}^{t} \lambda(s)ds} \tag{5.61}$$

where $\lambda = \sqrt{k_0^2 + (\varphi_0^T \hat{\theta}_0)^2} - \varphi_0^T \tilde{\theta}_0$. As a consequence, x_0 does not escape and $x_0(\bar{t}) \neq 0, \forall \bar{t} > 0$ and the discontinuous state scaling discussed in Subsection 5.2.3 can be applied. The control law u_0 defined by (5.59) is applied during time interval $[t_0, \bar{t}]$. A new second order sliding mode control law u_1^* and a new update law $\dot{\hat{\theta}}^*$ for time interval $[t_0, \bar{t}]$ can be obtained following the procedure described in Subsections 5.2.3, 5.2.4 and 5.2.5. Since $x_0(\bar{t}) \neq 0$, at time $\bar{t}$ the control input u_0 and u_1 can be switched to (5.8) and (5.52), respectively.

5.2.7 Stability considerations

In this subsection, the stability properties of the presented control scheme are analyzed.

Theorem 5.4 *Under assumptions (5.3)–(5.7), control laws (5.8) and (5.52)–(5.55) with adaptation laws (5.10) and (5.44) along with the switching strategy described in Subsection 5.2.6 are capable of globally asymptotically regulating the uncertain system (5.2) at the origin, while keeping the estimated parameters bounded.*

Proof: To analyse the stability properties of the overall closed loop system (5.2)–(5.8)–(5.52)–(5.55), consider the Lyapunov function candidate

$$V = V_0 + V_{n-1} = \frac{1}{2}x_0^2 + \frac{1}{2}\tilde{\theta}_0^T\Gamma^{-1}\tilde{\theta}_0 + \sum_{j=1}^{n-1}\frac{1}{2}e_j^2 + \frac{1}{2}\tilde{\theta}^T\Gamma^{-1}\tilde{\theta} \tag{5.62}$$

Then, the first time derivative of (5.62) results in

$$\dot{V} \leq -k_0 x_0^2 - \sum_{j=1}^{n-1} k_j e_j^2 + e_{n-1}e_n g_0 \tag{5.63}$$

From (5.63)

$$\forall\, |e_{n-1}| \geq \frac{|e_n g_0|}{\sigma k_{n-1}} \Rightarrow \dot{V} \leq -k_0 x_0^2 - \sum_{j=1}^{n-2} k_j e_j^2 - k_{n-1}(1-\sigma)e_{n-1}^2 \tag{5.64}$$

where $\sigma \in (0,1)$. From (5.64), the closed–loop system with state $E = [x_0, e_1, \ldots, e_{n-1}]^T$ is ISS with respect to $e_n g_0$. This implies that $E \in \mathcal{L}_\infty^n$ and $\tilde{\theta}_0, \tilde{\theta} \in \mathcal{L}_\infty^l$, i.e., x_0, $e_1, \ldots, e_{n-1}$, $\tilde{\theta}_0$, $\tilde{\theta}$ are bounded. Since θ is a constant vector, one also has that $\hat{\theta}_0$ and $\hat{\theta}$ are bounded. Moreover, since $e_n(t)$ is steered to zero in finite time by control law (5.52)–(5.55) as discussed in Subsection 5.2.5.1, from LaSalle's Invariant Theorem (LaSalle, 1960), it follows that $[E, \tilde{\theta}_0, \tilde{\theta}]$ converges to the largest invariant set M contained in the set where $\dot{V} = 0$, which implies that $E(t) \to 0$ as $t \to \infty$. Hence, $[x_0, e_1, \ldots, e_n]^T \to 0$ as $t \to \infty$.
From (5.34) all the virtual controls $\alpha_i(0, \ldots, 0, \hat{\theta}_0, \hat{\theta}) = 0$ and, as a consequence, it follows that $E \to 0$ as $t \to \infty$ imply that $[x_0, z] \to 0$ as $t \to \infty$, and, consequently, $[x_0, x] \to 0$ as $t \to \infty$.

5.2.8 Simulation results

The control scheme presented in this section is applied to the bilinear model of a mobile robot with small angle measurement error considered in Morin *et al.* (1998). The model equations are given by

$$\begin{cases} \dot{x}_l &= \left(1-\frac{\varepsilon^2}{2}\right)v \\ \dot{y}_l &= \theta_l v + \varepsilon v \\ \dot{\theta}_l &= \omega \end{cases} \tag{5.65}$$

where x_l, y_l denote the coordinates of the center of mass on the plane, θ_l denotes the heading angle measured from the x–axis, v denotes the magnitude of the translational velocity of the center of mass, and w denotes the angular velocity of the robot. System (5.65) can be transformed into form (5.2) through the following change of coordinates

$$\begin{array}{rcl} x_0 &=& x_l \\ x_1 &=& y_l \\ x_2 &=& \theta_l + \varepsilon \\ u_0 &=& v \\ u_1 &=& \omega \end{array} \tag{5.66}$$

The resulting transformed system is

$$\begin{cases} \dot{x}_0 &= (1-\frac{\varepsilon^2}{2})u_0 \\ \dot{x}_1 &= x_2 u_0 \\ \dot{x}_2 &= u_1 \end{cases} \tag{5.67}$$

5.2.8.1 Simulation Case A

For the sake of simplicity, it is assumed that $\theta = 1-\frac{\varepsilon^2}{2} > 0$ and $x_0(t_0) \neq 0$. Since $\dot{x}_0 = \theta u_0$, with $\theta > 0$, control signal u_0 can be chosen as

$$u_0 = -k_0 x_0 \tag{5.68}$$

with $k_0 > 0$. As a result, one has that $x_0 \to 0$ as $t \to \infty$.
Applying the discontinuous state scaling (5.14) to (5.65), the resulting z–subsystem is

$$\begin{array}{rcl} \dot{z}_1 &=& -k_0 z_2 + k_0 z_1 \theta \\ \dot{z}_2 &=& u_1 \end{array} \tag{5.69}$$

Table 5.1: Simulation parameters

Parameter	Value
$x_0(0)$	2
$x_1(0)$	2
$x_2(0)$	2
k_0	1
k_1	1
Γ	10
U_{Max}	10
$\hat{\theta}(0)$	0

Applying the backstepping procedure to system (5.69), the following quantities are obtained

$$\dot{\hat{\theta}} = \tau_1 = \Gamma k_0 z_1^2 \tag{5.70}$$

$$\alpha_1 = \frac{k_1 + k_0\hat{\theta}}{k_0} z_1 \tag{5.71}$$

According to (5.49), the sliding variable is

$$s \;=\; z_2 - \alpha_1 \tag{5.72}$$

The control signal u_1 is calculated as in (5.52), i.e.,

$$u_1 \;=\; \overline{u}_1 - (k_1 + k_0\hat{\theta})(z_2 - z_1\hat{\theta}) + \Gamma k_0 z_1^3 \tag{5.73}$$

where $\overline{u}_1$ is given, according to (5.55), by integrating

$$\dot{\overline{u}}_1 = -U_{Max}\ \text{sign}(s - \frac{1}{2}s_{Max}) \tag{5.74}$$

The simulation parameters are reported in Table 5.1. The time evolution of the control signals u_0 and u_1 is given in Fig. 5.1. Note that control u_1 is a continuous control signal as previously discussed. From Fig. 5.2 it appears that all the states x_0, x_1, and x_2 converge to zero. In Fig. 5.3 the time evolution of the sliding variable is reported: it is steered to zero quite rapidly. Note that also the first time derivative of the sliding variable is steered to zero as shown in Fig. 5.4, since a second order sliding mode is enforced. Fig 5.5 shows the real value of the unknown constant parameter θ and its estimate $\hat{\theta}$. One can note that the estimation error is bounded

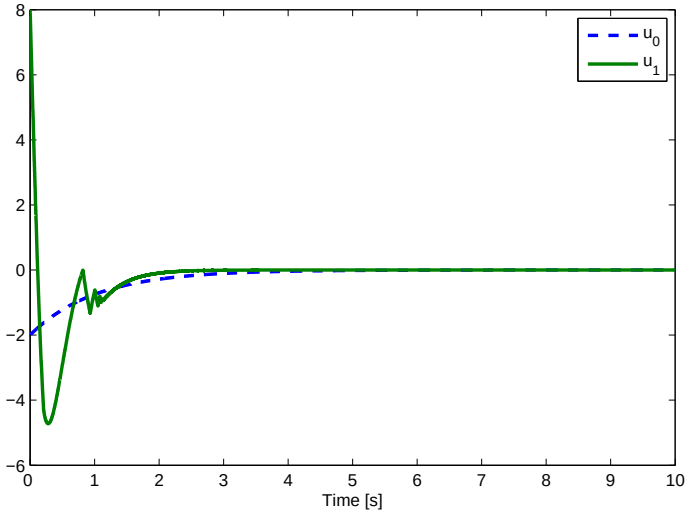

Figure 5.1: Case A: the evolution of control signals u_0 and u_1

but $\hat{\theta}$ does not approach the actual value of θ. In fact, the convergence of the parameter values is not necessary to attain the pre–specified control objective. This also happens in conventional backstepping control with tuning functions.

5.2.8.2 Simulation Case B

In this simulation case, it is again assumed that $\theta > 0$ but the initial state condition is $x(0) = [x_0(0), x_1(0), x_2(0)]^T = [0, 1, 1]^T$. Since the nonlinearity of the considered system satisfies the Lipschitz condition $|\phi_0^T \theta| \leq c_0 |x_0|$, which is a particular case of the problem addressed in this chapter, the constant control based switching strategy (Jiang, 1996) can be applied. The control signal u_0 is chosen as

$$u_0 = u_0^* \tag{5.75}$$

with $u_0^* > 0$. System (5.67) can be rewritten as

$$\begin{aligned} x_1 &= u_0^* x_2 && (5.76) \\ x_2 &= u_1 && (5.77) \end{aligned}$$

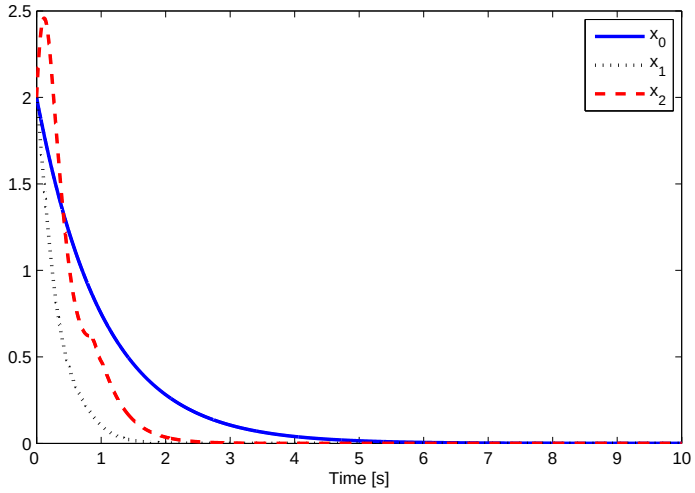

Figure 5.2: Case A: the time evolution of x_0, x_1 and x_2

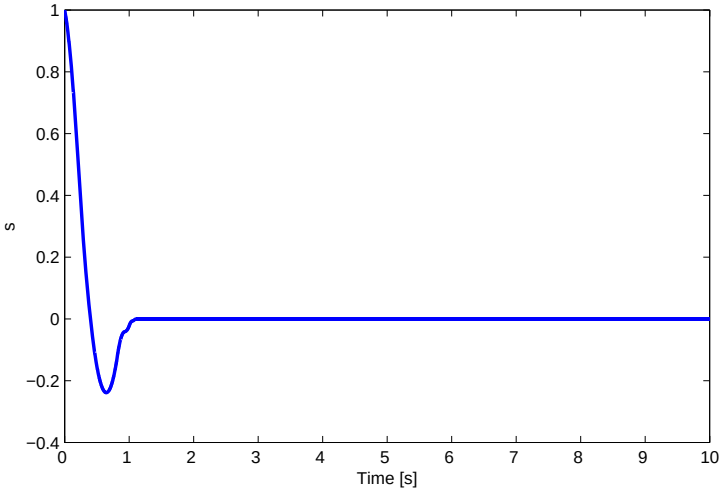

Figure 5.3: Case A: the sliding variable s

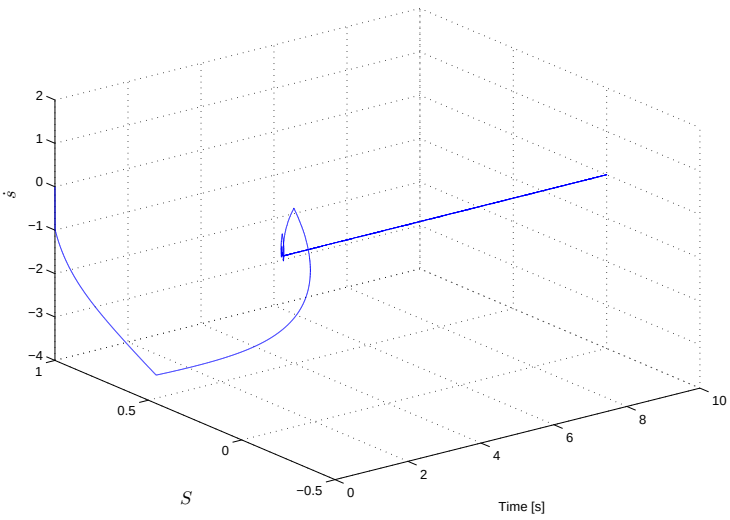

Figure 5.4: Case A: the time evolution of the sliding quantity s and its first time derivative $\dot{s}$

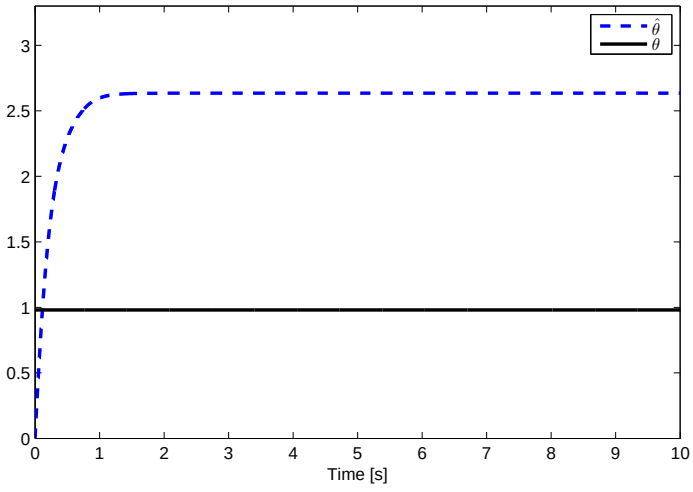

Figure 5.5: Case A: parameter θ and its estimates $\hat{\theta}$

and the backstepping based procedure can be directly applied, yielding

$$\begin{aligned} e_1 &= x_1 \\ \alpha_1 &= -\tfrac{k_1}{u_0^*} e_1 \\ e_2 &= x_2 - \alpha_1 \end{aligned} \tag{5.78}$$

According to (5.49), the sliding variable is

$$s = x_2 - \alpha_1 \tag{5.79}$$

The control signal u_1 is calculated as in (5.52), i.e.,

$$u_1 = \overline{u}_1 - k_1 x_2 \tag{5.80}$$

where $\overline{u}_1$ is given, according to (5.55), as

$$\dot{\overline{u}}_1 = -U_{max}\ \text{sign}(s - \frac{1}{2} s_{max}) \tag{5.81}$$

The simulation parameters k_1, U_{max} are reported in Table 5.1, and $u_0^* = 1$. The control signals u_0 and u_1, given respectively by (5.75) and (5.80), are applied for $t \in [0, 1s]$. At $t = 1s$ the control signals u_0 and u_1 are switched to (5.68) and (5.73), respectively.
The time evolution of the control signals u_0 and u_1 is reported in Fig. 5.6. As shown in Fig. 5.7, all the states x_0, x_1, and x_2 converge to zero. In Fig. 5.8 the time evolution of the sliding variable which is steered to zero in finite time is illustrated. Fig 5.9 shows the real value of the unknown constant parameter θ and its estimate $\hat{\theta}$. As in Case A, the estimation error is bounded but $\hat{\theta}$ does not approach the real value of θ.

5.2.9 Conclusions

In this section an adaptive second order sliding mode control scheme has been presented for stabilizing a class of nonholonomic systems in chained form affected by uncertain drift nonlinearity and parametric uncertainties. The key idea is to transform the original system, through a backstepping–based procedure, into a form suitable to design a sliding manifold upon which to enforce a second order sliding mode. In this way the overall stabilization problem can be solved relying on a continuous control signal. This fact enables the application of the presented strategy even to systems, such

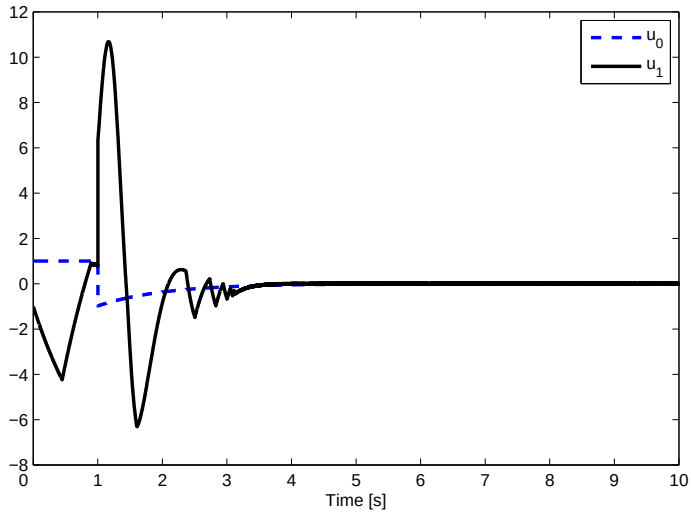

Figure 5.6: Case B: the evolution of control signals u_0 and u_1

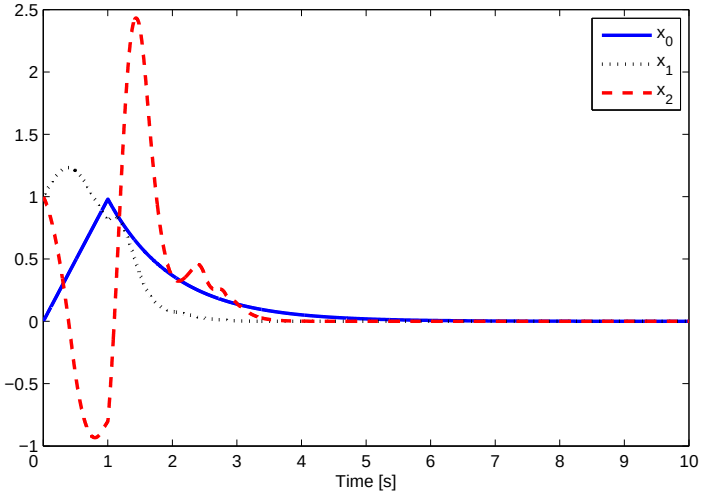

Figure 5.7: Case B: the time evolution of x_0, x_1 and x_2

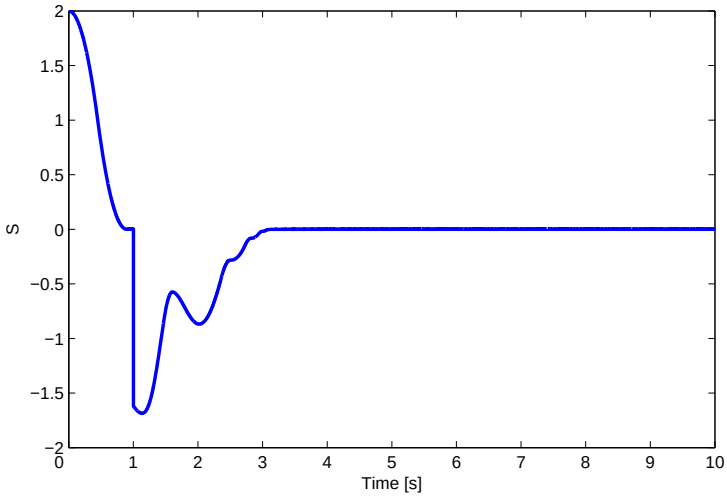

Figure 5.8: Case B: the sliding variable s

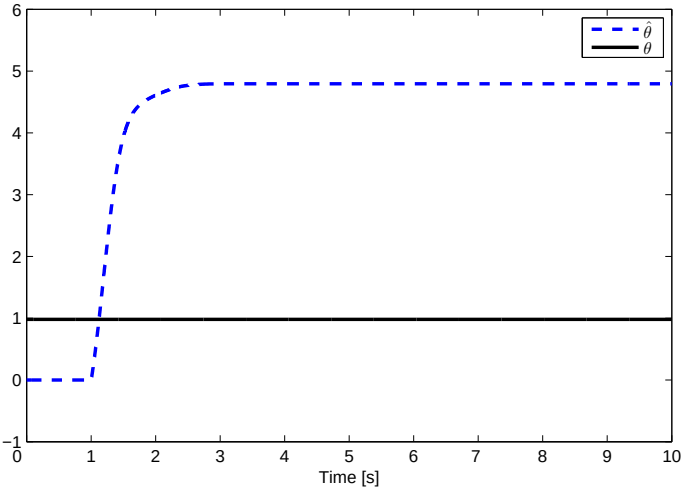

Figure 5.9: Case B: parameter θ and its estimates $\hat{\theta}$

as mechanical ones, for which the chattering effect, typical of conventional first order sliding mode control, may be unacceptable. By applying the presented control strategy, in spite of the presence of uncertainties, the system states converge to the origin, while the estimated parameters remain bounded. Simulation results have shown the effectiveness of the presented control scheme.

5.3 Chained form system affected by matched and unmatched uncertainties

In this section the more complicated problem of stabilizing a class of chained form systems affected by both matched and unmatched uncertainties is addressed. The presence of unmatched uncertainties is particularly critical for any sliding mode controller. A controller which can be classified as an adaptive multiple–surface sliding mode controller is designed in this section relying on a suitable function approximation approach.
Function approximation based adaptive multiple–surface sliding controllers have been introduced in Huang and Chen (2004) to deal with nonlinear systems, relying on the concept of multiple–surface sliding mode proposed by Won and Hedrick (1996) to cope with unmatched uncertainties. In the considered case the problem is further complicated by the complexity of the system model necessary to capture the nonholonomic nature of the systems. The function approximation technique here adopted (Huang and Kuo, 2001) is used to transform the uncertain terms into a finite combination of orthonormal basis functions. Since the coefficients of the approximation series are time–invariant, the update laws for the approximating series can thus be derived relying on a standard Lyapunov approach to ensure the closed–loop stability of the overall controlled system.
As a novelty with respect to other proposals appeared in the literature to deal with nonholonomic uncertain system (Jiang, 1996, 2000; Do and Pan, 2002; Xi *et al.*, 2003; Ge *et al.*, 2003), it is not assumed that the uncertain terms are bounded by some known functions of the system states.
Another positive aspect of the presented control scheme, is that the control signal is designed so that a second order sliding mode (Bartolini *et al.*, 1999; Levant, 2003) is enforced. This implies that the actual control is continuous and this allows us to circumvent the problems usually associated with the

application of conventional sliding mode control to real plants, mainly due to the notorious chattering effect (Fridman, 2001*b*; Levant, 2007).

5.3.1 The problem statement

In this section, the following class of systems, which can be viewed as systems in perturbed chained form affected by uncertainties, is considered

$$\begin{cases} \dot{x}_0 &= d_0 u_0 + x_0 f_0(x_0) \\ &\vdots \\ \dot{x}_i &= x_{i+1} u_0 + \delta_i(x_0, u_0, \overline{x}_i) \qquad 1 \leq i \leq n \\ &\vdots \\ \dot{x}_n &= d_n u_1 + \delta_n(x_0, u_0, x) \end{cases} \tag{5.82}$$

where $x = [x_1, x_2, \ldots, x_n]^T$, $[x_0, x^T]^T \in I\!R^{n+1}$ are the system states, $\overline{x}_i = [x_1, \ldots, x_i]^T$, u_0 and u_1 are scalar control inputs, $f_0(x_0)$ and $\delta_i(x_0, u_0, \overline{x}_i)$ are unknown functions which represent the possible modeling errors and parametric uncertainties affecting the system, and d_0 and d_n are the unknown control gains. Note that $\delta_i(x_0, u_0, \overline{x}_i)$ can also include uncertain drift terms or parametric uncertainties.
As for the uncertain term $f_0(x_0)$ and $\delta_i(x_0, u_0, \overline{x}_i)$ it is assumed that a known smooth nonnegative function $c_0(x_0)$, and unknown smooth nonnegative functions $\varphi_j(u_0, x_0, \overline{x}_i)$ exist such that

$$|f_0(x_0)| \leq c_0(x_0) \tag{5.83}$$

$$\delta_i(u_0, x_0, \overline{x}_i) = \sum_{j=1}^{i} x_j \varphi_j(u_0, x_0, \overline{x}_i) \qquad 0 \leq i \leq n \tag{5.84}$$

Assumption (5.84) implies that the uncertainties $\delta_i(u_0, x_0, \overline{x}_i)$ satisfy a triangularity structure requirement. Note that this assumption is a quite common assumption in the framework of robust and adaptive nonlinear control (Krstić *et al.*, 1995). As a consequence of (5.84), the origin is a possible equilibrium point of the considered system (5.82). It is important to observe that this assumption is significantly less stringent than requiring the knowledge of a function of the state bounding the uncertainty terms as usually done in the classical nonholonomic literature.
As for the control gain d_0 and d_n it is assumed that there are known positive

constants $\overline{d}_0$, d_{n1} and d_{n2} such that

$$0 < \overline{d}_0 \leq \quad d_0 \tag{5.85}$$

$$0 < d_{n1} \leq \quad d_n \quad \leq d_{n2} \tag{5.86}$$

Taking into account the foregoing problem formulation, the control objective is to design the control laws u_0 and u_1 appearing in (5.82) such that $[x_0, x^T]^T$, as $t \to \infty$, converge to a small vicinity of the equilibrium point, which will be formally defined in the sequel of this section relying on the concept of Input–to–State Stability (Isidori, 1999), and all the other signals in the closed–loop system are bounded.
As in Section 5.2, the control inputs u_0 and u_1 will be designed in two separate steps.

5.3.2 The x_0–subsystem

In this section, the case $x_0(t_0) \neq 0$ is considered. The case when $x_0(t_0) = 0$ deserve a special treatment, and will be dealt with in Section 5.3.6. when $x_0(t_0) \neq 0$, the following theorem can be proved.

Theorem 5.5 *Consider the chained form uncertain system (5.82). Then, for any initial condition $x_0(t_0) \neq 0$, the control law u_0 given by*

$$u_0(x_0) = x_0 g_0(x_0) \tag{5.87}$$

with

$$g_0(x_0) = -\frac{c_0(x_0) + k_0}{\overline{d}_0} \tag{5.88}$$

where $k_0 > 0$ is a design parameter, can globally asymptotically regulate the state x_0 to zero, i.e.

$$\lim_{t \to \infty} x_0(t) = 0$$

Moreover, since $x_0(t_0) \neq 0$ is assumed, u_0 ensures that x_0 does not cross zero $\forall t \in [t_0, \infty)$.

Proof: Consider the Lyapunov function candidate

$$V_0 = \frac{1}{2} x_0^2 \tag{5.89}$$

The first time derivative of (5.89) is given by

$$\begin{aligned}\dot{V}_0 &= x_0(d_0 g_0(x_0)x_0 + x_0 f_0(x_0)) \\ &\leq x_0\left[\frac{d_0}{\overline{d}_0}(-c_0(x_0)-k_0)x_0 + x_0 c_0(x_0)\right] \\ &\leq -\frac{d_0}{\overline{d}_0}k_0 x_0^2 - \frac{d_0}{\overline{d}_0}c_0(x_0)x_0^2 + c_0(x_0)x_0^2 \\ &\leq -k_0 x_0^2 \end{aligned} \tag{5.90}$$

then one can conclude that $x_0 \to 0$ as $t \to \infty$.
Applying the control law (5.87) to system (5.82), the solution $x_0(t)$ of the closed–loop system is given by

$$x_0(t) = x_0(t_0)e^{-\int_{t_0}^{t}\left((k_0+c_0(\tau))d_0/\overline{d}_0 - f_0(\tau)\right)d\tau} \tag{5.91}$$

Thus, for any initial instant $t_0 \geq 0$, and any initial condition $x_0(t_0) \neq 0$, u_0 ensures that x_0 does not cross zero $\forall t \in [t_0, \infty)$.

5.3.3 Discontinuous state scaling

As proved in Section 5.3.2, the control law (5.87) can globally asymptotically regulate the state x_0 to zero. To overcome the loss of controllability of the x–subsystem in the limiting case, when $u_0 = 0$, the discontinuous state scaling transformation discussed in Subsection 5.2.3 is adopted. Then, by applying the state transformation (5.14) to system (5.82), it yields

$$\begin{aligned}\dot{z}_i &= \frac{\dot{x}_i}{x_0^{n-i}} - (n-i)\frac{\dot{x}_0 x_i}{x_0^{n-i+1}} \\ &= \frac{u_0 x_{i+1} + \delta_i}{x_0^{n-i}} - (n-i)\frac{x_i(d_0 u_0 + x_0 f_0)}{x_0^{n-i+1}} \\ &= g_0(x_0)z_{i+1} + \Delta_i(x_0, \overline{z}_i) \end{aligned} \tag{5.92}$$

where

$$\Delta_i(x_0, \overline{z}_i) = \frac{\delta_i(u_0, x_0, \overline{x}_i)}{x_0^{n-i}} - (n-i)(d_0 g_0(x_0) + f_0(x_0))z_i \tag{5.93}$$

Then, the resulting z–subsystem is given by

$$\begin{cases} \dot{z}_i &= g_0(x_0)z_{i+1} + \Delta_i(x_0, \overline{z}_i), \qquad 1 \leq i \leq n \\ \dot{z}_n &= d_n u_1 + \Delta_n(x_0, z) \end{cases} \tag{5.94}$$

where $\overline{z}_i = [z_1, \ldots, z_i]^T$.

5.3.4 The adaptive multiple–surface sliding procedure

Differently from the case considered in Section 5.2, the backstepping design procedure cannot be applied to the considered z–subsystem (5.163) due to the time–variant nature of the uncertainties. Moreover, since the bounds of the uncertainty terms $\Delta_i(x_0, \overline{z}_i)$ are unknown, even traditional sliding mode controllers (Utkin *et al.*, 1999) and multiple–surface sliding controllers (Won and Hedrick, 1996) cannot be designed. To deal with the particularly hard kind of uncertainty considered in this section, the controller is designed relying on the function approximation based adaptive multiple–surface sliding control approach proposed in Huang and Chen (2004).
The function approximation technique is based on the fact that if a piecewise continuous real–valued function $f(t)$ satisfies the Dirichlet conditions, then it can be transformed into the Fourier series within a time interval $[0; T_s]$ as

$$f(t) = a_0 + \sum_{n=1}^{\infty}(a_n \cos(v_n t) + b_n \sin(v_n t)) \tag{5.95}$$

where $v_n = 2n\pi/T_s$ are the frequencies of the sinusoidal function. Equation (5.95) can be rewritten as

$$f(t) = W^T h(t) + \varepsilon \tag{5.96}$$

where

$$h(t) = [1, \cos(v_1 t), \sin(v_1 t), \ldots, \cos(v_{n_f} t), \sin(v_{n_f} t)]^T \tag{5.97}$$

$$W = [a_0, a_1, b_1, \ldots, a_{n_f}, b_{n_f}]^T \tag{5.98}$$

$$\varepsilon = \sum_{n=n_f+1}^{\infty} (a_n \cos(v_n t) + b_n \sin(v_n t)) \tag{5.99}$$

Then, if n_f is chosen sufficiently large function $f(t)$ can be approximated by

$$f(t) \approx W^T h(t) \tag{5.100}$$

Note that (5.100) is a linear approximation of the time-varying function $f(t)$ characterized by a basis function vector and a time–invariant coefficient vector.
In this section, (5.100) is used to represent the unmatched uncertainties affecting the system model. Since the coefficients of the approximation series are time–invariant, the update laws for tuning such coefficients can be

derived relying on a standard Lyapunov approach to ensure the closed–loop stability. Note that, as a novelty with respect to other proposals, no knowledge of the bounds of the uncertainty terms is required to apply the presented control scheme in analogy with Huang and Kuo (2001).
Differently from the multiple-surface sliding approach proposed in Huang and Kuo (2001) and in Huang and Chen (2004), the control signal is designed relying on second order sliding mode control technique (Levant, 1993; Bartolini *et al.*, 1999). The design procedure is carried out so that the discontinuity necessary to enforce a sliding mode is confined to the control vector derivative, while the actual control is continuous.

The control design procedure can be subdivided into several steps:

5.3.4.1 Step 1

With reference to system (5.94) the following quantities are defined

$$s_1 = z_1 \tag{5.101}$$
$$s_2 = z_2 - \alpha_1 \tag{5.102}$$

By differentiating (5.101), it yields

$$\dot{s}_1 = g_0 s_2 + g_0 \alpha_1 + \overline{\Delta}_1 \tag{5.103}$$

where $\overline{\Delta}_1 = \Delta_1$. Using the function approximation technique introduced in Huang and Kuo (2001), the quantity $\overline{\Delta}_1$ can be represented as

$$\overline{\Delta}_1 = \omega_1 C_1 + \varepsilon_1 \tag{5.104}$$

where $\omega_1 \in I\!R^{n_1}$ is a weighting vector, $C_1 \in I\!R^{n_1}$ is a vector of orthonormal basis, and $\varepsilon_1 \in I\!R$ is the approximation error, n_1 being the number of basis used in the approximation. The uncertain term $\overline{\Delta}_1$ can be approximated as

$$\hat{\overline{\Delta}}_1 = \hat{\omega}_1 C_1 \tag{5.105}$$

where $\hat{\omega}_1$ is a suitable estimate of ω_1, specified in the sequel.
Consider the candidate Lyapunov function

$$V_1 = \frac{1}{2} s_1^2 + \frac{1}{2} \tilde{\omega}_1^T Q_1^{-1} \tilde{\omega}_1 \tag{5.106}$$

where $Q_1 = Q_1^T > 0$, and $\tilde{\omega}_1 = \omega_1 - \hat{\omega}_1$. By differentiating (5.106), it yields

$$\dot{V}_1 = s_1(g_0 s_2 + g_0\alpha_1 + \overline{\Delta}_1) - \tilde{\omega}_1^T Q_1^{-1}\dot{\hat{\omega}}_1 \tag{5.107}$$

Choosing the virtual control α_1, and the update law for the estimate $\hat{\omega}_1$ as follows

$$\alpha_1 = \frac{1}{g_0}\left(- k_1 s_1 - \hat{\overline{\Delta}}_1 \right) \tag{5.108}$$

$$\dot{\hat{\omega}}_1 = Q_1 C_1 s_1 \tag{5.109}$$

where $k_1 > 0$ is a positive parameter design, one has that

$$\dot{V}_1 \leq -k_1 s_1^2 + g_0 s_1 s_2 + s_1\varepsilon_1 \tag{5.110}$$

5.3.4.2 Step i

Introduce the quantity

$$s_i = z_i - \alpha_{i-1} \tag{5.111}$$

From (5.111), it yields

$$\dot{s}_i = g_0 s_{i+1} + g_0\alpha_i + \overline{\Delta}_i - \sum_{k=1}^{i-1} \frac{\partial \alpha_{i-1}}{\partial z_k} g_0 z_{k+1} \tag{5.112}$$

where the lumped uncertainty term $\overline{\Delta}_i$ is given by

$$\overline{\Delta}_i = \Delta_i - \sum_{k=1}^{i-1} \frac{\partial \alpha_{i-1}}{\partial z_k}\Delta_k - \frac{\partial \alpha_{i-1}}{\partial \hat{\overline{\Delta}}_{i-1}} \dot{\hat{\overline{\Delta}}}_{i-1} \tag{5.113}$$

This term can be represented as

$$\overline{\Delta}_i = \omega_i C_i + \varepsilon_i \tag{5.114}$$

where $\omega_i \in I\!R^{n_i}$ is a weighting vector, $C_i \in I\!R^{n_i}$ is a vector of orthonormal basis, and $\varepsilon_i \in I\!R$ is the approximation error, n_i being the number of basis used in the approximation. The uncertain term $\overline{\Delta}_i$ can be approximated as

$$\hat{\overline{\Delta}}_i = \hat{\omega}_i C_i \tag{5.115}$$

where $\hat{\omega}_i$ is a suitable estimate of ω_i, specified in the sequel.

Consider the Lyapunov function candidate

$$V_i = V_{i-1} + \frac{1}{2}s_i^2 + \frac{1}{2}\tilde{\omega}_i^T Q_i^{-1}\tilde{\omega}_i \tag{5.116}$$

where $Q_i = Q_i^T > 0$, yielding

$$\begin{aligned}\dot{V}_i &\leq -\sum_{j=1}^{i-1} k_j s_j^2 + \sum_{j=1}^{i-1} s_j\varepsilon_j - \tilde{\omega}_i^T Q_i^{-1}\dot{\hat{\omega}}_i + s_i\Big[g_0 s_{i-1} \\ &\quad + g_0 s_{i+1} + g_0\alpha_i - \sum_{k=1}^{i-1}\frac{\partial\alpha_{i-1}}{\partial z_k}g_0 z_{k+1} + \overline{\Delta}_i\Big]\end{aligned} \tag{5.117}$$

By selecting the virtual control α_i as

$$\alpha_i = \frac{1}{g_0}\big(-k_i s_i - g_0 s_{i-1} - \hat{\overline{\Delta}}_i + \sum_{k=1}^{i-1}\frac{\partial\alpha_{i-1}}{\partial z_k}g_0 z_{k+1}\big) \tag{5.118}$$

with $k_i > 0$, then (5.117) results in

$$\dot{V}_i \leq -\sum_{j=1}^{i} k_j s_j^2 + \sum_{j=1}^{i} s_j\varepsilon_j + g_0 s_i s_{i+1} - \tilde{\omega}_i^T Q_i^{-1}(\dot{\hat{\omega}}_i - Q_i C_i s_i) \tag{5.119}$$

By choosing the update law for the estimate $\hat{\omega}_i$ as

$$\dot{\hat{\omega}}_i = Q_i C_i s_i \tag{5.120}$$

one has

$$\dot{V}_i \leq -\sum_{j=1}^{i} k_j s_j^2 + \sum_{j=1}^{i} s_j\varepsilon_j + g_0 s_i s_{i+1} \tag{5.121}$$

5.3.4.3 Step $n-1$

At step $n-1$, introduce the quantity

$$s_{n-1} = z_{n-1} - \alpha_{n-2} \tag{5.122}$$

Its first time derivative is given by

$$\dot{s}_{n-1} = g_0 s_n + g_0\alpha_{n-1} + \overline{\Delta}_{n-1} - \sum_{k=1}^{n-2}\frac{\partial\alpha_{n-2}}{\partial z_k}g_0 z_{k+1} \tag{5.123}$$

where

$$s_n = z_n - \alpha_{n-1} \tag{5.124}$$

and, according to (5.113), the lumped uncertainty term $\overline{\Delta}_{n-1}$ results in

$$\overline{\Delta}_{n-1} = \Delta_{n-1} - \sum_{k=1}^{n-2} \frac{\partial \alpha_{n-2}}{\partial z_k} \Delta_k - \frac{\partial \alpha_{n-2}}{\partial \hat{\overline{\Delta}}_{n-2}} \dot{\hat{\overline{\Delta}}}_{n-2} \tag{5.125}$$

According to (5.116), introduce the Lyapunov function candidate

$$V_{n-1} = V_{n-2} + \frac{1}{2} s_{n-1}^2 + \frac{1}{2} \tilde{\omega}_{n-1}^T Q_{n-1}^{-1} \tilde{\omega}_{n-1} \tag{5.126}$$

where $Q_{n-1} = Q_{n-1}^T > 0$. From (5.118) and (5.120), at step $n-1$, the virtual control and the update law, respectively, result in

$$\begin{aligned} \alpha_{n-1} &= \frac{1}{g_0} \big(- k_{n-1} s_{n-1} - g_0 s_{n-2} - \hat{\overline{\Delta}}_{n-2} \\ &\quad + \sum_{k=1}^{n-2} \frac{\partial \alpha_{n-2}}{\partial z_k} g_0 z_{k+1} \big) \end{aligned} \tag{5.127}$$

$$\dot{\hat{\omega}}_{n-1} = Q_{n-1} C_{n-1} s_{n-1} \tag{5.128}$$

with $k_{n-1} > 0$. From (5.127) and (5.128), the first time derivative of (5.126) is

$$\dot{V}_{n-1} \leq - \sum_{j=1}^{n-1} k_j s_j^2 + \sum_{j=1}^{n-1} s_j \varepsilon_j + g_0 s_n s_{n-1} \tag{5.129}$$

Then, by relying on the concept of input-to-state stability (Isidori, 1999), the following result can be proved.

Theorem 5.6 *The dynamic system*

$$\begin{cases} \dot{s}_1 = \dot{z}_1 \\ \dot{s}_2 = \dot{z}_2 - \dot{\alpha}_1 \\ \quad \vdots \\ \dot{s}_{n-1} = \dot{z}_{n-1} - \dot{\alpha}_{n-2} \end{cases} \tag{5.130}$$

where the states s_i, $i = 1, \ldots, n-1$, are given by (5.111), z_i, $i = 1, \ldots, n$, are defined in (5.94), α_i, $i = 1, \ldots, n-1$, as in (5.118), is input-to-state-stable (ISS) (Isidori, 1999) with respect to $\mu = [0, 0, \ldots, g_0 s_n]^T$ and $\varepsilon = [\varepsilon_1, \varepsilon_2, \ldots, \varepsilon_{n-1}]^T$, and if both μ and ε goes to zero then

$$\lim_{t \to \infty} \|s\| = 0$$

where $s = [s_1, s_2, \ldots, s_{n-1}]^T$.

Proof: The Lyapunov function (5.126) is an ISS Lyapunov function (Isidori, 1999). Indeed, from (5.129) one has that

$$\begin{aligned} \dot{V}_{n-1} &\leq -\bar{k}\|s\|^2 + s^T\varepsilon + s^T\mu \\ &\leq -\bar{k}\|s\|^2 + \|s\|\|\varepsilon\| + \|s\|\|\mu\| \end{aligned} \tag{5.131}$$

where $\bar{k} = \min_{1\leq j\leq n-1}\{k_j\}$. Thus, from (5.131), it turns out that

$$\forall\ \|s\| \geq \frac{2}{\sigma\bar{k}} \max\{\|\mu\|; \|\varepsilon\|\} \tag{5.132}$$

where $\sigma \in (0,1)$, the following inequality holds

$$\dot{V}_{n-1} \leq -\bar{k}(1-\sigma)\|s\|^2 \tag{5.133}$$

This implies that there exist a function $\chi(\cdot,\cdot)$ of class $\mathcal{KL}$ and functions $\rho_\varepsilon(\cdot)$ and $\rho_\mu(\cdot)$ of class $\mathcal{K}$ (called ISS gain functions) such that, for any initial state $s(0)$ one has that

$$\|s(t)\| \leq \chi(\|s(0)\|, t) + \rho_\varepsilon(\|\varepsilon\|_\infty) + \rho_\mu(\|\mu\|_\infty) \tag{5.134}$$

Hence, if $\|\varepsilon\|$ and $\|\mu\|$ are bounded, then $\|s\|$ is bounded (Isidori, 1999). Moreover, if $\mu \to 0$ and $\varepsilon \to 0$, for $t \to \infty$, then $s \to 0$ asymptotically. Furthermore, by applying the LaSalle's Invariant Theorem (LaSalle, 1960), it follows that $\tilde{\omega}_i$, $1 \leq i \leq n-1$, and, as a consequence, $\hat{\omega}_i$, $1 \leq i \leq n-1$, are bounded.

Note that ε can be steered to zero by choosing a sufficiently large number of basis functions, while μ can be turned to zero, for instance, by designing a control law u_1 such that s_n is steered to zero in finite time.

5.3.5 The control signal u_1

From Theorem 5.6 one can observe that, if a sufficiently large number of basis functions are chosen so as to have $\varepsilon \approx 0$, it is possible to steer s to zero with a control law u_1 capable of steering s_n to zero.
In this section, a second order sliding mode control law is designed to steer to zero not only s_n but also its first time derivative $\dot{s}_n$, and this is attained in finite time. As in Subsection 5.2.5, the design procedure is carried relying

on the second order sliding mode control methodology so that the actual control u_1 results in being continuous.

From (5.124), one has

$$\dot{s}_n = d_n u_1 + \overline{\Delta}_n - \sum_{k=1}^{n-1} \frac{\partial \alpha_{n-1}}{\partial z_k} g_0 z_{k+1} \tag{5.135}$$

where the lumped uncertainty term $\overline{\Delta}_n$ is given by

$$\overline{\Delta}_n = \Delta_n - \sum_{k=1}^{n-1} \frac{\partial \alpha_{n-1}}{\partial z_k} \Delta_k - \frac{\partial \alpha_{n-1}}{\partial \hat{\overline{\Delta}}_{n-1}} \dot{\hat{\overline{\Delta}}}_{n-1} \tag{5.136}$$

Now, consider the Lyapunov function candidate

$$V_n = \frac{1}{2} s_n^2 + \frac{1}{2} \tilde{\omega}_n^T Q_n^{-1} \tilde{\omega}_n + \frac{1}{2} \gamma_n^{-1} \tilde{d}_n^2 \tag{5.137}$$

where $Q_n = Q_n^T > 0$, $\gamma_n > 0$, and $\tilde{d}_n = d_n - \hat{d}_n$, with $\hat{d}_n$ being a suitable estimate of d_n. The first derivative of (5.137) is

$$\dot{V}_n \leq s_n \left(d_n u_1 + \overline{\Delta}_n - \sum_{k=1}^{n-1} \frac{\partial \alpha_{n-1}}{\partial z_k} g_0 z_{k+1} \right) - \tilde{\omega}_n^T Q_n^{-1} \dot{\tilde{\omega}}_n - \gamma_n^{-1} \tilde{d}_n \dot{\tilde{d}}_n \tag{5.138}$$

Thus, the control signal u_1 can be chosen as

$$u_1 = \bar{u}_1 + \tau_1 \tag{5.139}$$

with

$$\bar{u}_1 = \frac{1}{\hat{d}_n} \left(-k_n s_n - \hat{\overline{\Delta}}_n + \sum_{k=1}^{n-1} \frac{\partial \alpha_{n-1}}{\partial z_k} g_0 z_{k+1} \right) \tag{5.140}$$

where $k_n > 0$ is a design parameter, and τ_1 will be designed later so as to robustly steer s_n to zero in finite time.
By substituting (5.139) in (5.138), it results

$$\begin{aligned} \dot{V}_n = & -k_n s_n^2 - \tilde{\omega}_n^T Q_n^{-1} (\dot{\tilde{\omega}}_n - Q_n C_n s_n) \\ & -\gamma_n^{-1} \tilde{d}_n (\dot{\tilde{d}}_n - \gamma_n u_1 s_n) + s_n (\tau_1 / d_n + \varepsilon_n) \end{aligned} \tag{5.141}$$

By choosing the update laws for the estimates $\hat{d}_n$ and $\hat{\omega}_n$ as follows

$$\dot{\hat{\omega}}_n = Q_n C_n s_n \tag{5.142}$$

$$\dot{\hat{d}}_n = \begin{cases} \pi_n = \gamma_n u_1 s_n, & \text{if } \hat{d}_n > d_{n1} \text{ or } \pi_n > 0 \\ 0, & \text{if } \hat{d}_n \leq d_{n1} \text{ and } \pi_n < 0 \end{cases} \tag{5.143}$$

it yields

$$\dot{V}_n \leq -k_n s_n^2 + s_n(\tau_1/d_n + \varepsilon_n) + \begin{cases} 0, & \text{if } \hat{d}_n > d_{n1} \text{ or } \pi_n > 0 \\ \gamma_n^{-1}\tilde{d}_n \pi_n, & \text{if } \hat{d}_n \leq d_{n1} \text{ and } \pi_n < 0 \end{cases} \tag{5.144}$$

Since the last term in (5.144) is nonpositive, one has

$$\dot{V}_n \leq -k_n s_n^2 + s_n(\tau_1/d_n + \varepsilon_n) \tag{5.145}$$

Relying on the concept of ISS, (5.145) implies that if τ_1 and ε_n are bounded, then s_n is also bounded. Moreover, it turns out that $\tilde{\omega}_n$ and $\tilde{d}_n$, and consequently $\hat{\omega}_n$ and $\hat{d}_n$ are bounded.

5.3.5.1 The second order sliding mode control

Now the point is to design τ according to the second order sliding mode control technique in order to steer s_n to zero in finite time in presence of uncertainties. To this end, the chosen sliding variable is

$$s_n = z_n - \alpha_{n-1} \tag{5.146}$$

The first and second time derivatives of (5.146) are given by

$$\begin{aligned} \dot{s}_n &= d_n \bar{u}_1 + d_n \tau_1 + \overline{\Delta}_n - \sum_{k=1}^{n-1} \frac{\partial \alpha_{n-1}}{\partial z_k} g_0 z_{k+1} \\ &= \tilde{d}_n \bar{u}_1 - k_n s_n + \tilde{\overline{\Delta}}_n + \varepsilon_n + d_n \tau_1 \end{aligned} \tag{5.147}$$

$$\ddot{s}_n = \tilde{d}_n \dot{\bar{u}}_1 - \dot{\hat{d}}_n \bar{u}_1 - k_n \dot{s}_n + \dot{\tilde{\overline{\Delta}}}_n + d_n \dot{\tau}_1 \tag{5.148}$$

where $\dot{\tau}_1$ can be regarded as an auxiliary control signal. Now, by using the sliding variable and its first time derivative as states of a new dynamical system, i.e., by introducing the auxiliary variables $y_1 = s_n$ and $y_2 = \dot{s}_n$, equations (5.146)–(5.148) can be rewritten as

$$\begin{cases} \dot{y}_1 = y_2 \\ \dot{y}_2 = \xi + d_n \dot{\tau}_1 \end{cases} \tag{5.149}$$

The auxiliary system (5.149) is a double integrator affected by the uncertainty terms d_n and

$$\xi \;=\; \tilde{d}_n\dot{\bar{u}}_1 - \dot{\hat{d}}_n\bar{u}_1 - k_n\dot{s}_n + \dot{\bar{\Delta}}_n$$

Relying on assumptions (5.86) and on the previous results, one can observe that the term ξ is uncertain but its components are bounded, i.e.,

$$|\xi| \leq F \tag{5.150}$$

where $F > 0$ is assumed to be a known constant. Note that the quantity y_2 can be viewed as an unmeasurable quantity.
Then, the following theorem can be proved:

Theorem 5.7 *Given system (5.149), where ξ, and d_n satisfy (5.150) and (5.86), respectively, and y_2 is not measurable, the auxiliary control signal $\dot{\tau}_1$ given by*

$$\dot{\tau}_1(t) \;=\; -U\ \text{sign}\left\{y_1(t) - \frac{1}{2}y_{1_M}\right\} \tag{5.151}$$

where

$$U \;>\; \max\left\{\frac{F}{d_{n1}}; \frac{4F}{3d_{n1} - d_{n2}}\right\} \tag{5.152}$$

and y_{1_M} is a piece–wise constant function representing the value of the last singular point of $y_1(t)$ (i.e., the most recent value y_{1_M} such that $\dot{y}_1(t) = 0$) causes the convergence of the system trajectory to the origin of the y_1Oy_2 plane in finite time.

Proof: The control law (5.151) can be classified as a sub–optimal second order sliding mode control law (Bartolini *et al.*, 1999), and by following a theoretical development as that provided in Bartolini *et al.* (1999) for the general case, it can be proved that the trajectories on the y_1Oy_2 plane are confined within limit parabolic arcs which include the origin. As shown in Bartolini *et al.* (1998*b*), under condition (5.152), the following relationships hold

$$|y_1| \leq |y_{1_M}|, \qquad |y_2| \leq \sqrt{|y_{1_M}|}$$

and the convergence of y_{1_M} to zero takes place in finite time. As a consequence, the origin of the plane, i.e., $y_1 = y_2 = 0$, is reached in finite since y_1 and y_2 are both bounded by $\max(|y_{1_M}|, \sqrt{|y_{1_M}|})$.

5.3.6 The case $x_0(t_0) = 0$

As previously mentioned, the case $x_0(t_0) = 0$ is a critical case to cope with separately. The control scheme adopted to circumvent the loss of controllability is the same described in Subsection 5.2.6, i.e., when $x_0(t_0) = 0$, the control signal u_0 is chosen as

$$u_0 = x_0 g_0 + u_0^* \tag{5.153}$$

where g_0 is given by (5.88), and $u_0^* \in I\!R^+$ is a constant. Choosing the Lyapunov function (5.89), its first time derivative is given by

$$\dot{V}_0 \leq -k_0 x_0^2 + d_0 u_0^* x_0 \tag{5.154}$$

which leads to the boundedness of x_0. Moreover, $x_0(\bar{t}) \neq 0$, $\forall \bar{t} > t_0$. The control law u_0 defined by (5.153) and a new control law u_1^*, obtained following the procedure previously described, are applied for the time interval $[t_0, \bar{t}]$. Since $x_0(\bar{t}) \neq 0$, at time $\bar{t}$ the control input u_0 and u_1 are switched to (5.87) and (5.139), respectively.

5.3.7 Stability analysis

In this subsection, the stability properties of the designed control scheme are analyzed.

Theorem 5.8 *Under assumptions (5.85) and (5.86), the control laws (5.87) and (5.139) with adaptation laws (5.120), along with the switching strategy described in Subsection 5.3.6, makes the nonholonomic uncertain system (5.82) ISS with respect to the approximation error* $\bar{\varepsilon} = [0, \varepsilon_1, \varepsilon_2, \ldots, \varepsilon_{n-1}]^T$, *while keeping the estimated parameters bounded. Moreover, if a sufficiently large number of basis functions are chosen such that* $\varepsilon_i \approx 0$, $1 \leq i \leq n-1$, *then, system (5.82) is globally asymptotically regulated to the origin.*

Proof: To analyse the stability properties of the overall closed loop system (5.82)–(5.87)–(5.139), consider the Lyapunov function candidate

$$V = V_0 + V_{n-1} \quad = \quad \frac{1}{2}x_0^2 + \sum_{j=1}^{n-1} \frac{1}{2} s_j^2 + \sum_{j=1}^{n-1} \frac{1}{2} \tilde{\omega}_i^T Q_i^{-1} \tilde{\omega}_i \tag{5.155}$$

Then, the first time derivative of (5.155) results in

$$\dot{V} \leq -k_0 x_0^2 - \sum_{j=1}^{n-1} k_j s_j^2 + s_{n-1} s_n g_0 + \sum_{j=1}^{n-1} s_j \varepsilon_j \tag{5.156}$$

Now, define $\bar{s} = [x_0, s_1, s_2, \ldots, s_{n-1}]^T$, then one has that

$$\forall \, \|\bar{s}\| \geq \frac{2}{\sigma\kappa} \max\{\|\bar{\varepsilon}\|, |s_n|\}$$

where $\sigma \in (0,1)$ and $\kappa = \min_{0 \leq j \leq n-1}\{k_j\}$, it results that

$$\dot{V} \leq -(1-\sigma)\kappa \|\bar{s}\|^2 \tag{5.157}$$

Since (5.155) is an ISS Lyapunov function, the closed–loop system with state $\bar{s}$ is ISS with respect to $\bar{\varepsilon}$ and s_n. Moreover, $\tilde{\omega}_i$, $1 \leq i \leq n-1$, and $\hat{\omega}_i$, $1 \leq i \leq n-1$, remain bounded.
As proved by Theorem 5.8, s_n is steered to zero in finite time by the control law u_1. Then, if a sufficient large number of basis functions are chosen so that $\varepsilon_i \approx 0$, $1 \leq i \leq n-1$, one has that

$$\lim_{t \to \infty} \|\bar{s}\| = 0 \tag{5.158}$$

In this latter case one has that (5.111) gives

$$\lim_{t \to \infty} z_i = \alpha_{i-1}, \qquad 1 \leq i \leq n \tag{5.159}$$

and, from (5.118) and the assumption that $\varepsilon_i \approx 0$, it follows that

$$\lim_{t \to \infty} z_i = \hat{\overline{\Delta}}_{i-1} \approx \overline{\Delta}_{i-1}, \qquad 1 \leq i \leq n \tag{5.160}$$

Taking into account (5.84) and (5.14) it results

$$\lim_{t \to \infty} x_i = 0, \qquad 1 \leq i \leq n \tag{5.161}$$

Thus, the perturbed nonholonomic system (5.82) is globally asymptotically regulated to the origin.

5.3.8 Simulation results

In this subsection, the presented control scheme is applied to the parking problem of a tricycle-type robot affected by parametric uncertainty (Hespanha *et al.*, 1999). The model equations are

$$\begin{cases} \dot{x}_l &= p_1^* v \cos\theta \\ \dot{y}_l &= p_1^* v \sin\theta \\ \dot{\theta}_l &= p_2^* \omega \end{cases} \tag{5.162}$$

where x_l, y_l denote the coordinates of the center of mass on the plane, θ_l denotes the heading angle measured from the x–axis, v denotes the magnitude of the translational velocity of the center of mass, w denotes the angular velocity of the robot, and p_1^* and p_2^* are unknown positive parameters determined by the radius of the rear wheels and the distance between them.
System (5.162) can be transformed into form (5.82) through the following change of coordinates

$$\begin{aligned} x_0 &= \theta \\ x_1 &= x_l \sin\theta - y_l \cos\theta \\ x_2 &= x_l \cos\theta + y_l \sin\theta \\ u_1 &= v \\ u_0 &= \omega \end{aligned} \tag{5.163}$$

So that the resulting transformed system is

$$\begin{cases} \dot{x}_0 &= p_2^* u_0 \\ \dot{x}_1 &= x_2 u_0 + \delta_1 \\ \dot{x}_2 &= p_1^* u_1 + \delta_2 \end{cases} \tag{5.164}$$

where $\delta_1 = (p_2^* - 1) x_2 u_0$ and $\delta_2 = -p_2^* x_1 u_0$. It is assumed that the unknown parameters are such that $p_2^* \geq \bar{p}_2^*$ and $p_{11}^* \leq p_1^* \leq p_{12}^*$. The simulation parameters are $[x_0(0), x_1(0), x_2(0)] = [1, 1, 1]$, $k_0 = 1$, $k_1 = 10$, $k_2 = 20$, $U = 10$, $p_1^* = p_2^* = 2$, $\bar{p}_2^* = 1$, $p_{11}^* = 1$ and $p_{12}^* = 5$.
The number of basis for the approximation of δ_1 and δ_2 are 10. This number is determined in simulation on the basis of the regulation performance. The time evolution of the control signals u_0 and u_1 is reported in Fig. 5.10. Note that control u_1 is a continuous control signal as previously discussed. From Fig. 5.11 it appears that all the states x_0, x_1, and x_2 converge to zero as

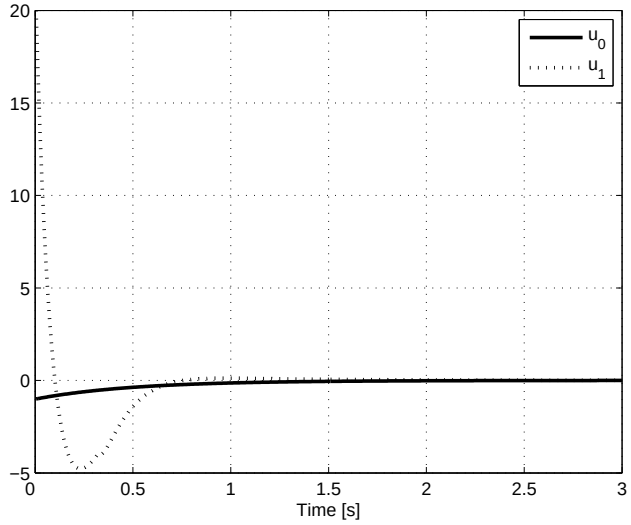

Figure 5.10: The evolution of control signals u_0 and u_1

expected.
The time evolution of the sliding variable s_2 is reported in Fig. 5.12. As one cane note, the sliding variable s_2 is steered to zero quite rapidly. Note that also the first time derivative of the sliding variable is steered to zero as shown in Fig. 5.13, since a second order sliding mode is enforced. The time evolution of the state of the system (5.164) starting from the critical initial condition $[x_0(0), x_1(0), x_2(0)] = [0, 1, 1]$, is still satisfactory, since the global asymptotically convergence to zero is maintained as can be seen in Fig. 5.14.

5.3.9 Conclusions

In this section an adaptive multiple–surface sliding control generating second order sliding modes has been presented for stabilizing a class of nonholonomic systems in chained form affected by matched and unmatched uncertainties. Differently from other proposals appeared in the literature, no knowledge of the bounds of the uncertainty terms is required. The key idea is to apply the function approximation technique in order to deal with the unmatched uncertainties while the matched uncertainty are coped with

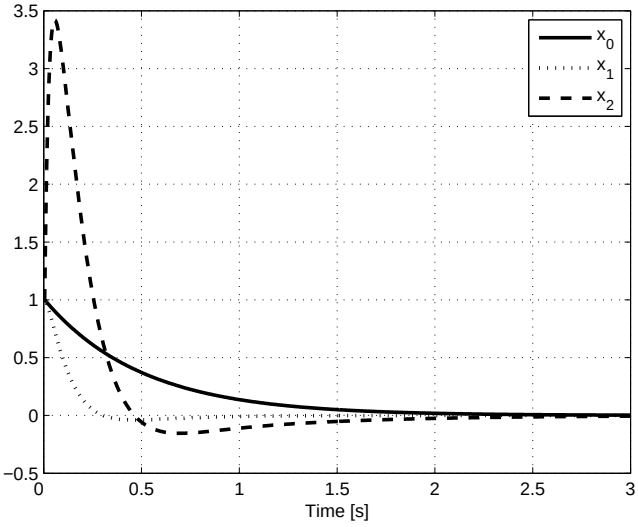

Figure 5.11: The time evolution of x_0, x_1 and x_2

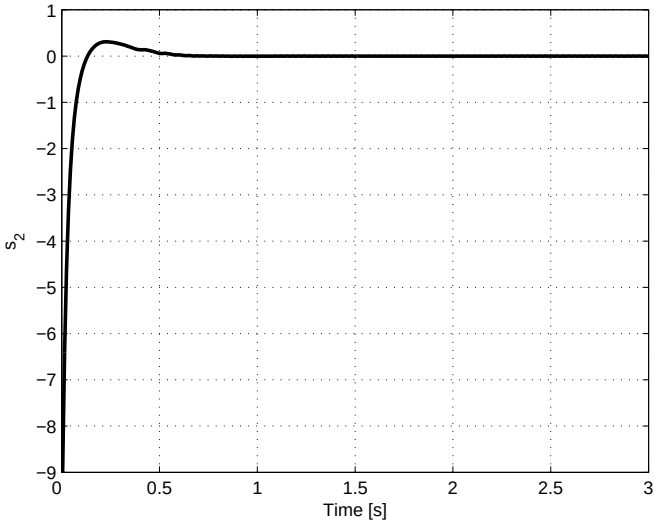

Figure 5.12: The sliding variable s

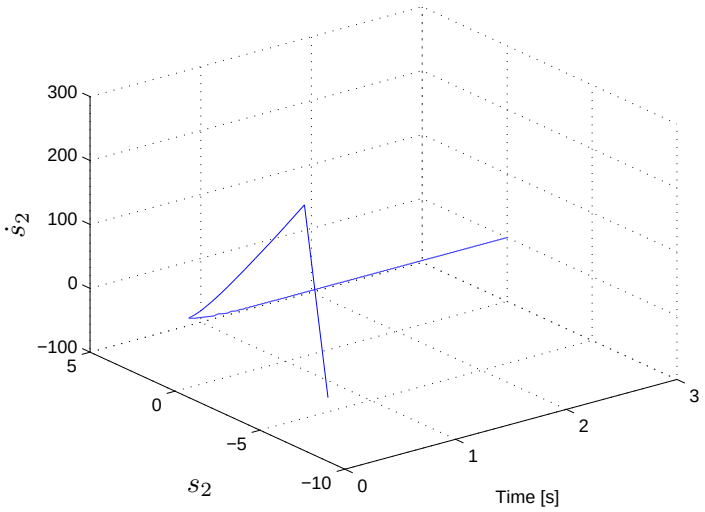

Figure 5.13: The time evolution of the sliding quantity s and its first time derivative $\dot{s}$

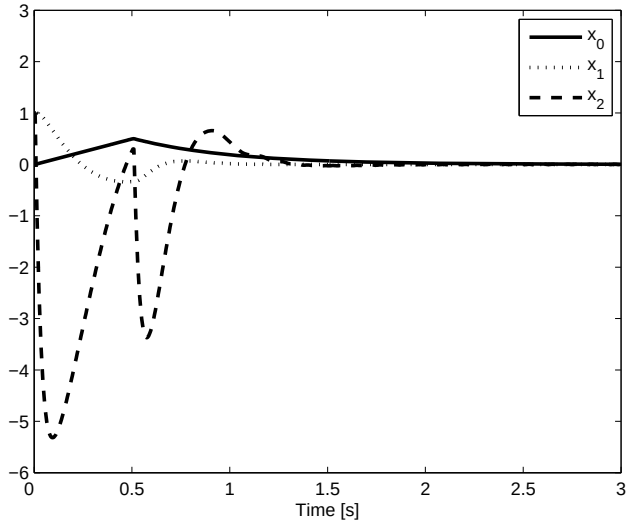

Figure 5.14: The time evolution of the system state with initial condition $[x_0(0), x_1(0), x_2(0)] = [0, 1, 1]$

by the sliding mode controller. By virtue of the second order nature of the generated sliding modes, the overall stabilization problem is solved relying on a continuous control signal. This fact enables the application of the presented strategy even to systems, such as the mechanical ones, for which the chattering effect, typical of conventional first order sliding mode control, may be unacceptable. By applying the presented control strategy, in spite of the presence of uncertainties, the system states globally asymptotically converge to the origin, while the estimated parameters remain bounded. Simulation results have shown the effectiveness of the control scheme presented in this section.

Chapter 6

Formation control of multi-agent systems

Contents

This chapter focuses on the control of a team of agents designated either as leaders or followers and exchanging information over a directed communication network. The generalized consensus state for a follower agent is defined as a target state that depends on the state of its neighbors. In order to guarantee generalized consensus, a decentralized control scheme based on sliding mode techniques is presented and the position error propagation within the network is studied using the notion of Input–to–State Stability (ISS). In particular, sufficient conditions on the control parameters are derived for guaranteeing that the error dynamics is ISS with respect to the leaders' velocities. Moreover, under suitable assumptions, the sliding mode

part of the control law is capable of steering the position errors to zero in finite time. The theoretical results are backed up by numerical simulations.

Part of this Chapter is taken from Ferrara *et al.* (2007) and Ferrara *et al.* (2008*a*).

6.1 Introduction

Over the last few years, the problem of designing decentralized control laws for multi–agent systems has received considerable attention, motivated by applications such as formation flight for unmanned aerial vehicles (Giulietti *et al.*, 2001), cooperative control for swarms of robots (Ögren *et al.*, 2002), or automated highway systems (Horowitz and Varaiya, 2000). In a typical scenario, agents are modeled as dynamical systems that can sense the state of a limited number of team members, hence giving rise to incomplete communication graphs. The main goal is then to control individual agents so as to guarantee the emergence of a global coordinated behaviour. As an example, in consensus problems agents must converge asymptotically to a common state without exploiting the knowledge of a common set–point (Ferrari-Trecate *et al.*, 2006*a*; Jadbabaie *et al.*, 2003; Olfati-Saber and Murray, 2004). Another form of consensus is leader–following where a leader moves independently of all other agents and followers must reach, asymptotically, a formation defined in terms of the leader position (Desai *et al.*, 1998; Ji *et al.*, 2006). Finally, a large stream of research was devoted to formation control problems (Balch and Arkin, 1998; Lawton *et al.*, 2003; Egerstedt *et al.*, 2001; Ren, 2007; Sorensen and Ren, 2007) most of which can be considered as special cases of consensus problems (Ren, 2007).
Beside the asymptotic achievement of the coordination objective, it is also important to quantify how errors propagate through the network during transients, especially when the agent closed–loop dynamics is nonlinear. In Tanner *et al.* (2002); Tanner and Pappas (2002) and Tanner *et al.* (2004) it has been shown that Input–to–State Stability (ISS) provides a suitable framework for studying the team performance since error amplification can be captured by ISS gains. Results in Tanner and Pappas (2002) assume nonlinear agent dynamics and acyclic communication graphs, while Tanner *et al.* (2002) focuses on linear agent dynamics and graphs that can be decomposed into basic interconnection structures including cycles.
In this chapter multi-agent systems with at least one leader are considered

and the problem of driving each follower towards the generalized consensus state, that is a time–varying target location defined in terms of the position of its neighboring agents, is addressed. Generalized consensus encompasses various coordination objectives such as leader–following and achievement of a reference formation. Moreover, when the leaders' formation is not maintained over time, generalized consensus guarantees a containment property for each follower.
A decentralized control scheme composed by a linear term and a sliding mode term is presented. Differently from Gazi (2005), where sliding mode control is used in order to make agents minimize a potential function encoding the desired cooperation goals, here the sliding mode component is introduced for speeding up the convergence to the generalized consensus state.
In order to analyze the error propagation within the network, as in Tanner *et al.* (2004), sufficient conditions guaranteeing that the error dynamics of a follower is ISS with respect to the velocities of its neighbors are derived. As far as the whole network is considered, sufficient conditions on the control parameters for guaranteeing ISS of the collective error with respect to the leaders' velocities are also provided. However, differently from the rationale used in Tanner *et al.* (2004), where ISS is proved through the composition of elementary ISS interconnections, relying on recent results on ISS for networks of systems (Dashkovskiy *et al.*, 2007) the collective error is analyzed at once and without assuming constraints on the structure of the communication graph.
Finally, when bounds on the leader velocities are known, it is possible to tune the sliding mode component of the control input in order to steer errors to zero in finite time. This feature is in sharp contrast with other control schemes available in the literature (see, e.g. Ren (2007); Sorensen and Ren (2007) and the references therein) that guarantee formation achievement just in the asymptotic regime.

This chapter is organized as follows. The control problem is described in Section 6.2. In Section 6.3 the sliding mode control scheme is introduced. In Section 6.4 conditions on the control parameters are given in order to guarantee that the position error of a follower is ISS with respect to the position error of its neighboring followers and to the velocity of its neighboring leaders. Sufficient conditions for extending the ISS property to the whole team of agents are given in Section 6.5. Section 6.6 is devoted to

the derivation of conditions for zeroing the errors of follower agents in finite time. A discussion on how the control parameters can be chosen in order to fulfill the assumptions of the main theorems are given in Section 6.7. Simulation results are reported in Section 6.8, and final comments in Section 6.9 conclude this chapter.

6.2 Problem statement

Consider a multi–agent system composed by N_L leader agents, and N_F follower agents. Followers and leaders will be indexed by elements of the sets $\mathcal{F}$ and $\mathcal{L}$, respectively defined as

$$\mathcal{F} := \{1, 2, \ldots, N_F\} \tag{6.1}$$
$$\mathcal{L} := \{N_F + 1, N_F + 2, \ldots, N_F + N_L\} \tag{6.2}$$

with $N_F > 0$ and $N_L > 0$. The total number of agents is $N = N_L + N_F$. Leaders are autonomously driven, while followers are controlled so as to maintain a desired relative distance with respect to their neighboring agents. In order to capture the topology of the communication network among agents, leaders and followers are arranged into a graph structure. More precisely, a directed graph $\mathcal{G} = (\mathcal{N}, \mathcal{E})$ with nodes $\mathcal{N} = \mathcal{L} \cup \mathcal{F}$ and arcs $\mathcal{E} \subseteq \mathcal{N} \times \mathcal{N}$ is considered. Each node $v \in \mathcal{N}$ represents an agent, and an arc $e = (k, i)$ from agent k to agent i means that agent i has access to the state of agent k. Furthermore, it is assumed that:

$$\mathcal{E} \subseteq \mathcal{N} \times \mathcal{F} \quad \text{(leaders send information only to followers)} \tag{6.3}$$
$$(i, i) \notin \mathcal{E} \quad \text{(no self loops)} \tag{6.4}$$

For $i \in \mathcal{F}$, let $\mathcal{L}_i = \{j : (j, i) \in \mathcal{E}, j \in \mathcal{L}\}$ and $\mathcal{F}_i = \{j : (j, i) \in \mathcal{E}, j \in \mathcal{F}\}$ be the sets of neighboring leaders and followers, respectively, and $\mathcal{N}_i = \mathcal{F}_i \cup \mathcal{L}_i$. The cardinality of $\mathcal{N}_i$ will be denoted with μ_i. In the spirit of the behavioural approach to formation control (Balch and Arkin, 1998; Lawton *et al.*, 2003), each arc $(i, j) \in \mathcal{E}$ is associated to weights $\alpha_{ij} \geq 0$ verifying

$$\sum_{k \in \mathcal{N}_i} \alpha_{ki} = 1 \tag{6.5}$$

Note that in Section 6.5 suitable choices of the weights α_{ij} will be suggested so as to solve the control problem in question.

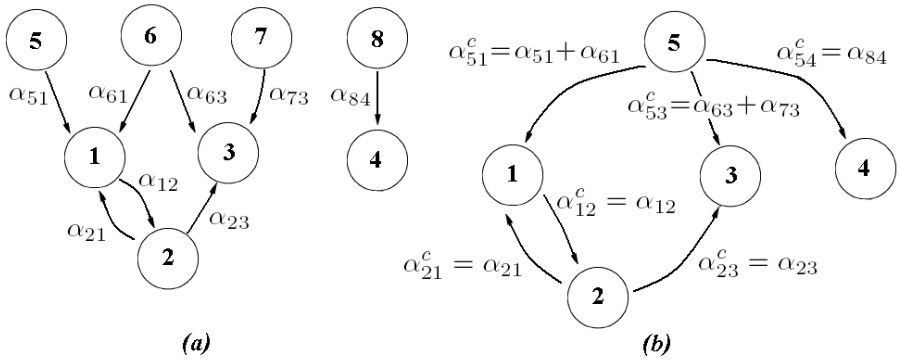

Figure 6.1: An example of graph $\mathcal{G}$ (Panel a) and the associated $\mathcal{G}^c$ graph (Panel b).

In order to specify the connectivity property of the graph, the following definition is introduced

Definition 6.1 *The graph $\mathcal{G}^c$ is given by the set of nodes $\mathcal{N}^c = \mathcal{F} \cup \{N_F + 1\}$, the set of edges $\mathcal{E}^c = \mathcal{E}^c_1 \cup \mathcal{E}^c_2$, where $\mathcal{E}^c_1 = \{(i,j) \in \mathcal{E} \cap (\mathcal{F} \times \mathcal{F})\}$ and $\mathcal{E}^c_2 = \{(N_F+1, j), \forall j : \mathcal{L}_j \neq \emptyset\}$, and the weights α^c_{ij} verifying*

$$\alpha^c_{ij} = \quad \alpha_{ij} \qquad \text{if} \quad (i,j) \in \mathcal{E}^c_1 \tag{6.6}$$

$$\alpha^c_{N_F+1,j} = \quad \textstyle\sum_{i \in \mathcal{L}_j} \alpha_{ij} \qquad \text{if} \quad (N_F+1, j) \in \mathcal{E}^c_2 \tag{6.7}$$

Roughly speaking, $\mathcal{G}^c$ is obtained by collapsing all leader nodes in a single node. As an example, for the graph $\mathcal{G}$ in Fig. 6.1.a with $\mathcal{F} = \{1,2,3,4\}$ and $\mathcal{L} = \{5,6,7,8\}$ the corresponding graph $\mathcal{G}^c$ is depicted in Fig. 6.1.b. The superscript "c" will be used for denoting quantities defined with reference to $\mathcal{G}^c$. Hence, $\mathcal{L}^c_i$ and $\mathcal{F}^c_i$ will denote the set of neighboring leaders and followers of follower i in $\mathcal{G}^c$, respectively. As an example, in Fig 6.1 we have $\mathcal{L}_1 = \{5,6\}$ and $\mathcal{L}^c_1 = \{5\}$. Note also that one has

$$\sum_{k \in \mathcal{N}_i} \alpha^c_{ki} = 1 \tag{6.8}$$

and

$$\mathcal{F}^c_i = \mathcal{F}_i \tag{6.9}$$

In a directed graph, a path is a sequence of edges $e_i = (u_i, v_i)$ such that $u_{i+1} = v_i$ and two nodes i and j are connected if there is a path starting

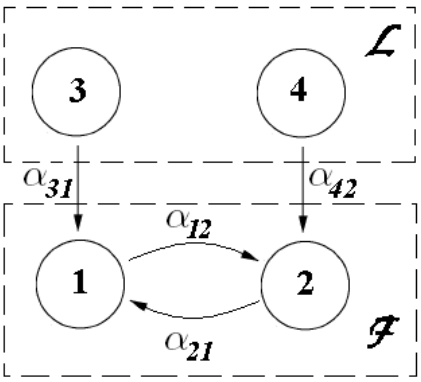

Figure 6.2: An example of communication topology with $\mathcal{L} = \{3, 4\}$ and $\mathcal{F} = \{1, 2\}$ which verifies Assumption 6.1.

from i and ending in j. Moreover, a directed graph is a rooted tree if every node has just one incoming arc except for one node (the root) which has no incoming arc and is connected to all other nodes. Then, the connectivity structure of $\mathcal{G}$ can be introduced.

Assumption 6.1 *The graph $\mathcal{G}^c$ contains a rooted spanning tree, i.e., there is a subgraph $(\mathcal{N}^c, \hat{\mathcal{E}})$ with $\hat{\mathcal{E}} \subseteq \mathcal{E}^c$ that is a rooted tree.*

An example of a graph verifying Assumption 6.1 is depicted in Fig. 6.1.a. Note that Assumption 6.1 does not imply that $\mathcal{G}$ is connected. However, Assumption 6.1 implies that no follower is disconnected, i.e. $\mathcal{N}_i \neq \emptyset$, $i \in \mathcal{F}$. Note also that in view of (6.3) the root of $(\mathcal{N}^c, \hat{\mathcal{E}})$ is necessarily the node $N_F + 1$ in which all leaders node have been collapsed. Another example of a communication topology which verifies the previous constraints is depicted in Fig. 6.2.

All followers are modeled as a single-integrator systems, i.e.,

$$\dot{x}_i = u_i, \qquad i \in \mathcal{F} \tag{6.10}$$

where $x_i \in \mathbb{R}^n$, and $u_i \in \mathbb{R}^n$. Moreover, x_i, $i \in \mathcal{L}$, is used to denote the state of the i–th leader although it is not assumed the knowledge of leaders'

dynamics. States x_i will be also called "positions" and $\dot{x}_i$ "velocities".
Each node $i \in \mathcal{N}$ is associated with a reference position $p_i \in \mathbb{R}^n$ and the relative distance is defined as $d_{ij} = p_i - p_j$. Positions p_i are used for defining a reference formation. The target position of agent i, with $i \in \mathcal{F}$, is the generalized consensus state that is defined as follows.

Definition 6.2 *The generalized consensus state of agent $i \in \mathcal{F}$, is defined as*

$$x_i^d = \sum_{k \in \mathcal{L}_i} \alpha_{ki}(x_k - d_{ki}) + \sum_{j \in \mathcal{F}_i} \alpha_{ji}(x_j - d_{ji}) \tag{6.11}$$

and the error of agent $i \in \mathcal{F}$ is

$$\tilde{x}_i \;\; = \;\; x_i^d - x_i \tag{6.12}$$

Note that, in view of (6.5), one has

$$\tilde{x}_i = \sum_{k \in \mathcal{L}_i} \alpha_{ki}(x_k - p_k - (x_i - p_i)) + \sum_{j \in \mathcal{F}_i} \alpha_{ji}(x_j - p_j - (x_i - p_i)) \quad i \in \mathcal{F} \tag{6.13}$$

and the error dynamics is given by

$$\dot{\tilde{x}}_i = \sum_{k \in \mathcal{L}_i} \alpha_{ki}\dot{x}_k + \sum_{j \in \mathcal{F}_i} \alpha_{ji}\dot{x}_j - \dot{x}_i \tag{6.14}$$

In Section 6.3–6.6 control laws for the followers capable of steering errors $\tilde{x}_i(t)$ to zero when $t \to \infty$ or in finite time are presented.
The coordinated behaviour of the system is then encoded by the equation

$$\tilde{x}_i = 0 \qquad i \in \mathcal{F} \tag{6.15}$$

and depends on the evolution of leader positions.

First, consider the case of leaders with fixed positions given by

$$x_i = p_i + \nu \qquad i \in \mathcal{L} \tag{6.16}$$

where $\nu \in \mathbb{R}^n$ is a translation term.

Theorem 6.1 *The system of linear equations (6.15)–(6.16) with unknown x_i, $i \in \mathcal{N}$, has a unique solution if and only of Assumption 6.1 holds. Moreover, the solution is given by (6.16) and*

$$x_i = p_i + \nu \qquad i \in \mathcal{F} \tag{6.17}$$

Proof: The proof is reported in Appendix 6.9.

In view of the previous theorem, zero errors means that leaders and followers are in the reference formation. Note that this result is achieved independently of the precise values of the weights α_{ki}, as far as condition (6.5) holds.

Consider now the case where leaders are not fixed but leaders' formation is maintained over time, i.e. (6.16) is replaced by

$$x_i(t) = p_i + \nu(t) \qquad i \in \mathcal{L} \tag{6.18}$$

In view of Theorem 6.1, convergence to zero of all follower errors implies that, asymptotically, also follower positions will be given by

$$x_i(t) = p_i + \nu(t) \qquad i \in \mathcal{F} \tag{6.19}$$

Moreover, if errors are zeroed in finite time then there exists $\bar{t}$ such that leaders and followers will maintain the reference formation for all $t \geq \bar{t}$.

Consider now the case when the leader positions do not evolve according to (6.18). Note that, because of (6.5), the generalized consensus state of follower $i \in \mathcal{F}$ lies in $H_i = Co(\{x_k - d_{ki}, k \in \mathcal{N}_i\})$ where $Co(\cdot)$ denotes the convex hull. Hence $\tilde{x}_i = 0$ implies that $x_i \in H_i$ and this can be interpreted as a containment property that is desirable when the reference formation cannot be attained. Moreover, note that the containment property is independent on the precise value of the weights α_{ij} as far as (6.5) holds. As a special case, assume that $p_i = 0$, $i \in \mathcal{N}$, and that $\mathcal{G}_F = (\mathcal{F}, \mathcal{E} \cap (\mathcal{F} \times \mathcal{F}))$ is an undirected and connected graph (i.e. $(i,j) \in \mathcal{E} \cap (\mathcal{F} \times \mathcal{F}) \Leftrightarrow (j,i) \in \mathcal{E} \cap (\mathcal{F} \times \mathcal{F})$ and $\mathcal{G}_F$ is strongly connected). Then, in Ferrari-Trecate *et al.* (2006*b*) it has been shown that $\tilde{x}_i = 0$, $i \in \mathcal{F}$, implies that the polytope spanned by the leader positions contains all follower positions.

Remark 6.1 *Note that, followers obeying to a linear fully actuated dynamics, i.e.,*

$$\dot{x}_i = A_i x_i + B_i u_i, \qquad i \in \mathcal{F} \tag{6.20}$$

where $x_i \in R^n$, $u_i \in \mathbb{R}^n$, $A_i \in \mathbb{R}^{n \times n}$, and $B_i \in \mathbb{R}^{n \times n}$ is a full rank matrix, can be easily converted to agents with single integrator dynamics and inputs $\bar{u}_i$ by using the control inputs

$$u_i = B_i^{-1}(-A_i x_i + \bar{u}_i), \qquad i \in \mathcal{F} \tag{6.21}$$

The first control objective is to design a decentralized control law, i.e., $u_i(\{x_j\}_{j\in\mathcal{N}_i})$, $\forall i \in \mathcal{F}$, in order to guarantee bounded position errors, as far as the leaders' velocities $\dot{x}_k$, $k \in \mathcal{L}$, are bounded. As in Tanner *et al.* (2002); Tanner and Pappas (2002) and Tanner *et al.* (2004), this concept will be precisely captured by the notion of Input–to–State Stability (Isidori, 1999) for the multi–agent system.

For a signal $x(t)$, $t \geq 0$, its restriction to the time interval $[t_1, t_2]$ will be denoted as $x_{[t_1,t_2]}$ and its supremum norm with $\|x\|_\infty$.

Definition 6.3 *The position error of a follower $i \in \mathcal{F}$, is Input–to–State Stable (ISS) with respect to $\tilde{x}_j, j \in \mathcal{F}_i$, and $\dot{x}_k, k \in \mathcal{L}_i$, if there exist a function $\beta_i(\cdot,\cdot)$ of class $\mathcal{KL}$ and functions $\gamma_{ij}(\cdot)$, $\gamma_{ik}(\cdot)$ of class $\mathcal{K}$ (called ISS gain functions) such that, for any initial error $\tilde{x}_i(0)$, the solution $\tilde{x}_i(t)$ of (6.14) verifies, for all $t \geq 0$*

$$\|\tilde{x}_i(t)\| \leq \beta_i(\|\tilde{x}_i(0)\|, t) + \sum_{j\in\mathcal{F}_i} \gamma_{ij}(\|\tilde{x}_{j[0,t]}\|_\infty) + \sum_{k\in\mathcal{L}_i} \gamma_{ik}(\|\dot{x}_{k[0,t]}\|_\infty) \tag{6.22}$$

Let us introduce the collective error $\tilde{x}$ as

$$\tilde{x} = [\tilde{x}_1, \tilde{x}_2, \ldots, \tilde{x}_{N_F}]^T \tag{6.23}$$

Definition 6.4 *The collective error is ISS with respect to $\dot{x}_k, k \in \mathcal{L}$, if there exist a class $\mathcal{KL}$ function $\beta(\cdot,\cdot)$, and functions $\gamma_k(\cdot)$ of class $\mathcal{K}$ such that*

$$\|\tilde{x}(t)\| \leq \beta(\|\tilde{x}(0)\|, t) + \sum_{k\in\mathcal{L}} \gamma_k(\|\dot{x}_{k[0,t]}\|_\infty) \tag{6.24}$$

for all $t \geq 0$.

Note that in the case when all leaders are in a fixed position, i.e., $\|\dot{x}_k(t)\| = 0$, $\forall t, k \in \mathcal{L}$, and when the leaders' velocities tends to zero, i.e., $\lim_{t\to\infty} \sum_{k\in\mathcal{L}} \|\dot{x}_k(t)\| = 0$, Definition 6.4 implies that $\tilde{x} = 0$ is a global asymptotically stable equilibrium for the error dynamics (6.14).

6.3 The proposed control scheme

In this section a control scheme capable of guaranteeing the ISS property for the followers' errors and the collective error is presented. Moreover, when bounds on leaders' velocities and followers' position errors are known, in addition to the attainment of the ISS property, the presented control scheme will be also able to steer the position errors to zero in finite time which implies the reaching of the generalized consensus state.

The proposed control law for agent $i \in \mathcal{F}$, is

$$u_i = K_i \tilde{x}_i + \eta_i \frac{\tilde{x}_i}{\|\tilde{x}_i\|} \tag{6.25}$$

where $K_i, \eta_i \in \mathbb{R}^{n \times n}$. Note that $\tilde{x}_i/\|\tilde{x}_i\| = sign(\tilde{x}_i)$ for $\tilde{x}_i \in \mathbb{R}$. The control law is characterized by two parameters, i.e., K_i and η_i. The matrix K_i is the feedback gain, while η_i is the gain of $\tilde{x}_i/\|\tilde{x}_i\|$. The term $K_i\tilde{x}_i$ is a classical linear state feedback while the term $\eta_i\tilde{x}_i/\|\tilde{x}_i\|$ introduces a unit vector sliding mode component (Edwards and Spurgeon, 1998). In particular, the sliding mode component will be used to enforce the finite time convergence to the sliding manifold $\tilde{x}_i = 0$, as discussed in Section 6.6.

Remark 6.2 *Note that, in view of (6.5), the error of agent i can be written as*

$$\tilde{x}_i = \sum_{k \in \mathcal{L}_i} \alpha_{ki}(x_k - x_i - d_{ki}) + \sum_{j \in \mathcal{F}_i} \alpha_{ji}(x_j - x_i - d_{ji}) \quad i \in \mathcal{F} \tag{6.26}$$

and only the relative distance between follower agent i and its neighboring agent k is needed to calculate the error $\tilde{x}_i$ and hence the control law (6.25). In particular, differently from formation control strategies based on virtual structures (see (Sorensen and Ren, 2007) and the references therein), followers do not need to know or to estimate a virtual coordinate frame for the whole formation.

The closed–loop followers' dynamics can be obtained by substituting (6.25) in (6.10), thus obtaining

$$\dot{x}_i = K_i \tilde{x}_i + \eta_i \frac{\tilde{x}_i}{\|\tilde{x}_i\|} \tag{6.27}$$

From (6.27) and (6.14), the closed–loop error dynamics results in

$$\dot{\tilde{x}}_i = -K_i\tilde{x}_i - \eta_i\frac{\tilde{x}_i}{\|\tilde{x}_i\|} + \sum_{k\in\mathcal{L}_i}\alpha_{ki}\dot{x}_k + \sum_{j\in\mathcal{F}_i}\alpha_{ji}\Big(K_j\tilde{x}_j + \eta_j\frac{\tilde{x}_j}{\|\tilde{x}_j\|}\Big) \tag{6.28}$$

6.4 The ISS property for the followers' error

In this section, conditions on the control parameter K_i, and η_i in (6.25) are given in order to guarantee that the position error of each agent is ISS. In this case, a closed–form expression of the ISS gain functions is also provided.

In the sequel, $\lambda_{min}(Q)$, and $\lambda_{max}(Q)$ will be used to denote the minimum and maximum eigenvalue of the positive–semidefinite matrix Q, respectively.

Theorem 6.2 *Assume that the closed–loop dynamics of the follower $i \in \mathcal{F}$ is given by (6.27) where K_i is positive–definite, and η_i is positive- semidefinite. If the matrices η_i and $\eta_j, j \in \mathcal{F}_i$ verify*

$$\lambda_{min}(\eta_i) \geq \sum_{j\in\mathcal{F}_i}\alpha_{ji}\lambda_{max}(\eta_j) \tag{6.29}$$

then the position error of the i–th follower is ISS with respect to $\tilde{x}_j$, $j \in \mathcal{F}_i$, and $\dot{x}_k$, $k \in \mathcal{L}_i$. Moreover, the functions

$$\gamma_{ij}(r) = \frac{\mu_i\alpha_{ji}}{\theta}\frac{\lambda_{max}(K_j)}{\lambda_{min}(K_i)}r \qquad j \in \mathcal{F}_i \tag{6.30}$$

$$\gamma_{ik}(r) = \frac{\mu_i\alpha_{ki}}{\theta}\frac{1}{\lambda_{min}(K_i)}r \qquad k \in \mathcal{L}_i \tag{6.31}$$

where $\theta \in (0,1)$, provide the ISS gains appearing in (6.22).

Proof: Consider the following candidate Lyapunov function for the error dynamics (6.28)

$$V_i(\tilde{x}_i) = \frac{1}{2}\tilde{x}_i^T\tilde{x}_i \tag{6.32}$$

Then,

$$\begin{aligned}\dot{V}_i(\tilde{x}_i) &= -\tilde{x}_i^TK_i\tilde{x}_i - \tilde{x}_i^T\eta_i\frac{\tilde{x}_i}{\|\tilde{x}_i\|} + \tilde{x}_i^T\sum_{k\in\mathcal{L}_i}\alpha_{ki}\dot{x}_k \\ &\quad + \tilde{x}_i^T\sum_{j\in\mathcal{F}_i}\alpha_{ji}K_j\tilde{x}_j + \tilde{x}_i^T\sum_{j\in\mathcal{F}_i}\alpha_{ji}\eta_j\frac{\tilde{x}_j}{\|\tilde{x}_j\|}\end{aligned} \tag{6.33}$$

If η_i verifies the inequality (6.29), one has

$$\begin{array}{l} -\tilde{x}_i^T \eta_i \frac{\tilde{x}_i}{\|\tilde{x}_i\|} + \tilde{x}_i^T \sum_{j\in\mathcal{F}_i} \alpha_{ji}\eta_j \frac{\tilde{x}_j}{\|\tilde{x}_j\|} \\ \leq -\lambda_{min}(\eta_i)\|\tilde{x}_i\| + \sum_{j\in\mathcal{F}_i} \alpha_{ji}\lambda_{max}(\eta_j)\|\tilde{x}_i\| \\ \leq -\Big(\lambda_{min}(\eta_i) - \sum_{j\in\mathcal{F}_i} \alpha_{ji}\lambda_{max}(\eta_j)\Big)\|\tilde{x}_i\| \leq 0 \end{array} \tag{6.34}$$

Therefore, if (6.29) holds, it follows that

$$\begin{array}{rcl} \dot{V}_i(\tilde{x}_i) & \leq & -\tilde{x}_i^T K_i \tilde{x}_i + \tilde{x}_i^T \sum_{k\in\mathcal{L}_i} \alpha_{ki}\dot{x}_k + \tilde{x}_i^T \sum_{j\in\mathcal{F}_i} \alpha_{ji} K_j \tilde{x}_j \\ & \leq & -\lambda_{min}(K_i)\|\tilde{x}_i\|^2 + \sum_{k\in\mathcal{L}_i} \alpha_{ki}\|\tilde{x}_i\|\|\dot{x}_k\| \\ & & + \sum_{j\in\mathcal{F}_i} \alpha_{ji}\lambda_{max}(K_j)\|\tilde{x}_i\|\|\tilde{x}_j\| \end{array} \tag{6.35}$$

From (6.35), it turns out that for all $\|\tilde{x}_i\|$ such that

$$\|\tilde{x}_i\| \geq \mu_i \max_{j\in\mathcal{F},k\in\mathcal{L}} \left\{ \frac{\alpha_{ki}\|\dot{x}_k\|}{\theta\lambda_{min}(K_i)}; \frac{\alpha_{ji}\lambda_{max}(K_j)\|\tilde{x}_j\|}{\theta\lambda_{min}(K_i)} \right\} \tag{6.36}$$

where $\theta \in (0,1)$, the following inequality holds

$$\dot{V}_i(\tilde{x}_i) \leq -(1-\theta)\lambda_{min}(K_i)\|\tilde{x}_i\|^2 \tag{6.37}$$

Thus, by applying Theorem 10.4.1 in Isidori (1999), from (6.36) and (6.37), it results that $V_i(\tilde{x}_i)$ is an ISS–Lyapunov function for (6.28), i.e., there exist $\beta_i(\cdot,\cdot)$ of class $\mathcal{KL}$ such that

$$\|\tilde{x}_i(t)\| \leq \beta_i(\|\tilde{x}_i(0)\|, t) + \sum_{j\in\mathcal{F}_i} \gamma_{ij}(\|\tilde{x}_{j[0,t]}\|_\infty) + \sum_{k\in\mathcal{L}_i} \gamma_{ik}(\|\dot{x}_{k[0,t]}\|_\infty) \tag{6.38}$$

for all $t \geq 0$, where gain functions $\gamma_{ij}(\cdot)$, and $\gamma_{ik}(\cdot)$ are defined by (6.30) and (6.31).

6.5 ISS property of the collective error

It is known that, under suitable assumptions, the interconnections of ISS systems is ISS as well. In particular, if two ISS systems are arranged in a feedback loop, one can apply the small–gain theorem (Isidori, 1999) which states that if the composition of the gain functions $\gamma_1(\cdot)$, $\gamma_2(\cdot)$ of the ISS

subsystems is small enough, then the whole system is ISS. In Dashkovskiy *et al.* (2007), the small–gain theorem has been generalized to arbitrary interconnections of ISS systems. This is precisely the tool that will be used for establishing the ISS property of the collective error (6.23) under the control law (6.25) and for general network topologies. In the sequel, $\rho(A)$ will denote the spectral radius of a given matrix A. The results obtained in this section are mainly based on Corollary 7 in Dashkovskiy *et al.* (2007), which is here reported for the reader convenience:

Lemma 6.1 *(Dashkovskiy* et al.*, 2007) Consider n interconnected systems*

$$\begin{aligned} \dot{x}_1 &= f_1(x_1, \ldots, x_n, u) \\ &\vdots \\ \dot{x}_n &= f_n(x_1, \ldots, x_n, u) \end{aligned} \tag{6.39}$$

where $x_i \in \mathbb{R}^{N_i}$, $u \in \mathbb{R}^L$. *Assume that each subsystem i is ISS, i.e., there exist a function* $\beta_i(\cdot,\cdot)$ *of class* $\mathcal{KL}$ *and functions* $\gamma_{ij}(\cdot)$, $\gamma(\cdot)$ *of class* $\mathcal{K}$ *such that the state* $x_i(t)$*, with initial condition* $x_i(0)$*, satisfies*

$$\|x_i(t)\| \leq \beta_i(\|x_i(0)\|, t) + \sum_{j=1}^{n} \gamma_{ij}(\|x_{j[0,t]}\|_\infty) + \gamma(\|u_{[0,t]}\|_\infty) \tag{6.40}$$

for all $t \geq 0$. *Introduce the function* $\Gamma : \mathbb{R}_+^n \to \mathbb{R}_+^n$ *defined as*

$$\Gamma(s_1, \ldots, s_n)^T = \Big(\sum_{j=1}^{n} \gamma_{1j}(s_j), \ldots, \sum_{j=1}^{n} \gamma_{nj}(s_j) \Big)^T \tag{6.41}$$

where $s = (s_1, \ldots, s_n)^T \in \mathbb{R}_+^n$. *If the function* Γ *is a linear operator, i.e.,* $\Gamma(s) = \Gamma s$*, and its spectral radius* $\rho(\Gamma)$ *fulfills*

$$\rho(\Gamma) < 1 \tag{6.42}$$

then system (6.39) is ISS.

Then, the following theorem can be proved.

Theorem 6.3 *Assume that all followers verify the assumptions of Theorem 6.2. If in addition, for all followers* $i \in \mathcal{F}$*, the scalars* α_{ji} *and* α_{ki} *in (6.11) and the matrices* K_i *in (6.25) are chosen such that*

$$\rho(\Gamma_1) < 1 \tag{6.43}$$

where $\Gamma_1 \in \mathbb{R}^{N_F \times N_F}$ *is the matrix with elements*

$$(\Gamma_1)_{ij} = \begin{cases} 0 & \text{if } j \notin \mathcal{F}_i \\ \mu_i \alpha_{ji} \frac{\lambda_{max}(K_j)}{\lambda_{min}(K_i)} & \text{if } j \in \mathcal{F}_i \end{cases} \tag{6.44}$$

then the collective error is ISS with respect to $\dot{x}_k$, $k \in \mathcal{L}$.

Proof: From Theorem 6.2, it results that, $\forall t \geq 0$, and $\forall i \in \mathcal{F}$,

$$\|\tilde{x}_i(t)\| \leq \beta_i(\|\tilde{x}_i(0)\|, t) + \sum_{j \in \mathcal{F}} \gamma_{ij}(\|\tilde{x}_{j[0,t]}\|_\infty) + \sum_{k \in \mathcal{L}} \gamma_{ik}(\|\dot{x}_{k[0,t]}\|_\infty) \tag{6.45}$$

where, for notation simplicity,

$$\begin{aligned} \gamma_{ij}(r) &= 0 \quad \text{if } j \notin \mathcal{F}_i \\ \gamma_{ik}(r) &= 0 \quad \text{if } k \notin \mathcal{L}_i \end{aligned}$$

The collective error $\tilde{x}$, defined as in (6.23), can be interpreted as the interconnection of the N_F ISS systems with state $\tilde{x}_i$, $i \in \mathcal{F}$. The gain functions (6.30) of the position error of an agent $i \in \mathcal{F}$ are linear functions. Hence, the function $\Gamma(s)$ is a linear operator and (6.41) can be written as

$$\Gamma(s) = \Gamma s = \begin{bmatrix} 0 & \gamma_{12} & \cdots & \gamma_{1N_F} \\ \gamma_{21} & 0 & \cdots & \gamma_{2N_F} \\ \vdots & \vdots & \ddots & \vdots \\ \gamma_{N_F 1} & \gamma_{N_F 2} & \cdots & 0 \end{bmatrix} s \tag{6.46}$$

where the expression of γ_{ij} is given in (6.30). The function (6.46) can be rewritten as

$$\Gamma = \frac{\Gamma_1}{\theta} \tag{6.47}$$

where $\theta \in (0, 1)$. Thus, since $\rho(\Gamma) = \rho(\Gamma_1)/\theta$, if (6.43) holds then $\exists\ \theta \in (0, 1)$ such that $\rho(\Gamma) < 1$. The result follows from the application of Lemma 6.1.

6.6 Finite time convergence to the generalized consensus state

Under the assumptions of Theorem 6.3, the collective error is ISS with respect to $\dot{x}_k$, $k \in \mathcal{L}$. Therefore, from (6.24) one has that if $\dot{x}_k$, $k \in \mathcal{L}$, are

bounded, then $\tilde{x}$ is also bounded. As a further result, in this section it will be shown that the presented control law is also capable to drive all followers to the generalized consensus state.

Theorem 6.4 *Under the assumption of Theorem 6.3, if all matrices η_i, $i \in \mathcal{F}$, are chosen such that*

$$\eta_i = diag(\varepsilon_1, \ldots, \varepsilon_n) \tag{6.48}$$

are positive–definite, and

$$\tilde{x}_i^T(\Omega_i + \eta_i)\frac{\tilde{x}_i}{\|\tilde{x}\|} \geq \tilde{x}_i^T\Big(\sum_{k\in\mathcal{L}_i}\alpha_{ki}\dot{x}_k + \sum_{j\in\mathcal{F}_i}\alpha_{ji}(K_j\tilde{x}_j + \eta_j\frac{\tilde{x}_j}{\|\tilde{x}_j\|})\Big) \tag{6.49}$$

for some $\Omega_i = diag(\omega_1, \ldots, \omega_n) > 0$, then the position errors $\tilde{x}_i$ are steered to zero in finite time.

Proof: If η_i are chosen such that (6.49) is satisfied then the derivative of the Lyapunov function $V_i(\tilde{x}_i)$ in (6.32) results in

$$\begin{aligned}\dot{V}_i(\tilde{x}_i) &= -\tilde{x}_i^T K_i\tilde{x}_i - \tilde{x}_i^T\eta_i\tfrac{\tilde{x}_i}{\|\tilde{x}_i\|} + \tilde{x}_i^T\textstyle\sum_{k\in\mathcal{L}_i}\alpha_{ki}\dot{x}_k \\ &\quad +\tilde{x}_i^T\textstyle\sum_{j\in\mathcal{F}_i}\alpha_{ji}K_j\tilde{x}_j + \tilde{x}_i^T\sum_{j\in\mathcal{F}_i}\alpha_{ji}\eta_j\tfrac{\tilde{x}_j}{\|\tilde{x}_j\|} \\ &\leq -\tilde{x}_i^T K_i\tilde{x}_i - \tilde{x}_i^T\Omega_i\tfrac{\tilde{x}_i}{\|\tilde{x}_i\|} \leq -\lambda_{min}(\Omega_i)\|\tilde{x}_i\|\end{aligned} \tag{6.50}$$

Equation (6.50) can be rewritten as

$$\dot{V}_i(\tilde{x}_i) \leq -\lambda_{min}(\Omega_i)\sqrt{2V_i(\tilde{x}_i)} \tag{6.51}$$

By integrating (6.51), the time taken to reach $\tilde{x}_i = 0$, denoted by t_{s_i} fulfills

$$t_{s_i} \leq \frac{\sqrt{2}\sqrt{V_i(\tilde{x}_i(0))}}{\lambda_{min}(\Omega_i)} \tag{6.52}$$

and this implies that $\tilde{x}_i$ is steered to zero in finite time.

Relying on Theorem 6.4, the quantity $\tilde{x}_i$ can be regarded as a sliding variable S_i (Edwards and Spurgeon, 1998). If (6.49) is verified, it turns out that

$$S_i^T\dot{S}_i \leq -\lambda_{min}(\Omega_i)\|S_i\| \tag{6.53}$$

Equation (6.53) is the so–called reachability condition (Edwards and Spurgeon, 1998) and this implies that the proposed control law (6.25) will enforce a sliding mode on the sliding manifolds $S_i = 0$, $\forall i \in \mathcal{F}$, in finite time. This means that, after a finite time interval, position errors are steered to zero, i.e., $\tilde{x}_i = 0$, which implies that the generalized consensus state is reached.

6.7 Discussion on the control synthesis procedure

In this section, it is discussed how to choose the control parameters in order to verify all the assumptions of Theorems 6.2, 6.3, and 6.4.

As for Theorem 6.2, one has that the inequality (6.29) can be fulfilled by choosing $\hat{\eta} \in \mathbb{R}$, $\hat{\eta} \geq 0$ and setting

$$\eta_i = \hat{\eta} I, \qquad \forall i \in \mathcal{F} \tag{6.54}$$

From (6.54) we have that (6.29) results into the inequality

$$\hat{\eta} \geq \hat{\eta} \sum_{j \in \mathcal{F}_i} \alpha_{ji}, \quad \forall i \in \mathcal{F} \tag{6.55}$$

that, in view of (6.5), is always verified.

As for Theorem 6.3, the key difficulty is that the computation of matrices K_i and weights α_{ij} verifying (6.43) is a nonconvex optimization problem. However, if the positive–definite matrices K_i are fixed, the problem of finding scalars α_{ij} that verify (6.43) is much easier, as it is shown in the sequel. If we choose the matrices K_i such that

$$\lambda_{max}(K_i) = \delta, \qquad \lambda_{min}(K_i) = \alpha, \qquad \forall i \in \mathcal{F} \tag{6.56}$$

we have that $\rho(\Gamma_1) = \frac{\delta}{\alpha}\rho(\Gamma_2)$ where $\Gamma_2 \in \mathbb{R}^{N_F \times N_F}$ is the matrix with elements

$$(\Gamma_2)_{ij} = \begin{cases} 0 & \text{if } j \notin \mathcal{F}_i \\ \mu_i \alpha_{ji} & \text{if } j \in \mathcal{F}_i \end{cases} \tag{6.57}$$

If $\rho(\Gamma_2) < 1$ then it is always possible to find δ and α verifying $\delta/\alpha \geq 1$ and then yielding $\rho(\Gamma_1) < 1$. The problem of finding coefficients α_{ji} in Γ_2 guaranteeing that $\rho(\Gamma_2) < 1$, and verifying the constraints

$$\sum_{j \in \mathcal{F}_i} \alpha_{ji} < 1 \qquad \forall i : \mathcal{L}_i \neq \emptyset \tag{6.58}$$

$$\sum_{j \in \mathcal{F}_i} \alpha_{ji} = 1 \qquad \forall i : \mathcal{L}_i = \emptyset \tag{6.59}$$

is a semidefinite programming problem (Boyd and Vandenberghe, 2004) for which efficient solvers exist. If, on the one hand, the computation of the coefficients α_{ij} is the most computationally demanding part of the control

design procedure, on the other hand it must be carried out offline and as such it does not impact on the performance of the closed-loop system.
Note that, if the graph of the communication network is a tree, in which the leader corresponds to the root node and all edges are directed from parent to child nodes then the matrix Γ_2 is upper triangular with null entries on the diagonal. In this case, $\rho(\Gamma_2) = 0$ and condition (6.43) is satisfied.

As for Theorem 6.4, if matrices η_i are chosen such that (6.54) holds, then condition (6.48) is satisfied. Moreover, a suitable value for $\hat{\eta}$ in (6.54) can be found according to the following theorem.

Theorem 6.5 *Assume that matrices K_i are chosen so that (6.56) holds, matrices η_i are chosen according to (6.54), and there exists*

$$\xi = \max_{k \in \mathcal{L}} \{\|\dot{x}_k\|_\infty\}$$

. Let $d(i,j)$ be the number of arcs composing the shortest path from node i to node j in $\mathcal{G}^c$. Then, there exists $\psi > 0$ such that $\psi > \|\tilde{x}_i(t)\|$, $i \in \mathcal{F}$, $\forall t \geq 0$. Moreover, if $\hat{\eta}$ verifies

$$\hat{\eta} > \max_{i \in \mathcal{F}} \left\{ \frac{(1-\theta_i)\delta\psi + \xi}{\theta_i} \right\} \tag{6.60}$$

where

$$\theta_i = \begin{cases} 1 - \sum_{j \in \mathcal{F}_i} \alpha_{ji} & \text{if } d(N_F+1, i) = 1 \\ \min_{z \in \Xi_i} \left\{ 1 - \sum_{j \in \mathcal{F}_i / \{z\}} \alpha_{ji} \right\} & \text{otherwise} \end{cases} \tag{6.61}$$

and

$$\Xi_i = \{ j \in \mathcal{F}_i : d(N_F+1, j) = d(N_F+1, i) - 1 \} \tag{6.62}$$

then condition (6.49) is fulfilled and the generalized consensus state is reached in finite time.

Proof: From (6.54) and (6.56) one has that Theorem 6.3 holds and then the collective error is ISS with respect to $\dot{x}_k$, $k \in \mathcal{L}$. As a consequence, if $\dot{x}_k$, $k \in \mathcal{L}$, are bounded then there exist $\psi > 0$ such that $\psi \geq \|\tilde{x}_i(t)\|$, $\forall i \in \mathcal{F}$. From Assumption 6.1, the graph $\mathcal{G}^c$ has a rooted spanning tree and for each follower i there is at least one path from node $N_F + 1$ to node i.

The theorem will be proved by induction. Consider a follower $i \in \mathcal{F}$, such that $d(N_F+1,i)=1$ in $\mathcal{G}^c$. From (6.61), one obtains

$$\theta_i = 1 - \sum_{j\in\mathcal{F}_i} \alpha_{ji} \tag{6.63}$$

If $\hat{\eta}$ is chosen according to (6.60) one has that

$$\theta_i\hat{\eta}\|\tilde{x}_i\| > \Big((1-\theta_i)\delta\psi + \xi\Big)\|\tilde{x}_i\| \tag{6.64}$$

and hence, adding $(1-\theta_i)\hat{\eta}\|\tilde{x}_i\|$ to both sides of the inequality

$$\begin{aligned}
\hat{\eta}\|\tilde{x}_i\| &> \Big((1-\theta_i)\delta\psi + \xi + (1-\theta_i)\hat{\eta}\Big)\|\tilde{x}_i\| \\
&\geq \Big(\sum_{j\in\mathcal{F}_i}\alpha_{ji}\delta\psi + \sum_{k\in\mathcal{L}_i}\alpha_{ki}\xi + \sum_{j\in\mathcal{F}_i}\alpha_{ji}\hat{\eta}\Big)\|\tilde{x}_i\| \\
&> \Big(\sum_{j\in\mathcal{F}_i}\alpha_{ji}\delta\|\tilde{x}_j\| + \sum_{k\in\mathcal{L}_i}\alpha_{ki}\|\dot{x}_k\| + \sum_{j\in\mathcal{F}_i}\alpha_{ji}\hat{\eta}\Big)\|\tilde{x}_i\| \\
&> \tilde{x}_i^T\Big(\sum_{j\in\mathcal{F}_i}\alpha_{ji}K_j\tilde{x}_j + \sum_{k\in\mathcal{L}_i}\alpha_{ki}\dot{x}_k + \sum_{j\in\mathcal{F}_i}\alpha_{ji}\hat{\eta}I\frac{\tilde{x}_j}{\|\tilde{x}_j\|}\Big)
\end{aligned} \tag{6.65}$$

Note that the second inequality in (6.65) follows from the fact that $\sum_{k\in\mathcal{L}_i}\alpha_{ki} \leq 1$. In the last inequality in (6.65) we used (6.56) and the fact that $\tilde{x}_i^T\frac{\tilde{x}_j}{\|\tilde{x}_j\|} \leq \|\tilde{x}_i\|\frac{\|\tilde{x}_j\|}{\|\tilde{x}_j\|} = \|\tilde{x}_i\|$. From (6.65), there exists $\Omega_i = \omega_i I > 0$ such that

$$\begin{aligned}
\tilde{x}_i^T(\Omega_i + \hat{\eta}I)\frac{\tilde{x}_i}{\|\tilde{x}_i\|} &\geq \tilde{x}_i^T\Big(\sum_{j\in\mathcal{F}_i}\alpha_{ji}K_j\tilde{x}_j + \sum_{k\in\mathcal{L}_i}\alpha_{ki}\dot{x}_k \\
&\quad + \sum_{j\in\mathcal{F}_i}\alpha_{ji}\hat{\eta}I\frac{\tilde{x}_j}{\|\tilde{x}_j\|}\Big)
\end{aligned} \tag{6.66}$$

and (6.49) is fulfilled. As a consequence of Theorem 6.4, there is a time t_{s_i} such that agent i exhibits a sliding mode on the sliding manifold $\tilde{x}_i = 0$ for $t \geq t_{s_i}$.

As induction hypothesis it is assumed that all follower agents h, $h \in \mathcal{F}$, such that $d(N_F+1,h) < j$ in $\mathcal{G}^c$ have reached the generalized consensus state in finite time.

Let z be a follower agent such that $d(N_F+1,z) = j$ in $\mathcal{G}^c$ and let $\pi_z =$

$\{(N_F+1, i_{j-1})\ (i_{j-1}, i_{j-2}), \ldots, (i_1, z)\}$ a path connecting node z to node N_F+1. If $\hat{\eta}$ is chosen according to (6.60) one has that

$$\begin{aligned}
\hat{\eta}\|\tilde{x}_z\| &> \Big((1-\theta_z)\delta\psi + \xi + (1-\theta_z)\hat{\eta}\Big)\|\tilde{x}_z\| \\
&\geq \Big(\sum_{j\in\mathcal{F}_z/\{i_1\}} \alpha_{jz}\delta\psi + \sum_{k\in\mathcal{L}_z} \alpha_{kz}\xi + \sum_{j\in\mathcal{F}_z/\{i_1\}} \alpha_{jz}\hat{\eta}\Big)\|\tilde{x}_z\| \\
&> \Big(\sum_{j\in\mathcal{F}_z/\{i_1\}} \alpha_{jz}\delta\|\tilde{x}_j\| + \sum_{k\in\mathcal{L}_z} \alpha_{kz}\|\dot{x}_k\| + \sum_{j\in\mathcal{F}_z/\{i_1\}} \alpha_{jz}\hat{\eta}\Big)\|\tilde{x}_z\| \\
&> \tilde{x}_z^T\Big(\sum_{j\in\mathcal{F}_z/\{i_1\}} \alpha_{jz}K_j\tilde{x}_j + \sum_{k\in\mathcal{L}_z} \alpha_{kz}\dot{x}_k + \sum_{j\in\mathcal{F}_z/\{i_1\}} \alpha_{jz}\hat{\eta}I\frac{\tilde{x}_j}{\|\tilde{x}_j\|}\Big)
\end{aligned} \tag{6.67}$$

By assumption, since $d(N_F+1, i_1) \leq j-1$ in $\mathcal{G}^c$, for $t \geq t_{s_{i_1}}$, $\tilde{x}_{i_1} = 0$ and, in equivalent sense (Edwards and Spurgeon, 1998), $\tilde{x}_{i_1}/\|\tilde{x}_{i_1}\| = 0$. Then (6.67) can be rewritten as

$$\begin{aligned}
\hat{\eta}\|\tilde{x}_z\| &> \tilde{x}_z^T\Big(\sum_{j\in\mathcal{F}_z/\{i_1\}} \alpha_{jz}K_j\tilde{x}_j + \sum_{k\in\mathcal{L}_z} \alpha_{kz}\dot{x}_k + \sum_{j\in\mathcal{F}_z/\{i_1\}} \alpha_{jz}\hat{\eta}I\frac{\tilde{x}_j}{\|\tilde{x}_j\|}\Big) \\
&= \tilde{x}_z^T\Big(\sum_{j\in\mathcal{F}_z} \alpha_{jz}K_j\tilde{x}_j + \sum_{k\in\mathcal{L}_z} \alpha_{kz}\dot{x}_k + \sum_{j\in\mathcal{F}_z} \alpha_{jz}\hat{\eta}I\frac{\tilde{x}_j}{\|\tilde{x}_j\|}\Big)
\end{aligned} \tag{6.68}$$

From (6.68), there exists $\Omega_z = \omega_z I > 0$ such that

$$\begin{aligned}
\tilde{x}_z^T(\Omega_z + \hat{\eta}I)\frac{\tilde{x}_z}{\|\tilde{x}_z\|} \;\geq\; & \tilde{x}_z^T\Big(\sum_{j\in\mathcal{F}_z} \alpha_{jz}K_j\tilde{x}_j + \sum_{k\in\mathcal{L}_z} \alpha_{kz}\dot{x}_k \\
& + \sum_{j\in\mathcal{F}_z} \alpha_{jz}\hat{\eta}I\frac{\tilde{x}_j}{\|\tilde{x}_j\|}\Big)
\end{aligned} \tag{6.69}$$

and (6.49) is satisfied. As a consequence of Theorem 6.4, there is a time t_{s_z} such that agent z exhibits a sliding mode on the sliding manifold $\tilde{x}_z = 0$ for $t \geq t_{s_z}$.

Note that, by choosing $\hat{\eta} > 0$ one obtains a formation error $\|\tilde{x}\|$ which is lower with respect to the case $\hat{\eta} = 0$, even if the chosen value for $\hat{\eta}$ is not capable of guaranteeing the finite time convergence to the generalized consensus state. Moreover, the greater $\hat{\eta}$, the lower formation error $\|\tilde{x}\|$ in the asymptotic regime.

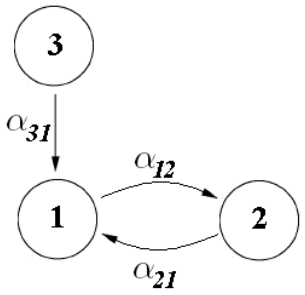

Figure 6.3: The topology of the multi–agent system considered in Section 6.8, Case A.

6.8 Simulation results

6.8.1 Case A

As a first example, the multi–agent system represented in Fig. 6.3 is considered. It is composed by two followers and one leader, indexed by the sets $\mathcal{F} = \{1, 2\}$, and $\mathcal{L} = \{3\}$, respectively. Assume that all agents $i \in \{1, 2, 3\}$ obey to the dynamics

$$\dot{x}_i = \begin{bmatrix} \dot{x}_{ix} \\ \dot{x}_{iy} \end{bmatrix} = \begin{bmatrix} u_{ix} \\ u_{iy} \end{bmatrix} = u_i \tag{6.70}$$

The reference position are chosen as $p_1 = [0, 0]^T$, $p_2 = [1, 1]^T$, and $p_3 = [2, 3]^T$ then the relative distance are given by $d_{21} = [1, 1]^T$, $d_{31} = [2, 3]^T$, and $d_{12} = [-1, -1]^T$. According to (6.12), the position error for agent 1 is defined as

$$\tilde{x}_1 = (1 - \alpha)(x_2 - d_{21}) + \alpha(x_3 - d_{31}) - x_1$$

with $\alpha \in (0, 1)$. Similarly, the position error for agent 2 is

$$\tilde{x}_2 = x_1 - d_{12} - x_2$$

The control law (6.25) is applied to the follower agents. In order to satisfy the assumptions of Theorem 6.2, K_1, and K_2 are chosen as positive–definite matrices and η_1, and η_2 are chosen as positive–semidefinite matrices. In order to fulfill (6.29), η_1 is chosen such that

$$\lambda_{min}(\eta_1) \geq (1 - \alpha)\lambda_{max}(\eta_2) \tag{6.71}$$

Then, from Theorem 6.2, $\tilde{x}_1$ is ISS with respect to $\tilde{x}_2$ and $\dot{x}_3$, and, from (6.30) and (6.31), the ISS gain functions are

$$\gamma_{12}(r) = \frac{2(1-\alpha)\lambda_{max}(K_2)}{\theta\lambda_{min}(K_1)}r \qquad \gamma_{13}(r) = \frac{2\alpha}{\theta\lambda_{min}(K_1)}r$$

As for agent 2, η_2 is chosen such that (6.29) is satisfied, i.e.,

$$\lambda_{min}(\eta_2) \geq \lambda_{max}(\eta_1) \tag{6.72}$$

Then, $\tilde{x}_2$ is ISS with respect to $\tilde{x}_1$, and, from (6.30), the ISS gain function is given by

$$\gamma_{21}(r) = \frac{\lambda_{max}(K_1)}{\theta\lambda_{min}(K_2)}r$$

In order to make the collective error, i.e., $\tilde{x} = [\tilde{x}_1, \tilde{x}_2]^T$, ISS with respect to $\dot{x}_3$, parameters α, K_1, and K_2 must be chosen so as to satisfy the assumptions of Theorem 6.3. The matrix Γ_1 for the considered multi–agent system is given by

$$\Gamma_1 = \begin{bmatrix} 0 & \frac{2(1-\alpha)\lambda_{max}(K_2)}{\lambda_{min}(K_1)} \\ \frac{\lambda_{max}(K_1)}{\lambda_{min}(K_2)} & 0 \end{bmatrix} \tag{6.73}$$

Note that, in this case, condition (6.43) is equivalent to the well-known small gain theorem (Dashkovskiy *et al.*, 2007).
From Theorem 6.3, the collective error is ISS if and only if

$$\gamma_{12}\gamma_{21} = (1-\alpha)\frac{\lambda_{max}(K_2)\lambda_{max}(K_1)}{\lambda_{min}(K_1)\lambda_{min}(K_2)} < 1 \tag{6.74}$$

By selecting

$$\alpha = \frac{2}{3} \qquad K_1 = 2I \qquad K_2 = 2I$$

condition (6.74) is satisfied, thus the collective error is ISS. In order to satisfy conditions (6.71), and (6.72), a possible choice for η_1, and η_2 is

$$\eta_1 = \eta_2 = \hat{\eta}I, \qquad \hat{\eta} \geq 0$$

6.8.1.1 Case A1

A first simulation is performed with $u_3 = [0.5, 0.5]^T$, and $\hat{\eta} = 0$. This means that the sliding mode component of the control law is not used. Fig. 6.4 shows the evolution of $\|\tilde{x}_1\|$, and $\|\tilde{x}_2\|$. As one can note, both $\|\tilde{x}_1\|$ and $\|\tilde{x}_2\|$ are bounded but they do not reach zero. More specifically, $\|\tilde{x}_1(t)\| \leq 0.4$, and $\|\tilde{x}_2(t)\| \leq 0.4$ for all $t \geq 3s$.

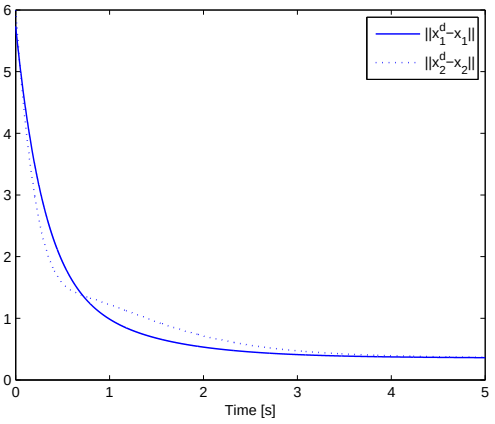

Figure 6.4: The evolution of $\|\tilde{x}_1(t)\|$ and $\|\tilde{x}_2(t)\|$ for the Case A1 discussed in Section 6.8.

6.8.1.2 Case A2

The second simulation case is performed with u_3 as in Case A1, but with $\hat{\eta} = 1$. Fig 6.5 shows the evolution in time of $\|\tilde{x}_1\|$, and $\|\tilde{x}_2\|$. Differently from Case A1, now both $\|\tilde{x}_1\|$ and $\|\tilde{x}_2\|$ go to zero in finite time. More specifically, $\|\tilde{x}_1(t)\| = \|\tilde{x}_2(t)\| = 0$ for all $t \geq 2.5s$.

6.8.2 Case B

Consider the multi–agent system represented in Fig. 6.6, composed by three followers and two leaders, indexed by the sets $\mathcal{F} = \{1, 2, 3\}$, and $\mathcal{L} = \{4, 5\}$, respectively. As in the previous simulation example, assume that all agents obey to the dynamics (6.70), for $i \in \{1, 2, 3, 4, 5\}$. The reference position are chosen as $p_1 = [0, 0]^T$, $p_2 = [2, 0]^T$, $p_3 = [1, -2]^T$, $p_4 = [0, 1]^T$, and $p_5 = [2, 1]^T$. The position errors for agent 1, 2, and 3 are given by

$$\begin{aligned}
\tilde{x}_1 &= \alpha_{21}(x_2 - d_{21}) + \alpha_{31}(x_3 - d_{31}) + \alpha_{41}(x_4 - d_{41}) - x_1 \\
\tilde{x}_2 &= \alpha_{12}(x_1 - d_{12}) + \alpha_{52}(x_5 - d_{52}) - x_2 \\
\tilde{x}_3 &= \alpha_{13}(x_1 - d_{13}) + \alpha_{23}(x_2 - d_{23}) - x_3
\end{aligned}$$

where $d_{21} = [2, 0]^T$, $d_{31} = [1, -2]^T$, $d_{41} = [0, 1]^T$, $d_{12} = -d_{21}$, $d_{52} = [0, 1]^T$, $d_{13} = -d_{31}$, $d_{23} = [1, 2]^T$, $\alpha_{21} + \alpha_{31} + \alpha_{41} = 1$, $\alpha_{12} + \alpha_{52} = 1$, and

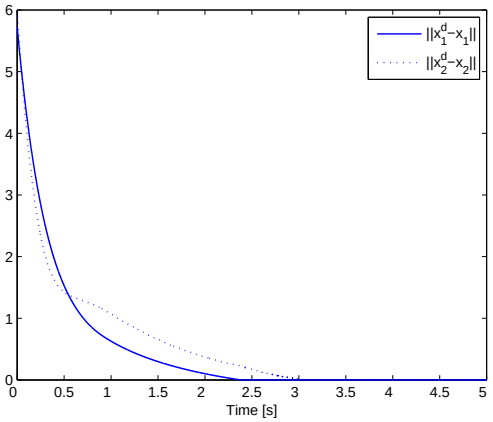

Figure 6.5: The evolution of $\|\tilde{x}_1(t)\|$ and $\|\tilde{x}_2(t)\|$ for the Case A2 discussed in Section 6.8.

$\alpha_{13} + \alpha_{23} = 1$.
The control law (6.25) is applied to the follower agents. In order to fulfill the assumptions of Theorem 6.2, K_1, K_2, K_3 are chosen as positive–definite matrices and η_1, η_2, η_3 are chosen as positive–semidefinite matrices. In order to fulfill (6.29), the matrices η_1, η_2, and η_3 are chosen as

$$\eta_1 = \eta_2 = \eta_3 = \hat{\eta} I, \qquad \hat{\eta} \geq 0$$

From (6.30), the gain functions γ_{ij} are

$$\gamma_{12} = \frac{3\alpha_{21}\lambda_{max}(K_2)}{\theta\lambda_{min}(K_1)} \qquad \gamma_{13} = \frac{3\alpha_{31}\lambda_{max}(K_3)}{\theta\lambda_{min}(K_1)} \qquad \gamma_{21} = \frac{2\alpha_{12}\lambda_{max}(K_1)}{\theta\lambda_{min}(K_2)}$$
$$\gamma_{31} = \frac{2\alpha_{13}\lambda_{max}(K_1)}{\theta\lambda_{min}(K_3)} \qquad \gamma_{32} = \frac{2\alpha_{23}\lambda_{max}(K_2)}{\theta\lambda_{min}(K_3)}$$

The control parameters K_1, K_2, and K_3 are chosen as

$$K_1 = K_2 = K_3 = \hat{K} I, \qquad \hat{K} > 0$$

From (6.57), the matrix Γ_2 is

$$\Gamma_2 = \begin{bmatrix} 0 & 3\alpha_{21} & 3\alpha_{31} \\ 2\alpha_{12} & 0 & 0 \\ 2\alpha_{13} & 2\alpha_{23} & 0 \end{bmatrix}$$

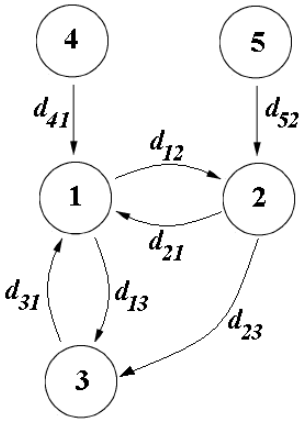

Figure 6.6: The topology of the multi–agent system considered in Section 6.8, Case B.

The characteristic polynomial of Γ_2 results in

$$\lambda^3 - (6\alpha_{12}\alpha_{21} + 6\alpha_{13}\alpha_{31})\lambda - 12\alpha_{12}\alpha_{23}\alpha_{31} = 0$$

In order to fulfill condition (6.43), a possible choice of the parameters α_{ij} is

$$\begin{array}{llll} \alpha_{21} = 1/6, & \alpha_{31} = 1/6, & \alpha_{41} = 4/6, & \alpha_{12} = 1/6, \\ \alpha_{52} = 5/6, & \alpha_{13} = 1/2, & \alpha_{23} = 1/2 & \end{array}$$

6.8.2.1 Case B1

A first simulation case is performed with $u_4 = u_5 = [2\sin(10t), 2\cos(10t)]^T$, $\hat{\eta} = 0$, and $\hat{K} = 1$. Therefore the sliding mode component of the control law is turned off. Fig 6.7 shows the evolution in time of $\|\tilde{x}_1\|$, $\|\tilde{x}_2\|$, and $\|\tilde{x}_3\|$. As one can note, all position errors are bounded since $\|\tilde{x}_1(t)\| \leq 0.2$, $\|\tilde{x}_2(t)\| \leq 0.2$, and $\|\tilde{x}_3(t)\| \leq 0.1$ for all $t \geq 5s$, but they do not reach zero.

6.8.2.2 Case B2

The second simulation case is performed with u_4, u_5 and $\hat{K}$ as in Case B1, but with $\hat{\eta} = 1$. The evolution in time of $\|\tilde{x}_1\|$, $\|\tilde{x}_2\|$, and $\|\tilde{x}_3\|$ is reported

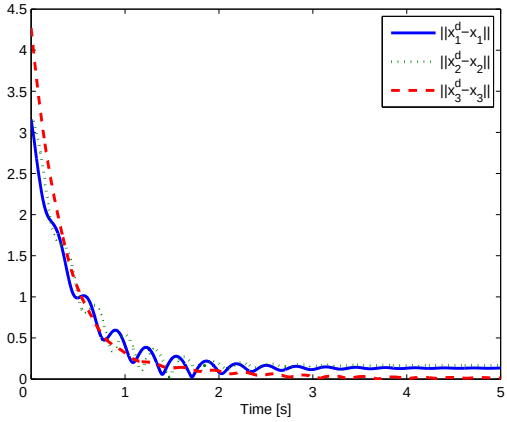

Figure 6.7: The evolution of the position errors for the Case B1 discussed in Section 6.8.

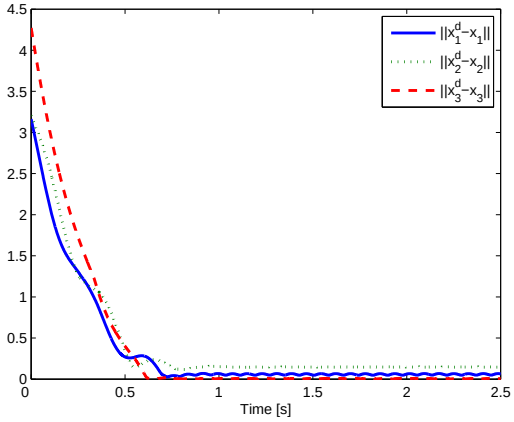

Figure 6.8: The evolution of the position errors for the Case B2 discussed in Section 6.8.

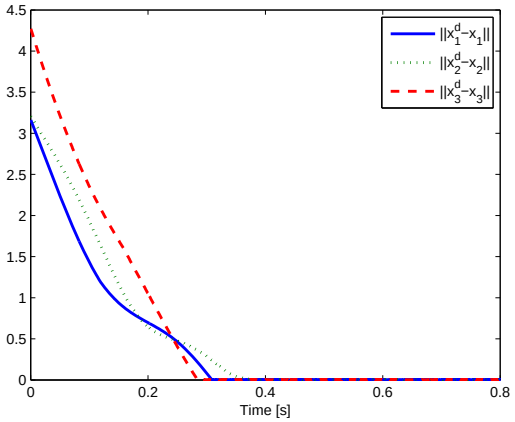

Figure 6.9: The evolution of the position errors for the Case B3 discussed in Section 6.8.

in Fig 6.8. As one can note, all position errors are bounded, in particular, $\|\tilde{x}_1(t)\| \leq 0.1$, $\|\tilde{x}_2(t)\| \leq 0.2$, and $\|\tilde{x}_3(t)\| \leq 0.1$ for all $t \geq 1s$, but they do not reach zero. Note that the formation error obtained in this case is lower than the one obtained in Case B1. This is due to the fact that the value of $\hat{\eta}$ has been increased.

6.8.2.3 Case B3

This last simulation case is performed with u_4, u_5 and $\hat{K}$ as in Case B1, but with $\hat{\eta} = 2.5$. The evolution in time of $\|\tilde{x}_1\|$, $\|\tilde{x}_2\|$, and $\|\tilde{x}_3\|$ is reported in Fig 6.9. In this case, all the position errors go to zero in finite time. More specifically, $\|\tilde{x}_1(t)\| = \|\tilde{x}_2(t)\| = \|\tilde{x}_3(t)\| = 0$ for all $t \geq 0.4s$.

6.9 Conclusions

In this chapter a decentralized sliding mode control for a multi–agent system with a directed communication network has been presented. The control objective is to drive each follower agent to the generalized consensus state. The propagation of the position errors within the network has been studied using the notion of ISS. In particular, it has been shown that, under suf-

ficient conditions on the control parameters, the proposed control scheme is capable to guarantee that the collective error dynamics is ISS with respect to the leaders' velocities. Moreover, it has been proved that, under suitable assumptions, the sliding mode part of the control law is capable of steering the position errors to zero in finite time, thus reaching the generalized consensus state. Simulation results are presented to demonstrate the effectiveness of the proposed control approach. Future researches will focus on the generalizations of the control scheme to the case of perturbations affecting the follower behaviour and the transmission channels and on the design of a second order sliding mode control law capable of guaranteeing the finite time reaching of the generalized consensus state.

Appendix A

This section is devoted to the proof of Theorem 6.1. First, a preliminary Lemma that relies on results derived in Ren *et al.* (2007) is introduced.

Lemma 6.2 *Assume that $\mathcal{L}$ is a singleton and $p_i = 0$, $i \in \mathcal{N}$. Then system*

$$\tilde{x}_i = 0 \qquad i \in \mathcal{F} \tag{6.75}$$

$$x_i = 0 \qquad i \in \mathcal{L} \tag{6.76}$$

has an unique solution if and only if $\mathcal{G}$ contains a rooted spanning tree. Moreover the solution is given by $x_i = 0$, $i \in \mathcal{N}$.

Proof: Since $\mathcal{L}$ is a singleton one has that $N = N_F + 1$. Consider the matrix $L \in \mathbb{R}^{N \times N}$ with entries $L_{ii} = 1$, $i = 1, \ldots, N_F$, $L_{NN} = 0$, $L_{ij} = -\alpha_{ji}$ if $(j,i) \in \mathcal{E}$ and $L_{ij} = 0$ if $(j,i) \notin \mathcal{E}$. Since $L_{ij} \leq 0$, $i \neq j$, and, in view of (6.5), $\sum_{j=1}^{N} L_{ij} = 0$, $i \in \mathcal{N}$, it follows that L is a graph Laplacian (Ren *et al.*, 2007). Moreover, as shown in Ren *et al.* (2007), 0 is a simple eigenvalue of L with associated eigenvector $\mathbf{1} = [1, \ldots, 1]^T$ if and only if Assumption 6.1 holds. Note also that the last row of L contains only zeros. Hence, introducing the vectors $\tilde{x}_i = [\tilde{x}_1^T, \ldots, \tilde{x}_N^T]^T$, $x = [x_1^T, \ldots, x_N^T]^T$ and setting $\tilde{x}_N = 0$ and $x_N = 0$, one has that $\tilde{x} = (I_n \otimes L)x$, where $\otimes$ denotes the Kronecker product. In view of the properties of L, 0 is an eigenvalue of $I_n \otimes L$ with multiplicity n and associated eigenspace

$$Z = \{[v^T, \ldots, v^T]^T \in \mathbb{R}^{N \times n},\ v \in \mathbb{R}^n\}$$

Therefore all solutions to $\tilde{x} = 0$ lie in Z and since $x_N = 0$ one has that $x_i = 0$, $\forall i \in \mathcal{F}$.

Proof of Theorem 6.1. Let $x = [x_1^T, \ldots, x_N^T]^T$. Obviously $x = [(p_1 + \nu)^T, \ldots, (p_N + \nu)^T]^T$ is a solution to (6.15)–(6.16). Next, it will be shown that it is unique. Let $z = [z_1^T, \ldots, z_N^T]^T$, $z_i \in \mathbb{R}^n$, and $v = [v_1^T, \ldots, v_N^T]^T$, $v_i \in \mathbb{R}^n$, be two solutions to (6.15)–(6.16).
Then, one has

$$\sum_{j \in \mathcal{N}_i} \alpha_{ji}(z_j - v_j - (z_i - v_i)) = 0 \qquad i \in \mathcal{F} \tag{6.77}$$

$$z_i - v_i = 0 \qquad i \in \mathcal{L} \tag{6.78}$$

or equivalently, $w = z - v$ verifies

$$\sum_{j \in \mathcal{N}_i} \alpha_{ji}(w_j - (w_i)) = 0 \qquad i \in \mathcal{F} \tag{6.79}$$

$$w_i = 0 \qquad i \in \mathcal{L} \tag{6.80}$$

Note that, because of (6.80), equation (6.79) can be written as $\tilde{w}_i = 0$, $i \in \mathcal{F}$, where

$$\tilde{w}_i = \sum_{k \in \mathcal{L}_i} \alpha_{ki}(-w_i) + \sum_{j \in \mathcal{F}_i} \alpha_{ji}(w_j - w_i) \tag{6.81}$$

Note that from Definition 6.1 and (6.9) one has

$$\tilde{w}_i = -w_i \alpha^c_{N_F+1,i} + \sum_{j \in \mathcal{F}_i^c} \alpha^c_{ji}(w_j - w_i) \tag{6.82}$$

Comparing the previous formula with (6.13) one has that $\tilde{w}_i$, $i \in \mathcal{F}$, are just the follower errors defined with respect to the graph $\mathcal{G}^c$ when $x_i = w_i$, $i \in \mathcal{F}$, $p_i = 0$, $i = 1, \ldots, N_F + 1$, and $x_{N_F+1} = w_{N_F+1} = 0$. Since $\mathcal{L}^c$ is a singleton one can apply Lemma 6.2 with respect to the graph $\mathcal{G}^c$ and conclude that the solution to the system

$$\tilde{w}_i = 0 \qquad i \in \mathcal{F} \tag{6.83}$$

$$w_{N_F+1} = 0 \tag{6.84}$$

is unique and given by $w_i = 0$, $i \in \mathcal{F}$, if and only if Assumption 6.1 holds. Hence, it has been shown that the following conditions are equivalent

- Assumption 6.1 holds

- (6.79)–(6.80) has an unique solution given by $w_i = 0$, $i \in \mathcal{N}$
- $x = [(p_1 + \nu)^T, \ldots, (p_n + \nu)^T]^T$ is the unique solution to (6.15)

thus concluding the proof

Chapter 7

Summary and conclusions

In this thesis it has been presented a survey of the theoretical background of sliding mode control, in particular higher order sliding mode control, and it has been shown by presenting also new theoretical developments, that the second order sliding mode approach is an effective solution to the drawbacks of first order sliding mode control laws, which are particularly evident when dealing with mechanical systems since rapidly changing control actions induce stress and wear in mechanical parts and the system could be damaged in a short time.

The basic notions of the sliding mode control theory has been given in Chapter 2, while a brief introduction to the higher order sliding mode control theory and a description of the main features and advantages of higher order sliding modes have been discussed in Chapter 3. In particular, the second order sliding mode control problem has been described and several second order sliding mode controllers have been presented.

The major contribution of the present thesis is the application of sliding mode control methodology to different important control problems involving uncertain mechanical systems which have been addressed and solved in Chapters 4, 5 and 6.
More specifically, in Chapter 4 different second order sliding mode active safety systems for vehicle have been proposed.
In particular the design of a second order sliding mode control for vehicle yaw stability is illustrated in Section 4.1. A traction control system based on second order sliding mode methodology is presented in Section 4.2 for vehicle and in Section 4.3 for sport motorbike. In Section 4.4 a driver assistance system for a platoon of vehicles capable of keeping the desired inter–vehicular spacing, but also capable, in case of detection of a possible collision with static or moving obstacles, of making a decision between the generation of an emergency braking or a collision avoidance manoeuvre is proposed. The different modules of this latter safety system are design re-

lying on sliding mode methodology.
The effectiveness of the control schemes proposed in Chapter 4 has been tested in simulations. All of them have shown good performances even in presence of disturbances and parametric uncertainties. Another advantage of the proposed control laws, apart from the robustness features against the uncertainty sources and disturbances typical of automotive applications, relies in the fact that they are characterized by low complexity compared to other robust control approaches (H_∞, LMI, adaptive control, etc.) and thus they appear particularly suitable to be implemented in the Electronic Control Unit (ECU) of a controlled vehicle. Moreover, the proposed controllers generate continuous control actions, since the discontinuity is confined to the derivative of the control signal, and the generated sliding modes are ideal, in contrast to what happens for solutions which relies on continuous approximations of the discontinuous control laws.

In Chapter 5 the problem of controlling a class of nonholonomic systems in chained form affected by two different kind of uncertainties has been addressed and solved by means of second order sliding mode control laws.
More specifically, the problem of stabilizing chained form systems affected by uncertain drift term and parametric uncertainties is addressed in Section 5.2, while in Section 5.3 the same problem is solved for a class of chained form systems affected by both matched and unmatched uncertainties.
The design methodologies described in Chapter 5 are both based on suitable transformations of the system model so that, on the basis of the transformed system state, it is possible to design a particular sliding manifold, as well as to re–formulate the control problem in question as a second order sliding mode control problem. As a consequence, the control input results in being continuous, thus more acceptable in the considered context. Note that the approaches here proposed are applicable to a wide class of perturbed nonholonomic systems. In particular, as a novelty with respect to the conventional sliding mode approach, the control scheme proposed in Section 5.3 is capable to deal also with unmatched uncertainties without requiring any knowledge of the uncertainty terms.

Finally, Chapter 6 has been focuses on the control of a team of agents designated either as leaders or followers and exchanging information over a directed communication network. The generalized consensus state for a follower agent has been defined as a target state that depends on the state of its neighbors. A decentralized control scheme based on the sliding

mode technique capable of steering the state of each follower agent to the generalized consensus state in finite time has been proposed. This feature is in sharp contrast with other control schemes available in the literature that guarantee formation achievement just in the asymptotic regime.

7.1 Ideas for future research

There are a number of possible interesting suggestions for further research.

As for the second order sliding mode control scheme for vehicle yaw stability proposed in Section 4.1, future work needs to be devoted to test stability and performance with low and non–uniform road friction coefficients. Moreover, it will be interesting to investigate the possibility of combining the second order sliding mode and the internal model control techniques presented in Section 4.1 in order to exploit their respective benefits in vehicle stability control.
Another important aspect that will be investigated in future research is the coupling of the traction force controller presented in Section 4.2 with throttle angle and brake controllers, taking into account the actuators dynamics, as well as vehicle pitch dynamics. As for the traction control for sport motorbike proposed in Section 4.3, ongoing work is being devoted to devise an adaptation of the controller gains in order to achieve high safety levels also at low speed, which is a very critical situation for traction control.
The control scheme for a platoon of vehicles proposed in Section 4.4 could be also regarded as an hybrid control problem. Future works will be devoted to investigate the problem from this point of view in particular as for as the stability issues are concerned and to the design of second order sliding mode low level controllers for the “collision avoidance" module. Furthermore, it will be interesting to investigate the possibility of introducing communication between vehicles in order to perform more complex collision manoeuvre.

An interesting future development of the control schemes proposed in Chapter 5 could be the design of a second order sliding mode control law for the input u_0 and the design of an output feedback control scheme.

Finally, future developments of the control scheme for multi–agent systems proposed in Chapter 6 will focus on the generalization of the control scheme to the case of perturbations affecting the follower behaviour and the

transmission channels and on the design of a second order sliding mode control law capable of guaranteeing the finite time reaching of the generalized consensus state.

Bibliography

Ackermann, J. and W. Sienel (1993). Robust yaw damping of cars with front and rear wheel steering. *IEEE Transactions on Control Systems Technology* **1**(1), 15–20.

Ackermann, J., J. Guldner, W. Sienel, R. Steinhauser and V.I. Utkin (1995). Linear and nonlinear controller design for robust automatic steering. *IEEE Transactions on Control Systems Technology* **3**(1), 132–143.

Amodeo, M., A. Ferrara, R. Terzaghi and C. Vecchio (2007*a*). Slip control for vehicles platooning via second order sliding modes. In: *Proceedings of the Intelligent Vehicle Symposium*. Istanbul, Turkey. pp. 761–766.

Amodeo, M., A. Ferrara, R. Terzaghi and C. Vecchio (2007*b*). Wheel slip control via second order sliding modes generation. In: *Proceedings of the 2007 Conference on Decision and Control*. New Orleans, LA, USA. pp. 3889–3894.

Amodeo, M., A. Ferrara, R. Terzaghi and C. Vecchio (2008). Wheel slip control via second order sliding modes generation. *IEEE Transactions on Intelligent Transportation Systems*. Submitted.

Arnold, V.I. (1996). *Geometrical methods in the theory of ordinary differential equations*. Springer–Verlag. Berlin.

Astolfi, A. (1996). Discontinuous control of nonholonomic systems. *Systems and Control Letters* **27**(1), 37–45.

Avenati, R., S. Campo and L. Ippolito (1998). A rear active differential: theory and practice of a new type of controlled splitting differential and its impact on vehicle behaviour. In: *Proceedings of the Global powertrain conference*. Detroit, MI, USA.

Balch, T. and R.C. Arkin (1998). Behavior-based formation control for multirobot teams. *Robotics and Automation, IEEE Transactions on* **14**(6), 926–939.

Bartolini, G. (1989). Chattering phenomena in discontinuous control systems. *International Journal of Systems Science* **20**(12), 2471–2481.

Bartolini, G., A. Ferrara, A. Pisano and E. Usai (1998*a*). Adaptive reduction of the control effort in chattering-free sliding-mode control of uncertain nonlinear systems. *Applied Mathematics and computer science* **8**, 51–72.

Bartolini, G., A. Ferrara, A. Pisano and E. Usai (2001). On the convergence properties of a 2-sliding control algorithm for non-linear uncertain systems. *International Journal of Control* **74**(7), 718–731.

Bartolini, G., A. Ferrara and E. Usai (1997*a*). Applications of a sub–optimal discontinuous control algorithm for uncertain second order systems. *International Journal of Robust and Nonlinear Control* **7**, 299–319.

Bartolini, G., A. Ferrara and E. Usai (1997*b*). Output Tracking Control of Uncertain Nonlinear Second-Order Systems. *Automatica* **33**, 2203–2212.

Bartolini, G., A. Ferrara and E. Usai (1998*b*). Chattering avoidance by second-order sliding mode control. *IEEE Transactions on Automatic Control* **43**(2), 241–246.

Bartolini, G., A. Ferrara, F. Levant and E. Usai (1999). On second order sliding mode controller. In: *Lecture Notes in Control and Information Sciences* (K. D. Young and Ü. Özgüner, Eds.). Vol. 247. Springer–Verlag. Berlin. pp. 329–350.

Bartolini, G., A. Ferrara, L. Giacomini and E. Usai (2000). Properties of a combined adaptive/second-order sliding mode control algorithm for some classes of uncertain nonlinear systems. *IEEE Transactions on Automatic Control* **45**(7), 1334–1341.

Bartolini, G. and T. Zolezzi (1996). Discontinuous feedback in nonlinear tracking problems. *Dynamics and Control* **6**(4), 323–332.

Beghi, A., L. Nardo and M. Stevanato (2006). Observer-based discrete-time sliding mode throttle control for drive-by-wire operation of a racing motorcycle engine. *IEEE Transactions on Control Systems Technology* **14**, 767–775.

Bevly, D.M., J.C. Gerdes and C. Wilson (2003). The Use of GPS Based Velocity Measurements for Measurement of Sideslip and Wheel Slip. *Vehicle System Dynamics* **38**(2), 127–147.

Bishop, R., R.B. Consulting and MD Granite (2000). A survey of intelligent vehicle applications worldwide. In: *Proceeding of the Intelligent Vehicles Symposium*. pp. 25–30.

Boiko, I., L. Fridman, A. Pisano and E. Usai (2007*a*). Analysis of chattering in systems with second-order sliding modes. *IEEE Transactions on Automatic Control* **52**(11), 2085–2102.

Boiko, I., L. Fridman, A. Pisano and E. Usai (2007*b*). Performance Analysis of Second-Order Sliding-Mode Control Systems With Fast Actuators. *IEEE Transactions on Automatic Control* **52**(6), 1053–1059.

Boiko, I., L. Fridman and M.I. Castellanos (2004). Analysis of second–order sliding–mode algorithms in the frequency domain. *IEEE Transactions on Automatic Control* **49**(6), 946–950.

Bom, J., B. Thuilot, F. Marmoiton and P. Martinet (2005). A global control strategy for urban vehicles platooning relying on nonlinear decoupling laws. In: *Proceedings of the IEEE/RSJ International Conference Intelligent Robots and Systems*. Edmonton, Canada. pp. 2875–2880.

Boniolo, I., S.M. Savaresi and M. Tanelli (2008). Roll angle estimation in two-wheeled vehicles. *IET Control Theory & Applications*. To appear.

Borrelli, F., A. Bemporad, M. Fodor and D. Hrovat (2006). an mpc/hybrid approach to traction control. *IEEE Transactions on Control System Technology* **14**(3), 541–552.

Boyd, S. and L. Vandenberghe (2004). *Convex optimization*. Cambridge University Press.

Brent, R. P. (1973). *Algorithms for Minimization without Derivatives*. Prentice–Hall. Englewood Cliffs, NJ, USA.

Brockett, R.W. (1983). Asymptotic stability and feedback stabilization. *Differential Geometric Control Theory* **27**, 181–191.

Brogliato, B. and C. De Wit (1999). Stability issues for vehicle platooning in automated highway systems. In: *Proceedings of the IEEE Conference on Control Applications*. Kohala Coast, Hawaii, USA. pp. 1377–1382.

Buckholtz, K.R. (2002). Reference input wheel slip tracking using sliding mode control. *Sae Transactions* **111**(6), 477–483.

Canale, M. (2004). Robust control from data in presence of input saturation. *International Journal of Robust and Nonlinear Control* **14**(11), 983–997.

Canale, M. and L. Fagiano (2008). Stability control of 4WS vehicles using robust IMC techniques. *Vehicle System Dynamics* **46**(11), 991–1011.

Canale, M., L. Fagiano, A. Ferrara and C. Vecchio (2008*a*). Comparing internal model control and sliding mode approaches for vehicle yaw control. *IEEE Transactions on Intelligent Transportation*. to appear.

Canale, M., L. Fagiano, A. Ferrara and C. Vecchio (2008*b*). A comparison between imc and sliding mode approaches to vehicle yaw control. In: *Proceedings of the 2008 American Control Conference*. Seattle, Washington, USA. pp. 248–253.

Canale, M., L. Fagiano, A. Ferrara and C. Vecchio (2008*c*). Vehicle yaw control via second order sliding mode technique. *IEEE Transactions on Industrial Electronics*. to appear.

Canale, M., L. Fagiano, M. Milanese and P. Borodani (2007). Robust vehicle yaw control using an active differential and IMC techniques. *Control Engineering Practice* **15**(8), 923–941.

Chakravarthy, A. and D. Ghose (1998). Obstacle avoidance in a dynamic environment: a collision cone approach. *IEEE Transactions on Systems, Man and Cybernetics* **28**(5), 562–574.

Chien, C.C., P. Ioannou and M.C. Lai (1994). Entrainment and vehicle following controllers design for autonomous intelligent vehicles. In: *Proceeding of the 1994 American Control Conference*. Baltimore, Maryland, USA. pp. 6–10.

Chikhi, F., A. El Hadri and J.C. Cadiou (2005). Abs control design based on wheel-slip peak localization. In: *Fifth International Workshop on Robot, Motion and Control*. Dymaczewo, Poland. pp. 73–77.

Corless, M.J. and G. Leitmann (1981). Continuous state feedback guaranteeing uniform ultimate boundedness for uncertain dynamic systems. *IEEE Transactions on Automatic Control* **26**(5), 1139–1144.

Corno, M., M. Tanelli, S.M. Savaresi, L. Fabbri and L. Nardo (2008*a*). Electronic throttle control for ride-by-wire in sport motorcycles. In: *IEEE*

Multi-conference on Systems and Control, San Antonio, Texas, USA. pp. 233–238.

Corno, M., S.M. Savaresi, M. Tanelli and L. Fabbri (2008*b*). On optimal motorcycle braking.. *Control Engineering Practice* **16**(6), 644–657.

Cossalter, V. (2002). *Motorcycle Dynamics*. Race Dynamics. Milwaukee, USA.

Cossalter, V., A. Doria and R. Lot (1999). Steady Turning of Two-Wheeled Vehicles. *Vehicle System Dynamics* **31**, 157–181.

Cossalter, V., R. Lot and F. Maggio (2004). On the Stability of Motorcycle during Braking. In: *SAE Small Engine Technology Conference & Exhibition*. Graz, Austria, September 2004. SAE Paper number: 2004-32-0018 / 20044305.

Dashkovskiy, S., B. S. Rüffer and F. R. Wirth (2007). An ISS small gain theorem for general networks. *Mathematics of Control, Signals, and Systems* **19**(2), 93–122.

Data, S. and F. Frigerio (2002). Objective evaluation of handling quality. *Journal of Automobile Engineering* **216**(4), 297–305.

De Nicolao, G., A. Ferrara and L. Giacomini (2007). Onboard sensor–based collision risk assessment to improve pedestrians' safety. *IEEE Trans. on Vehicular Technology* **56**(5), 2405–2413.

De Wit, C.C. and R. Horowitz (1999). Observers for tire/road contact friction using only wheel angular velocity information. In: *Proceedings of the 38th Conference on Decision and Control*. Phoenix, AZ, USA. pp. 3932–3937.

De Wit, C.C., G. Bastin and B. Siciliano (1996). *Theory of Robot Control*. Springer–Verlag. New York, NY, USA.

DeCarlo, R.A., S.H. Zak and G.P. Matthews (1988). Variable structure control of nonlinear multivariable systems: a tutorial. *Proceedings of the IEEE* **76**(3), 212–232.

Desai, J., J. P. Ostrowski and V. Kumar (1998). Controlling formations of multiple mobile robots. In: *Proc. IEEE Int. Conf. Robot. Automat.* pp. 2864–2869.

Deur, J., D. Pavkovic, P. Nedjeljko, M. Jansz and D. Hrovat (2004). An electronic throttle control strategy including compensation of friction and limp-home effects. *IEEE Transactions on Industrial Electronics* **40**, 821–834.

Do, K.D. and J. Pan (2002). Adaptive global stabilization of nonholonomic systems with strong nonlinear drifts. *Systems and Control Letters* **46**(3), 195–205.

Drakunov, S., Ü. Özgüner, P. Dix and B. Ashrafi (1995). Abs control using optimum search via sliding modes. *IEEE Transactions on Control, System, Technology* **3**(1), 79–85.

Drazenovic, B. (1969). The invariance conditions in variable structure systems. *Automatica* **5**(3), 287–295.

Edwards, C. and K. S. Spurgeon (1998). *Sliding mode control: theory and applications*. Taylor & Francis. London, U.K.

Egerstedt, M., X. Hu and A. Stotsky (2001). Control of mobile platforms using a virtual vehicle approach. *Automatic Control, IEEE Transactions on* **46**(11), 1777–1782.

Emel'yanov, S.V. (1970). *Theory of Variable Structure Systems*. Nauke. Moscow, Russia. (in Russian).

Emel'yanov, S.V. and V.A. Taran (1962). On a class of variable structure control systems. In: *USSR Academy of Sciences, Energy and Automation*. Moskov, Russia. (in Russian).

Ferrara, A. and C. Vecchio (2006*a*). Controlling a platoon of vehicles via second order sliding mode approach. In: *11–th IFAC Symposium on Control in Transportation Systems, CTS06*. Delft, The Netherlands.

Ferrara, A. and C. Vecchio (2006*b*). Controlling a platoon of vehicles with distributed collision avoidance capabilities. In: *Proceedings of the 12th IFAC Symposium on Information Control Problems in Manufacturing*. Sant'Etienne, France.

Ferrara, A. and C. Vecchio (2006*c*). Cruise control with collision avoidance for cars via sliding modes. In: *Proceedings of the IEEE International Conference on Control Applications*. Munich, Germany. pp. 2808–2813.

Ferrara, A. and C. Vecchio (2006*d*). Sliding mode control for automatic driving of a platoon of vehicles. In: *Proceedings of the 9th International Workshop on Variable Structure Systems*. Alghero, Sardinia, Italy. pp. 262–267.

Ferrara, A. and C. Vecchio (2007*a*). Collision avoidance strategies and coordinated control of passenger vehicles. *Nonlinear Dynamics* **49**(4), 475–492.

Ferrara, A. and C. Vecchio (2007*b*). Low vibration vehicle traction control to solve fastest acceleration/deceleration problems via second order sliding modes. In: *Proceeding of the 2007 American Control Conference*. New York, N.Y., USA.

Ferrara, A. and C. Vecchio (2008*a*). Adaptive multiple–surface sliding mode control of nonholonomic systems with matched and unmatched uncertainties. *Automatica*. Submitted.

Ferrara, A. and C. Vecchio (2008*b*). Second order sliding mode control of a platoon of vehicles. *International Journal of Modelling, Identification and Control*.

Ferrara, A. and C. Vecchio (2008*c*). Second order sliding mode control of vehicles with distributed collision avoidance capabilities. *IFAC Mechatronics*. to appear.

Ferrara, A. and M. Rubagotti (2008). A sub–optimal second order sliding mode controller for systems with saturating actuators. In: *Proceedings of the 2008 American Control Conference*. Seattle, WA, USA.

Ferrara, A., G. Ferrari-Trecate and C. Vecchio (2007). Sliding–mode control for coordination in multi–agent systems with directed communication graphs. In: *European Control Conference, ECC07*. Kos, Greece.

Ferrara, A., G. Ferrari-Trecate and C. Vecchio (2008*a*). Sliding mode control for generalized consensus problems in leader–following systems with directed communication graphs. *SIAM journal on control and optimization*. Submitted.

Ferrara, A., L. Giacomini and C. Vecchio (2006). Control of nonholonomic systems with uncertainties via second order sliding modes. In: *Proceedings of the American Control Conference*. Minneapolis, MI, USA. pp. 5384–5389.

Ferrara, A., L. Giacomini and C. Vecchio (2008*b*). Adaptive second order sliding mode control of uncertain nonholonomic systems. In: *Proceedings of the 10th International Workshop on Variable Structure Systems*. Antalya, Turkey. pp. 191–196.

Ferrara, A., L. Giacomini and C. Vecchio (2008*c*). Adaptive sliding mode control of nonholonomic systems in chained form with unknown control direction and uncertainties. In: *International Conference on Mathematical Problems in Engineering, Aerospace and Sciences*. Genova, Italy.

Ferrara, A., L. Giacomini and C. Vecchio (2008*d*). Control of nonholonomic systems with uncertainties via second order sliding modes. *International Journal of Robust and Nonlinear Control* **18**(4–5), 515–528.

Ferrara, A., L. Giacomini and C. Vecchio (2008*e*). Stabilization of nonholonomic uncertain systems via adaptive second order sliding mode control. In: *Modern Sliding Mode Control Theory. New Perspectives and Applications* (Bartolini G, L. Fridman, A. Pisano and E. Usai, Eds.). pp. 223–245. Lecture Notes in Control and Information Sciences. Springer–Verlag. Berlin.

Ferrara, A., R. Librino, A. Massola, M. Miglietta and C. Vecchio (2008*f*). Sliding mode control for urban vehicles platooning. In: *Proceedings of the Intelligent Vehicle Symposium*. Eindhoven, the Netherlands. pp. 877–882.

Ferrari-Trecate, G., A. Buffa and M. Gati (2006*a*). Analysis of coordination in multi-agent systems through partial difference equations. *IEEE Trans. on Autom. Control* **51**(6), 1058–1063.

Ferrari-Trecate, G., M. Egerstedt, A. Buffa and M. Ji (2006*b*). Laplacian sheep: A hybrid, stop-go policy for leader-based containment control.. In: *Proc. 9th International Workshop on Hybrid Systems: Computation and Control* (J. Hespanha and A. Tiwari, Eds.). Vol. 3927 of *Lecture Notes in Computer Science*. pp. 212–226. Springer-Verlag.

Filippov, A.F. (1988). *Differential Equations with Discontinuous Right–hand Sides*. Kluwer. Dordrecht, the Netherlands.

Floquet, T., J.P. Barbot and W. Perruquetti (2003). Higher-order sliding mode stabilization for a class of nonholonomic perturbed systems. *Automatica* **39**(6), 1077–1083.

Fodor, M., J. Yester and D. Hrovat (1998). Active control of vehicle dynamics. In: *Proceeding of the 17th Digital Avionics System Conference*. Bellevue, WA, USA. pp. I14/1–I14/8.

Frediani, S., R. Gianoglio and F. Giuliano (2002). System for the active control of a motor vehicle differential. Patent no. US 2002/0016661 A1.

Fridman, L. (2001*a*). An averaging approach to chattering. *IEEE Transactions on Automatic Control* **46**(8), 1260–1265.

Fridman, L. (2001*b*). An average approach to chattering. *IEEE Transactions on Automatic Control* **46**(8), 1260–1264.

Fridman, L (2003). Chattering analysis in sliding mode systems with inertial sensors. *International Journal of Control* **76**(9), 906–912.

Fridman, L. and A. Levant (1996). Higher Order Sliding Modes as a Natural Phenomenon in Control Theory. *Robust Control Via Variable Structure and Lyapunov Techniques*.

Fridman, L. and F. Levant (2002). Higher order sliding modes. In: *Sliding Mode Control in Engineering* (W. Perruquetti and J.P. Barbot, Eds.). Vol. 217. Marcel Dekker. New York. pp. 53–101.

Fu, L.C. (1991). A Robust Model–Reference Adaptive Control Using Variable–Structure Adaptation for a Class of Plants. *Internation Journal of Control* **53**, 1359–1375.

Gazi, V. (2005). Swarm aggregations using artificial potentials and sliding mode control. *IEEE Trans. on Robotics* **21**(6), 1208–1214.

Ge, S.S., Z. Wang and T.H. Lee (2003). Adaptive stabilization of uncertain nonholonomic systems by state and output feedback. *Automatica* **39**(8), 1451–1460.

Genta, G. (1997). *Motor vehicle dynamics. Modeling and Simulation*. World Scientific. Singapore.

Gillespie, T.D. (1992). *Fundamentals of Vehicle Dynamics*. Society of Automotive Engineers. Warrendale, PA, USA.

Giulietti, F., L. Pollini and M. Innocenti (2001). Autonomous formation flight. *IEEE Control System Magazine* **20**(6), 34–44.

Guldner, J. and V.I. Utkin (1995). Sliding mode control for gradient tracking and robot navigation using artificial potential fields. *IEEE Transactions on Robotics and Automation* **11**(2), 247–254.

Gustafsson, F. (1997). Slip-based tire-road friction estimation. *Automatica* **33**(6), 1087–1099.

Gutman, S. and Z. Palmor (1982). Properties of Min-Max Controllers in Uncertain Dynamical Systems. *SIAM Journal on Control and Optimization* **20**(6), 850–861.

Güvenç, B.A., T. Bünte, D. Odenthal and L. Güvenç (2004). Robust two degree-of-freedom vehicle steering controller design. *IEEE Transactions on Control Systems Technology* **12**(4), 627–636.

Hajek, O. (1979). Discontinuous differential equations I-II. *Journal of Differential Equations* **32**(2), 149–170.

Hallouzi, R., V. Verdult, H. Hellendoorn, PLJ Morsink and J. Ploeg (2004). Communication based Longitudinal Vehicle Control using an Extended Kalman Filter. In: *Proceedings of the IFAC Symposium on Advances in Automotive Control*. Salerno, Italy. pp. 19–23.

Haskara, I., C. Hatipoglu and Ü. Özgüner (2002). Sliding mode compensation, estimation and optimization methods in automotive control. *Variable Structure Systems: Towards the 21st Century, Control and Information Sciences* **274**, 155–174.

Haskara, I., Ü. Özgüner and J. Winkelman (2000). Wheel slip control for antispin acceleration via dynamic spark advance. *Control Engineering Practice* **8**(10), 1135–1148.

Hespanha, J.P., D. Liberzon and A.S. Morse (1999). Towards the supervisory control of uncertain nonholonomic systems. In: *Proceedings of the American Control Conference*. San Diego, CA, USA. pp. 3520–3524.

Hong, D., P. Yoon, H. Kang, I. Hwang and K. Huh (2006). Wheel slip control systems utilizing the estimated tire force. In: *Proceedings of the 2006 American Control Conference*. Minneapolis, MI, USA. pp. 5873–5878.

Horowitz, R. and P. Varaiya (2000). Control design of an automated highway system. *Proc. IEEE* **88**(7), 913–925.

Hsu, L. and R.R. Costa (1989). Variable structure model reference adaptive control using only input and output measurements Part 1. *International Journal of Control* **49**(2), 399–416.

Huang, A.C. and Y.C. Chen (2004). Adaptive multiple-surface sliding control for non-autonomous systems with mismatched uncertainties. *Automatica* **40**(11), 1939–1945.

Huang, A.C. and Y.S. Kuo (2001). Sliding control of non-linear systems containing time-varying uncertainties with unknown bounds. *International Journal of Control* **74**(3), 252–264.

Ippolito, L., G. Lupo and A. Lorenzini (1992). System for controlling torque distribution between the wheels of a common vehicle axle. EU Patent no. 92121621.4.

Isidori, A. (1999). *Nonlinear Control Systems II*. Springer–Verlag. Berlin.

Itkis, U. (1976). *Control systems of variable structure*. Wiley. New York, NY, USA.

Jadbabaie, A., J. Lin and A. S. Morse (2003). Coordination of groups of mobile autonomous agents using nearest neighbor rules. *IEEE Trans. on Automatic Control* **48**(6), 988–1001.

Ji, M., A. Muhammad and M. Egerstedt (2006). Leader-based multi-agent coordination: Controllability and optimal control. *Proc. of the American Control Conference*.

Jiang, Z.P. (1996). Iterative design of time-varying stabilizers for multi-input systems in chained form. *Systems and Control Letters* **28**(5), 255–262.

Jiang, Z.P. (2000). Robust exponential regulation of nonholonomic systems with uncertainties. *Automatica* **36**(2), 189–209.

Johansen, T.A., I. Petersen, J. Kalkkuhl and J. Lüdemann (2003). Gain-scheduled wheel slip control in automotive brake systems. *IEEE Transactions on Control Systems Technology* **11**(6), 799–811.

Kabganian, M. and R. Kazemi (2001). A new strategy for traction control in turning via engine modeling. *IEEE Transactions on Vehicular Technology* **50**(6), 1540–1548.

Kang, S.M., M. Yoo and M. Sunwoo (2005). Traction control using a throttle valve based on sliding mode control and load torque estimation. *Proceedings of the I MECH E Part D Journal of Automobile Engineering* **219**(5), 645–653.

Khatir, M.E. and E.J. Davison (2004). Decentralized control of a large platoon of vehicles using non-identical controllers. *Proceedings of the 2004 American Control Conference* pp. 2769–2776.

Kiencke, U. (1993). Real time estimation of adhesion characteristic between tyres and road. In: *Proceedings of the IFAC World Congress*. Sydney, Australia. pp. 15–22.

Kiencke, U. and L. Nielsen (2000). *Automotive Control Systems*. Springer–Verlag. Berlin.

Kolmanovsky, I. and N.H. McClamroch (1995). Developments in nonholonomic control problems. *IEEE Control Systems Magazine* **15**(6), 1271–1282.

Krstić, M., P.V. Kokotović and I. Kanellakopoulos (1995). *Nonlinear and Adaptive Control Design*. John Wiley & Sons, Inc.. New York, NY, USA.

Kwak, B. and Y. Park (2001). Robust vehicle stability controller based on multiple sliding mode control. *SAE transactions* **110**(7), 513–520.

LaSalle, J. (1960). Some extension of Liapunov's second method. *IRE Transactions on Circuit Theory* **4**(7), 510–517.

Lawton, J.R.T., R.W. Beard and B.J. Young (2003). A decentralized approach to formation maneuvers. *Robotics and Automation, IEEE Transactions on* **19**(6), 933–941.

Lee, H. and M. Tomizuka (2003). Adaptive vehicle traction force control for intelligent vehicle highway systems (ivhss). *IEEE Transactions on Industrial Electronics* **50**(1), 37–47.

Levant, A. (1993). Sliding order and sliding accuracy in sliding mode control. *International Journal of Control* **58**(6), 1247–1263.

Levant, A. (2003). Higher-order sliding modes, differentiation and output-feedback control. *International Journal of Control* **76**(9), 924–941.

Levant, A. (2007). Chattering analysis. *Proceedings of the European Control Conference*.

Levantosky, L.V. (1985). Second order sliding algorithms: their realization. *Dynamics of heterogeneous systems* pp. 32–43. in Russian.

Li, Li, Fei-Yue Wang and Qunzhi zhou (2006). Integrated longitudinal and lateral tire/road friction modeling and monitoring for vehicle motion control. *IEEE Transactions on Intelligent Transportation Systems* **7**(1), 1–19.

Liaw, D.C., H.H. Chiang and T.T. Lee (2007). Elucidating Vehicle Lateral Dynamics Using a Bifurcation Analysis. *IEEE Transactions on Intelligent Transportation Systems* **8**(2), 195–207.

Limebeer, D. J. N., R. S. Sharp and S. Evangelou (2001). The stability of motorcycles under acceleration and braking. *Proc. I. Mech. E., Part C, Journal of Mechanical Engineering Science* **215**, 1095–1109.

Ljung, L. (1999). *System identification, theory for the user*. Prentice Hall. New Jersey, USA.

Marino, R. and P. Tomel (1992). Global adaptive observer for nonlinear systems via filtered transformations. *IEEE Transaction on Automatic Control* **37**, 1239–1245.

Milanese, M. and M. Taragna (2005). H-∞ set membership identification: A survey. *Automatica* **41**(12), 2019–2032.

Morari, M. and E. Zafiriou (1989). *Robust process control*. Prentice Hall. Englewood Cliffs, N.J., USA.

Morin, P., J.B Pomet and C. Samson (1998). Developments in time-varying feedback stabilization of nonlinear systems. *Proceedings of the Nonlinear Control Systems Design Symposium*.

M'sirdi, N.K., A. Rabhi, L. Fridman, J. Davila and Y. Delanne (2006). Second order sliding mode observer for estimation of velocities, wheel slip, radius and stiffness. In: *Proceedings of the 2006 American Control Conference*. Minneapolis, MI, USA. pp. 3316–3321.

Murray, R.M. and S.S. Sastry (1993). Nonholonomic motion planning: steering using sinusoids. *IEEE Transactions on Automatic Control* **38**(5), 700–716.

Nuessle, M., R. Rutz, M. Leucht, M. Nonnenmacher and H. Volk (2007). Objective Test Methods To Assess Active Safety Benefits Of ESP. In: *in 20th International Technical Conference on the Enhanced Safety of Vehicles (ESV)*. Lyon, France. pp. paper no. 07–0230.

Ögren, P., M. Egerstedt and X. Hu (2002). A control Lyapunov function approach to multi-agent coordination. *IEEE Trans. on Robotics and Automation* **18**(5), 847–851.

Olfati-Saber, R. and R. Murray (2004). Consensus problems in networks of agents with switching topology and time-delays. *IEEE Trans on Autom. Control* **49**(9), 1520–1533.

Pacejka, H.B. (2002). *Tyre and Vehicle Dynamics*. Buttherworth Heinemann. Oxford.

Perruquetti, W. and J.P. Barbot (2002). *Sliding Mode Control in Engineering*. CRC Press.

Petti, S. and T. Fraichard (2005). Safe motion planning in dynamic environments. In: *IEEE International Conference on Robotics and Automation*. Barcelona, Spain. pp. 2210–2215.

Pintelon, R. and J. Schoukens (2001). *System Identification: a Frequency Domain Approach*. IEEE Press. New York, USA.

Rajamani, R. (2006). *Vehicle Dynamics and Control*. Springer–Verlag. New York, NY, USA.

Ray, L. R. (1997). Nonlinear tire force estimation and road friction identification: simulation and experiments. *Automatica* **33**(10), 1819–1833.

Reichart, G., R. Haller and K. Naab (1995). Towards future driver assistance systems. *Automotive Technology International* pp. 25–29.

Ren, W. (2007). Consensus strategies for cooperative control of vehicle formations. *Control Theory & Applications, IET* **1**(2), 505–512.

Ren, W., R.W. Beard and E.M. Atkins (2007). Information consensus in multivehicle cooperative control. *IEEE Control Systems Magazine* **27**(2), 71–82.

Ryan, E.P. (1994). On Brocketts' condition for smooth stabilizability and its necessity in a context of nonsmooth feedback. *SIAM Journal of Control and Optimization* **32**(6), 1597–1604.

Scarratt, J.C., A. Zinober, R.E. Mills, M. Rios-Bolívar, A. Ferrara and L. Giacomini (2000). Dynamical adaptive first and second-order sliding backstepping control of nonlinear nontriangular uncertain systems. *Journal of Dynamic Systems, Measurement, and Control* **122**, 746–752.

Schinkel, M. and Ken Hunt (2002). Anti-lock braking control using a sliding mode like approach. In: *Proceedings of the 2002 American Control Conference*. Anchorage, AK, USA. pp. 2386–2391.

Sharp, R. S. (2001). Stability, control and steering responses of motorcycles. *Vehicle System Dynamics* **35**, 291–318.

Sharp, R. S. and D. J. N. Limebeer (2001). A motorcycle model for stability and control analysis. *Multibody System Dynamics* **6**, 123–142.

Sharp, R. S., S. Evangelou and D. J. N. Limebeer (2004). Advances in the modelling of motorcycle dynamics. *Multibody System Dynamics* **12**, 251–283.

Sharp, R. S., S. Evangelou and D.J.N. Limebeer (2005). Multibody aspects of motorcycle modelling with special reference to Autosim. In: *Advances in computational multibody systems* (J.A.C. Ambrosio, Ed.). pp. 45–68. Springer-Verlag.

Sharp, R.S. (1971). The stability and control of motorcycles. *Journal of Mechanical Engineering Science* **13**, 316–329.

Sheikholeslam, S. and C.A. Desoer (1990). Longitudinal control of a platoon of vehicles. In: *Proceeding of the American Control Conference*. San Diego, CA, USA. pp. 291–297.

Shladover, S.E., C.A. Desoer, J.K. Hedrick, M. Tomizuka, J. Walrand, W.B. Zhang, D.H. McMahon, H. Peng, S. Sheikholeslam and N. McKeown

(1991). Automated vehicle control developments in the PATH program. *IEEE Transactions on Vehicular Technology* **40**(1), 114–130.

Sira-Ramirez, H. (1992). On the sliding mode control of nonlinear systems. *Systems & control letters* **19**(4), 303–312.

Skogestad, S. and I. Postlethwaite (2005). *Multivariable Feedback Control: Analysis and Design*. John Wiley & Sons, Inc.. New York, NY, USA.

Slotine, J.J.E. and W. Li (1991). *Applied nonlinear control*. Prentice Hall. Englewood Cliffs, NJ, USA.

Sorensen, N. and W. Ren (2007). A Unified Formation Control Scheme with a Single or Multiple Leaders. *American Control Conference, 2007. ACC'07* pp. 5412–5418.

Stéphant, J., A. Charara and D. Meizel (2007). Evaluation of a sliding mode observer for vehicle sideslip angle. *Control Engineering Practice* **15**(7), 803–812.

Swaroop, D. and J.K. Hedrick (1996). String stability of interconnected systems. *IEEE Transactions on Automatic Control* **41**(3), 349–357.

Tanelli, M., A. Astolfi and S.M. Savaresi (2008*a*). Robust nonlinear output feedback control for brake-by-wire control systems.. *Automatica* **44**(4), 1078–1087.

Tanelli, M., M. Prandini, F. Codecà, A. Moia and S.M. Savaresi (2008*b*). Analysing the interaction between braking control and speed estimation: the case of two-wheeled vehicles. In: *47th IEEE Conference on Decision and Control, Cancun, Mexico*. To appear.

Tanner, H. and G. Pappas (2002). Formation input–to–state stability. In: *Proceedings of* 15^{th} *IFAC World Congress*. Barcelona, Spain.

Tanner, H., G. Pappas and V. Kumar (2004). Leader–to–formation stability. *IEEE Trans. on Robotics and Automation* **20**(3), 433–455.

Tanner, H., V. Kumar and G. Pappas (2002). Stability properties of interconnected vehicles. In: *Proceedings of the* 15^{th} *International Symposium on Mathematical Theory of Networks and Systems*. South Bend, IN.

Tomizuka, M., J.K. Hedrick and H. Pham (1995). Integrated manoeuvring control for automated highway systems based on magnetic reference/sensing system. Technical Report PATH Rep. UCB-ITS-PRR-95-12. University of California, Berkeley.

Ünsal, C. and P. Kachroo (1999). Sliding mode measurement feedback control for antilock braking systems. *IEEE Transactions on Control Systems Technology* **7**(2), 271–281.

Utkin, V.I. (1974). *Sliding Modes and Their Application in Variable Structure Systems*. Nauka. Moscow, Russia. (in Russian).

Utkin, V.I. (1977). Variable structure systems with sliding modes. *IEEE Transactions on Automatic Control* **22**(2), 212–222.

Utkin, V.I. (1992). *Sliding modes in control optimization*. Springer–Verlag. Berlin.

Utkin, V.I., J. Guldner and J. Shi (1999). *Sliding–Mode Control in Electromechanical Systems*. Taylor & Francis. London, U.K.

Vahidi, A. and A. Eskandarian (2003). Research advances in intelligent collision avoidance and adaptive cruise control. *IEEE Transactions on Intelligent Transportation Systems* **4**(3), 143–153.

Vecchio, C., M. Tanelli, M. Corno, A. Ferrara and S.M. Savaresi (2008). Second order sliding mode for traction control in ride-by-wire sport motorcycles. In: *Proceeding of the 2009 American Control Conference*. Submitted.

Vecchio, C., M. Tanelli, M. Corno, A. Ferrara and S.M. Savaresi (2009). Traction control for ride-by-wire sport motorcycles: a second order sliding mode approach. *IEEE Transactions on Industrial Electronics*. Submitted.

White, B.A. and P.M. Silson (1984). Reachability in variable structure control systems. *IEE proceedings. Part D. Control theory and applications* **131**(3), 85–91.

Won, M. and J.K. Hedrick (1996). Multiple-surface sliding control of a class of uncertain nonlinear systemsm. *International Journal of Control* **64**(4), 693–706.

Xi, Z., G. Feng, Z.P. Jiang and D. Cheng (2003). A switching algorithm for global exponential stabilization of uncertain chained systems. *IEEE Transactions on Automatic Control* **48**(10), 1793–1798.

Xy, L., H.S. Tan, S. Shladover and J.K. Hedrick (2001). Nonlinear longitudinal controller implementation and comparison for automated cars. *Journal of Dynamic Systems measurement and control* **123**, 161–167.

Yip, P. (1997). Robust and adaptive nonlinear control using dynamic surface control with applications to intelligent vehicle highway systems. PhD thesis. University of California, Berkeley, USA.

Yoshida, T., H. Kuroda and T. Nishigaito (2004). Adaptive driver-assistance Systems. *Hitachi Review* **53**(4), 213.

Young, K., V. Utkin and Ü. Özgüner (1999). A control engineers guide to sliding mode control. *IEEE Transactions On Control Systems Technology* **7**(3), 328–342.

Zambou, N., M. Enning and D. Abel (2004). Longitudinal control of following vehicle within platoon, a model-based predictive approach. In: *Proceedings of the IFAC Symposium on Advances in Automotive Control.* Salerno, Italy. pp. 733–738.

Zhang, Y., B. Kosmatopoulos, P.A Ioannou and C.C. Chien (1999). Using front and back information for tight vehicle following maneuvers. *IEEE Transactions on Vehicular Technology* **48**(1), 319–328.

Zheng, A., M.V. Kothare and M. Morari (1994). Anti-windup design for internal model control. *International Journal of Control* **60**(5), 1015–1024.

Zheng, N.N., S. Tang, H. Cheng, Q. Li, G. Lai and F.Y. Wang (2004). Toward intelligent driver-assistance and safety warning systems. *IEEE Intelligent Systems* **19**(2), 8–11.

Zhou, J. and H. Peng (2000). String stability conditions of adaptive cruise control algorithms. *JSME International Journal Series C* **43**, 671–677.

Zinober, A.S.I. (1994). *Variable Structure and Lyapunov Control.* Springer-Verlag. New York, NY, USA.